An investigation into murine pericyte shape change in response to inflammatory stimuli *in vitro* and *in vivo*

A thesis submitted for the degree of

Doctor of Philosophy
University of London
Queen Mary University

By

Doris Proebstl, M.Sc.

Centre for Microvascular Research
William Harvey Research Institute
Barts & The London School of Medicine and Dentistry
Queen Mary University of London
Charterhouse Square
London EC1M 6BQ
United Kingdom

Acknowledgements

At this point, I would like to thank all the individuals without whom this PhD thesis would not have been possible:

First and foremost, I would like to thank my supervisor Prof. Sussan Nourshargh for giving me the opportunity to join her group and to work on this important, novel and exciting project. I also want to thank her for her time, help and extraordinary support. Her excellent teaching and guidance helped me to achieve so much.

Furthermore, I wish to thank Prof. Rod Flower for the friendly welcome to the William Harvey Research Institute and for acting as my second supervisor.

Moreover, I would like to thank Dr. Mathieu-Benoit Voisin for the excellent introduction to the project, for many valuable discussions, advice and all his help and time.

Many thanks also go to the whole Microvascular Research group for all the help and support and the very nice working atmosphere. Special thanks go to Dr. James Whiteford for his help regarding cell culture work and for proof reading this thesis and to Dr. Abigail Woodfin for her constant availability as a “rent-a-surgeon”. I would also like to thank Dr. Martina Bauer and Dr. Mathieu-Benoit Voisin for proof reading parts of this thesis.

I wish to thank the Biochemical Pharmacology group for the friendly welcome to the Institute and their great helpfulness.

A big thank you goes to all my friends for their understanding and support, especially to Dr. Anna Bauer-Mehren, who also did a PhD in a foreign country, for all the long telephone chats and for organising plenty of “PhD islands” together.

A special thank you goes to Fabian Gerick for his love, enormous support and tremendous help by motivating me and constantly taming my document, which had developed a mind of its own after a certain amount of pages and had a “nice” surprise in store almost every day.

Most importantly, I like to thank my mother Irmgard Proebstl and my grandmother Emilie Schmidbauer for all their love and support, not just during the last three years.

My final acknowledgement goes to the Barts and The London Research Advisory Board as well as The Wellcome Trust for funding of my PhD studentship.

Abstract

Leukocyte transmigration through venular walls into the surrounding tissue is a crucial event during inflammatory responses. Despite increased understanding of the mechanisms associated with leukocyte migration through endothelial cells, little is known about the mechanisms mediating the subsequent migration through the pericyte layer and the basement membrane. We previously reported that gaps between adjacent pericytes are co-localised with matrix protein low expression regions in the basement membrane, regions that are preferentially used by leukocytes to penetrate venular walls (Wang et al., 2006; Voisin et al., 2009; Voisin et al., 2010). This study extended these findings to other vascular beds showing that pericyte morphology is heterogeneous in different tissues (Voisin et al., 2010). To investigate whether pericytes facilitate the transmigration process through direct morphological changes at sites of inflammation, neutrophil transmigration and pericyte shape change was analysed in whole mounted TNF-α- and IL-1β-stimulated murine cremaster muscles by immunofluorescence labelling and confocal microscopy. Post-capillary pericytes exhibited shape change resulting in a significant increase in mean gap size between adjacent cells. Time-course studies indicated that TNF-α-induced shape change preceded neutrophil transmigration. This response was PMN-independent as it was also noted in PMN depleted mice. Parallel studies investigated the effect of these cytokines on shape change of murine pericyte-like C3H/10T1/2 cells *in vitro* by time lapse microscopy. C3H/10T1/2 cells also exhibited significant shape change in response to direct TNF-α- and IL-1β-stimulation *in vitro.* Post-capillary venular pericytes *in vivo* and C3H/10T1/2 cells *in vitro* expressed the respective cytokine receptors, TNFRI, TNFRII and IL-1RI, indicating that pericytes can respond directly to pro-inflammatory cytokines. Finally, pericyte involvement in neutrophil transmigration *in vivo* was investigated in real time by confocal intra vital microscopy using α-SMA-RFPcherryxLys-EGFP mice. Neutrophils preferentially used enlarged gaps to migrate into the surrounding tissue.

Table of contents

List of Figures

List of Tables

Abbreviations

ANOVA	analysis of variance
α-SMA	alpha-smooth muscle actin
BM	basement membrane
Ca2+	calcium ions
CCL2	chemokine: C-C motif ligand 2
CD	cluster of differentiation
dNTP	deoxynucleotide triphosphate
EC	endothelial cell
EDTA	ethylene diamine tetraacetate
EGFP	enhanced Green Fluorescent Protein
ESAM	endothelial cell-selective adhesion molecule
ESL-1	E-selectin ligand-1
FCS	fetal calf serum
GAG	glycosaminoglycan
GFP	Green Fluorescent Protein
GPCR	G-protein coupled receptor
ICAM	intercellular cell adhesion molecule
i.d.	intradermal
Ig	immunoglobulin
IL-1β	interleukin-1beta
IL-1RI	interleukin-1 receptor type I
i.m.	intramuscular
i.p.	intraperitoneal
I/R injury	ischemia/reperfusion injury

i.s.	intrascrotal
IVM	intravital microscopy
JAM	junctional adhesion molecule
KO	knockout
LER	Low expression region (of matrix protein in the vascular basement membrane)
LFA-1	leukocyte function-associated antigen-1
LSM	laser scanning microscope
LTB_4	leukotriene B_4
Lys	Lysozyme
Mac-1	macrophage antigen-1
MeOH	methanol
MFI	mean fluorescence intensity
$MgCl_2$	magnesium chloride
NGS	normal goat serum
NH_4^+	ammonium ion
PBS	phosphate buffered saline
PCR	polymerase chain reaction
PECAM-1	platelet endothelial cell adhesion molecule-1
PFA	paraformaldehyde
PSGL-1	P-selectin glycoprotein ligand-1
RFI	relative fluorescence intensity
RFPcherry	cherry variant of the Red Fluorescent Protein
SEM	standard error of mean
TNF-α	tumour necrosis factor alpha
TNFRI	tumour necrosis factor receptor type I

TNFRII	tumour necrosis factor receptor type II
VCAM-1	vascular endothelial cell adhesion molecule
VE-cadherin	vascular endothelial cadherin
VEGF	vascular endothelial growth factor
VLA-4	very late antigen-4
WT	wild-type

List of presentations at national and international meetings

Pröbstl D., Voisin M.B. and Nourshargh S. (2009). **Pericytes Facilitate Leukocyte Transmigration *In Vivo*.** FASEB Experimental Biology Meeting (New Orleans, LA, USA, 18th – 22nd April 2009). The abstract was selected for three oral presentations.

Pröbstl D., Voisin M.B. and Nourshargh S. (2009). **Pericytes: A Role in Facilitating Leukocyte Transmigration *In Vivo*.** London Vascular Biology Forum Christmas Poster Meeting (London, 9th December 2009). Poster presentation.

Pröbstl D., Voisin M.B., Woodfin A., Whiteford J.R., D'Acquisto F., Rowe D., Jones G.E. and Nourshargh S. (2010). **Inflammatory Cytokines Induce Pericyte Shape Change *In Vivo*: Role in Facilitating Leukocyte Transmigration?** UK adhesion meeting (Manchester, 13th – 15th September 2010). Poster presentation.

Pröbstl D., Voisin M.B., Woodfin A., Whiteford J.R., D'Acquisto F., Rowe D., Jones G.E. and Nourshargh S. (2010). **Inflammatory Cytokines Induce Pericyte Shape Change *In Vivo*: Role in Facilitating Leukocyte Transmigration?** London Vascular Biology Forum Christmas Poster Meeting (London, 8th December 2010). Poster presentation.

Publications arising from this work

Voisin M.B., Pröbstl D., and Nourshargh S.: **Venular Basement Membranes Ubiquitously Express Matrix Protein Low-Expression Regions.** *Am J Path, 2009*.

Pröbstl D., Voisin M.B., Woodfin A., Whiteford J.R., D'Acquisto F., Rowe D., Jones G.E. and Nourshargh S.: **Pericytes Support Neutrophil Sub-endothelial Cell Crawling and Migration Through Venular Walls *In Vivo*.** *In preparation*.

Statement of Originality

The approach and experiments presented here are novel. The author has personally undertaken all the work described here, unless stated otherwise.

Chapter 1: General Introduction

1.1 Inflammation

Inflammation is a complex multi-cellular host response to harmful stimuli, such as pathogens (e.g. viruses, bacteria, fungi or parasites), damaged cells or irritants. The innate immune response is part of an inflammatory response and forms the front line of host defence. The innate immune response is based on non-specific pathogen recognition systems that identify common surface patterns of pathogenic microorganisms (e.g. lipopolysaccharides (LPS) on Gram-negative bacteria) and involves key phagocytic leukocytes including neutrophils, monocytes and macrophages (Figure 1.1). The two major tasks of the innate immune response are resolving or confining the infection via phagocytosis and priming the other branch of host immunity, the adaptive immune response. Upon the initial encounter of foreign antigens, certain cells of the innate immune response act to induce the adaptive branch through the activation of specialised B and T lymphocytes that are highly specific for defined pathogens.

Inflammatory responses involve five characteristic symptoms: Heat, pain, redness, swelling and loss of functions. These symptoms are caused by the effects of inflammatory mediators on local blood vessels and the resulting recruitment of leukocytes to the surrounding tissue. In the early phase of inflammation, tissue resident macrophages and dendritic cells phagocytose pathogens and generate inflammatory mediators such as cytokines (e.g. tumour necrosis factor α (TNF-α) and interleukin-1β (IL-1β)), chemokines (e.g. CCL2/monocyte chemoattractant protein-1 (MCP-1) and CXCL8/interleukin 8 (IL-8)) and chemoattractants (e.g. leukotriene B_4 (LTB_4)) indicating the site of infection (Figure 1.1 a). These inflammatory stimuli activate endothelial cells of local blood vessels leading to vasodilatation, increased permeability and an upregulation of pro-inflammatory adhesion molecules on the luminal surface of the endothelium. Vasodilatation and increased permeability enhance local blood flow and vascular leakage, accounting for the heat, redness, and swelling observed during inflammatory responses. Collectively these events promote the recruitment of leukocytes from the vascular lumen to the site of infection, to which they are attracted, largely through the actions of chemokines (Figure 1.1 b).

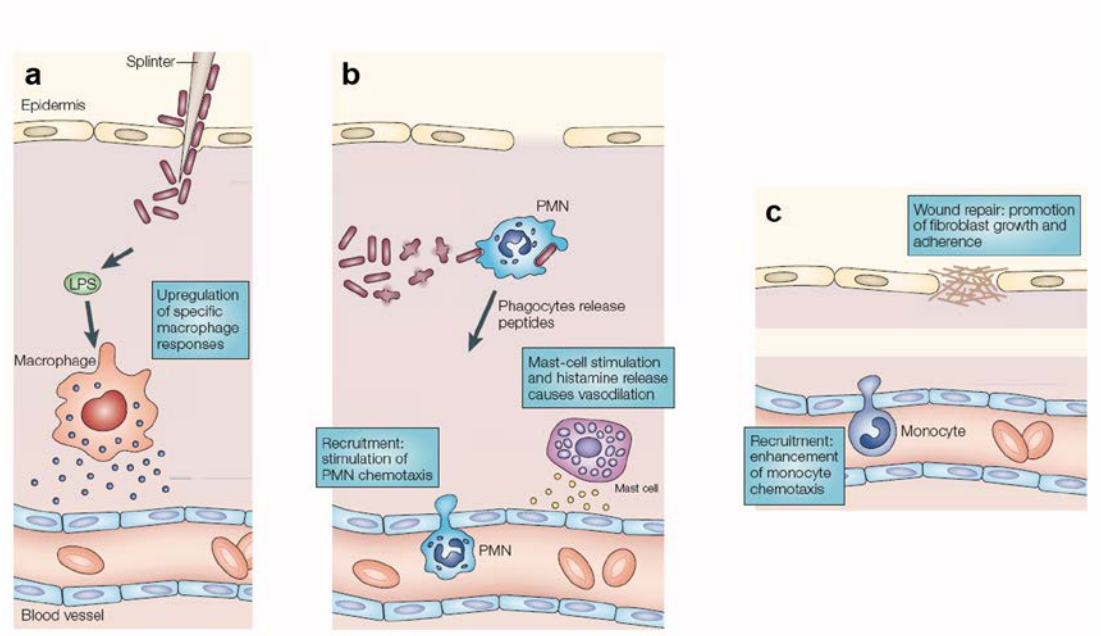

Figure 1.1: Aspects of innate immune responses during acute inflammation. (a) After injury, pathogens are detected by tissue-resident macrophages via the recognition of common surface patterns such as lipopolysaccharides (LPS). This interaction triggers macrophages to release inflammatory mediators such as cytokines and chemokines. (b) Inflammatory mediators stimulate local blood vessels, which initiates the recruitment of polymorphonuclear leukocytes (PMNs) such as neutrophils. PMNs can also be stimulated directly and once in the tissue they help clearing the infection via phagocytosis of pathogens as well as secretion of cytotoxic components. In addition, mast cells in the tissue get activated to release histamine from intracellular stores which induces vasodilation. (c) In most reactions neutrophil transmigration is followed by monocyte infiltration into the tissue, where they rapidly differentiate into macrophages. Finally, repair mechanisms are activated to initiate wound healing. Adapted from Finlay and Hancock, 2004.

The migration of cells into the tissue and their local responses such as the release of lytic enzymes and cytotoxic components activate sensory nerves causing the pain felt during inflammatory conditions. Neutrophils and monocytes are present in high numbers in the circulation and are therefore immediately available to react to inflammatory signals. Neutrophils are the most abundant subtype of blood leukocytes and are the first to be recruited into the infected tissue. Like macrophages, neutrophils express surface receptors for common bacterial components and are therefore able to engulf and destroy pathogenic microorganisms (Figure 1.1 b). In addition, neutrophils have numerous granules containing potent anti-microbial substances such as lytic enzymes and are able to generate reactive oxygen species that are cytotoxic for both pathogens and host tissue at high concentrations (Figure 1.1 b). Hence, neutrophil recruitment and activation has to be a controlled event in host defence so that it effectively eliminates pathogens while injury to host

cells is kept to a minimum. Neutrophil infiltration is often followed by monocyte transmigration into the tissue upon which monocytes rapidly differentiate into macrophages (Figure 1.1 c). Following internalisation and degradation of pathogens, macrophages become activated and present foreign antigens on their cell surface. However, the cells that are more specialised in presenting antigens and initiating adaptive immunity are dendritic cells, which reside in the tissue and become activated upon antigen encounter. During inflammatory responses the flow of lymph increases which promotes the migration of antigen-bearing macrophages and dendritic cells into lymphatic vessels and finally lymphoid tissues where they activate B and T lymphocytes initiating the slower but highly specific adaptive immune response. Activated dendritic cells migrate into lymph vessels to reach lymphoid tissues and prime the adaptive immune response by presenting the foreign antigens to T lymphocytes, resulting in the development of a highly specific population of B and T lymphocytes. Inflammation can be classified into either acute or chronic. Acute inflammatory responses are transient episodes, whereas chronic inflammation occurs when the infection persists or during autoimmune diseases.

Collectively, inflammation is a complex response that plays a vital role in host defence via a number of means such as regulating the spread of pathogens, delivering additional effector molecules and cells to sites of infection, priming the adaptive immune response and finally activating repair mechanisms to promote healing of the injured tissue. Immunity is a carefully balanced process targeting specifically foreign antigens while tolerating host antigens, however, in certain disorders the system is inappropriately triggered, excessive or prolonged or self-tolerance is lost leading to damage to the host. Therefore, it is important to investigate and understand the mechanisms that mediate and regulate leukocyte recruitment to be able to target this process when developing treatments for pathological inflammatory conditions.

1.2 The leukocyte adhesion cascade

The recruitment of leukocytes from blood to inflammatory sites is a crucial event during inflammatory responses. The mechanisms involved in the transmigration of leukocytes from the vascular lumen through venular walls into the surrounding tissue are summarised in a paradigm known as the leukocyte adhesion cascade. Initially, three steps had been described: Rolling, activation and arrest/firm adhesion of leukocytes (Butcher, 1991; Springer, 1994, 1995). These steps have been extended and refined, which led to the addition of extra steps such as slow rolling, adhesion strengthening, intraluminal crawling and paracellular and transcellular migration through the endothelium (Ley et al., 2007) (Figure 1.2).

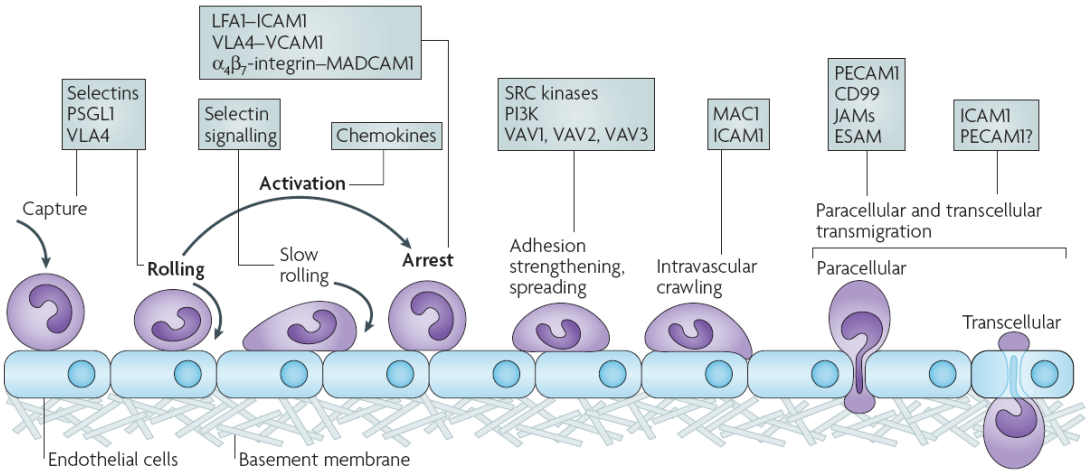

Figure 1.2: The leukocyte adhesion cascade. Originally known steps are shown in bold print compared to recently added ones. Key molecules involved in each step are indicated in boxes. Taken from Ley et al., 2007.

Furthermore, more insight has been gained into the mechanisms that mediate leukocyte transmigration through the endothelium (Woodfin et al., 2010) and some progress has been made in understanding how leukocytes breach the underlying vascular basement membrane and migrate within the extravascular tissue (Ley et al., 2007; Voisin et al., 2009; Nourshargh et al., 2010). However, the leukocyte adhesion cascade as it is recognised at present does not include the role of pericytes. By surrounding endothelial cells, they represent the second cellular component of venular walls, but very little is known about the role of these cells in inflammatory responses. Therefore, this study aims to elucidate the potential role of pericytes in

regulating leukocyte transmigration to understand the possible contribution of these cells to the overall molecular events during leukocyte extravasation.

1.2.1 Leukocyte capture and rolling

The earliest step in the leukocyte adhesion cascade is the capture of leukocytes from the circulation (also termed leukocyte tethering), which is followed by leukocyte rolling along activated endothelial cells. During inflammatory conditions, the endothelium is activated by inflammatory stimuli such as endotoxins, cytokines, chemokines and chemoattractants resulting in the expression of selectins (E-selectin and P-selectin) and cell adhesion molecules (intercellular adhesion molecule 1 (ICAM-1) and vascular cell adhesion molecule 1 (VCAM-1)) on the luminal surface. Subsequently, leukocytes are captured from the blood stream and start rolling along the activated endothelial cells, a process that is mainly mediated by the interaction of selectins and their respective ligands (Figure 1.3) (Kansas, 1996; Vestweber and Blanks, 1999).

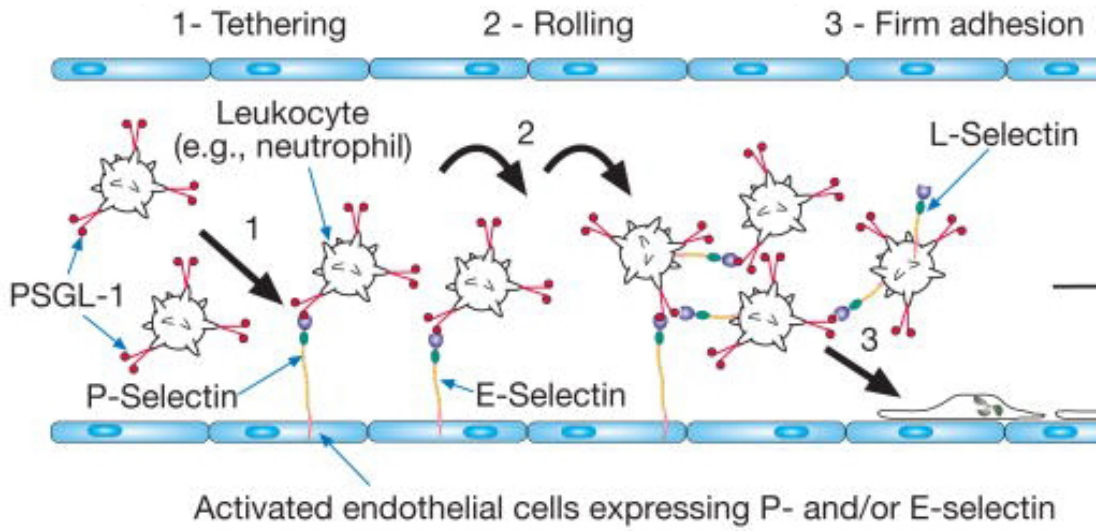

Figure 1.3: Capture of circulating leukocytes and subsequent rolling on activated endothelium mediated via interactions between selectins and their ligands. The diagram shows leukocytes constitutively expressing PSGL-1 and L-selectin. Upon activation through inflammatory stimuli endothelial cells express P-selectin and E-selectin and leukocytes start interacting by random contact with the activated endothelium through PSGL-1-P-selectin binding. E-Selectin also participates in these interactions by binding to PSGL-1 or other ligands on leukocytes. These interactions enable leukocytes to tether to and roll along the endothelium. Leukocyte–leukocyte interactions involving L-selectin and PSGL-1 are also depicted. Adapted from Varki A, 2009.

Selectins are type I transmembrane proteins with long extracellular and short cytoplasmic domains. The extracellular domain contains the ligand binding lectin domain located at the aminoterminus followed by an epidermal growth factor (EGF)-like domain and short consensus repeats (Vestweber and Blanks, 1999). At present three selectins are known: E-selectin (CD62E) which is expressed on activated endothelial cells (Bevilacqua et al., 1987; Pober et al., 1987; Bevilacqua et al., 1989), L-selectin (CD62L) which is found on all circulating leukocytes (Gallatin et al., 1983) and P-selectin (CD62P) which is present on activated endothelial cells and platelets (Hsu-Lin et al., 1984; McEver and Martin, 1984; Johnston et al., 1989). All selectin ligands are fucosylated carbohydrate structures containing sulfated-sialyl-Lewis^x, which is a tetrasaccharide carbohydrate recognised by the lectin domain of selectins. Circulating leukocytes express selectin ligands as shown in Table 1.1.

Selectin ligand	**Expressed on**	**Binding partner**	**Corresponding references**
E-selectin ligand 1 (ESL-1)	Leukocytes	E-selectin	Levinovitz et al., 1993
CD44	Leukocytes	E-selectin	Dimitroff et al., 2001; Katayama et al., 2005
P-selectin glycoprotein ligand 1 (PSGL-1)	Leukocytes	All selectins	Bargatze et al., 1994; Asa et al., 1995; Moore et al., 1995; Jutila and Kurk, 1996; Goetz et al., 1997

Table 1.1: Expression of selectin ligands on leukocytes.

The formed selectin bonds have very high on- and off-rates allowing the captured leukocytes to roll along the activated endothelial layer (Figure 1.3) (Lawrence and Springer, 1991; Hammer and Apte, 1992; Alon et al., 1995). In fact, the high shear rate along the vessel wall is necessary to promote and support P-selectin and L-selectin mediated leukocyte rolling (Finger et al., 1996; Lawrence et al., 1997). This is due to the catch bond character of selectins, meaning that each bond is strengthened as shear stress is applied (Marshall et al., 2003). P-selectin is the main selectin mediating leukocyte capture and early rolling events, since it is rapidly translocated from intracellular granules called Weibel-Palade bodies to the luminal surface of endothelial cells upon endothelial activation through inflammatory stimuli (Hsu-Lin et al., 1984; McEver and Martin, 1984; Geng et al., 1990). In addition, P-selectin synthesis can be induced by TNF-α, IL-1β and IL-4 (Pan and McEver, 1995;

Yao et al., 1996; Yao et al., 1999; Woltmann et al., 2000). In contrast, there are no intracellular stores of E-selectin, hence this molecule is newly synthesized as a result of endothelial cell activation by LPS or by inflammatory cytokines such as TNF-α and IL-1β (Bevilacqua et al., 1987; Pober et al., 1987). Therefore, E-selectin expression peaks at 3-4 h after stimulation (Bevilacqua et al., 1987; Pober et al., 1987). PSGL-1 seems to be the main selectin ligand involved in mediating leukocyte recruitment and rolling *in vivo* (Norman et al., 1995; Borges et al., 1997a; Borges et al., 1997b). The interaction of L-selectin with PSGL-1 initiates leukocyte-leukocyte interactions which facilitates the capture of secondary leukocytes (Figure 1.3) (Bargatze et al., 1994; Eriksson et al., 2001).

Apart from mediating rolling, selectin-mediated leukocyte-endothelial interactions also trigger signalling events in both cells, inducing the activation of integrins and subsequent integrin-mediated firm adhesion (Simon et al., 2000). Integrins are heterodimeric cell surface proteins consisting of an α- and a β-subunit and are basally expressed on leukocytes but are able to adopt different conformation states that vary in affinity for their ligand (low, intermediate and high affinity; Figure 1.4) (Arnaout et al., 2005). Leukocyte rolling on E-selectin induces conformational changes in integrins from low affinity to intermediate affinity. This is true for integrin $\alpha_L\beta_2$ (also known as lymphocyte-function-associated antigen 1 (LFA-1) or CD11a/CD18) and integrin $\alpha_M\beta_2$ (macrophage receptor 1 (Mac-1) or CD11b/CD18) which are both expressed on neutrophils. Their activation leads to the formation of transient bonds with their ligand ICAM-1 on activated endothelial cells supporting neutrophil rolling (Lo et al., 1991; Salas et al., 2004; Chesnutt et al., 2006). Another ligand for LFA-1 and Mac-1 is ICAM-2. In contrast to ICAM-1, which is expressed in a continuous manner on the luminal surface of the endothelium (Sumagin and Sarelius, 2006), ICAM-2 is mostly expressed at endothelial cell junctions (Huang et al., 2006) indicating a role for this molecule in leukocyte transmigration rather than rolling and adhesion. Indeed, to date ICAM-2 has only been implicated in leukocyte transmigration (Issekutz et al., 1999; Huang et al., 2006; Woodfin et al., 2009). T-cells and monocytes have been shown to express integrin $\alpha_4\beta_1$ (also termed very late integrin 4 (VLA-4) or CD49d/CD29) which interacts with VCAM-1 on activated endothelium to mediate leukocyte rolling *in vitro* and *in vivo* such as in the central nervous system (CNS) (Berlin et al., 1995; Grabovsky et al., 2000; Huo et al., 2000;

Chan et al., 2001; Singbartl et al., 2001). It has been shown *in vivo* that leukocyte rolling velocity eventually decreases at sites of inflammation, a phenomenon that is termed slow rolling and requires not only E-selectin, but also engagement of LFA-1 and/or Mac-1 with their ligand ICAM-1 (Kunkel and Ley, 1996; Jung et al., 1998; Dunne et al., 2002; Zarbock et al., 2008).

1.2.2 Leukocyte arrest and intravascular crawling to sites of transendothelial migration

Integrin-mediated slow rolling of leukocytes represents the transition from selectin-mediated rolling to integrin-mediated firm arrest (Simon et al., 2000; Zarbock and Ley, 2008). Chemokines and chemoattractants, synthesized by endothelial cells upon activation by inflammatory cytokines, are transported to the luminal surface where they are presented by being bound to glucosaminoglycans (GAGs) (Spillmann et al., 1998; Halden et al., 2004; Johnson et al., 2005). In addition, it has been shown that activated endothelial cells are able to transport chemokines and chemoattractants, which have been generated in the infected tissue such as the chemokine CCL2 and the bacteria-derived chemoattractant peptide formylated methionine-leucine-proline (fMLP), from their abluminal to their luminal side (Middleton et al., 1997; Rot, 2005). Leukocyte slow rolling allows for the binding of chemokines and chemoattractants on the luminal surface of endothelial cells to G-protein coupled receptors (GPCRs) on leukocytes. This interaction induces intracellular signalling pathways in leukocytes leading to a further activation of integrins from intermediate affinity to high affinity conformation (Figure 1.4), a process termed inside-out signalling (Constantin et al., 2000; Laudanna et al., 2002).

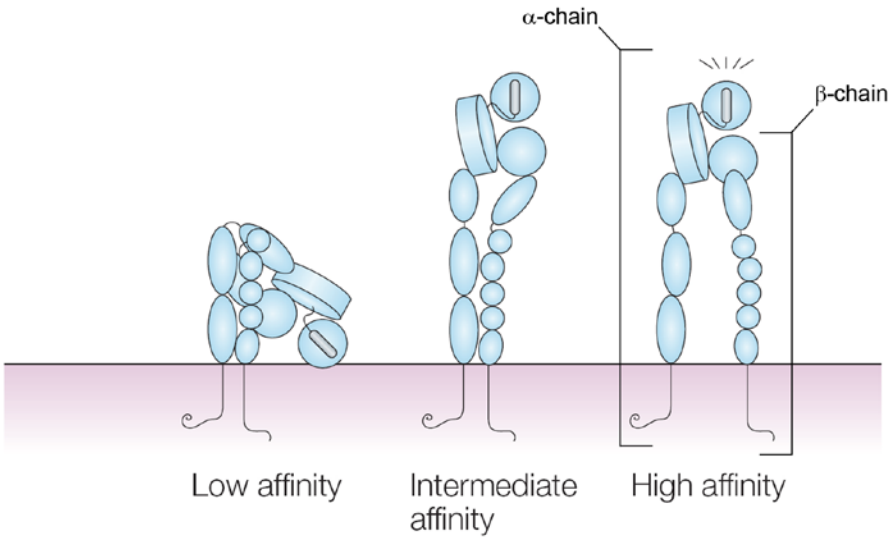

Figure 1.4: Different integrin conformation states and their associated ligand affinities. The diagram shows the three different conformations that integrins can adopt. In the bent head-piece conformation integrins exhibit low ligand affinity, whereas extension of the head-piece leads to conformations with intermediate and high affinity. Adapted from Kinashi, 2005.

The intracellular signalling induced in slow rolling leukocytes by the high affinity binding of fully activated integrins to their ligands on the endothelium is known as outside-in signalling (Arnaout et al., 2005; Shattil, 2005; Giagulli et al., 2006). The integrins primarily involved in this process are LFA-1, Mac-1 and VLA-4. The high affinity interaction with their endothelial ligands, mainly ICAM-1 and VCAM-1, results in adhesion strengthening leading to leukocyte arrest (Campbell et al., 1998; Constantin et al., 2000; Kim et al., 2003; Shamri et al., 2005).

Upon arrest leukocytes undergo changes in cell shape, which results in an elongated polarised phenotype and the formation of a leading edge (lammellipod or pseudopod) and a trailing edge (uropod) (Rose et al., 2007). This process, termed cell spreading, enables subsequent intravascular crawling to sites of transendothelial migration. This is important, since leukocyte arrest does not necessarily result in subsequent transendothelial migration at the same location. Leukocytes often show intravascular crawling from the initial site of arrest to preferred spots of transmigration, an event that requires Mac-1 and ICAM-1 interactions (Schenkel et al., 2004; Phillipson et al., 2006; Ryschich et al., 2006). However, details of the mechanisms involved in initiating and mediating intravascular crawling remain to be elucidated. Recently, it has been shown *in vivo* that Vav1, a guanine exchange factor for the Rho family

GTPases Rac and Cdc42, is a major regulator of the actin cytoskeleton organization during leukocyte polarization and plays an important role in intravascular crawling (Mor et al., 2007; Phillipson et al., 2009). Additionally, junctional adhesion molecule A (JAM-A), an adhesion molecule expressed on the surface of both leukocytes and endothelial cells, has recently been implicated in leukocyte motility (Corada et al., 2005; Cera et al., 2009).

Intravascular crawling seems to be important in finding ideal exit points for migration through the endothelium such as endothelial junctions since its blockade reportedly increases the frequency of transcellular migration (migration through the body of an endothelial cell, detailed in section 1.2.3.2) as opposed to paracellular migration (migration through endothelial cell junctions, detailed in section 1.2.3.1) (Phillipson et al., 2006).

1.2.3 Leukocyte transmigration through the endothelial layer

Intravascular crawling is followed by leukocyte adhesion at sites of transendothelial migration. Endothelial cells actively support leukocyte adhesion and transendothelial migration via the formation of pro-adhesive sites termed endothelial adhesive platforms (EAPs) (Barreiro et al., 2008; Ley and Zhang, 2008) and pro-transmigratory structures termed docking structures or transmigratory cups (Barreiro et al., 2002; Carman and Springer, 2004) (Figure 1.5).

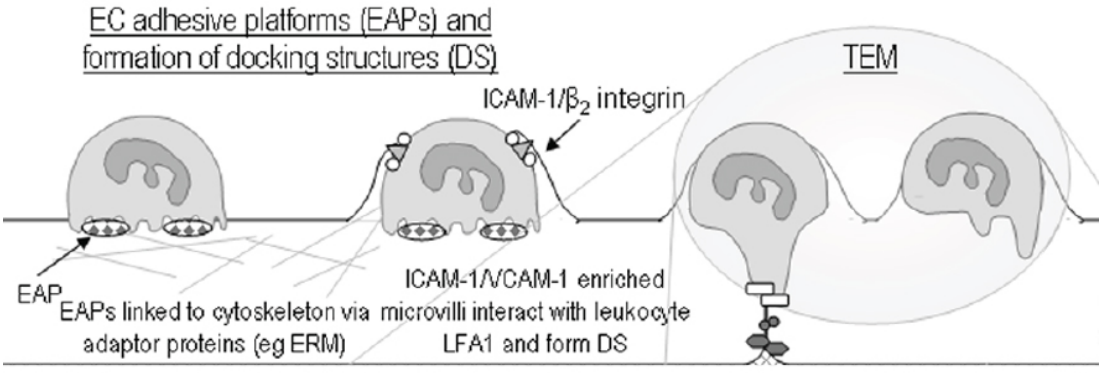

Figure 1.5: Formation of endothelial cell adhesion platforms and docking structures. After firm arrest, leukocytes crawl on the luminal surface to the point of transendothelial migration (TEM). Subsequently, leukocytes adhere to the endothelium via adhesive platforms (EAPs) resulting in the formation of docking structures (DSs). These structures facilitate transendothelial migration, which may occur via the paracellular or the transcellular route. ERM: Ezrin, radixin and moesin. Adapted from Woodfin et al., 2010.

EAPs form independently of leukocyte-endothelial cell interactions and are determined by pre-existing tetraspanin-enriched microdomains (composed of e.g. CD9, CD151 and CD81) on the endothelial cell surface into which ICAM-1 and VCAM-1 are incorporated (Barreiro et al., 2008). Subsequently, the interaction of leukocyte integrins with their endothelial-cell ligands (ICAM-1 and VCAM-1) triggers the formation of docking structures in endothelial cells around leukocytes adhering to EAPs. These docking structures are endothelial protrusions that are rich in ICAM-1 and VCAM-1, the cytoskeletal protein α-actinin and cytoplasmic adaptor molecules such as vinculin, talin-1 and ERM proteins (ezrin, radixin and moesin) (Barreiro et al., 2002; Barreiro et al., 2007). Docking structures partially embrace adherent leukocytes and initiate leukocyte passage through the endothelium which can occur either via the paracellular or the transcellular route.

1.2.3.1 Paracellular route

Leukocyte transmigration through post-capillary venules occurs mainly via the paracellular route, through endothelial junctions (Figure 1.7 a). Endothelial cell junctions contain a number of adhesion molecules many of which interact in a homophilic manner to maintain the integrity of the endothelium and regulate its barrier function to macromolecules (Figure 1.6) (Dejana, 2004).

The following junctional adhesion molecules also actively mediate the migration of leukocytes through endothelial cell junctions: Platelet endothelial cell adhesion molecule 1 (PECAM-1), ICAM-2, CD99, endothelial cell selective adhesion molecule (ESAM), JAM-A, JAM-B and JAM-C (Figure 1.7 a) (Thompson et al., 2001; Muller, 2003; Huang et al., 2006; Bixel et al., 2007; Woodfin et al., 2007). Junctional molecules that are not involved in leukocyte transmigration such as VE-cadherin transiently disappear from the junction (Allport et al., 2000; Shaw et al., 2001). Recently, our group could show that adhesion molecules located within different regions of the endothelial cell junction can act in a sequential manner during leukocyte transmigration (Woodfin et al., 2009). By analysing the site of arrest of neutrophils in IL-1β-stimulated cremasteric post-capillary venules of ICAM-2, JAM-A and PECAM-1 knockout mice we proposed the following sequence: ICAM-2, which is expressed on the luminal side of endothelial junctions and interacts with Mac-1 and LFA-1 on leukocytes (Staunton et al., 1989; Xie et al.,

1995), might be involved in guiding leukocytes to endothelial junctions. JAM-A, which is located within junctions and binds to LFA-1 and possibly JAM-A on leukocytes (Dejana, 2004; Weber et al., 2007), is involved in facilitating leukocyte migration through endothelial junctions. Finally, homophilic PECAM-1 interactions (Muller, 2003) induce signalling pathways within leukocytes leading to the up-regulation of the laminin receptor $\alpha_6\beta_1$ integrin, which seems to be necessary to breach the vascular basement membrane (Dangerfield et al., 2002). These adhesion molecules also exhibit a stimulus-specific role. In contrast to IL-1β, other inflammatory mediators such as TNF-α, fMLP or LTB_4 induce neutrophil transmigration that occurs independently of ICAM-2, JAM-A and PECAM-1 (Huang et al., 2006; Nourshargh et al., 2006; Woodfin et al., 2007).

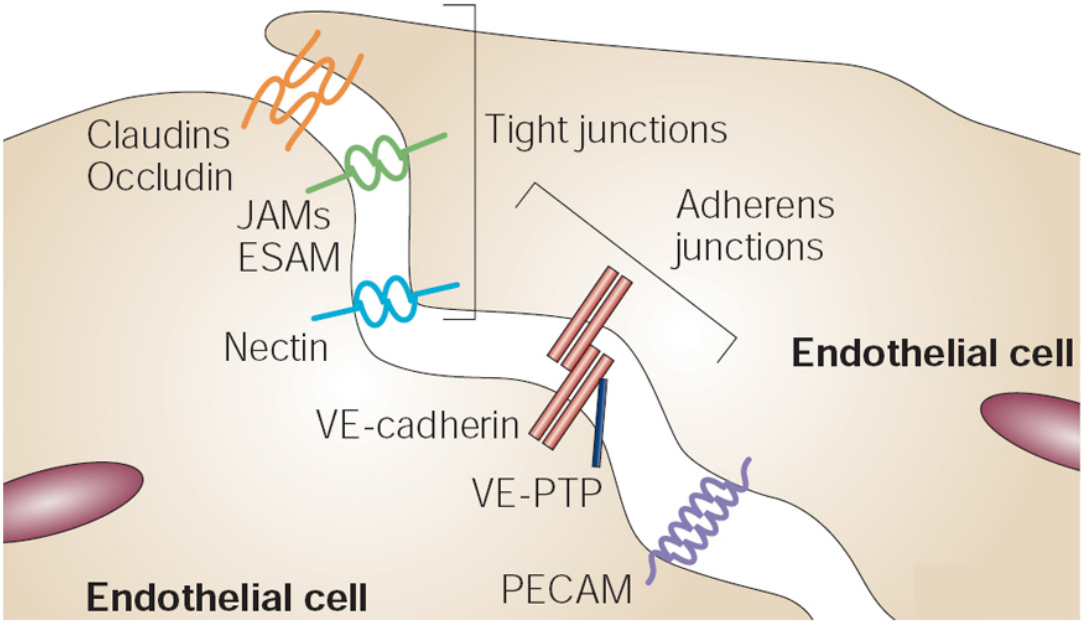

Figure 1.6: Transmembrane adhesion proteins at endothelial cell junctions. At tight junctions, cell-cell connection is mediated by claudins, occludin, members of the junctional adhesion molecule (JAM) family and endothelial cell selective adhesion molecule (ESAM). Junctional integrity at adherens junctions is mostly promoted by vascular endothelial cadherin (VE-cadherin). Nectin participates in the organization of both tight junctions and adherens junctions. Platelet endothelial cell adhesion molecule (PECAM), which does not form a part of tight or adherens junctions, also contributes to endothelial cell-cell adhesion. Adapted from Dejana, 2004.

A second mechanism that keeps the paracellular seal between endothelial cells and transmigrating leukocytes intact is shape change (Huang et al., 1988; Huang et al., 1993). Both leukocytes and endothelial cells undergo shape change to facilitate

leukocyte passage. Leukocytes squeeze through endothelial junctions while endothelial cells contract resulting in the opening of endothelial junctions. Endothelial contraction is mediated by a transient rise in endothelial intracellular calcium, leading to the activation of myosin light chain kinase and ultimately to actin-induced retraction of endothelial cells (Huang et al., 1993; Hixenbaugh et al., 1997; Su et al., 2000; Muller, 2003; Ley et al., 2007).

1.2.3.2 Transcellular route

Leukocytes have also been reported to migrate through the endothelial cell body via the transcellular route (Figure 1.7 b) (Feng et al., 1998; Carman and Springer, 2004). At present, the contributions and mechanisms of this pathway are not fully understood, but recently some mechanistic insights have been gained.

Leukocyte transcellular migration seems to be initiated by the formation of leukocyte protrusions, termed podosomes, which reach into endothelial invaginations to search for permissive sites (Cinamon et al., 2004; Millan et al., 2006; Carman et al., 2007; Carman, 2009). Podosomes are actin-rich adhesion structures that are a characteristic of invasive cells such as cancer cells (Linder and Aepfelbacher, 2003) and bind to endothelial cell ICAM-1 clusters on the endothelium (Millan et al., 2006). Upon podosome binding, ICAM-1 is internalized into caveolae that link together forming vesicular vacuolar organelles (VVOs) (Millan et al., 2006). VVOs form a transcellular pore connected to F-actin stress fibers providing additional membrane and structural support during leukocyte passage and finally facilitating the fusion of the apical and basal membranes of endothelial cells (Carman et al., 2007; Marmon et al., 2009).

The physiological and pathological role of transendothelial migration via the transcellular route is unclear but the response appears to occur when mechanism involved in mediating paracellular transmigration are blocked (Phillipson et al., 2006).

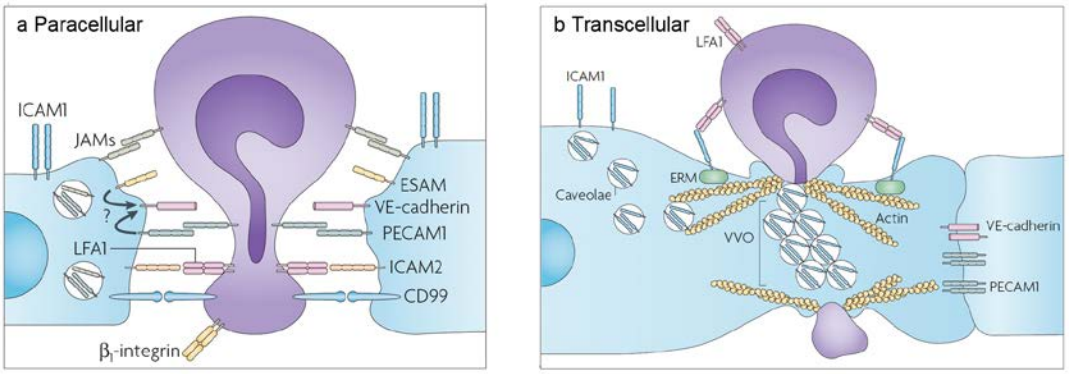

Figure 1.7: Leukocyte transmigration through the endothelial layer. Passage of leukocytes through the endothelium occurs either via the paracellular (a) or the transcellular route (b). (a) Junctional adhesion molecules on endothelial cells such as PECAM-1, ICAM-2, ESAM, CD99 JAM-A, JAM-B and JAM-C are involved in mediating leukocyte transendothelial migration via the paracellular pathway, through endothelial cell junctions. Junctional adhesion molecules not only guide the passage of leukocytes but also induce the expression of β_1 integrins on leukocytes, which might facilitate the subsequent step of leukocyte migration through the underlying basement membrane. (b) Transcellular migration is initiated by ICAM-1 ligation, which results in the internalization of ICAM-1 followed by it's translocation to actin- and caveolae-rich regions. ICAM-1 containing caveolae link together to form vesiculo-vacuolar organelles (VVOs) leading to the formation of an intracellular transmigratory pore supported by F-actin stress fibers. Taken from Ley et al., 2007.

1.3 Pericytes and the venular basement membrane: Additional barriers for transmigrating leukocytes

Despite the improved understanding of the mechanisms involved in leukocyte transmigration through endothelial cell junctions, at present little is known about the mechanisms by which leukocytes penetrate the remaining components of the vessel wall. The endothelial cell layer of collecting venules, post-capillary venules and capillaries is surrounded by pericytes, which are embedded in the vascular basement membrane (Diaz-Flores et al., 1991; Shimada et al., 1992; Hirschi and D'Amore, 1996; Voisin et al., 2010). Hence, the basement membrane and pericytes represent additional barriers for transmigrating leukocytes (Figure 1.8). Due to the complexity of vascular basement membranes and the technical difficulties associated with isolating primary pericytes hardly any *in vitro* models exist that can be used to investigate transmigration of leukocytes through these venular components. Therefore, only few investigations into the mechanisms that mediate and regulate leukocyte transmigration through these barriers exist.

Recent findings have provided more insight into how leukocytes breach the basement membrane (Wang et al., 2006; Rowe and Weiss, 2008; Voisin et al., 2009; Nourshargh et al., 2010; Voisin et al., 2010). The venular basement membrane is a complex network consisting of collagen type IV, laminin 8 and 10, perlecan and nidogen, which are interconnected to form a dense layer of extracellular matrix (Figure 1.9) (Hallmann et al., 2005; Rowe and Weiss, 2008). We could demonstrate that the venular basement membrane is discontinuous exhibiting numerous regions of low matrix protein deposition, which we termed low expression regions or LERs (Wang et al., 2006; Voisin et al., 2010). LERs seem to be preferential sites of leukocyte transmigration as observed in different inflammatory reactions (Sixt et al., 2001; Wang et al., 2006; Voisin et al., 2009; Voisin et al., 2010). This might be due to LERs being easier to breach by leukocytes since the protein density is significantly lower in these regions. LERs might also be more permissive for chemoattractants generated in the inflammed tissue leading to leukocyte attraction.

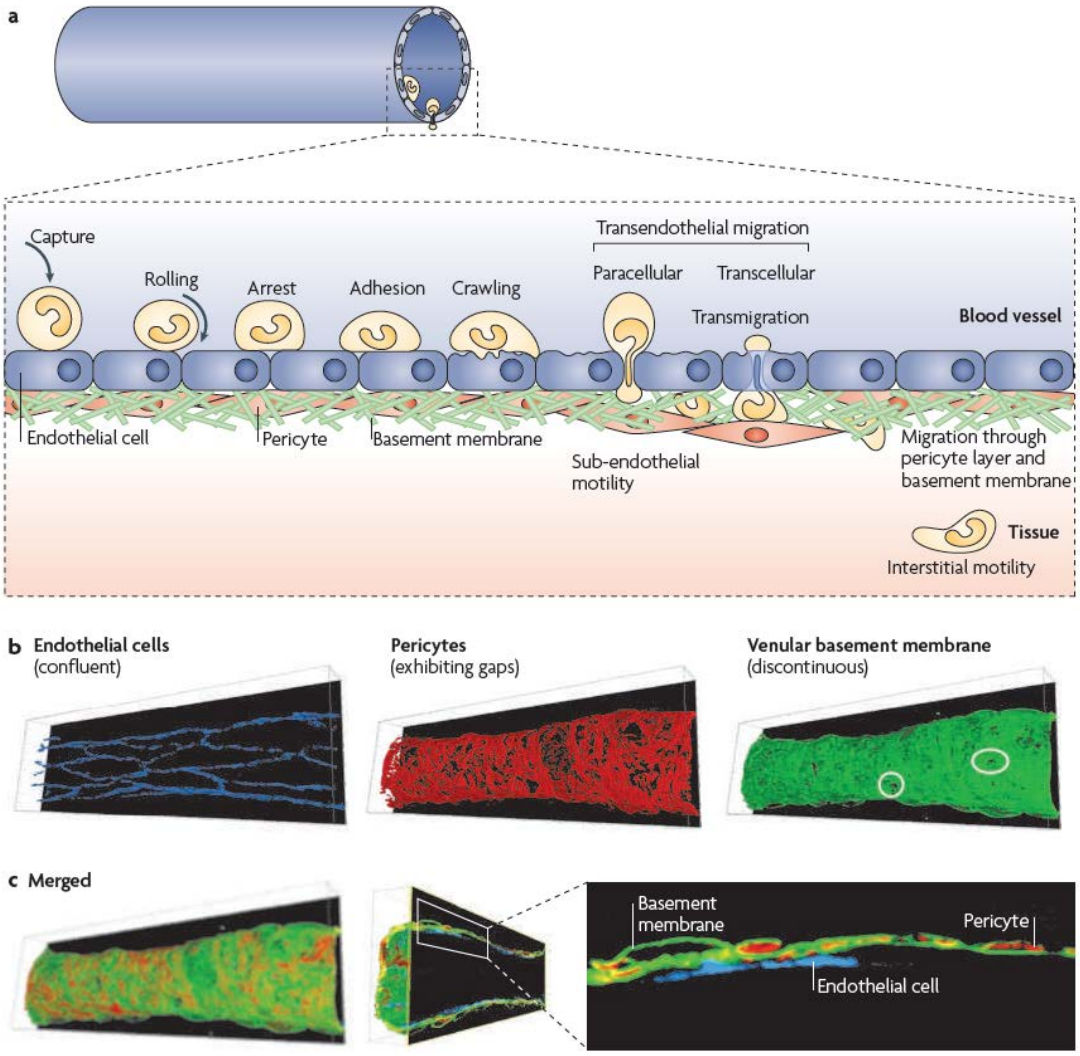

Figure 1.8: Pericytes and the venular basement membrane represent additional barriers for leukocytes after transendothelial migration. (a) The diagram illustrates the leukocyte adhesion cascade including leukocyte migration steps after transendothelial migration. After crossing the endothelium, leukocytes have to penetrate the remaining components of the venular wall, the venular basement membrane and the pericyte sheath and finally reach the site of infection via interstitial motility. (b) Three-dimensional (3D)-reconstructed confocal images depicting the different components of post-capillary venules visualised via triple immunofluorescence staining: Endothelial cells (PECAM-1 labelling, blue), pericytes (stained for α-smooth muscle actin (α-SMA), red) and the venular basement membrane (laminin staining, green). These structures differ greatly in terms of their morphology. Endothelial cells form a confluent monolayer, but the pericyte layer is discontinuous and exhibits gaps between adjacent cells. The expression of vascular basement membrane components is also heterogeneous exhibiting regions of low protein deposition, termed low expression regions or LERs (white circles indicate examples). (c) The cross-section of the triple stained post-capillary venule shown in (b) illustrates the relative localization of the vessel wall components. Endothelial cells line the lumen and are surrounded on their abluminal side by pericytes, which are embedded in the basement membrane. Taken from Nourshargh et al., 2010.

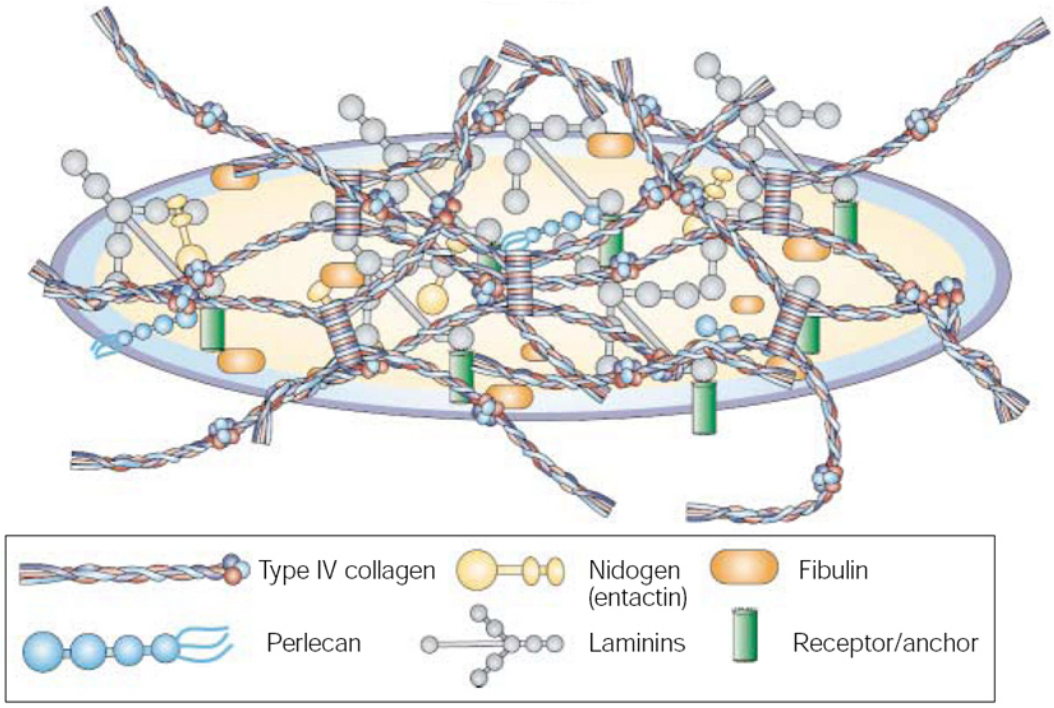

Figure 1.9: Components and structure of basement membranes. Basement membrane components are secreted as functional units: Type IV collagen protomers, laminin trimers, nidogen (also termed entactin) and perlecan. Laminins are anchored to the cell by receptor proteins such as integrins and then associate with the type IV collagen network that has formed extracellularly. Nidogen and perlecan crosslink laminins with the type IV collagen network. Taken from Kalluri, 2003.

The mechanisms involved in leukocyte migration through LERs differ among leukocyte subtypes. Monocytes have been observed to squeeze through LERs, however, the underlying mechanism remains unknown (Voisin et al., 2009). In contrary to that, neutrophils seem to be unable to squeeze through LERs and have been shown to remodel and enlarge these regions in a neutrophil elastase-dependent manner (Wang et al., 2006; Voisin et al., 2009; Voisin et al., 2010). Transendothelial migration of neutrophils triggers the release of proteases such as neutrophil elastase that are stored in granules (Cepinskas et al., 1999; Wang et al., 2005). In addition to protease release, leukocyte-endothelial cell interactions during transmigration also induce changes in the expression of β_1-integrins (receptors for main basement membrane components) on leukocytes aiding the passage of the vascular basement membrane (Dangerfield et al., 2002).

At present, very little is known about the role of pericytes in leukocyte transmigration. One *in vivo* study exists that has reported transcellular migration of leukocytes through pericytes in response to fMLP (Feng et al., 1998) and our group could demonstrate by using various other inflammatory conditions *in vivo* that leukocytes preferentially use the paracellular route to cross the pericyte layer (Wang et al., 2006), but the associated mechanisms remain to be elucidated.

1.4 Pericytes

1.4.1 Definition and Identification

Pericytes, also known as adventitial cells, perivascular cells, Rouget cells, mural cells, periendothelial cells and pericapillary cells, surround the endothelial cell layer of capillaries, post-capillary venules and collecting venules (Diaz-Flores et al., 1991; Shimada et al., 1992; Hirschi and D'Amore, 1996) (Figure 1.10). They are embedded in the vascular basement membrane and can contribute to the generation of basement membrane components (Cohen et al., 1980; Mandarino et al., 1993).

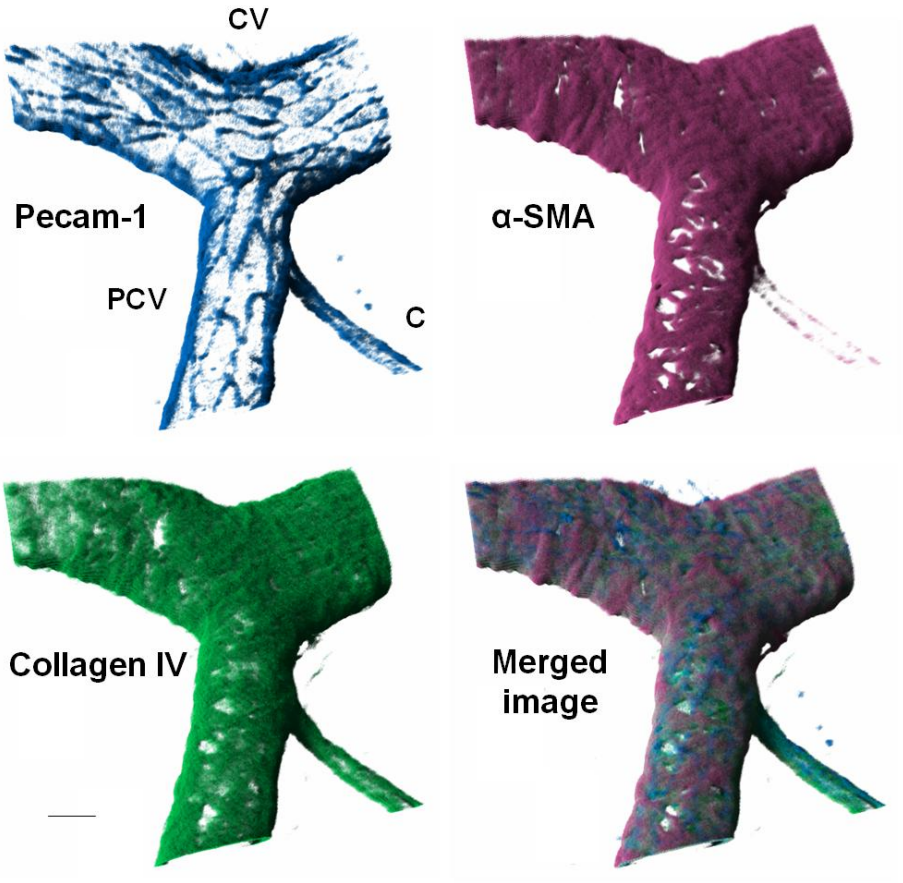

Figure 1.10: Vessel wall components of cremasteric collecting and post-capillary venules and capillaries. A representative 3D-reconstructed longitudinal confocal image section illustrating venular wall components such as endothelium, pericytes and basement membrane is shown. Cremaster muscles were isolated from unstimulated WT C57BL/6 mice and immunostained for PECAM-1 (blue, to visualize endothelial cell junctions), α-SMA (pink, to visualise pericytes) and collagen IV (green, to visualise this component of the vascular basement membrane). C, capillary; CV, collecting venule; PCV, post-capillary venule. Bar, 20 μm. The confocal image was kindly provided by Dr. Mathieu-Benoit Voisin.

Pericyes are derived from undifferentiated mesenchymal cells, but have also been shown to be of mesodermal (Hungerford and Little, 1999), neural crest (Etchevers et al., 2001) or bone marrow origin (Rajantie et al., 2004). They are able to differentiate into other cell types (Schor et al., 1995) such as fibroblasts (Sundberg et al., 1996), chondroblasts (Farrington-Rock et al., 2004), osteoblasts (Brighton et al., 1992; Diaz-Flores et al., 1992; Canfield et al., 1996; Doherty et al., 1998) and adipocytes (Farrington-Rock et al., 2004).

Several markers for pericytes have been reported to date, including intracellular markers such as smooth muscle α-actin (α-SMA), desmin, and the regulator of G-protein signalling 5 (RGS5) and extracellular markers like neuron-glia antigen 2 (NG2), platelet-growth factor receptor β (PDGFR-β), endosialin (CD 248), and the unknown antigen of the antibody 3G5 (Gerhardt and Betsholtz, 2003). However, unfortunately none of these markers is absolutely specific for pericytes or recognizes all pericytes. Their expression varies depending on vessel type (capillaries or venules), vascular bed and species (Nehls and Drenckhahn, 1991; Chan-Ling et al., 2004; Hughes and Chan-Ling, 2004; Murfee et al., 2005). For example, pericytes of post-capillary and collecting venules and smooth muscle cells on pre-capillary arteriols and arteries express α-SMA, but pericytes of midcapillary pericytes show hardly any α-SMA expression (Nehls and Drenckhahn, 1991). Additionally, marker expression was also shown to change during pathological conditions such as cancer (Morikawa et al., 2002). This has led to misinterpreted findings in previous studies, where pericyte loss on angiogenic sprouts and tumour vessels was described due to the use of markers, which have later been shown not to be expressed under pathological conditions (Morikawa et al., 2002; Baluk et al., 2005). More recently, pericytes were reported to be abundant on tumour vessels (Morikawa et al., 2002; Baluk et al., 2005).

1.4.2 Distribution, Morphology and Structure

Pericytes are the second cellular component of capillaries, post-capillary venules and collecting venules (Diaz-Flores et al., 1991; Shimada et al., 1992; Hirschi and D'Amore, 1996) (Figure 1.10). They form a discontinuous network with gaps between adjacent cells (Shimada et al., 1992; Wang et al., 2006) (Figure 1.11) and show close association to the underlying endothelium. Morphological differences

exist depending on vessel type (capillaries or venules), vascular bed, developmental stage, species and pathological conditions (Diaz-Flores et al., 1991; Morikawa et al., 2002). Furthermore, pericyte coverage of the abluminal vessel area varies in different organs, developmental stages and species (Shepro and Morel, 1993; Egginton et al., 1996). The ratio of pericytes to endothelial cells varies in different vascular beds ranging from 1:1 to 1:100. The retina exhibits one of the highest ratios of 1:3, but the highest pericyte abundance (1:1) is found in the CNS (Shepro and Morel, 1993). Pericytes can be distinguished from VSMC, which are wrapped tighly aroung arteriols, arteries and veins (Figure 1.11) by their location, their morphology and their marker expression. However, an absolute distinction between pericytes and VSMC is not always possible. There is a continuum of cells from true pericytes surrounding post-capillary venules and capillaries to intermediate cells resembling both pericytes and smooth muscle cells at the interface between arteriolar capillaries and arterioles, to true smooth muscle cells surrounding arterioles, arteries and veins (Shimada et al., 1992).

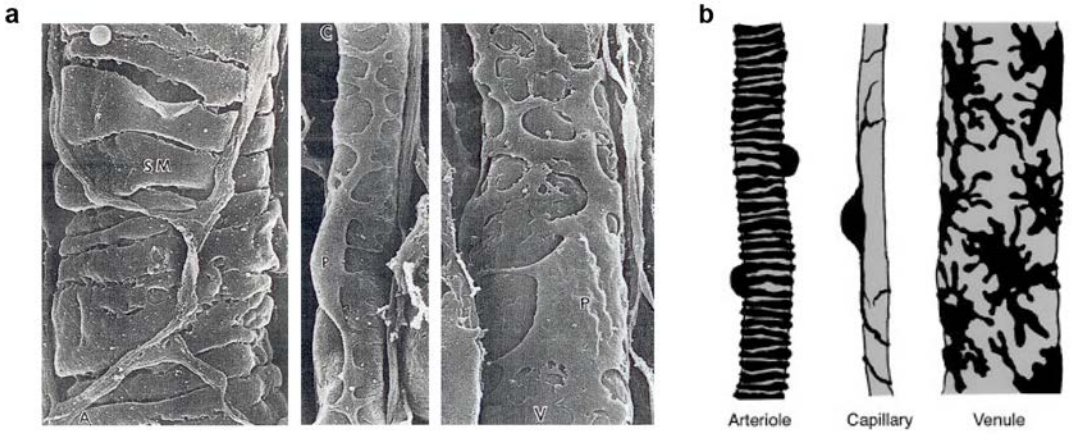

Figure 1.11: Morphology of smooth muscle cells on arterioles and pericytes on capillaries and venules. (a) Scanning electron microscopy images depicting smooth muscle cells (SM) surrounding an arteriole (A) as well as pericytes (P) on a capillary (C) and a venule (V). Taken from Shimada et al., 1992. (b) Schematic drawings illustrating morphological differences between smooth muscle cells and pericytes as well as among pericytes depending on the vessel type. Taken from Morikawa et al., 2002. (a and b) Smooth muscle cells on arterioles are uniformly shaped, circumferentially arranged, closely packed, and tightly associated with the endothelium. Pericytes on capillaries have two thin major processes that are oriented longitudinally along the vessel from which mutiple minor process extend surrounding the capillary. Capillary pericytes cover only a small proportion of the endothelial surface. Pericytes on venules exhibit an irregular shape and extend numerous major processes covering a great part of the endothelial surface.

Pericytes have a large kidney-shaped nucleus and their cytoplasm contains multivesicular bodies, osmiophilic bodies and lysosomes (Diaz-Flores et al., 1991). They also exhibit structures important for contraction. It has been shown by electron microscopy that pericytes contain a pronounced network of filaments (Forbes et al., 1977), including actin microfilaments of both smooth muscle and nonmuscle isoforms (Herman and D'Amore, 1985; Skalli et al., 1989). Pericytes also posses significant amounts of other regulator proteins of contractile responses such as GMP-dependent protein kinase (Joyce et al., 1984), and tropomyosin (Joyce et al., 1985b, a).

1.4.3 Functions

Pericytes play a critical role in maintaining the integrity of the vessel wall and in generating the vascular BM, in which they are embedded (Cohen et al., 1980; Mandarino et al., 1993). The close interaction of pericytes with endothelial cells provides mechanical support (Lindahl et al., 1997) and mediates endothelial metabolism, growth and motility. Pericytes interact with endothelial cells via soluble factors as well as cell-cell contacts (Armulik et al., 2005) such as tight junctions, gap junctions (Cuevas et al., 1984; Larson et al., 1987; Fujimoto, 1995; Little et al., 1995), adhesion plaques (Forbes et al., 1977), and peg and socket connections (Diaz-Flores et al., 1991). These are mediated via adhesion molecules such as CAMs, N-cadherin (Gilbertson-Beadling and Fisher, 1993; Gerhardt et al., 2000), VCAM-1 (Verbeek et al., 1995), substrate adherence molecules (SAMs) and integrins (Silva et al., 2008). Furthermore, mechanical linkage between pericytes and endothelial cells occurs via endothelial fibronectin-rich cytoplasmic fibrils, which are inserted into the plasma membrane of pericytes (Courtoy and Boyles, 1983). Pericyte processes in contrary do not frequently come into contact (Diaz-Flores et al., 1991) and intercellular junctions between pericytes have not been reported.

On newly formed vessel sprouts pericytes are recruited via soluble growth factors such as basic fibroblast growth factor (bFGF), heparin-binding epidermal growth factor (HB-EGF) and platelet-derived growth factor (PDGF) (Hirschi and D'Amore, 1996). After recruitment, pericytes suppress endothelial proliferation via a contact-dependent activation of TGF-β (Orlidge and D'Amore, 1986, 1987). Endothelial movement *in vitro* has also been shown to be blocked by the activation of latent

TGF-β (Sato and Rifkin, 1989). Pericyte proliferation on the other hand is regulated by bFGF, HB-EGF, PDGF (D'Amore and Smith, 1993) and endothelin, which have been shown to be mitogenic for pericytes *in vitro*. Endotoxins and platelet-activating factor (PAF) show also direct mitogenic activity on pericytes (Khoury and Langleben, 1996, 1998). Inhibition of pericyte growth and proliferation is mediated by TGF-β (D'Amore and Smith, 1993), heparin (Newcomb and Herman, 1993) and vascular endothelial growth factor (VEGF) (Greenberg et al., 2008).

Apart from providing mechanical support and stability for the vessel wall and regulating endothelial proliferation, pericytes have the ability to contract and thereby regulate vascular flow and permeability. Pericytes posses a contractile apparatus and structural components for contractile mechanisms by expressing numerous proteins, which are typical for contractile cells (Joyce et al., 1984; Joyce et al., 1985a, b; Skalli et al., 1989). Additionally, they posses high affinity binding sites for endothelin, which is a potent vasoconstrictive agent. Hence, pericytes are able to contribute to the regulation of capillary and venular blood flow and permeability (Peppiatt et al., 2006). Pericytes are also considered to posses potential phagocytotic activity (Brachvogel et al., 2007) and have been shown to exhibit numerous vesicles and lysosomes (Diaz-Flores et al., 1991). Therefore, pericytes might contribute to the clearance of pathogens via phagocytosis of pathogens or release of toxic components from their vesicles.

1.4.4 Related diseases

Many of the crucial functions of pericytes are highlighted by their implication in diseases such as diabetic retinopathy, multiple sclerosis, tumour angiogenesis, hypertension, central nervous system dementia and calcification of vascular tissues (Wallow et al., 1993; Verbeek et al., 1999; Yamagishi et al., 1999; Collett and Canfield, 2005). Apoptosis and loss of retinal capillary pericytes and disruption of pericyte-endothelial contacts are characteristic features of diabetic retinopathy and can also occur in other capillary beds in humans with diabetes (Sima et al., 1985). The absence of pericytes results in a loss of capillary tone, leading to dilatation, formation of micro-aneurysms and retinal neovascularisation. Pericytes on tumour vessels have multiple abnormalities such as variation in marker expression and changes in morphology. Here, pericytes are noted to detach from vessels and the

processes extend away from the endothelium into the surrounding tissue, resulting in a loss of endothelial growth control, which supports tumour angiogenesis (Morikawa et al., 2002). In Acute Respiratory Distress Syndrome (ARDS), increased permeability (pulmonary oedema) can be diagnosed in early stages of the disease (Matthay and Zimmerman, 2005). After direct lung injury pro-inflammatory cytokines are released resulting in pulmonary microvasculature injury and an increase in permeability (Matthay and Zimmerman, 2005). This might be mediated by pericytes, because these cells have been shown to be crucial in the development of microvascular permeability and capillary leak (Leveen et al., 1994; Hellstrom et al., 2001). Interestingly, pericytes have also been implicated in the regulation of leukocyte extravasation. During multiple sclerosis T-Lymphocyte adhesion and migration into the human brain is mediated via the interaction of very late antigen-4 (VLA-4) on T-lymphocytes and VCAM-1, which is expressed on endothelial cells and pericytes (Verbeek et al., 1995). Therefore, pericytes may also play a role in T-cell infiltration into the brain via direct adhesive interactions with extravasating T-cells.

1.5 Aim of this study

At present very little is known about the potential role of pericytes in leukocyte transmigration. Therefore, this project aimed to investigate the involvement of pericytes in regulating leukocyte transmigration *in vivo* by addressing the following key questions:

Does pericyte phenotype/morphology differ in different vessel types and vascular beds in the mouse?

To date no study has described and compared morphological characteristics of pericytes in different vascular beds in the mouse. Therefore, pericytes were characterized in different types of blood vessels in the cremaster muscle as well as in post-capillary venules in selected vascular beds in the mouse.

Does pericyte morphology change under inflammatory conditions?

To elucidate potential pericyte responsiveness during inflammatory conditions *in vivo*, changes in pericyte morphology upon stimulation with various inflammatory mediators were investigated in the murine cremaster muscle. Subsequently, the effects of TNF-α and IL-1β were further characterised over time and the involvement of neutrophils was examined using neutrophil depleted animals. Furthermore, the effects of TNF-α and IL-1β were investigated in an additional vascular bed - the skin of the ear - to explore the possibility of tissue-specific mechanisms.

Is the potential pericyte responsiveness a direct effect of inflammatory stimuli on pericytes?

To complement the *in vivo* findings and to investigate pericytes and their properties isolated from other cell types, murine pericyte-like C3H/10T1/2 cells and their responses to TNF-α and IL-1β stimulation were characterized *in vitro*. To determine whether pericytes are able to respond directly to TNF-α- and IL-1β, expression of the receptors for these cytokines was examined on C3H/10T1/2 cells *in vitro* as well as on cremasteric post-capillary venular pericytes *in vivo*.

Does pericyte morphology change under inflammatory conditions in a manner that would facilitate neutrophil transmigration?

By using pericyte reporter mice (α-SMA-GFP and α-SMA-RFPcherry mice) and 4D confocal Intravital Microscopy TNF-α-induced pericyte shape change and its involvement in leukocyte transmigration could be observed and analysed *in vivo*.

Chapter 2: Materials and Methods

2.1 Animals

All animal studies were performed according to the directions of the United Kingdom Home Office Animals (Scientific Procedures) Act (1986).

2.1.1 Strains

C57BL/6 mice Male wild type (WT) C57BL/6 mice were routinely used between the ages of 6-12 weeks (~ 25 g) and were purchased from Harlan-Olac (Bicester, UK).

α-SMA-GFP mice C57BL/6 mice which express Green Fluorescent Protein (GFP) under the control of the α-smooth muscle actin (α-SMA) promoter (Yokota et al., 2006) were obtained as a gift from Prof. Clare Isacke (Breakthrough Breast Cancer Research Centre, The Institute of Cancer Research, London, UK) with the authorisation of Prof. Sanai Sato (Department of Medicine, University of Oklahoma Health Science Center, Oklahoma City, USA).

α-SMA-RFPcherry mice C57BL/6 mice which express the cherry variant of Red Fluorescent Protein (RFPcherry) under the control of the α-SMA promoter were obtained as a gift from Dr. David Rowe (Department of Genetics and Developmental Biology, University of Connecticut Health Center, Farmington, USA).

Lys-EGFP mice This mouse strain was generated as described by Faust et al. in 2000 and contains the mutated murine lysozyme M (*lys*) locus into which coding sequence for eGFP has been inserted (Faust et al., 2000). Lys-EGFP mice exhibit EGFP labelled myelomonocytic cells and especially high fluorescence intensity is observed in mature neutrophil granulocytes. Homozygous *lys* knockout mice show normal development and are fertile. We noticed no differences in leukocyte

transmigration using the homozygous or heterozygous mice. This strain was generated in a C57BL/6 background and was obtained as a gift from Prof. Markus Sperandio (Walter Brendel Center of Experimental Medicine, Ludwig-Maximillians-Universität, Munich, Germany).

Tumour necrosis factor receptor (TNFR) double knockout mice

These mice are double mutant mice lacking both genes *Tnfrsf1a* (p55) and *Tnfrsf1b* (p75). They were generated by intercrossing the singly deficient mice whereupon the *Tnfrsf1b* mutation was transferred into the *Tnfrsf1a* background (C57BL/6). The mice are viable and fertile and animals were purchased from The Jackson Laboratory (stock number: 003243).

2.1.2 Genotyping and Phenotyping

2.1.2.1 Phenotyping of the α-SMA-GFP mice

α-SMA-GFP mice were phenotyped by fluorescence microscopy. For this purpose, ear notch samples were taken and the skin was separated carefully from the cartilage using forceps. The skin was then whole mounted for fluorescence microscopy to look for the presence of GFP positive vascular smooth muscle cells and pericytes (Figure 2.1 a).

2.1.2.2 Phenotyping of the α-SMA-RFPcherry mice

α-SMA-RFPcherry mice were phenotyped by fluorescence microscopy as described above for the α-SMA-GFP mice looking for the presence of RFP positive vascular smooth muscle cells and pericytes (Figure 2.1 b).

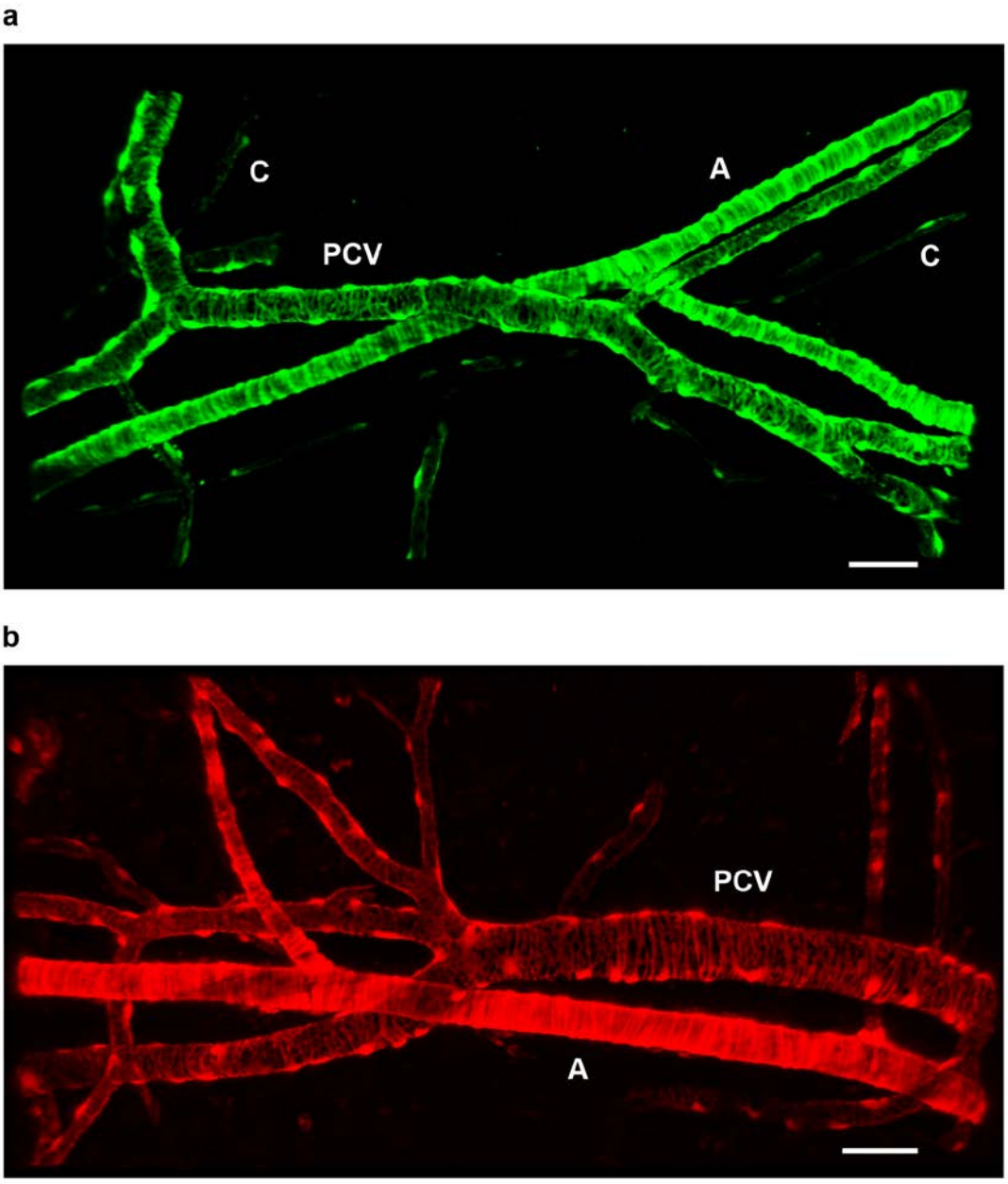

Figure 2.1: Phenotyping of α-SMA-GFP mice (a) and α-SMA-RFPcherry mice (b). 3D-reconstructed confocal images of skin from ear notch samples. A, arteriole; C, capillary; PCV, post-capillary venule. Bars, 20 μm.

2.1.2.3 Phenotyping of the Lys-EGFP mice

The phenotype of Lys-EGFP mice was established by flow cytometry analysis of blood leukocytes (performed by Dr. Abigail Woodfin). Homozygous samples could be distinguished from heterozygous samples by fluorescence intensity.

2.1.2.4 Genotyping of the TNFR double knockout mice

TNFR double knockout mice were genotyped by polymerase chain reaction (PCR). For this purpose, ear notch samples were taken and digested in 200 µl lysis buffer containing 100 µg/ml proteinase K for 3 h at 55 °C. Afterwards, tubes were shaken gently and cooled to room temperature (RT) prior to DNA purification using isopropanol/ethanol precipitation. The samples were spun down for 10 min at 20,000 g/RT and the resulting supernatant was transferred into new tubes containing 250 µl isopropanol and mixed well resulting in the formation of precipitates. The mix was centrifuged for 5 min at 20,000 g/RT and the resulting supernatant was discarded. The pellet was washed with 150 µl 70 % (v/v) Ethanol followed by centrifugation for 5 min at 20,000 g/RT. After removal of ethanol, the pellet was air dried for approximately 10 min. The DNA was resuspended in 50 µl molecular biology grade water and stored at 4 °C for short-term storage or at 20 °C for longer storage. 2 µl purified DNA were used for PCR. TNFRI and TNFRII gene knockouts were assessed in separate reactions.

Detection of TNFRI (tnfrsf1a) knockout

TNFRI knockout was detected using a slighty modified version of the Jackson Laboratory protocol resulting in separate PCRs for amplification of the WT allele and the knockout allele. Two primer pairs were used to either amplify the WT or the knockout allele (Table 2.1). PCR master mixes were prepared (Table 1.1 and Table 2.3) and mixed with 2 µl purified DNA. Subsequently, DNA fragments were amplified in a PCR block (DNAEngine® Peltier Thermal Cycler, Bio-Rad, Hemel Hempstead, UK) using either the TNFR1AWT program (Table 2.4) or the TNFR1AKO program (Table 2.5) to amplify the WT or the knockout allele respectively.

Primer	Primer sequence	Melting temperature	Primer type
oIMRo834	5'-GGA TTG TCA CGG TGC CGT TGA AG-3'	64.2 °C	WT
oIMRo835	5'-TGA CAA GGA CAC GGT GTG TGG C-3'	64.0 °C	WT
oIMRo836	5'-TGC TGA TGG GGA TAC ATC CAT C-3'	60.3 °C	Mutant
oIMRo837	5'-CCG GTG GAT GTG GAA TGT GTG-3'	61.8 °C	Mutant

Table 2.1: Primers used to amplify either the TNFRI WT or mutant (knockout) allele.

Reagent	Stock concentration	Volume per sample	Final concentration
Primer 1: oIMRo834	100 µM	0.12 µl	0.5 µM
Primer 2: oIMRo835	100 µM	0.12 µl	0.5 µM
dNTPs	10 mM	0.5 µl	0.2 mM
$MgCl_2$	50 mM	1 µl	2 mM
NH_4^+ buffer	10 x	2.50 µl	1 x
TAQ polymerase	5 U/µl	0.15 µl	0.03 U/µl
dH_2O (molecular biology grade)		18.61 µl	
Total		23 µl	

Table 2.2: PCR master mix to amplify the TNFRI WT allele.

Reagent	Stock concentration	Volume per sample	Final concentration
Primer 3: oIMRo836	100 µM	0.12 µl	0.5 µM
Primer 4: oIMRo837	100 µM	0.12 µl	0.5 µM
dNTPs	10 mM	0.5 µl	0.2 mM
$MgCl_2$	50 mM	1 µl	2 mM
NH_4^+ buffer	10 x	2.50 µl	1 x
TAQ polymerase	5 U/µl	0.15 µl	0.03 U/µl
dH_2O (molecular biology grade)		18.61 µl	
Total		23 µl	

Table 2.3: PCR master mix to amplify the TNFRI knockout allele.

Initial denaturation	94 °C for 3 min	x 1
Denaturation	94 °C for 30 sec	35 cycles
Annealing	68 °C for 1 min	
Elongation	72 °C for 1 min	
Final elongation	72 °C for 2 min	x 1

Table 2.4: PCR program TNFR1AWT.

Initial denaturation	94 °C for 3 min	x 1
Denaturation	94 °C for 30 sec	35 cycles
Annealing	64 °C for 1 min	
Elongation	72 °C for 1 min	
Final elongation	72 °C for 2 min	x 1

Table 2.5: PCR program TNFR1AKO.

After amplification, 2 µl of blue agarose gel electrophoresis loading buffer was added to the samples and 10 µl were run on a 3 % (w/v) agarose gel (in TAE buffer) supplemented with 2 µl GelRed. A 100 – 1,000 bp DNA ladder was used as a marker. Gels were left running in an electrophoresis chamber (Mupid®-One electrophoresis system, Eurogentec, Southampton, UK) for approximately 45 min at 90 V. Subsequently, gel pictures were taken under ultraviolet light on a UV White Darkroom BioImaging system (UVP, Cambridge, UK). 120 bp PCR products represented WT alleles whereas 155 bp PCR products corresponded to knockout alleles.

Detection of TNFRII (tnfrsf1b) knockout

Knockout of TNFRII was detected according to the Jackson Laboratory protocol. Three primers were used to amplify both the WT and the knockout allele (Table 2.6). A PCR master mix was prepared (Table 2.7) and mixed with 2 µl purified DNA. Subsequently, DNA was amplified in a PCR block (DNAEngine® Peltier Thermal Cycler, Bio-Rad, Hemel Hempstead, UK) using the TNFR1BKO programm (Table 2.8).

Primer	Primer sequence	Melting temperature	Primer type
oIMRo837	5'-CCG GTG GAT GTG GAA TGT GTG-3'	61.8 °C	Mutant
oIMRo838	5'-AGA GCT CCA GGC ACA AGG GC-3'	63.5 °C	Common
oIMRo839	5'-AAC GGG CCA GAC CTC GGG T-3'	63.1 °C	WT

Table 2.6: Primers used to amplify both the TNFRII WT and mutant (knockout) allele.

Reagent	Stock concentration	Volume per sample	Final concentration
Primer 1: oIMRo837	100 µM	0.13 µl	0.5 µM
Primer 2: oIMRo838	100 µM	0.26 µl	1 µM
Primer 3: oIMRo839	100 µM	0.13 µl	0.5 µM
dNTPs	10 mM	0.5 µl	0.2 mM
$MgCl_2$	50 mM	1 µl	2 mM
NH_4^+ buffer	10 x	2.50 µl	1 x
TAQ polymerase	5 U/µl	0.15 µl	0.03 U/µl
dH_2O (molecular biology grade)		18.33 µl	
Total		23 µl	

Table 2.7: PCR master mix to amplify both the TNFRII WT and knockout allele.

Initial denaturation	94 °C for 3 min	x 1
Denaturation	94 °C for 30 sec	35 cycles
Annealing	69 °C for 1 min	
Elongation	72 °C for 1 min	
Final elongation	72 °C for 2 min	x 1

Table 2.8: PCR program TNFR1BKO.

After amplification, samples were run on a 1 % (w/v) agarose gel as described above. 257 bp PCR products represented WT alleles whereas 160 bp PCR products corresponded to knockout alleles.

2.2 Cell lines

C3H/10T1/2 (clone 8) This adherent cell line was purchased from ATCC (Manassas, USA). These murine fibroblasts show pericyte-like properties and were isolated from a line

of C3H mouse embryo as described in Reznikoff et al. in 1973 (Reznikoff et al., 1973).

2.3 Bacterial strains

Top10F' Aliquots of this bacterial strain were received as a gift from Dr. Fulvio D'Acquisto (purchased from Invitrogen, Cat. No. 44-0301, Paisley, UK).

2.4 Plasmids

Lifeact-eGFP The Lifeact-eGFP plasmid encodes for a 17amino-acid probe against F-actin fused at the C-Terminus to eGFP. Therefore, the probe can be used to directly image changes in the actin cytoskeleton in real time (Riedl et al., 2008). Lifeact-eGFP has been reported not to interfere with actin dynamics *in vitro* and *in vivo* and was received as a gift from Dr. Michael Sixt (Max Planck Institute of Biochemistry, Martinsried, Germany).

2.5 Reagents

2.5.1 Anaesthetics

Ketamin Ketaset® Injection, c = 100 mg/ml, Cat. No. SH4401C, Fort Dodge Animal Health Ltd, Southampton, UK;

Xylazine Rompun® 2 %, c = 20 mg/ml, Cat. No. 79767161 Bayer plc., Newbury, UK;

2.5.2 Antibodies

Primary antibodies

α-SMA Purified monoclonal mouse anti-mouse α-SMA-Cy3, clone 1A4, c = 1.3 mg/ml, Sigma-Aldrich, Poole, Dorset, UK;

Collagen IV Purified polyclonal rabbit anti-mouse collagen IV, c = 1 mg/ml, abcam, Cambridge, UK;

GR1 Purified monoclonal rat anti-mouse Ly-6G and Ly-6C (GR1), clone RB6-8C5, c = 1 mg/ml, no azide/low endotoxin (NA/LE) formulation, BD Pharmingen, Oxford, UK;

Interleukin-1 receptor I (IL-1RI)

Armenian hamster anti-mouse IL-1RI, clone JAMA-147, c = 0.5 mg/ml, BioLegend (via Cambridge Bioscience, Cambridge, UK); Used for flow cytometry of cultered cells;

Goat anti-mouse IL-1RI, c = 0.2 mg/ml, R&D Systems, Abingdon, UK; Used for labelling of whole mounted tissues for confocal microscopy;

MRP-14 Rat anti-mouse MRP-14, clone 2B10, c = 1.4 mg/ml, received as a gift from Dr. Nancy Hogg (Leukocyte Adhesion Laboratory, Cancer Research UK, London Research Institute, Lincoln's Inn Fields Laboratories, London, UK), MRP14 is an intracellular marker for neutrophils (Hobbs et al., 2003);

NG2 Purified polyclonal rabbit anti-rat NG2 chondroitin sulfate proteoglycan (cross reacts with mouse), c = 1 mg/ml, Millipore, Watford, UK;

PECAM-1-647 Functional grade purified rat anti-mouse CD31 (PECAM-1), clone 390, c = 1 mg/ml, eBioscience, Hatfield, UK. This antibody was then directly conjugated to Alexa-647 using the APEX™ Alexa Fluor® 647 Antibody Labeling Kit (Cat. No. A10475, Invitrogen, Paisley, UK) according to the manufacturer's protocol.

TNFRI Armenian hamster anti-mouse TNFRI, clone 55R-286, c = 0.5 mg/ml, BioLegend (via Cambridge Bioscience,

Cambridge, UK); Used for flow cytometry of cultered cells;

Goat anti-mouse TNFRI, c = 0.2 mg/ml, R&D Systems, Abingdon, UK; Used for labelling of whole mounted tissues for confocal microscopy;

TNFRII Armenian hamster anti-mouse TNFRII, clone TR75-89, c = 0.5 mg/ml, BioLegend (via Cambridge Bioscience, Cambridge, UK); Used for flow cytometry of cultered cells;

Goat anti-mouse TNFRII, c = 0.2 mg/ml, R&D Systems, Abingdon, UK; Used for labelling of whole mounted tissues for confocal microscopy;

Isotype controls

for GR1 Rat IgG2b κ, c = 1mg/ml, Cat. No. MCA1125XZ, AbDSerotec, Oxford, UK;

for NG2 IgGs from rabbit serum, c = 5 mg/ml, Sigma-Aldrich, Poole, Dorset, UK;

for armenian hamster anti IL-1RI, TNFRI and TNFRII

armenian hamster IgG_1, clone G235-2356, c = 1 mg/ml, BD Pharmingen, Oxford, UK;

for goat anti IL-1RI, TNFRI and TNFRII

Normal goat IgGs, c = 1 mg/ml, R&D Systems, Abingdon, UK

Secondary antibodies and streptavidin conjugates

anti-armenian hamster-biotin

Purified biotin conjugated goat anti-armenian hamster IgGs antibody, c = 1 mg/ml, Invitrogen, Paisley, UK;

streptavidin-488 Alexa Fluor conjugated streptavidin, c = 2 mg/ml, Invitrogen, Paisley, UK;

anti-goat-488 Purified Alexa Fluor conjugated rabbit anti-goat IgGs antibody, c = 2 mg/ml, Invitrogen, Paisley, UK;

anti-rabbit-488 or -633 Purified Alexa Fluor conjugated goat anti-rabbit IgGs antibody, c = 2 mg/ml, Invitrogen, Paisley, UK;

anti-rat-488 or -633 Purified Alexa Fluor conjugated goat anti-rat IgGs antibody, c = 2 mg/ml, Invitrogen, Paisley, UK;

2.5.3 Cell culture reagents

Dulbecco's Modified Eagles Medium (DMEM)
high glucose, Cat. No. 11960-044, Gibco, Paisley, UK;

Ethylenediaminetetraacetic acid (EDTA)
Cat. No. E5134, Sigma-Aldrich, Poole, Dorset, UK;

Fetal bovine serum (FBS) Cat. No. 10270-106, Gibco, Paisley, UK;

Leibovitz Leibovitz's, Cat. No. 21083027, Gibco, Paisley, UK;

L-Glutamine c = 200 mM (100 x), Cat. No. 25030, Gibco, Paisley, UK;

Phosphate buffered saline (PBS)
1 × PBS, pH 7.2, Cat. No. 20012-019, Gibco, Paisley, UK;

Penicillin/Streptomycin 10 000 u/ml Penicillin and 10 000 μg/ml Streptomycin, Cat. No. 15140, Gibco, Paisley, UK;

Trypan blue Cat. No. 15250-061, Gibco, Paisley, UK;

Trypsin/EDTA 1 × solution (0.025 % Trypsin and 0.01% EDTA), Cat. No. R-001-100, Cascade Biologics (Invitrogen), Paisley, UK;

2.5.4 Fluorescent cell markers

Draq5 Draq5^{TM} nuclear dye, c = 5 mM, Cat. No. DR50051, Biostatus limited, Shepshed, UK;

Wheat Germ Agglutinin-488 (WGA-488)

WGA-488 conjugate, c = 1 mg/ml, Cat. No. Invitrogen, Paisley, UK, used as a cell surface marker;

2.5.5 Cytokines/Chemokines/Chemoattractants

CCL2 (Monocyte chemotactic protein-1 (MCP-1))

mouse CCL2, Cat. No. DY479, R&D Systems, Abingdon, UK;

Interleukin-1β (IL-1β) mouse IL-1β, Cat. No. 401-ML-005/CF, R&D Systems, Abingdon, UK;

Leukotriene B_4 (LTB_4) LTB_4, Cat. No. 434625, Merck, Hoddesdon Hets, UK;

Tumor necrosis factor-α (TNF-α)

mouse TNF-α, Cat. No. 401-ML-010/CF, R&D Systems, Abingdon, UK;

2.5.6 Enzymes

BamHI Cat. No. R0136S, New England Biolabs, Hitchin, UK;

DraIII Cat. No. R0510S, New England Biolabs, Hitchin, UK;

Proteinase K Cat. No. 3115879001, Roche, Burgess Hill, UK;

2.5.7 Kits

BD Cytofix/Cytoperm™ Kit

Fixation and Permeabilisation Kit, Cat. No. 554714, BD Biosciences, Oxford, UK;

2.5.8 Other reagents, solutions and buffers

Blue agarose gel electrophoresis loading buffer

25 mg Bromophenol Blue
4 g Sucrose
10 ml molecular biology grade water

Bovine serum albumin (BSA)

New England Biolabs, Hitchin, UK;

Bromophenol Blue	Cat. No. B0126, Sigma-Aldrich, Poole, Dorset, UK;
DNA ladders	SmartLadder SF (100 – 1,000 bp), Cat. No. MW-1800-04 or SmartLadder (200 – 10,000 bp), Cat. No. MW-, Eurogentec, Southampton, UK
Ethanol	Cat. No. 101077Y, VWR, Soulbury, UK;
GelRed	Cat. No. 41003, Biotium, via Cambridge BioScience, Cambridge, UK;
Genticin	Cat. No. 10131-019, Gibco, Paisley, UK;
Goat Serum	Normal goat serum
Isopropanol	Cat. No. 20839.322, VWR, Soulbury, UK;
Lipofectamine	Cat. No. 18324-012, Invitrogen, Paisley, UK;
Lysis buffer	100 mM Tris-HCl, pH 8.5 5 mM EDTA 200 mM NaCl 0.2 % sodium dodecyl sulphate (SDS)
Methanol	Cat. No. 20847.320, VWR, Soulbury, UK;
Molecular biology grade water	UltraPure™ DNase/RNase-free distilled water, Cat. No. 10977-049, Invitrogen, Paisley, UK;
NEB buffer 3	New England Biolabs, Hitchin, UK;
Paraformaldehyde (PFA)	Cat. No. 294474L, VWR, Soulbury, UK;
Plus reagent	Cat. No. 11514-015, Invitrogen, Paisley, UK;
Rabbit serum	Normal rabbit serum, Cat. No. C12SAZ, AbD Serotec, Kidlington, UK;
Saline	Sodium chloride, 0.9 % w/v, Cat. No. B1323, Baxter Healthcare, Northampton, UK;
Sodium chloride (NaCl)	Cat. No. 71376, Fluka BioChemika, Sigma-Aldrich, Poole, Dorset, UK;

Sodium dodecyl sulfate (SDS)

10 % SDS solution, Cat No. 20-4000-05, Severn Biotech Ltd., Kidderminster, UK;

Sucrose Cat. No. 102744, BDH AnalaR®, VWR, Soulbury, UK;

TAE buffer UltraPure™ 10x TAE buffer, Cat. No. 15558-026, Invitrogen, Paisley, UK;

Tris-HCL 1 M Tris-HCL solution, pH 8.5, Cat. No. 20-7901-10, Severn Biotech Ltd., Kidderminster, UK;

Triton X-100 Cat. No. X100, Sigma-Aldrich, Poole, Dorset, UK;

Tyrode's salt solution Cat. No. 127K8303, Sigma-Aldrich, Poole, Dorset, UK;

2.6 Induction of inflammation in murine tissues and analysis by immunofluorescence labeling and confocal microscopy

2.6.1 Induction of inflammatory reactions in the murine cremaster muscle

Neutrophil transmigration through cremasteric post-capillary venules was induced in male WT C57BL/6 mice (~ 25 g) either via intrascrotal (i.s.) injection of inflammatory stimuli like IL-1β or TNF-α or topical application of inflammatory mediators onto the exteriorised cremaster such as LTB_4 or CCL2 or through Ischemia Reperfusion Injury (I/R). Different concentrations and *in vivo* test periods were investigated as governed by the time course of action of these stimuli.

For i.s. injection of IL-1β (50 ng/400 µl saline) and TNF-α (300 ng/400 µl saline), mice were sedated via intramuscular (i.m.) injection of 1ml/kg anaesthetic (40 mg ketamine and 2 mg xylazine in saline). As a vehicle control, mice received 400 µl saline i.s. alone. Different *in vivo* test periods such as 2 h, 4 h, 8 h and 24 h for IL-1β and 0.5 h, 1 h, 2 h and 4 h for TNF-α, were employed.

For topical application of CCL2 (5×10^{-9} M) and LTB_4 (10^{-7} M), mice were anaesthetised via intraperitoneal (i.p.) injection of ketamine (100 mg/kg) and xylazine (10 mg/kg). The cremaster muscle was surgically exteriorised onto a purpose-built microscope stage and was continuously perfused with warm Tyrode's solution containing the inflammatory stimulus under investigation for 2 h. As control, cremaster muscles were superfused with Tyrode's solution alone. These experiments were performed by Dr. Mathieu-Benoit Voisin.

I/R was performed by inducing ischemia after placing an artery clamp at the base of the cremaster muscle (for 30 min), followed by the removal of the clamp to start vascular reflow for 2 h. These experiments were carried out by Dr. Abigail Woodfin and Dr. Mathieu-Benoit Voisin.

At the end of the *in vivo* test periods, mice were sacrificed and cremaster muscles were dissected away and fixed in 100 % Methanol or 4 % PFA for 30 min at 4 °C. Subsequently, analysis of venules by immunofluorescence labeling and confocal microscopy of whole mounted cremasters was performed.

2.6.2 Induction of dermal inflammation in the mouse ear

Mice were anesthetized and injected intradermally (i.d.) with TNF-α (150 ng in 30 µl PBS) or IL-1β (10 ng in 30 µl PBS) or 30 µl PBS alone (vehicle control) in the ear. At the end of the experiments, animals were sacrificed and ears were dissected for subsequent analysis of venules by immunofluorescent labeling and confocal microscopy.

2.6.3 Immunofluorescence labelling of murine tissues and analysis by confocal microscopy

To investigate pericyte morphology in murine post-capillary venules, confocal microscopy of whole mounted murine tissues such as cremaster muscle, diaphragm, mesentery, peritoneal wall and skin of the ear was performed. These tissues (unstimulated tissues, respective controls or tissues stimulated with different inflammatory mediators, as described above, 2.6.1) were dissected away from WT C57BL/6 mice and fixed in 100 % Methanol or 4 % PFA for 30 min to 1 h at 4 °C. Subsequently, immunofluorescent staining of whole mounted tissues was performed. For this purpose, the tissues were permeabilised after fixation with 0.5 % Triton

X-100 and blocked with 25 % serum (12.5 % FBS and 12.5 % goat serum or rabbit serum, depending on the species in which the secondary antibody was raised) in PBS for 2 h at RT. This was followed by the incubation with the primary antibodies for α-SMA, collagen IV, MRP14, IL-1RI (goat anti-IL-1RI), MRP14, NG2, TNFRI (goat anti-TNFRI) or TNFRII (goat anti-TNFRII) or appropriate control antibodies in PBS/20 % serum (10 % FBS and 10 % goat serum or rabbit serum, depending on the species in which the secondary antibody was raised) over night at 4 °C. After a washing step (tissues were washed three times for 5 min in PBS on the shaker), appropriate secondary antibodies conjugated with Alexa Fluor 488 or 633 were used if necessary (at a final concentration of 10 μg/ml in PBS for 3 h at 4 °C) followed by a final washing step in PBS. For confocal analysis the tissues were mounted on glass slides and scanned using a Zeiss LSM 5 PASCAL confocal laser-scanning microscope (Zeiss Ltd, Welwyn Garden City, UK) and a Zeiss 40x water-dipping ACHROPLAN objective (NA 0.75 W, Ph2) or a Zeiss 63x oil Plan-APOCHROMAT objective (NA 1.4). Z-stack images of post-capillary venules (analysed vessels were largely within a diameter of 20-50μm) were captured using the multiple track scanning mode at every 1 μm (40x) or 0.4 μm (63x) of tissue depth at a resolution of 1024 × 1024 pixels in the x × y plane, corresponding to a voxel size of approximately 0.26 × 0.26 × 1/0.4 μm in x × y × z, respectively. The resulting confocal images were analysed using softwares for 3D-reconstruction such as ImageJ (public domain Java-based image analysis and processing software, developed at the National Institutes of Health, USA) and IMARIS (Bitplane AG, Zurich, Switzerland) to quantify neutrophil transmigration, determine changes in pericyte morphology and assess IL-1RI, TNFRI and TNFRII expression on endothelial cells and pericytes of post-capillary venules. To quantify neutrophil transmigration, all neutrophils that have transmigrated into the tissue 50 μm above and below a post-capillary venule over a length of 200 μm were counted (per 0.02 mm^2 of tissue) (Figure 2.2). To determine changes in pericyte shape, 3D-reconstructed confocal images were split in half *in silico* along the longitudinal vessel axis. The resulting image sections of semi vessels were transformed into gray scale intensity projection and all the gaps between adjacent pericytes were encircled manually to measure their area (in μm^2) (Figure 2.3). Subsequently, the mean gap size was determined for each post-capillary venule. At least four post-capillary venules were investigated per cremaster and the resulting mean gap sizes were then plotted as mean per mouse. In addition, the

number of gaps per defined vessel area (per 1 mm^2) was determined to give a measure of gap density. The mean gap density was also plotted as mean per mouse. To assess IL-1RI, TNFRI and TNFRII expression on post-capillary venules, the mean fluorescence intensity (MFI) of isotype control (goat IgG), IL-1RI, TNFRI or TNFRII staining was determined using IMARIS software with the advice of expert IMARIS users in our group. To analyse endothelial cells and pericytes separately, an isosurface has to be created representing exclusively the endothelium or the pericyte sheath, respectively (Figure 2.4). This parameter depicts the limitation of the volume of interest in which IMARIS determines the MFI of other channels (in this case of the channel showing isotype control, IL-1RI, TNFRI or TNFRII staining). Isosurfaces embodying the endothelial cell or pericyte layer were built by using the channel showing immunofluorescence labeling of PECAM-1 or α-SMA as a source, respectively (Figure 2.4).

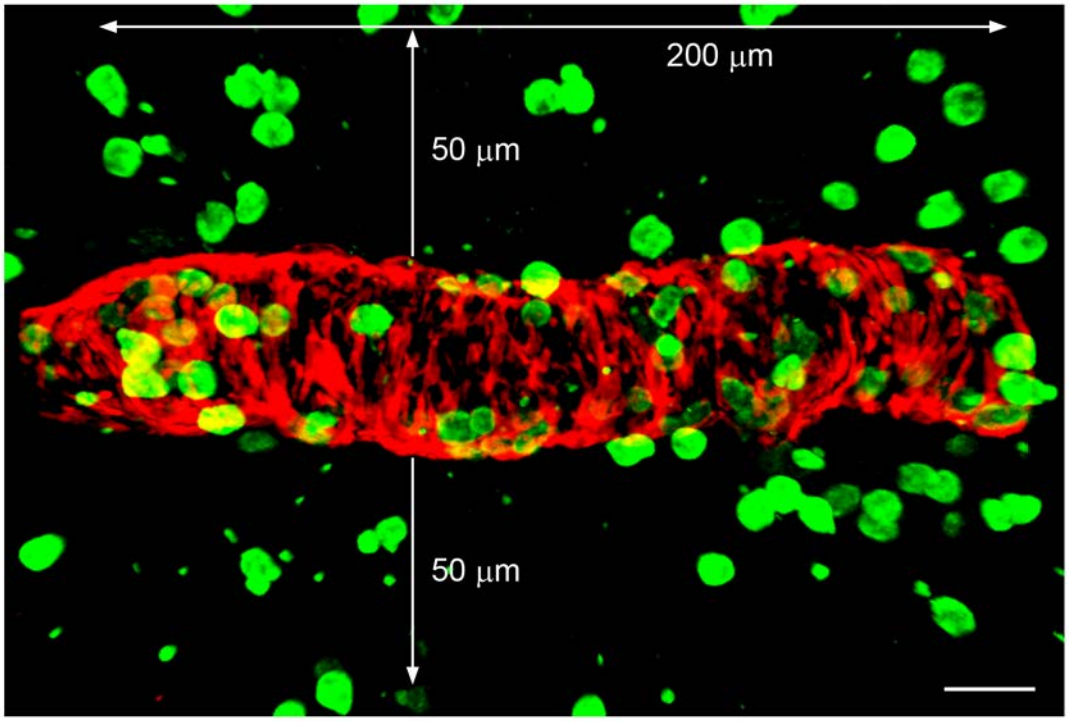

Figure 2.2: Quantification of neutrophil transmigration. 3D-reconstructed confocal image of a post-capillary venule (red, pericytes, α-SMA staining) from an IL-1β-stimulated cremaster muscle. Neutrophils (green, marker: MRP14) that have transmigrated into the tissue 50 µm away from the vessel were counted over a length of 200 µm. Bar, 20 µm.

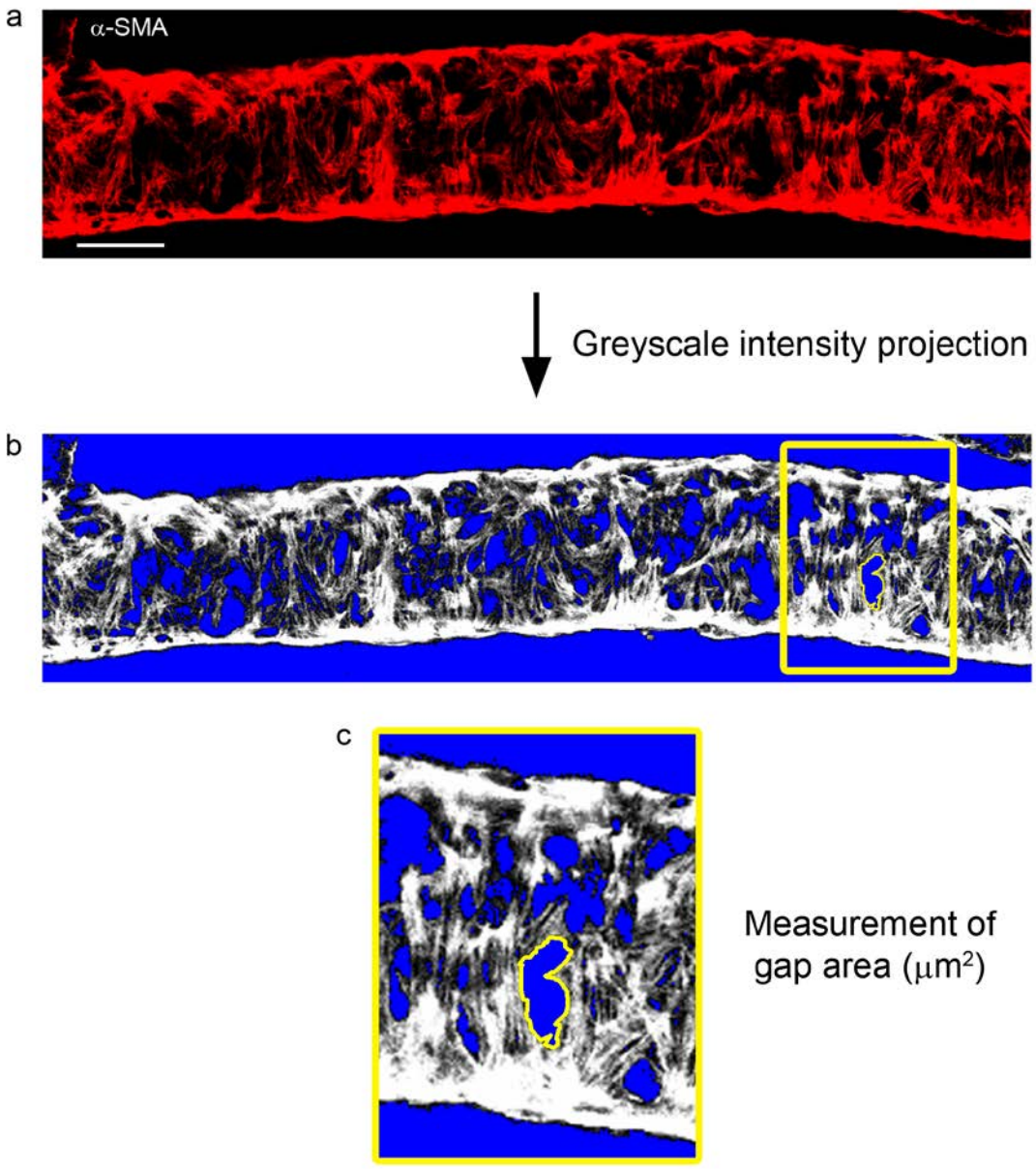

Figure 2.3: Quantification of the size of gaps between adjacent pericytes in post-capillary venules. (a) 3D-reconstructed confocal image section of a semi post-capillary venule (split in half *in silico* along the longitudinal vessel axis). Bar, 20 μm. (b) Gray scale intensity projection of the confocal image section. All gaps between adjacent pericytes were encircled manually as shown for an example gap (yellow line) to measure their area. Yellow boxed region enlarged in (c).

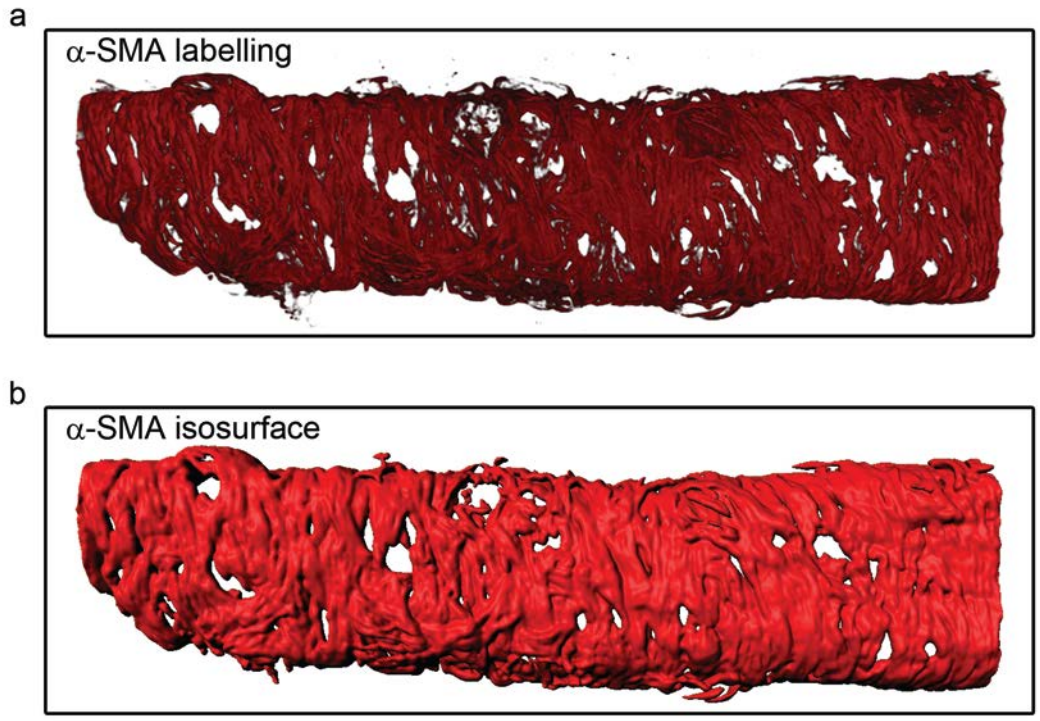

Figure 2.4: Creating isosurfaces using IMARIS software. A representative isosurface showing the pericyte layer (b) is illustrated, which has been generated using immunofluorescence labelling of α-SMA (a) as a source.

2.7 Neutrophil depletion

Neutrophil depletion was induced by i.p. injection of 100 µg of anti-GR1 antibody in 1 ml saline 24 h before i.s. administration of IL-1β or TNF-α. Control mice received the rat IgG2bκ isotype matched control antibody. To determine the level of neutrophil depletion, blood neutrophil counts were performed. For this purpose, tail vein blood samples were collected before and 24 h after antibody administration indicating an 82 % depletion of circulating neutrophils.

2.8 Confocal Intravital Microscopy

Confocal intravital microscopy was used to directly observe leukocyte responses and changes in pericyte morphology within murine cremasteric post-capillary venules upon TNF-α stimulation in real-time in 3D.

Observation of pericyte shape change

To observe changes in pericyte morphology *in vivo* male α-SMA-GFP mice were anaesthetised by i.p. injection of ketamine (100 mg/kg) and xylazine (10 mg/kg) and maintained at 37 °C on a custom-built heated microscope stage. The cremaster was exteriorized, pinned out flat over the optical window of the stage and superfused with Tyrode's solution (2.5.8). During confocal IVM Z-stack images of a post-capillary venule (analysed vessels were largely within a diameter of 20 - 50 µm) were captured every minute using a Leica SP5 confocal microscope (Leica Microsystems, Milton Keynes, UK) incorporating a 20x water-dipping objective (NA 1.0). Images were acquired with sequential scanning of different channels at a resolution of 1024 × 512 pixels in the x × y plane and 0.7 µm steps in z-direction, corresponding to a voxel size of ~ 0.23 × 0.23 × 0.7 µm in x × y × z, respectively. Subsequently, after 5 min of imaging, pericyte shape change was induced by adding TNF-α to the Tyrode's solution at 30 ng/ml and images were taken every minute for a further 2 h and 30 min. As control, cremasters were superfused with Tyrode's solution alone. The resulting 4D image sequences were processed using IMARIS software (Bitplane, Switzerland).

Investigation of leukocyte responses

Pericyte gap enlargement was induced in male α-SMA-RFPcherryxLys-eGFP mice (details of the crossing are described in Chapter 6) via i.s. injection of TNF-α (300 ng/400 µl saline). Additionally, an anti PECAM-1-647 antibody (3 µg in 300 µl saline) was injected i.s. to immunolabel endothelial cell junctions and so aid visualisation of the endothelial cell layer. As vehicle control, mice were injected with 400 µl saline containing the anti PECAM-1-647 antibody only. For i.s. administrations, mice were sedated via intramuscular (i.m.) injection of 1ml/kg anaesthetic (40 mg ketamine and 2 mg xylazine in saline). After 2 h, mice were anaesthetised by i.p. injection of ketamine (100 mg/kg) and xylazine (10 mg/kg) and maintained at 37 °C on a custom-built heated microscope stage. The cremaster was exteriorized, pinned out flat over the optical window of the stage (Figure 2.5) and superfused with Tyrode's solution. Z-stack images of a post-capillary venule were captured every 1 min for 2 h using a Leica SP5 confocal microscope (Leica Microsystems, Milton Keynes, UK) incorporating a 20x water-dipping objective (NA 1.0). Z-stacks were captured at every 0.7 µm of tissue depth at a resolution of 1024 × 512. The resulting 4D confocal image sequences were analyzed using IMARIS software by Dr. Mathieu-Benoit Voisin.

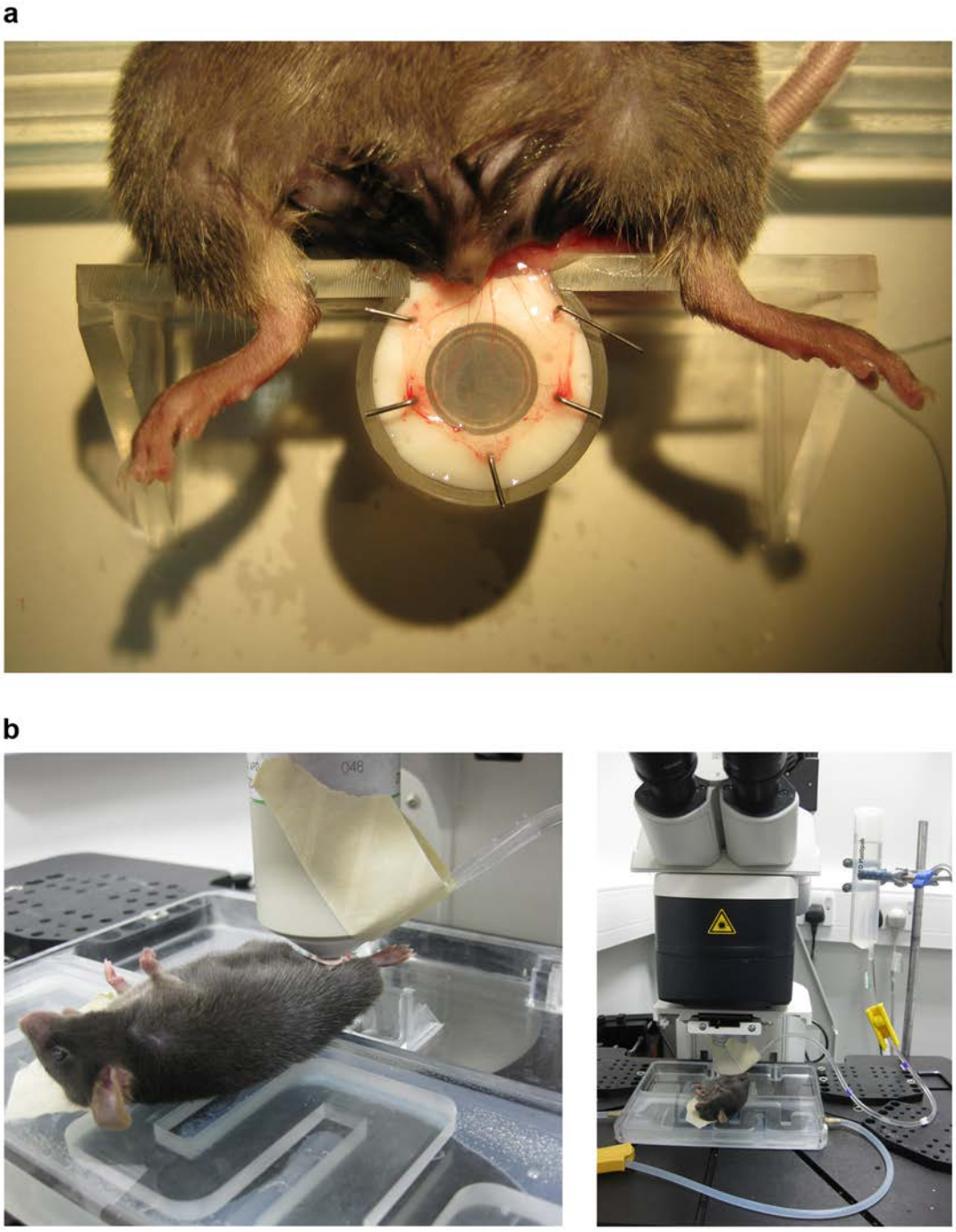

Figure 2.5: Surgical exteriorisation and preparation of the cremaster muscle for confocal intravital microscopy. (a) The cremaster was exteriorized and pinned out flat over the optical window of a heated microscope stage. (b) It was then positioned under the confocal microscope and constantly superfused with TNF-α (in Tyrode's solution) or Tyrode's solution alone.

2.9 Characterisation and analysis of the murine pericyte-like cell line C3H/10T1/2

2.9.1 Culture of C3H/10T1/2 cells

C3H/10T1/2 cells were maintained in Dulbecco's modified Eagle's medium (DMEM), supplemented with 10 % heat-inactivated fetal bovine serum (FBS), 4.5 g/l Glucose, 2 mM L-Glutamine, 100 U Penicillin and 100 µg/ml Streptomycin. Cells were grown at a confluence of 70 % to 80 %, at 37 °C and 5 % CO_2 and were not used beyond passage 20.

2.9.1.1 Thawing cells from liquid nitrogen

C3H/10T1/2 cells were stored in liquid nitrogen in cryovials containing 10 % DMSO in FBS. Cells were thawed at 37 °C and added to 9 ml of C3H/10T1/2 growth medium (composition described above, 2.9.1) prior to pelleting the cells by centrifugation for 10 min at 200 g/RT. The resulting cell pellet was resuspended in 5 ml medium. The cells were then plated in a 25 cm^2 cell culture flask and incubated at 37 °C and 5 % CO_2 using C3H/10T1/2 growth medium.

2.9.1.2 Passaging cells

To passage cells, the medium was removed and the cells were washed once with PBS. Subsequently, the cells were detached from the culture flasks using a trypsin/EDTA solution. Cell suspensions were diluted in 9 volumes medium and transferred into new cell culture flasks (5×10^3 cells/cm^2).

2.9.1.3 Determination of cell numbers

For determination of the total cell number, the cells were detached from the cell culture flasks and transferred into new medium (as described above, 2.9.1.2). Subsequently, the number of cells in the resulting cell suspension was determined using a Neubauer haematocytometer. For this purpose, 50 µl of the cell suspension were mixed with 50 µl of trypan blue stain in order to exclude dead cells. This solution was pipetted under the cover slip of the haematocytometer and the cells in two opposed squares were counted. This number reflects the amount of cells per 0.1 µl cell suspension, because the volume above one square is 0.1 µl and the dilution

factor resulting from the trypan blue staining was 1:2. To determine the number of cells per 1 ml, the number of cells counted was multiplied by 10^4.

2.9.1.4 Freezing cells

For long-term storage cells were stored in liquid nitrogen. For this purpose, the cells were detached from the cell culture flasks and were transferred into new medium (as described above, 2.9.1.2). Cell numbers were counted as described (2.9.1.4) and the cells pelleted by centrifugation for 10 min at 200 g/RT. The resulting cell pellet was resuspended in FBS containing 10 % DMSO such that the final concentration was 1×10^6 cells/ml. Cell suspensions were distributed into cryovials and stored at – 80 °C over night. After 24 h, the cryovials were transferred into storage under liquid nitrogen.

2.9.2 Flow cytometry

To examine the expression of pericyte markers (α-SMA and NG2) or cytokine receptors (IL-1RI, TNFRI or TNFRII) by the pericyte-like C3H/10T1/2 cells, Flow cytometry was used. For this purpose, the cells were harvested using 0.02 % EDTA in PBS to avoid shedding of surface molecules by trypsin. Afterwards the cells were counted, pelleted and resuspended in PBS/1 % FBS to obtain a concentration of 2.5×10^6 cells/ml. Per sample 5×10^5 cells were used to perform fluorescence immunostaining. Cells were incubated for 30 min on ice with the primary antibodies specific to IL-1RI (armenian hamster anti-IL-1RI), NG2, TNFRI (armenian hamster anti-TNFRI) or TNFRII (armenian hamster anti-TNFRII) or appropriate control antibodies in 200 µl PBS/1 % FBS. Where use of secondary antibodies was appropriate, the cells were washed three times with PBS/1 % FBS before incubation in the presence of secondary antibody in 200 µl PBS/1 % FBS for 30 min on ice. For detection of IL-1RI, TNFRI and TNFRII a third labelling step was necessary. In this instance, detection of the biotinylated anti-armenian hamster secondary antibody was performed after three washes in PBS/1 % FBS by incubating the cells with streptavidin conjugated with Alexa Fluor 488 in 200 µl for 30 min on ice. To visualise intracellular α-SMA, the cells were fixed and permeabilised by incubation in 100 µl Fixation/Permeabilisation Solution (BD Cytofix/Cytoperm™ Kit) for 20 min on ice. Subsequently, after two washes in Permeabilisation/Washing Buffer (P/W Buffer) from the same kit the anti-α-SMA antibody was applied in 200 µl P/W

Buffer and the cells were incubated for 30 min on ice. In all cases, after the final antibody step, samples were washed three times with PBS/1 % FBS and were subsequently analysed using a BD FACSCalibur flow cytometer (BD Biosciences, Oxford, UK) and the flow cytometry analysis software FlowJo (Tree Star, Inc., Ashland, USA).

2.9.3 Immunofluorescence labelling and analysis of C3H/10T1/2 cells grown on chambered slides

For analysis of pericyte marker and cytokine receptor expression profile by the pericyte-like C3H/10T1/2 cell line confocal microscopy was used. For this purpose, the cells were seeded on 4-well chamber slides for fluorescence immunostaining at a density of 9×10^3 cells/well in 900 µl of C3H/10T1/2 growth medium. After 48 h, the medium was removed and the cells were washed twice with cold PBS/1 % FBS. Subsequently, the cells were fixed by incubating in 300 µl of 4 % PFA per well for 10 min on ice and washed twice with cold PBS. This was followed by incubation for 30 min on ice with the primary antibodies for IL-1RI (armenian hamster anti-IL-1RI), NG2, TNFRI (armenian hamster anti-TNFRI) or TNFRII (armenian hamster anti-TNFRII) or appropriate control antibodies in 300 µl PBS. To label the cell membrane, cells were incubated with wheat germ agglutinin-488 (WGA-488) in 300 µl PBS for 20 min on ice. Where incubation with a secondary antibody was necessary, the cells were washed three times with PBS before incubating with the secondary antibody in 300 µl PBS for 30 min on ice. For detection of IL-1RI, TNFRI and TNFRII a third labelling step was necessary. In this instance, detection of the biotinylated anti-armenian hamster secondary antibody was performed after three washes in PBS by incubating the cells with streptavidin conjugated with Alexa Fluor 488 in 300 µl PBS for 30 min on ice. To visualise intracellular α-SMA, the cells were fixed and permeabilised by incubation in 300 µl Fixation/Permeabilisation Solution (BD Cytofix/Cytoperm^{TM} Kit) for 20 min on ice. Subsequently, after two washes with Permeabilisation/Washing Buffer (P/W Buffer) from the same kit the anti-α-SMA antibody was applied in 300 µl P/W Buffer and the cells were incubated for 30 min on ice. After the final antibody incubation, samples were washed three times with cold PBS. Cell nuclei were labelled using Draq5 in 300 µl PBS for 1 min on ice followed by a final washing step. For confocal analysis, the cells were scanned using a Zeiss LSM 5 PASCAL confocal laser-scanning microscope (Zeiss Ltd, Welwyn

Garden City, UK) and a Zeiss 20x (NA 0.5 W, Ph2) or Zeiss 40x (NA 0.75 W, Ph2) water-dipping ACHROPLAN objective.

2.9.4 Transfection of C3H/10T1/2 cells with Lifeact-eGFP plasmid DNA

To image changes in the actin cytoskeleton and visualise cell shape change in real time using fluorescence time lapse microscopy, C3H/10T1/2 cells were transfected to express Lifeact-eGFP.

2.9.4.1 Transformation of Top10F' bacteria with Lifeact-eGFP plasmid DNA

To amplify Lifeact-eGFP plasmids, competent Top10 bacteria were transformed. Bacteria were defrosted on ice, mixed with 10 ng Lifeact-eGFP plasmid DNA and incubated for 15 min on ice. Afterwards, the tube was placed into a 42 °C water bath and incubated for 1 min, followed by incubation on ice for 5 min. The bacteria were transferred to a 13 ml culture tube containing 500 µl of warm LB medium (without antibiotics!) and incubated at 37 °C for 1 h in an orbital shaker set at 225 rpm. Single colonies of transformed bacteria were obtained by streaking the cell suspension (20 µl and 200 µl) onto LB Agar culture plates containing Kanamycin (50 µg/ml) and incubating them over night at 37 °C. Plates were stored at 4 °C for a maximum of four weeks and single bacterial colonies were used to inoculate liquid cultures.

2.9.4.2 DNA isolation

To isolate plasmid DNA from bacteria QIAGEN Plasmid Purification Kits were used according to the manufacturer's protocol. These kits are based on alkaline lysis of bacteria, followed by a selective immobilisation of the plasmid DNA on a carrier substrate (anion-exchange resin). After several washing steps the DNA is eluted from the resin and stored at 4 °C for short-term storage or at 20 °C for longer storage. DNA minipreps were performed on 1 ml aliquots from 5 ml bacterial cultures inoculated from single colonies grown overnight at 37 °C in an orbital shaker set at 225 rpm. Plasmid DNA was analysed by restriction digest using the enzymes BamHI and DraIII to verify the correct version of Lifeact-eGFP using standard procedures. Correct fragment sizes are 1213 bp and 3548 bp. The remaining 4 ml of liquid culture from verified Lifeact-eGFP clones was used as an inoculum for 300 ml

cultures grown as described above and upon which larger scale plasmid extraction was performed using the QUIAGEN Maxi Prep Kit.

2.9.4.3 Quantitation of DNA concentration

To measure the DNA concentration of Lifeact-eGFP Maxi preparations, a NanoDrop ND-1000 spectrophotometer (NanoDrop Technologies, Labtech International Ltd, Ringmer, UK) was used according to the manufacturer's protocol. A sample volume of 1 µl was sufficient, because the NanoDrop is based on fibre optic technology. Due to surface tension this small sample volume was held in place between two optical surfaces. Each sample was assessed at two light path length (0.2 mM and 1 mM), providing an extensive dynamic range from 2 ng/µl to 3.7 µg/µl. All measurements producing a value higher than 3 µg/µl were repeated using appropriate dilutions of the sample. As a blank control the QIAGEN Elution Buffer was used. Between each sample the absorbance of QIAGEN Elution Buffer alone was measured to avoid potential contamination. Plasmid DNA was stored at 4 °C for short-term storage or at 20 °C for longer storage.

2.9.4.4 Transfection of C3H/10T1/2 cells

For fluorescence time lapse microscopy, C3H/10T1/2 cells were transfected in suspension with Lifeact-eGFP plasmid DNA according to the protocol from Alexopoulou et al., 2008. For this purpose, 0.5 µg pmeGFP-N1-Lifeact plasmid DNA and 1 µl Plus reagent were mixed and serum-free C3H/10T1/2 growth medium was added to a final volume of 25 µl. Serum-free C3H/10T1/2 growth medium was added to 5.5 µl Lipofectamine to a final volume of 25 µl and incubated for 15 min at RT. The diluted Lipofectamine was then added dropwise to the DNA and incubated for 20 min at RT. The DNA/Lipofectamine complexes were used to resuspend a C3H/10T1/2 cell pellet containing 3.5×10^5 cells, which had been washed with serum-free C3H/10T1/2 growth medium beforehand. After 10 min of incubation at RT, the cell suspension was transferred into a well of a 6-well-plate containing 2 ml warm C3H/10T1/2 growth medium. Fresh C3H/10T1/2 growth medium was added after 24 h containing 1 mg/ml Geneticin to select for transfected cells.

2.9.5 Fluorescence time lapse microscopy

To investigate the response of the pericyte-like C3H/10T1/2 cells to the inflammatory cytokines IL-1β and TNF-α *in vitro*, time lapse experiments were performed. For this purpose, Lifeact-eGFP transfected C3H/10T1/2 cells were seeded into 6-well plates at a density of 3.5×10^5 cells/well in normal growth medium 48 h prior to the experiment. For imaging, normal C3H/10T1/2 growth medium was exchanged for Leibovitz's medium without Phenol Red. This medium was developed for the support of cell growth in non-CO_2-equlibrated environments. The 6-well-plates were transferred into the heated chamber of an Olympus IX81 motorised inverted microscope (Olympus Medical, Southend-on-Sea, UK) and incubated at 37 °C throughout the whole experiment. Pictures of three different fields of view per dish were taken every 10 minutes for 4 h using an Olympus 20x dry long working distance LUCPlanFLN objective lens (NA 0.45, Ph2). Subsequently after the first picture, the inflammatory cytokines IL-1β (1, 10 or 100 ng/ml) or TNF-α (10 or 100 ng/ml) or the vehicle control (PBS) were added to the cells. The eccentricity of cells, which is the ratio of cell length to cell width, was manually measured at different time points using IMARIS software. The mean cell eccentricity (of all three fields of view per well and at least 5 randomly selected cells per field of view) was determined and the changes in mean cell eccentricity were plotted per stimulus and time point as percentage change normalised to the overall mean at time point 0 h (time point before addition of the cytokines or the vehicle control).

2.10 Statistical analysis

Results were plotted and statistically analysed using GraphPad Prism® 4. Values were expressed as means ± standard error of the mean (SEM) and significant differences between multiple groups were identified by one-way analysis of variance (ANOVA) followed by Newman-Keuls Multiple Comparison Test. Whenever two groups were compared a Student's *t* test was used. p values < 0.05 were considered as significant.

Chapter 3: Identification and characterisation of pericytes in different types of murine blood vessels and vascular beds

3.1 Introduction

Pericytes are phenotypically heterogeneous (Sims, 2000). They differ in marker expression, morphology and frequency depending on vessel type, vascular bed, developmental stage and species. Marker expression and morphology have also been shown to be altered during pathological conditions (Morikawa et al., 2002).

Several markers for pericytes have been reported to date. Intracellular markers include α-smooth muscle actin (α-SMA) (Nehls and Drenckhahn, 1991), desmin (Fujimoto and Singer, 1987; Hughes and Chan-Ling, 2004), aminopeptidase A and N (Schlingemann et al., 1996; Alliot et al., 1999) and the regulator of G-protein signalling 5 (RGS5) (Cho et al., 2003). Accepted extracellular markers are neuron-glia antigen 2 (NG2) (Ozerdem et al., 2001; Ozerdem et al., 2002; Murfee et al., 2005), platelet-growth factor receptor β (PDGFR-β) (Lindahl et al., 1997), the unknown antigen of the antibody 3G5 (Nayak et al., 1988), endosialin (CD248) (Rupp et al., 2006) and CD146 (Li et al., 2003). However, none of the known pericyte markers is absolutely specific for pericytes or recognizes all pericytes. Their expression varies depending on vessel type, vascular bed, developmental stage and species (Nehls and Drenckhahn, 1991; Chan-Ling et al., 2004; Hughes and Chan-Ling, 2004; Murfee et al., 2005). Additionally, marker expression was also shown to change during pathological conditions such as cancer (Morikawa et al., 2002). This has led to misinterpreted findings in previous studies, where pericyte loss on angiogenic sprouts and tumour vessels was described due to the use of markers, which have later been shown not to be expressed under pathological conditions (Morikawa et al., 2002; Baluk et al., 2005). More recently, pericytes were reported to be abundant on tumour vessels (Morikawa et al., 2002; Baluk et al., 2005).

Morphological differences exist, which also depend on vessel type (capillaries or venules), vascular bed, developmental stage, species and pathological conditions (Diaz-Flores et al., 1991; Morikawa et al., 2002). Furthermore, pericyte coverage of the abluminal vessel area varies in different organs, developmental stages and species (Shepro and Morel, 1993; Egginton et al., 1996). The ratio of pericytes to endothelial cells varies in different vascular beds ranging from 1:1 to 1:100. The retina exhibits one of the highest ratios of 1:3, but the highest pericyte abundance (1:1) is found in the CNS (Shepro and Morel, 1993). Pericytes can be distinguished

from VSMC, which are wrapped tightly around arteriols, arteries and veins by their location, their morphology and their marker expression (Armulik et al., 2005). However, an absolute distinction between pericytes and VSMC is not always possible. There is a continuum of cells from characteristic pericytes surrounding post-capillary venules and capillaries to intermediate cells resembling both pericytes and smooth muscle cells at the interface between arteriolar capillaries and arterioles, to true smooth muscle cells surrounding arterioles, arteries and veins (Shimada et al., 1992).

This chapter aims to investigate the expression profile of various known pericyte markers in the mouse cremaster muscle with a focus on finding the best possible marker for pericytes on post-capillary venules of murine cremaster muscles. Additionally, pericyte morphology was compared in different types of blood vessels in the cremaster muscle as well as in post-capillary venules in selected vascular beds (cremaster muscle, mesentery, skin of the ear, peritoneal wall and diaphragm) as to date no study has described morphological characteristics of pericytes in these tissues.

3.2 Results

3.2.1 Pericyte marker expression in the murine cremaster muscle

In initial studies I aimed to investigate the best possible marker for pericytes on post-capillary venules of murine cremaster muscles, to be used for subsequent analysis of pericyte morphology under basal and inflammatory conditions. The cremaster muscle was used for investigations because of its thin and transparent nature, which enables it to be used whole mounted for immunofluorescence staining and confocal microscopy.

In this tissue I found an α-SMA expression pattern in line with previous reports using other tissues (Nehls and Drenckhahn, 1991; Morikawa et al., 2002). High amounts of α-SMA were found in pericytes surrounding post-capillary and collecting venules as well as in smooth muscle cells, which are wrapped tightly around arterioles, arteries and large veins (Figure 3.1). Pericytes in capillaries on the other hand showed low or no expression of α-SMA. However, capillary pericytes could be positively stained for the chondroitin sulphate proteoglycan NG2, which is a marker for pericytes and neural cells (Figure 3.1). This surface marker was also strongly expressed by smooth muscle cells and nerves, but was absent on pericytes of post-capillary venules (Figure 3.1).

Figure 3.1 also highlights the gradual transition of pericyte phenotypes, in this case relating to marker expression. Capillary pericytes on the venous side of the capillary - where the capillary meets the post-capillary venule - could sometimes be detected by α-SMA staining. However, the α-SMA expression here was not as strong as that detected on post-capillary venules. In the capillary in Figure 3.1 (marked with C), some pericytes were α-SMA positive and also showed weak as well as high NG2 expression representing intermediate pericyte phenotypes between post-capillary venular and capillary pericytes. In the same vessel, the adjacent pericytes appeared to show more typical capillary pericyte characteristics by expressing NG2 but no α-SMA.

Other surface markers tested include desmin, platelet derived growth factor-β (PDGFR-β) and the unknown antigen of the antibody 3G5. Desmin and PDGFR-β were found to be expressed at very low levels in post-capillary venular pericytes. No

staining could be detected in the cremaster muscle using the 3G5 antibody. Functionality of the 3G5 antibody could be verified on rat brain cryosections.

Based on these findings, for the rest of this study α-SMA was used as a marker to visualise pericytes on post-capillary venules in the murine cremaster muscle as well as in various other murine tissues. In addition, transgenic mice became available, which express either the Green Fluorescent Protein (GFP) (Yokota et al., 2006) or the more recently described cherry variant of the Red Fluorescent Protein (RFPcherry) under the control of the α-SMA promoter (see 2.1.1). These mice provide an excellent tool for direct *in vivo* real time imaging of post-capillary venular pericytes using confocal intravital microscopy (IVM) (results produced using these mice are described in Chapter 6). In addition, using the same marker permits direct comparison of data obtained by *ex vivo* immunofluorescence labelling of whole mounted cremaster muscles with real time analysis of post-capillary venular pericytes using direct 4D confocal IVM.

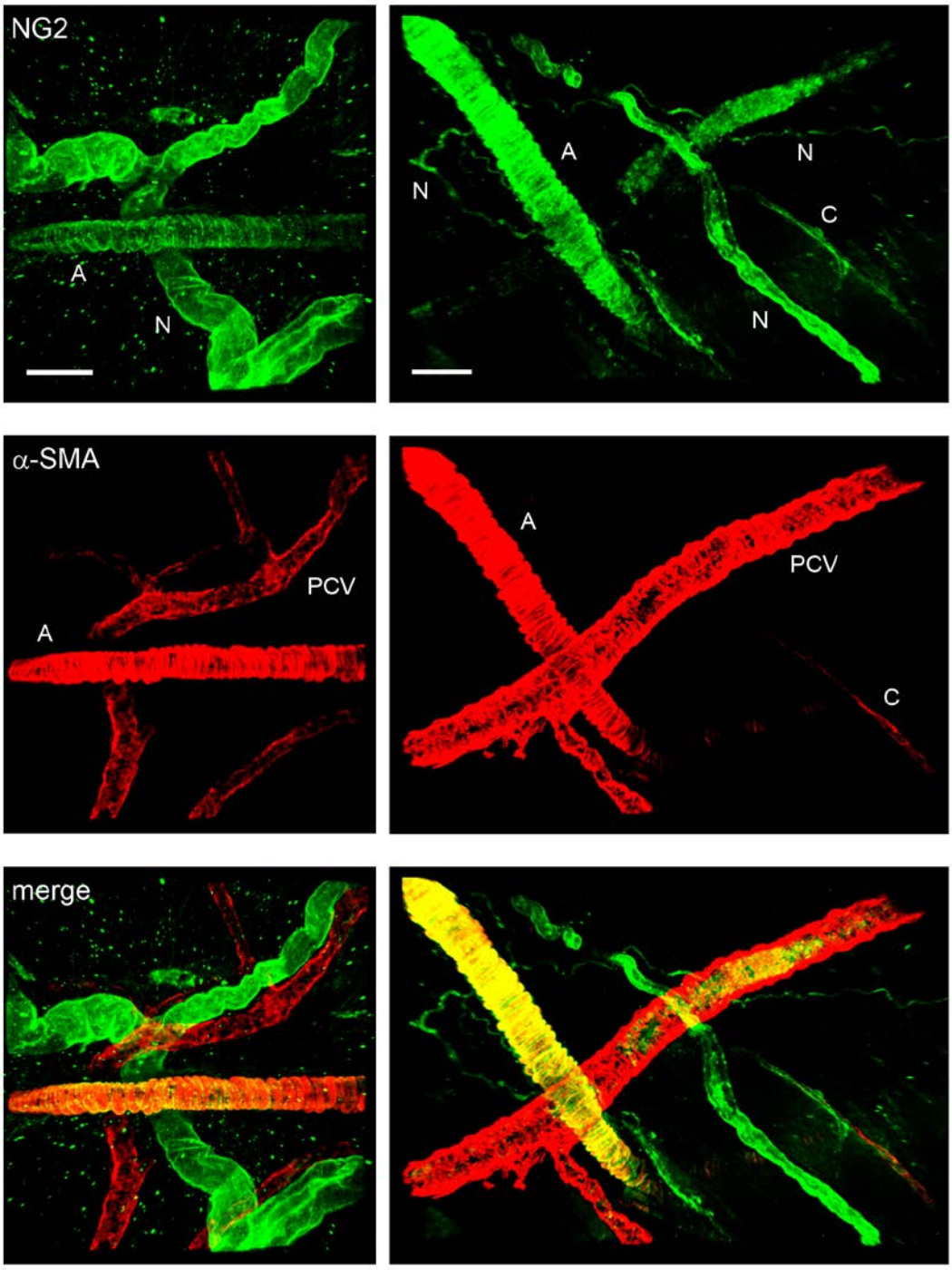

Figure 3.1: Expression of the pericyte markers α-SMA (red) and NG2 (green) by pericytes and smooth muscle cells on unstimulated murine cremasteric vessels. Representative 3D-reconstructed confocal images are shown. Cremaster muscles from unstimulated WT C57BL/6 mice were used. A, arteriole; C, capillary; N, nerve; PCV, post-capillary venule. Bars, 50 μm.

3.2.2 Pericyte morphology in different types of blood vessels in the murine cremaster muscle

Pericyte morphology was characterised in different types of cremasteric blood vessels using immunofluorescence staining and confocal microscopy of whole mounted cremaster muscles. To visualise pericytes, the intracellular marker α-SMA was used, which was found to be highly expressed in most pericytes and all smooth muscle cells in the mouse cremaster muscle (3.2.1). Although pericytes on capillaries are usually α-SMA negative, some capillary pericytes expressed α-SMA (described in more detail in 3.2.1) and could therefore be investigated as well in terms of their morphology.

In general, pericytes are large cells, which exhibit cytoplasmic processes extending from the body of the cell embracing the endothelium (Shepro and Morel, 1993). In the cremaster muscle, capillary pericytes showed an elongated shape with two major processes expanding along the longitudinal axis of the vessel (Figure 3.2). From these two major processes emanated numerous small processes, which encircled the capillaries. Consequently, pericytes on capillaries cover only a small proportion of the endothelial surface. Pericytes in post-capillary venules on the other hand were irregular in shape and orientation and exhibited multiple major processes spreading in all directions (Figure 3.2). Hence, pericytes on post-capillary venules form a discontinuous layer with significant gaps between adjacent cells. As a consequence of the difference in morphology, the percentage of coverage of the underlying endothelium is higher in post-capillary venules compared to capillaries. Collecting venules were almost completely covered by pericytes with very few small gaps between adjacent cells. These pericytes exhibited many major processes, which were arranged mainly circumferentially. Therefore, these cells resembled smooth muscle cells, which are wrapped tightly around arterioles, arteries and large veins leaving no gaps between adjacent cells.

Hence, besides differences in marker expression, there were also great variances in pericyte shape between different vessel types in the cremaster muscle. In this case as well, there was a continuum of cell morphology existing between all pericyte shapes described above. Furthermore, pericytes on collecting venules resembled more like smooth muscles cells than pericytes, which indicates that a gradual transition occurs between pericyte and smooth muscle cell phenotypes.

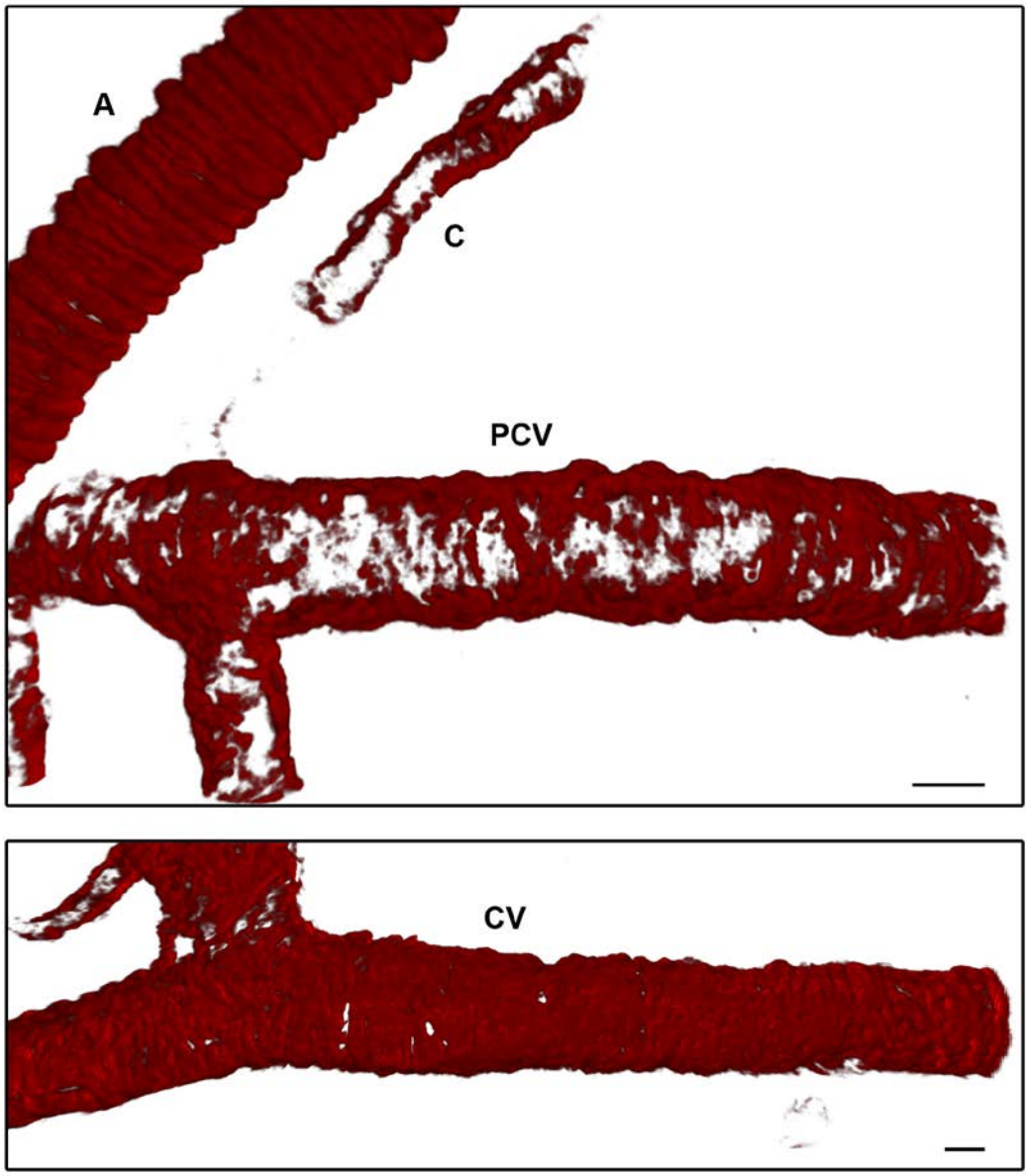

Figure 3.2: Morphological differences among pericytes as well as between pericytes and smooth muscle cells on unstimulated murine cremasteric vessels. Representative 3D-reconstructed longitudinal confocal image sections depicting different cremasteric vessel types are shown. Cremaster muscles were isolated from unstimulated WT C57BL/6 mice, fixed and immunostained for α-SMA to visualise pericytes and smooth muscle cells. A, arteriole; C, capillary; CV, collecting venule; PCV, post-capillary venule. Bars, 20 μm.

3.2.3 Pericyte morphology in post-capillary venules in various murine vascular beds

In the cremaster muscle, pericytes in post-capillary venules form a net-like layer with significant gaps between adjacent cells (3.2.2) (Morikawa et al., 2002; Wang et al., 2006; Voisin et al., 2010). The aim of the following experiments was to investigate whether the pericyte layer surrounding post-capillary venules in other murine vascular beds also exhibited a discontinuous profile. Tissues such as mesentery, skin of the ear, peritoneal wall and diaphragm were chosen for investigation because, like the cremaster muscle, they are thin and transparent tissues and can therefore be used whole mounted for immunofluorescence staining (using α-SMA to visualise pericytes) and confocal microscopy. Confocal images of post-capillary venules (analysed vessels were largely within a diameter of 20 - 50 μm) in different vascular beds from unstimulated WT C57BL/6 mice were captured and analysed.

In all tissues analysed, pericytes were present in post-capillary venules and 3D reconstructed confocal images consistently indicated a discontinuous nature of the pericyte sheath (Figure 3.3) (Voisin et al., 2010). However, a significant diversity existed in terms of pericyte shape and distribution, especially regarding size of gaps between adjacent cells. Confocal images were then analysed to quantify and compare the size of gaps between adjacent pericytes (as described in 2.6.3). The average gap size varied among these tissues ranging from $7.1 \pm 0.6\ \mu m^2$ in the cremaster to $17.2 \pm 2.5\ \mu m^2$ in the mesentery (Figure 3.4 a). Skin (ear) ($8.1 \pm 1.2\ \mu m^2$) and peritoneal wall ($8.2 \pm 2.3\ \mu m^2$) exhibited mean gap sizes similar to the cremaster, whereas mean gap sizes were significantly higher in the diaphragm ($16.4 \pm 2.8\ \mu m^2$) and the mesentery compared to the other three vascular beds (Figure 3.4 a).

Furthermore, the density of gaps was determined, which is the average number of gaps per defined vessel area (per $1\ mm^2$). The investigated vascular beds exhibited differences in gap density ranging from $11{,}007 \pm 964$ gaps/mm^2 in the mesentery to $27{,}936 \pm 3{,}191$ gaps/mm^2 in the skin of the ear (Figure 3.4 b). Interestingly, cremaster muscle ($14{,}076 \pm 1063$ gaps/mm^2), mesentery, peritoneal wall ($13{,}032 \pm 1{,}803$ gaps/mm^2) and diaphragm ($13749 \pm 3{,}491$ gaps/mm^2) all revealed gap densities around 13,000 gaps/mm^2, whereas the gap density was significantly higher in the skin of the ear. The percentage of venular surface not covered by

pericytes (α-SMA negative area) also varied among all the vascular beds investigated and was calculated as follows:

$$\text{mean gap size } [\text{mm}^2] \times \frac{\text{number of gaps}}{1\,\text{mm}^2} \times 100 = \alpha\text{-SMA negative venular area } [\%]$$

This calculation revealed that the percentage of α-SMA negative venular area varied in the multiple vascular beds ranging from 9.58 ± 0.75 % in the cremaster muscle to 18.19 ± 2.25 % in the mesentery. Therefore, post-capillary venules either exhibited vascular pericyte coverage around 90 % as in cremaster muscle and peritoneal wall (α-SMA negative venular area: 9.58 ± 0.75 % and 10.15 ± 1.63 %, respectively) or around 82 % as seen for mesentery, skin (ear) and diaphragm (α-SMA negative venular area: 18.19 ± 2.25 %, 17.82 ± 2.40 % and 17.87 ± 1.92 %, respectively). This suggests the existence of a wide range of vascular pericyte coverage, as previously detailed in other species (Diaz-Flores et al., 1991; Shepro and Morel, 1993; Egginton et al., 1996). Of interest, the low percentage of vascular pericyte coverage in the skin (ear) resulted from a significantly higher gap density compared to the other tissues, whereas the low values observed for mesentery and diaphragm were due to a significantly higher mean gap size in these tissues as compared to the other vascular beds.

All the tissues investigated were also stained for type IV collagen to visualise the vascular basement membrane. Our group previously reported that the localization of gaps between adjacent pericytes in cremasteric post-capillary venules is directly in line with regions of low matrix protein deposition within the basement membrane (termed low expression regions, LE regions or LERs) (Wang et al., 2006). The findings of the present study demonstrate that the average size and density of type IV collagen LERs was directly in line with the average size and density of gaps in the pericyte layer in all the vascular beds examined (Figure 3.5 and Figure 3.6) (Voisin et al., 2010).

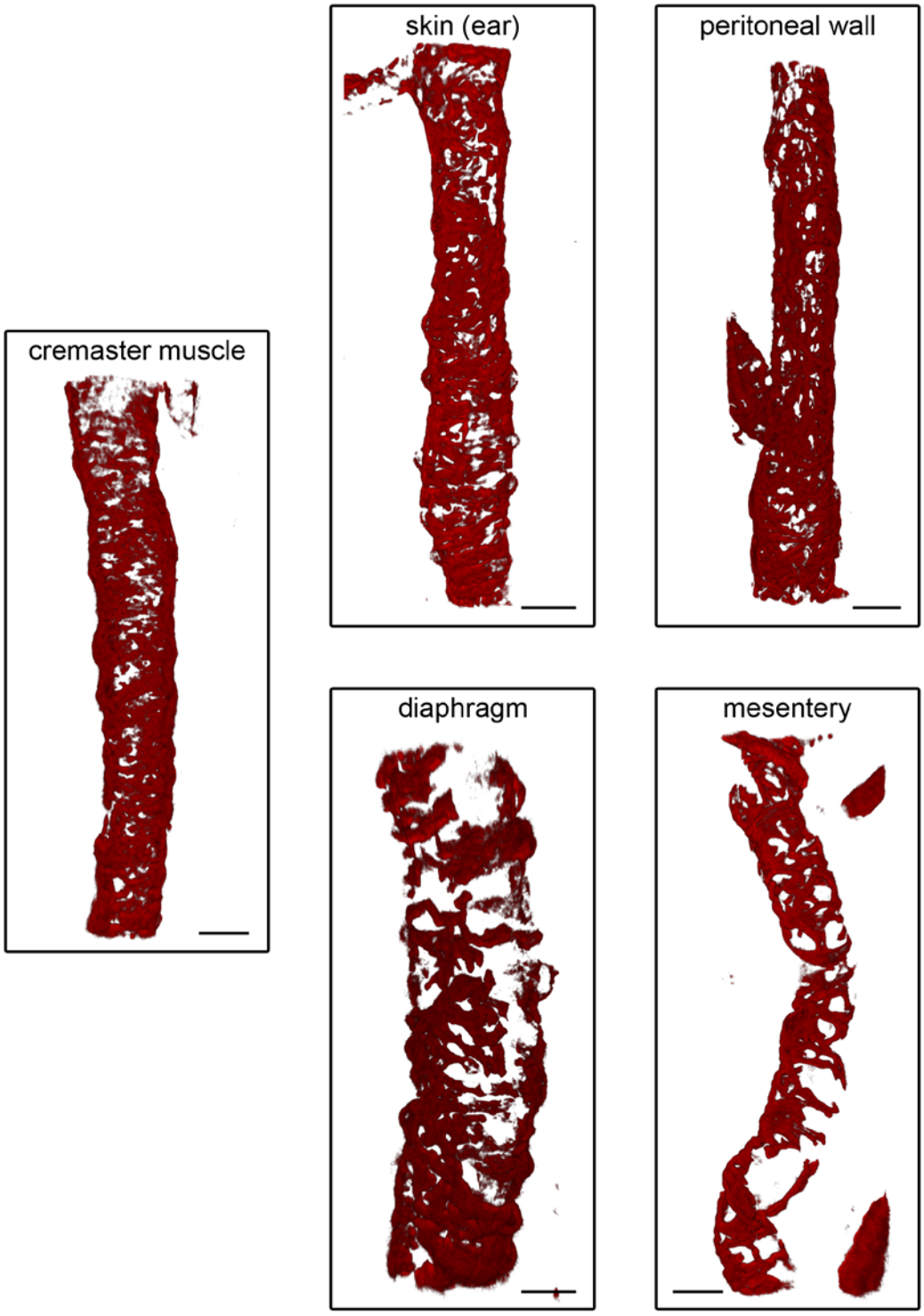

Figure 3.3: Differences in pericyte shape and coverage in various vascular beds in the mouse. Tissues were isolated from unstimulated WT C57BL/6 mice, fixed and immunostained for α-SMA to visualise pericytes. Representative 3D-reconstructed longitudinal confocal image sections of post-capillary venules from the indicated vascular beds are shown. Bars, 20 μm.

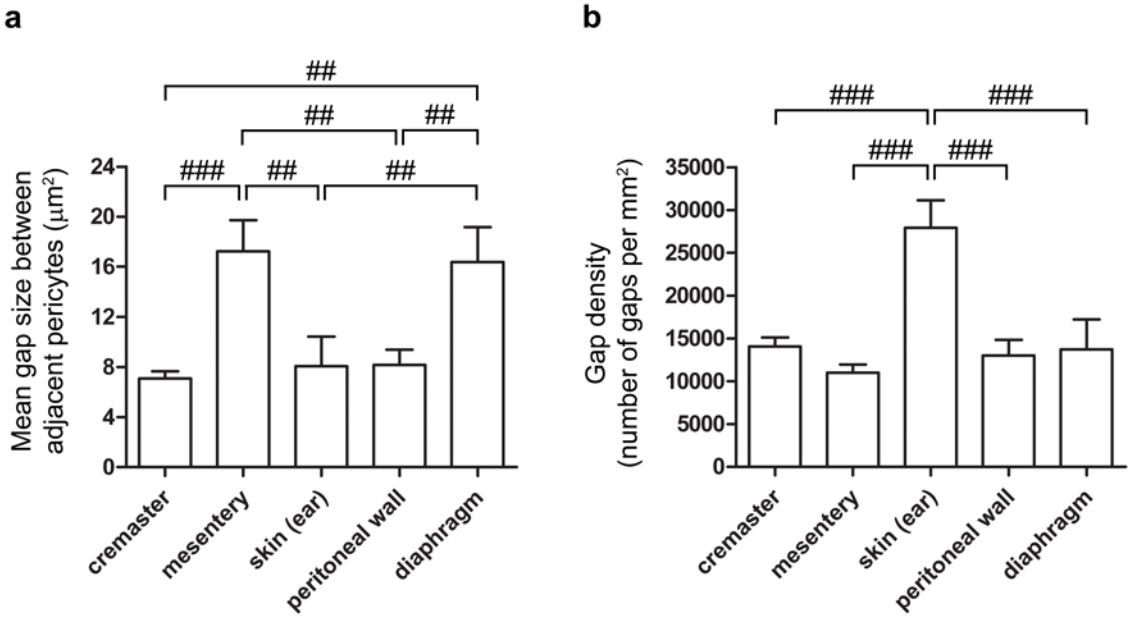

Figure 3.4: Mean size and density of gaps between adjacent pericytes in post-capillary venules in different murine vascular beds. Indicated tissues were isolated from unstimulated WT C57BL/6 mice, fixed and immunostained for α-SMA to visualize pericytes. Confocal images of post-capillary venules were acquired and subsequently 3D-reconstructed longitudinal image sections were analysed to determine the mean gap size and gap density per vessel (quantified as described in 2.6.3). (a) Mean gap size between adjacent pericytes. (b) Gap density represents the number of gaps per defined vessel area (per mm^2). In both graphs, for each bar a minimum of three up to nine mice were used. Overall, per vascular bed at least eight vessels were analysed. Significant differences between vascular beds were determined using one way Anova and are indicated by ## ($p < 0.01$) and ### ($p < 0.001$).

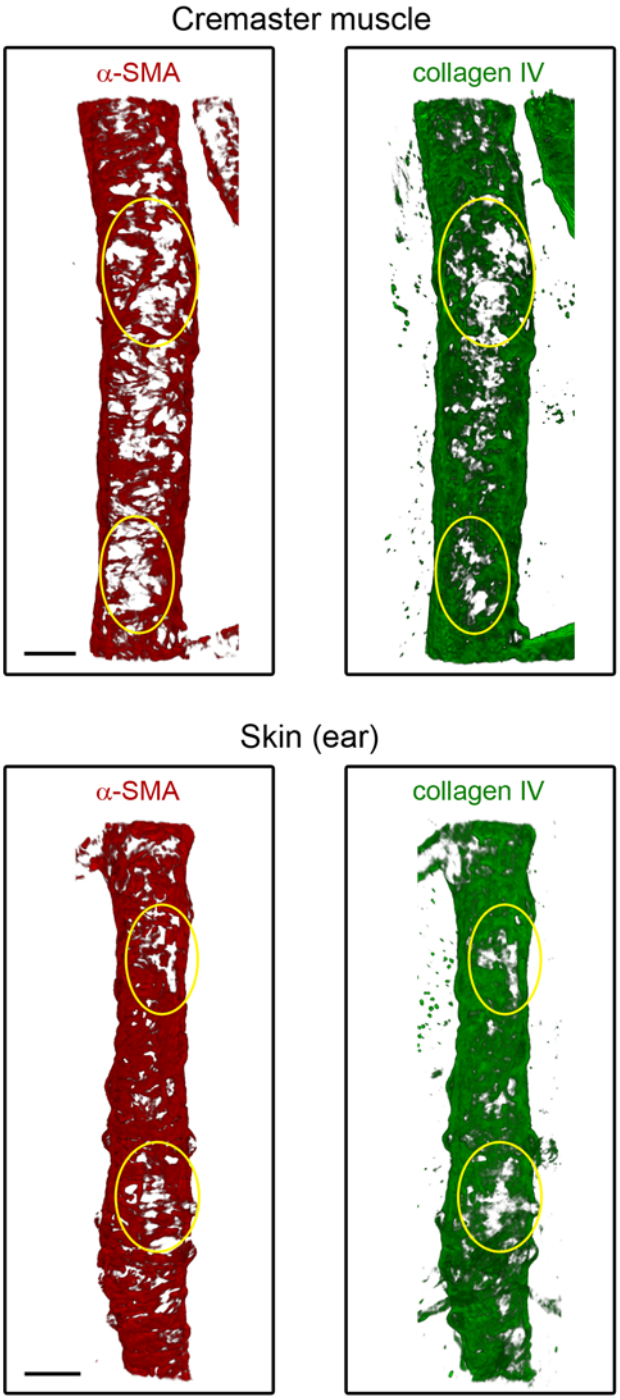

Figure 3.5: Association of pericyte gaps and collagen type IV low expression regions in the cremaster muscle and the skin (ear). Tissues were isolated from unstimulated WT C57BL/6 mice, fixed and immunostained for α-SMA and collagen type IV to visualise pericytes and the vascular basement membrane, respectively. Representative 3D-reconstructed longitudinal confocal image sections of post-capillary venules are shown. Bars, 20 μm.

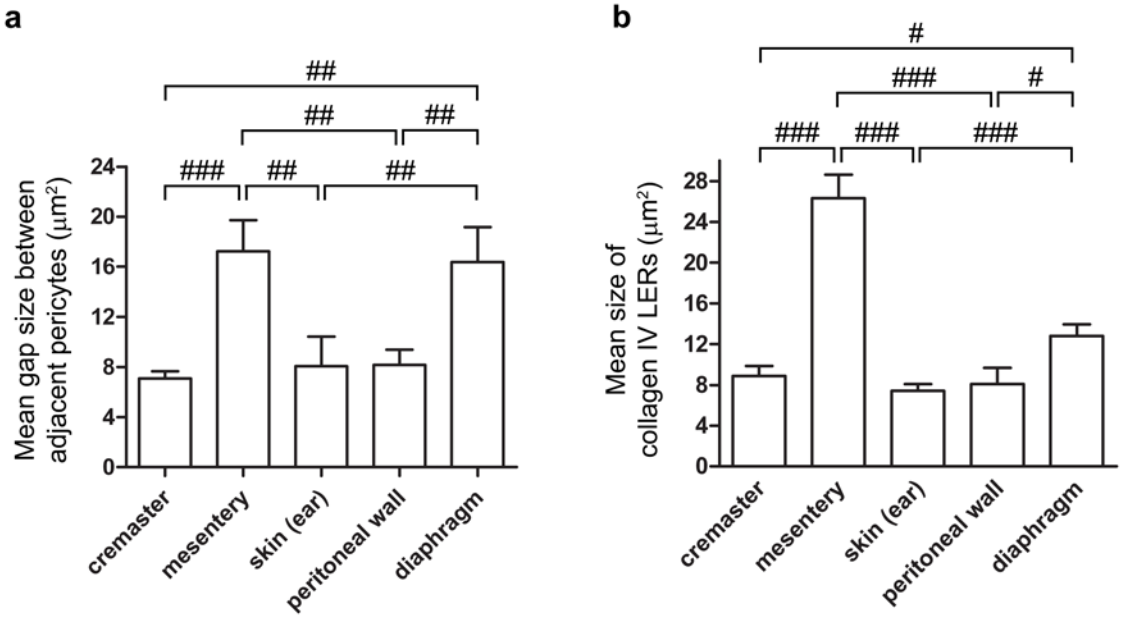

Figure 3.6: Association of the mean size of pericyte gaps and the mean size of collagen type IV LERs in post-capillary venules from different murine vascular beds. Indicated tissues were isolated from unstimulated WT C57BL/6 mice, fixed and immunostained for α-SMA and collagen type IV to visualise pericytes and the vascular basement membrane, respectively. Confocal images of post-capillary venules were acquired and subsequently 3D-reconstructed longitudinal image sections were analysed to determine the mean gap size and the mean size of collagen type IV LERs (quantified as described in 2.6.3). (a) Mean gap size between adjacent pericytes as shown in Figure 3.4a. (b) Mean size of collagen type IV LERs. In both graphs, for each bar a minimum of three up to nine mice were used. Overall, per vascular bed at least eight vessels were analysed. Significant differences between vascular beds were determined using one way Anova and are indicated by # ($p < 0.05$), ## ($p < 0.01$) and ### ($p < 0.001$).

3.3 Discussion

In this chapter, pericyte phenotypes such as marker expression and morphology were investigated in different types of blood vessels in the cremaster muscle. Additionally, pericyte morphology was compared in post-capillary venules of various vascular beds.

To find a highly expressed pericyte marker for analysis of pericyte morphology in the mouse cremaster muscle, the labelling of pericytes as achieved by antibodies directed against α-SMA and NG2 was investigated. These are two commonly used pericyte markers. α-SMA was found to be highly expressed by pericytes surrounding post-capillary and collecting venules as well as by smooth muscle cells tightly covering the endothelium of arterioles, arteries and veins confirming previous studies using rat mesentery, bovine retina and mouse pancreas (Nehls and Drenckhahn, 1991; Morikawa et al., 2002). Capillary pericytes showed weak or no expression of α-SMA. The pericyte/neural cell surface marker NG2 was strongly expressed on capillary pericytes, smooth muscle cells and nerves, but not on pericytes of post-capillary venules. These differences in NG2 expression had also been observed in a previous study using various rat tissues (Murfee et al., 2005).

Other known pericyte markers include desmin, PDGFR-β, antigen of the antibody 3G5, endosialin (CD248) and CD146. Desmin and PDGFR-β were expressed at very low levels in cremasteric post-capillary venular pericytes and no staining could be detected using the 3G5 antibody. The inability of the 3G5 antibody to detect pericytes in the mouse cremaster muscle could be caused by either the absence of this antigen in the mouse or a lack of cross-reactivity with the murine antigen. Unfortunately, murine as well as human endosialin is only expressed in embryonic and tumour-associated pericytes (Rupp et al., 2006; Bagley et al., 2008; Simonavicius et al., 2008) and CD146 is expressed in numerous cell types in mice and humans including endothelial cells (Bardin et al., 2001; Elshal et al., 2005; Despoix et al., 2008; Schrage et al., 2008). Due to these findings and because we found α-SMA to be highly expressed in cremasteric post-capillary venules, α-SMA was used for the rest of this study as a marker to visualise pericytes on post-capillary venules in the murine cremaster muscle as well as in various other murine tissues.

As a result of the lack of highly specific pericyte markers different pericyte reporter mice have been generated including promoter-trap transgene XlacZ4 mice (Tidhar et al., 2001), Anxa5-lacZ mice (Brachvogel et al., 2005; Brachvogel et al., 2007), RGS5-GFP mice (Nisancioglu et al., 2008), α-SMA-GFP mice (Yokota et al., 2006) and α-SMA-RFPcherry mice (see 2.1.1). α-SMA-GFP mice and α-SMA-RFPcherry mice are transgenic mice, which express the Green Fluorescent Protein (GFP) or the more recently described cherry variant of the Red Fluorescent Protein (RFPcherry) under the control of the α-SMA promoter, respectively. α-SMA-GFP and α-SMA-RFPcherry mice were used for direct *in vivo* real time imaging of post-capillary pericytes, because we found α-SMA to be highly expressed in cremasteric post-capillary venular pericytes and by using a fluorescent protein as reporter no additional staining step with fluorescent X-gal is required (results produced using these mice are described in Chapters 6).

In common with pericyte marker expression, differences were also evident in pericyte shape on the different vessel types in the cremaster muscle. Capillary pericytes showed an elongated cell body consisting of two major processes from which numerous small processes originated. This has also been reported in an electron microscopic study looking at rat submandibular glands, which named the two types of processes primary/longitudinal and secondary/circumferential processes (Shimada et al., 1992). Pericytes in post-capillary venules were irregular in shape and orientation and exhibited multiple major processes forming a discontinuous layer with gaps between adjacent cells, confirming observations that had previously been made using the mouse cremaster muscle (Wang et al., 2006) and pancreas (Morikawa et al., 2002). Pericytes on collecting venules exhibited many major processes, however, mainly arranged circumferentially. Due to this difference in morphology, the pericyte coverage of the underlying endothelium also varied between the different vessel types.

By investigating pericyte phenotypes in the mouse cremaster muscle, I discovered that the transition between different pericyte phenotypes happens gradually. Characteristic capillary pericytes express no α-SMA, but show high NG2 expression whereas post-capillary pericytes contain high amounts of α-SMA, but are NG2 negative. However, pericytes on the venous side of the capillary occasionally exhibited weak α-SMA staining. Both α-SMA negative capillary pericytes and

capillary pericytes expressing α-SMA weakly showed low to high NG2 expression representing various intermediate pericyte phenotypes between post-capillary and capillary pericytes. Additionally, a continuum of cell shapes existed between "classic" pericyte shapes characteristic for a certain vessel type as well as among pericytes and smooth muscle cells. Gradual pericyte phenotype transition has to date only been observed with regard to pericyte shape (Shimada et al., 1992). A gradual transition of pericytes to smooth muscle cells has been reported on the arterial side of capillaries, where capillary pericytes exhibit large, band-like, circumferential processes completely encircling the vessel (Shimada et al., 1992). This study, investigating thyroid glands and cardiac muscles of Japanese monkeys, even distinguishes three types of capillary pericytes based on their shape: Mid-capillary pericytes with two major longitudinal processes (Type I), pericytes on the arterial side of the capillary with large, band-like, circumferential processes (Type II) and pericytes on the venous side of the capillary with short irregular processes (Type III).

Pericyte morphology was also compared among post-capillary venules of different vascular beds, such as the cremaster muscle, the mesentery, the skin of the ear, the peritoneal wall and the diaphragm using immunofluorescence staining and confocal microscopy of whole mounted tissues. This study demonstrated in all vascular beds investigated, that the pericyte layer surrounding post-capillary venules is discontinuous with significant gaps between adjacent cells (Voisin et al., 2010). However, a significant diversity in pericyte shape and coverage was noted among these tissues, resulting in different mean size and density of gaps between pericytes. This highlights the existence of a wide range of vascular pericyte coverage, which has been reported previously to differ among organs (Diaz-Flores et al., 1991; Shepro and Morel, 1993; Egginton et al., 1996). Additionally, the ratio of pericytes to endothelial cells varies in different vascular beds ranging from 1:1 to 1:100. The retina exhibits one of the highest ratios of 1:3, but the highest pericyte abundance is found in the CNS (Shepro and Morel, 1993; Armulik et al., 2005).

Post-capillary venules of the mesentery for example showed the highest mean gap size but revealed the lowest gap density. Therefore, this tissue had the highest percentage of α-SMA negative vascular area meaning it exhibited the lowest percentage of vascular pericyte coverage. Skin (ear) and diaphragm showed similar percentages of vascular pericyte coverage. The low pericyte coverage in the

diaphragm was also a result of the significantly higher mean gap size, whereas in the skin of the ear it resulted from a gap density, which was significantly higher than in all other tissues investigated. Low percentage of α-SMA negative vascular area resulting in a higher percentage of venular pericyte coverage was seen in the cremaster and the peritoneal wall and these tissues exhibited low values for both mean gap size and pericyte density. This diversity could lead to differences in pericyte function and vascular permeability as well as contribute to tissue-specific mechanisms of leukocyte transmigration, which has been discussed in relation to the functional needs of different organs (Butcher and Picker, 1996; Petri et al., 2008). Therefore, the existence of pronounced gaps between adjacent pericytes within the mesentery may support the highly pathogenic environment of the intestine by reducing barrier function to emigrating leukocytes to control the dissemination of invasive pathogens as compared with an inflammatory response in an organ less prone to infection such as the cremaster muscle.

Co-staining all the tissues investigated for the vascular basement membrane component type IV collagen revealed that pericyte gaps corresponded to LERs. Hence, pericyte coverage is likely to be the determinant in collagen type IV deposition around these vessels. We obtained similar results by investigating laminin-511, which is another key basement membrane protein (Voisin et al., 2010). In this study, the expression profile of laminin-511 and collagen IV in cremasteric post-capillary venules was also compared with other components of the vascular basement membrane such as laminin-411, nidogen, and perlecan. Interestingly, all basement membrane proteins investigated are also expressed in a heterogeneous manner exhibiting LERs and are directly aligned with gaps between adjacent pericytes except for perlecan LERs, which could be observed at pericyte positive regions. These findings suggest that pericytes are an important source for most of the vascular basement membrane components *in vivo* and that their venular coverage determines the properties of the venular basement membrane. Several *in vitro* studies have shown that pericytes can generate key basement membrane constituents such as collagen IV, laminin and fibronectin (Cohen et al., 1980; Mandarino et al., 1993; Stratman et al., 2009). Therefore, the two main cell types linked to the generation of the venular basement membrane are endothelial cells and pericytes, however, differences may exist between the relative contributions of these two cell types to the

different basement membrane components. Perlecan LERs were mainly located at venular regions covered by pericytes indicating that pericytes are not involved in the generation of this basement membrane component despite its heterogenous expression profile forming LERs.

Of importance, previous findings from our group have shown that in response to IL-1β, transmigrating neutrophils preferentially use the permissive sites formed by pericyte gaps and aligned LERs illustrating a functional implication of pericyte coverage (Wang et al., 2006). Hence, pericytes represent an additional barrier for emigrating leukocytes and therefore play an important role during inflammatory conditions. The potential role of pericytes in inflammatory conditions was investigated further and the results are detailed in the following Chapters.

Chapter 4: Analysis of pericyte shape change in TNF-α- and IL-1β-stimulated tissues *in vivo*

4.1 Introduction

Despite the improved understanding of the mechanisms involved in leukocyte transmigration through the endothelium in inflammatory conditions, at present very little is known about the mechanisms by which leukocytes penetrate the residual components of the vessel wall, the pericyte sheath and the vascular basement membrane. Our group has previously shown that transmigrating leukocytes preferentially use permissive sites formed by gaps in the pericyte layer combined with aligned regions of low matrix protein deposition in the vascular basement membrane (termed low expression regions, LE regions or LERs) to migrate through venular walls (Wang et al., 2006; Voisin et al., 2009; Voisin et al., 2010). However, the role of pericytes during inflammatory conditions remains unknown.

The aim of this chapter was to elucidate potential pericyte responsiveness to pro-inflammatory stimuli. The murine cremaster muscle was chosen to extend investigations of pericyte morphology to inflammatory scenarios, because it permitted direct comparison of data obtained by *ex vivo* immunofluorescence staining and confocal analysis with real-time analysis of leukocyte transmigration as observed by intravital microscopy. Pericyte response - shape change - was investigated using inflammatory mediators such as the pro-inflammatory cytokines TNF-α and IL-1β, the chemokine CCL2, the chemoattractant LTB_4 and the disease model Ischemia Reperfusion (I/R) Injury. Furthermore, the effects of TNF-α and IL-1β were examined in an additional vascular bed - the skin of the ear - to explore the possibility of tissue-specific mechanisms. Subsequently, the effects of TNF-α and IL-1β were further characterised over time in the cremaster muscle and changes in pericyte shape were associated with neutrophil transmigration in the same tissues. In addition, the involvement of neutrophils in TNF-α- and IL-1β-induced pericyte shape change was examined using neutrophil depleted animals. To elucidate whether pericytes are able to respond directly to TNF-α- and IL-1β, the expression profile of IL-1RI, TNFRI and TNFRII on post-capillary venules in unstimulated cremaster muscles was analysed by immunofluorescence staining and confocal microscopy.

4.2 Results

4.2.1 Pericyte shape change in different inflammatory scenarios in the murine cremaster muscle

To study the response of pericytes in murine cremasteric post-capillary venules to different inflammatory mediators, cremaster muscles were stimulated either via topical application of the chemokine CCL2 or the chemoattractant LTB_4 or local injection of the inflammatory cytokines TNF-α or IL-1β or by induction of I/R injury. Dose and *in vivo* test periods employed were those known to elicit significant leukocyte transmigration in this model based on previous findings from our group. Subsequently, the cremaster muscles were dissected away from the mice, fixed and used whole mounted for immunofluorescence labelling and confocal analysis.

Local injection of TNF-α or IL-1β (300 ng or 50 ng in 400 µl saline, respectively) induced pericyte shape change resulting in an enhancement of gaps between adjacent cells (Figure 4.1 a). Confocal images were then analysed to determine the mean size of gaps between adjacent pericytes (as described in section 2.6.3). Saline injection (vehicle control) resulted in a mean gap size of $8.3 \pm 0.4\ \mu m^2$ and no significant changes were observed (unstimulated cremasters: $7.2 \pm 0.4\ \mu m^2$) (Figure 4.1 b). TNF-α and IL-1β stimulation led to a significant increase in mean gap size between adjacent pericytes compared to unstimulated and saline-injected controls. In comparison to saline injection alone, TNF-α stimulation for 2 h provoked a significant 65 % increase in mean gap size to $13.8 \pm 0.9\ \mu m^2$ and after 4 h stimulation with IL-1β a significant 63 % increase to $13.6 \pm 0.7\ \mu m^2$ could be seen ($p < 0.001$ for both).

Superfusion of exteriorised cremaster muscles with the chemokine CCL2 or the chemoattractant LTB_4 (10^{-7} M or 5×10^{-9} M in Tyrode's salt solution, respectively) for 2 h elicited no change in pericyte shape (Figure 4.2 a). Image analysis confirmed that topical application of CCL2 and LTB_4 induced no significant change in mean gap size between adjacent pericytes ($8.1 \pm 0.8\ \mu m^2$ and $8.9 \pm 1.0\ \mu m^2$, respectively) (Figure 4.2 b). Superfusion with Tyrode's salt solution alone (vehicle control) also evoked no significant change in mean gap size ($9.0 \pm 1.2\ \mu m^2$).

After I/R injury (30 min Ischemia followed by 2 h reperfusion under constant superfusion with Tyrode's salt solution) cremasteric post-capillary venules exhibited the most striking change in pericyte shape with large gaps between adjacent pericytes (Figure 4.3 a). Gap size quantifications revealed that I/R injury resulted in a 119 % enlargement of pericyte gaps (19.7 μm2 ± 4.8 μm^2) compared to sham operated cremasters (9.0 ± 1.2 μm^2) and a significant 175 % increase in mean gap size compared to unstimulated cremasters (Figure 4.3 b). The I/R tissues were prepared by Dr. Abigail Woodfin and Dr. Mathieu-Benoit Voisin.

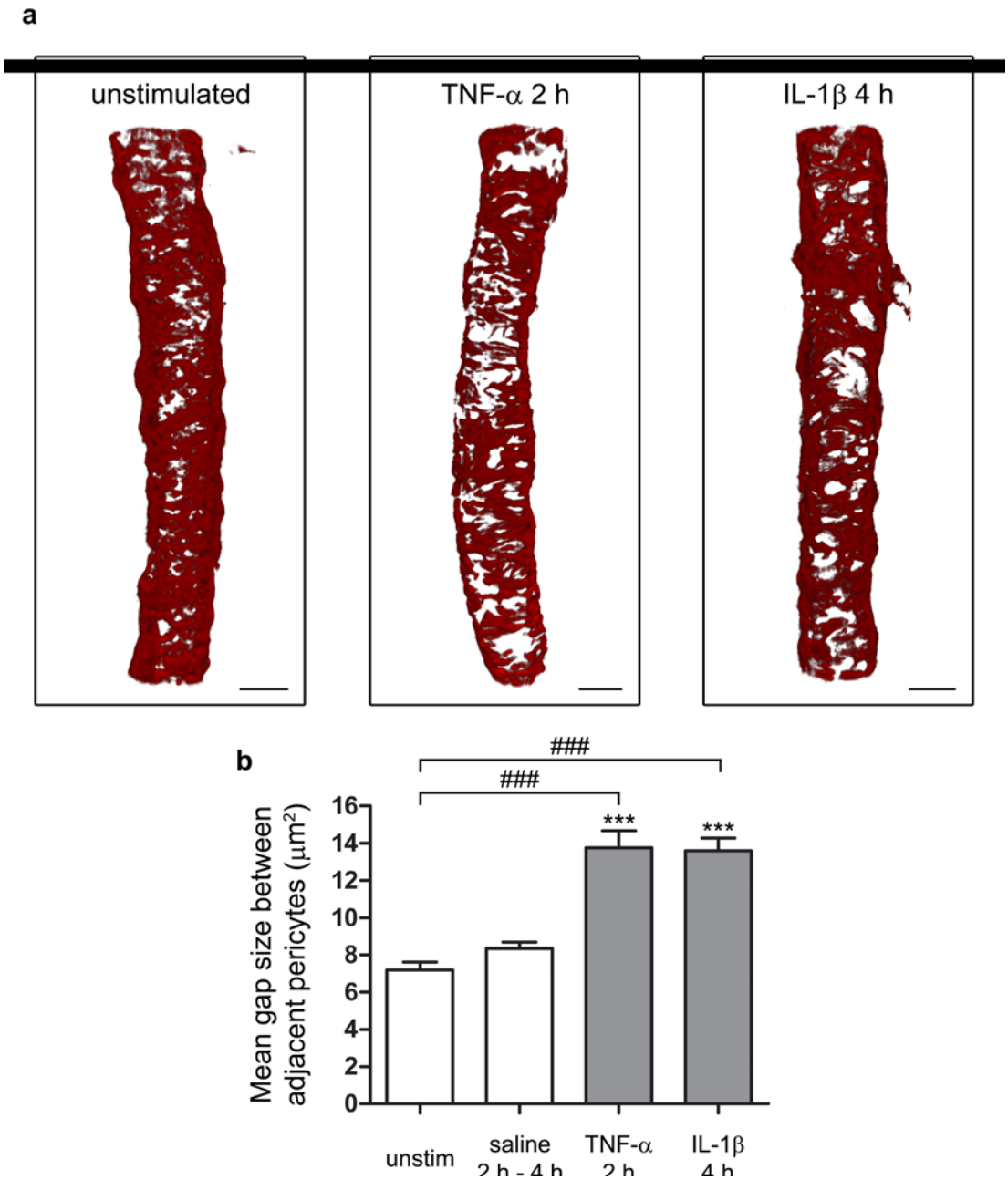

Figure 4.1: Shape change of pericytes in cremasteric post-capillary venules after TNF-α and IL-1β stimulation. Inflammatory conditions were induced in WT C57BL/6 mice via i.s. injection of TNF-α or IL-1β (300 ng or 50 ng in 400 µl saline, respectively). As controls, unstimulated and saline injected cremasters were used. After the *in vivo* test periods indicated cremasters were dissected, fixed and immunostained (α-SMA) for confocal analysis. (a) The panels show representative 3D-reconstructed longitudinal confocal image sections of post-capillary venules. Bars, 20 µm. (b) The graph shows the mean gap size between adjacent pericytes in μm^2 (quantified as described in 2.6.3). Per cremaster at least three vessels were analysed and the mean gap size was determined per vessel. Afterwards, the mean gap size per mouse was plotted. Each bar represents results from at least three mice. White bars represent control samples and grey bars correspond to stimulated cremasters. Significant differences between groups were determined using one way Anova. Compared to unstimulated controls significant differences are indicated by ### ($p < 0.001$). Significant differences from cremasters injected with vehicle control (saline) are indicated by *** ($p < 0.001$).

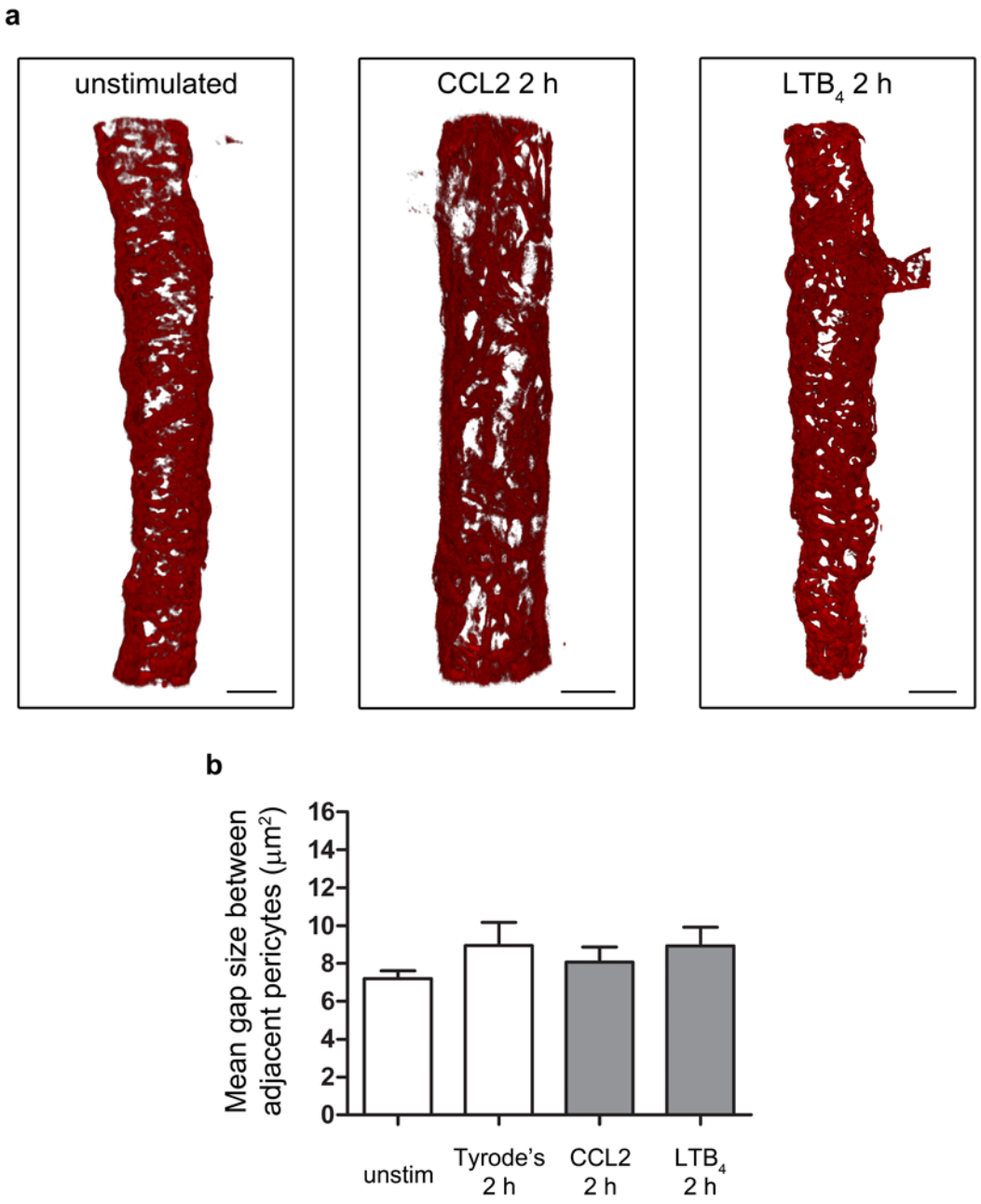

Figure 4.2: Morphology of pericytes on cremasteric post-capillary venules after CCL2 and LTB_4 stimulation. Inflammatory conditions were induced in WT C57BL/6 mice via topical application of LTB_4 or CCL2 (10^{-7} M or 5×10^{-9} M in Tyrode's solution, respectively) onto the exteriorised cremaster muscle. As controls, unstimulated cremasters and cremasters superfused with Tyrode's solution alone were used. After the *in vivo* test periods indicated cremasters were dissected from the mice, fixed and immunostained (α-SMA) for confocal analysis. (a) The panels show representative 3D-reconstructed longitudinal confocal image sections of unstimulated, CCL2- and LTB_4-stimulated post-capillary venules. Bars, 20 µm. (b) The graph shows the mean gap size between adjacent pericytes in μm^2 (quantified as described in 2.6.3). Per cremaster at least three vessels were analysed and the mean gap size was determined per vessel. Afterwards, the mean gap size per mouse was plotted. Each bar represents results from at least three mice. White bars represent control samples and grey bars correspond to stimulated cremasters. Significant differences between groups were investigated using one way Anova.

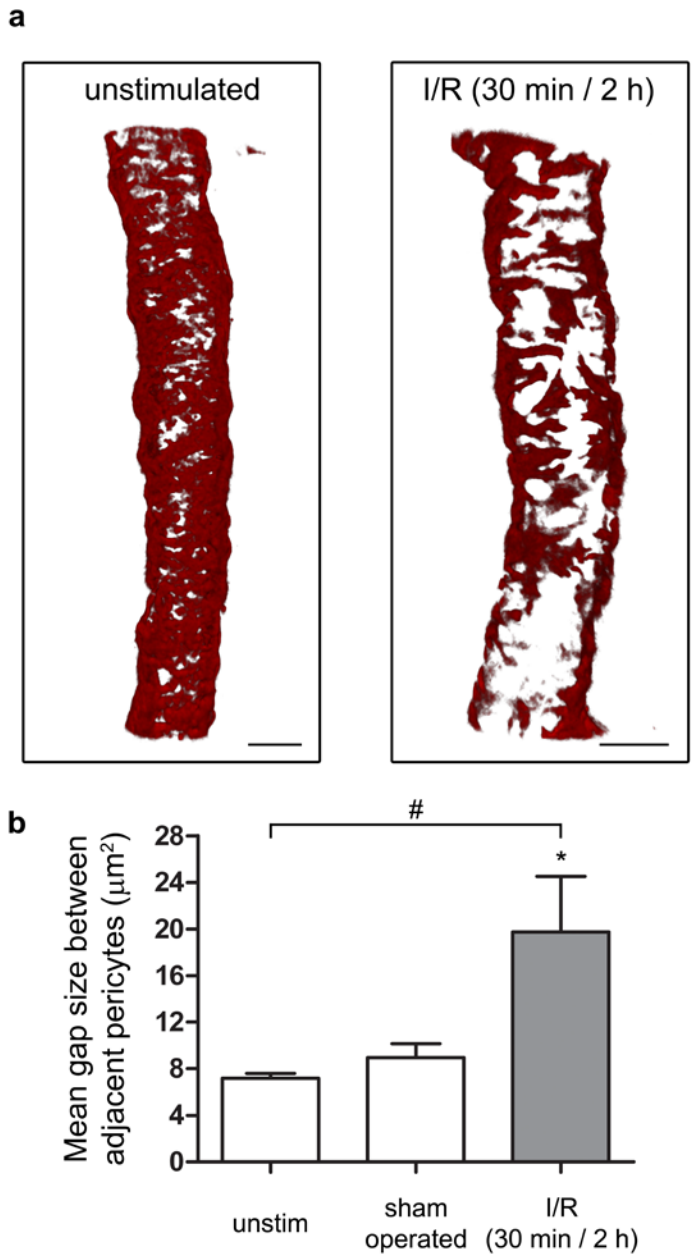

Figure 4.3: Response of pericytes on cremasteric post-capillary venules to I/R injury. Ischemia was induced in WT C57BL/6 mice by placing an artery clamp at the base of the cremaster (for 30 min). This was followed by 2 h of reperfusion under constant superfusion with Tyrode's salt solution. As control, unstimulated cremaster muscles and sham operated cremasters were used. After a 2 h reperfusion period, cremaster muscles were dissected from the mice, fixed and immunostained (α-SMA) for confocal analysis. (a) The panels show representative 3D-reconstructed longitudinal confocal image sections of post-capillary venules. Bars, 20 µm. (b) The graph shows the mean gap size between adjacent pericytes in μm^2 (quantified as described in 2.6.3). Per cremaster at least three vessels were analysed. Afterwards, the mean gap size per mouse was determined and plotted. Each bar represents data from at least four mice. White bars represent control samples and grey bars correspond to stimulated cremasters. Significant differences between groups were determined using one way Anova. Compared to unstimulated controls significant differences are indicated by # ($p < 0.05$) and significant differences from sham operated cremasters are indicated by * ($p < 0.05$).

4.2.2 Effects of TNF-α and IL-1β on pericyte morphology in the dorsal skin of the ear

Based on the findings described in 4.2.1, which showed a significant enhancement of gaps between adjacent pericytes in cremasteric post-capillary venules, the responses induced by TNF-α and IL-1β were investigated in more detail. Initially, to investigate whether there is evidence for tissue-specific mechanisms, the effects of TNF-α and IL-1β on pericyte shape change were analysed in the skin of the ear. The skin of the ear was chosen for this purpose because, like the cremaster muscle, it is a thin and transparent tissue and can therefore be used whole mounted for confocal microscopy. In addition, the pericyte sheath in this tissue exhibited the same mean gap size as in the cremaster but showed a significantly higher density of gaps, which resulted in an almost 2-fold higher percentage of pericyte gap coverage (see Chapter 3). Therefore, it is interesting to investigate whether this difference has an effect on pericyte shape change during inflammatory scenarios.

The dose and *in vivo* test periods that were used with TNF-α and IL-1β in the ear skin where those that had led to significant leukocyte transmigration in preliminary experiments. Hence 150 ng TNF-α or 10 ng IL-1β (both in 30 µl PBS) were injected intradermally and ears were dissected away from the mice after 2 h or 4 h, respectively. Subsequently, the skin was separated from the cartilage, fixed and used whole mounted for immunofluorescence labelling and confocal microscopy.

Intradermal injection of TNF-α or IL-1β induced pericyte shape change as seen in the cremaster muscle leading to an enhancement of gaps between adjacent cells (Figure 4.4 a). Confocal images were then analysed to determine the mean size of gaps between adjacent pericytes. PBS injection (vehicle control) resulted in a mean gap size of 8.1 ± 0.5 µm^2 causing no significant change in mean gap size compared to unstimulated skins (8.1 ± 2.4 µm^2) (Figure 4.4 b). TNF-α and IL-1β stimulation led to a significant increase in mean gap size between adjacent pericytes in comparison to PBS injection alone. After 2 h stimulation with TNF-α a significant 69 % increase in mean gap size to 13.8 ± 2.0 µm^2 could be observed and 4 h IL-1β stimulation induced a significant 94 % increase to 15.7 ± 2.1 µm^2 ($p < 0.05$ for both). Overall the results indicate that as found in the cremaster muscle, TNF-α and IL-1β can stimulate pericyte shape change in the mouse ear skin.

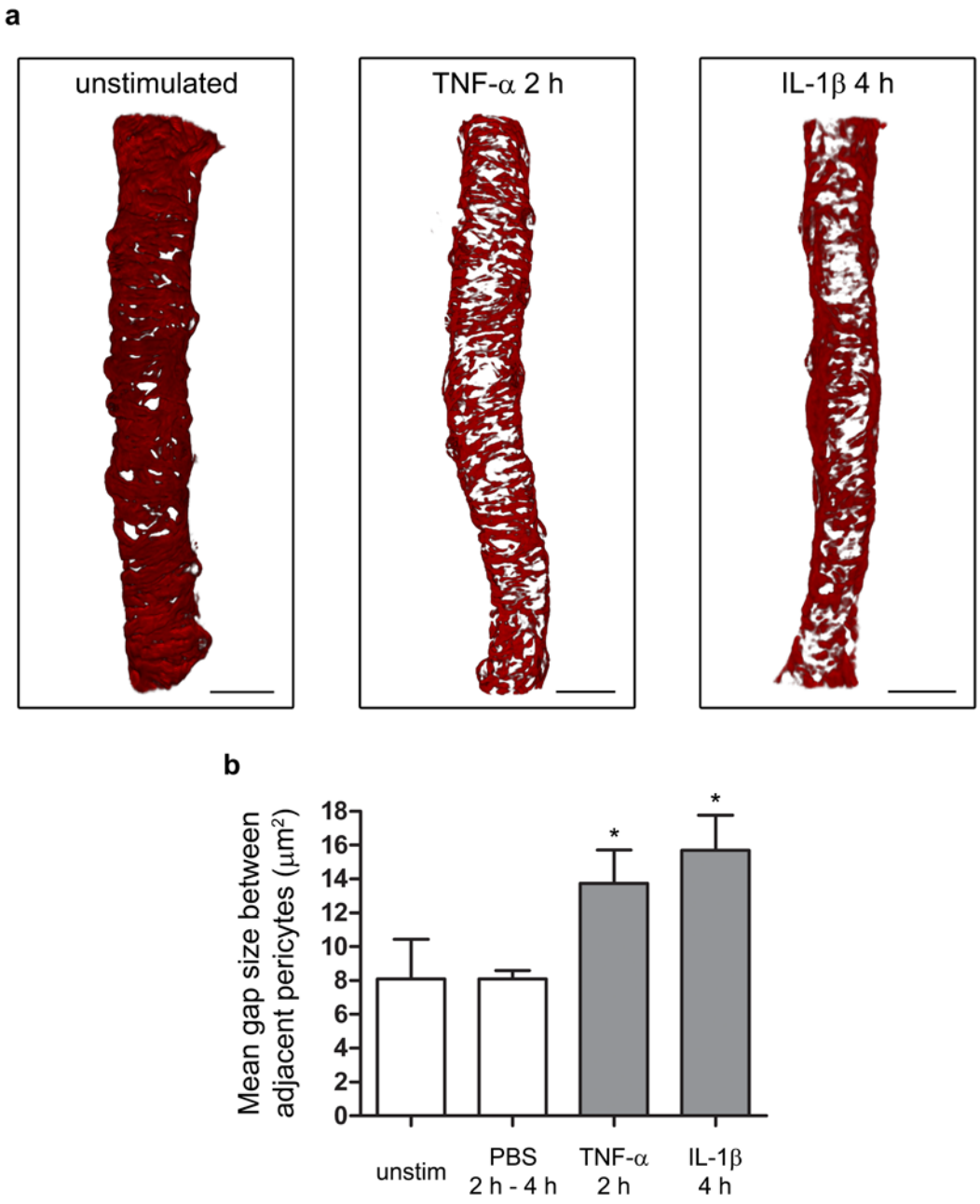

Figure 4.4: Shape change of pericytes in post-capillary venules in the skin of the ear after TNF-α and IL-1β stimulation. Inflammatory conditions were induced in the skin (ear) of WT C57BL/6 mice via i.d. injection of TNF-α or IL-1β (150 ng or 10 ng in 30 µl PBS, respectively). As controls, unstimulated ears and ears injected with PBS alone were used. After the *in vivo* test periods indicated ears were dissected and the skin was separated from the cartilage, fixed and immunostained (α-SMA) for confocal analysis. (a) The panels show representative 3D-reconstructed longitudinal confocal image sections of unstimulated, TNF-α- and IL-1β-stimulated post-capillary venules. Bars, 20 µm. (b) The graph shows the mean gap size between adjacent pericytes in μm^2 (quantified as described in 2.6.3). Each bar represents at least nine vessels. White bars represent control samples and grey bars correspond to stimulated cremaster muscles. Significant differences between groups were determined using one way Anova. Significant differences compared to vehicle controls (PBS) are indicated by * ($p < 0.05$).

4.2.3 Time-course of TNF-α- and IL-1β-induced pericyte shape change in post-capillary venules in the murine cremaster muscle

To further characterise the effects of TNF-α and IL-1β in the cremaster muscle in terms of pericyte shape change, the time-course of response elicited by these cytokines was investigated. For this purpose, TNF-α or IL-1β were injected as describe above and cremaster muscles were dissected from the mice after different *in vivo* test periods, fixed and used whole mounted for immunofluorescence staining and confocal analysis.

The significant change in mean size of gaps between adjacent pericytes upon local injection of both TNF-α and IL-1β occurred in a time-dependent manner (Figure 4.5). Specifically, in TNF-α-stimulated cremaster muscles a change in pericyte shape was already noted at 0.5 h, resulting in a 24 % increase in mean gap size ($10.4 \pm 1.1\ \mu m^2$) compared to saline injected tissues ($8.3 \pm 0.4\ \mu m^2$) (Figure 4.5 a). As described above, after 2 h of TNF-α stimulation a significant 65 % increase in mean gap size could be seen. The observed gap enlargement was a transient response and returned to basal level by 4 h after injection of TNF-α ($8.2 \pm 0.4\ \mu m^2$). IL-1β induced increase in mean gap size was slower in on-set and peaked at 4 h resulting in a significant 63 % gap enlargement (Figure 4.5 b). Time points beyond 4 h indicated a gradual decrease in mean pericyte gap size to $10.6 \pm 0.5\ \mu m^2$ 24 h after IL-1β injection.

The effects of the cytokines on the density of gaps between adjacent pericytes was also determined. This parameter is the average number of gaps per defined vessel area (per $1\ mm^2$) as detailed in Chapter 3 (3.2.3). In the same Chapter, the gap density for unstimulated cremaster muscles was established at $14{,}076 \pm 1{,}063$ gaps/mm^2. Intrascrotal saline injection led to a gap density of $11{,}640 \pm 2{,}844$ gaps/mm^2 and hence induced no significant change (Figure 4.6). In comparison to saline controls, upon local injection of TNF-α or IL-1β the gap density was slightly reduced but not significantly altered at all the time points investigated. The gap densities were in the order of 10,000 gaps/mm^2 for TNF-α injection (Figure 4.6 a) and 10,500 gaps/mm^2 for IL-1β stimulation (Figure 4.6 b). These data suggest that during inflammatory reactions in the cremaster muscle overall neither a

loss nor a generation of new gaps occurred between adjacent pericytes. The existing gaps mainly increased in size, indicating that pericytes have the ability to change their shape in response to these cytokines.

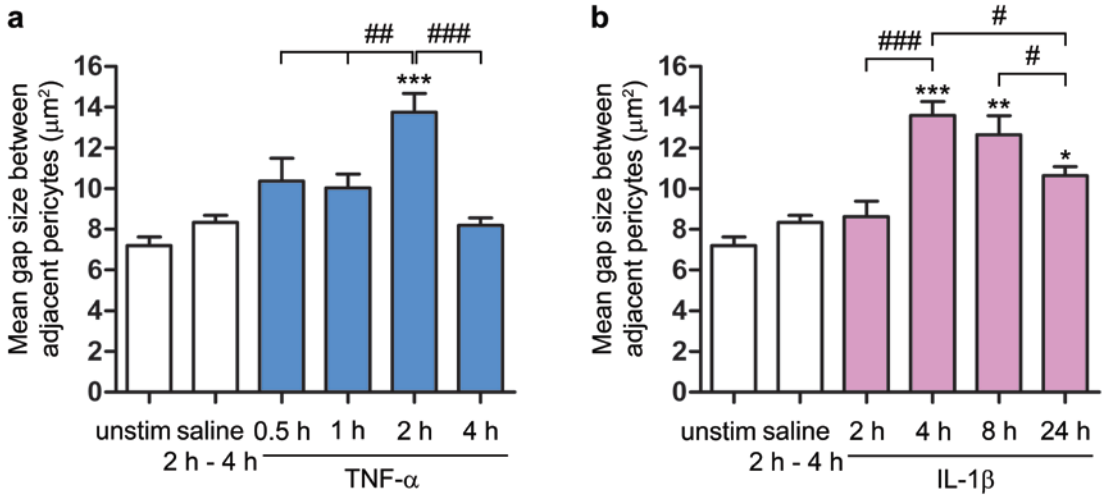

Figure 4.5: Time course of (a) TNF- α- and (b) IL-1β-induced pericyte shape change in the cremaster muscle. TNF-α and IL-1β (300 ng and 50 ng in 400 µl saline, respectively) were injected i.s. into WT C57BL/6 mice. Cremaster muscles were dissected away from the mice after the *in vivo* test periods indicated, fixed and immunostained (α-SMA staining) for confocal analysis. White bars represent unstimulated control samples and blue or pink bars correspond to stimulated cremasters (TNF-α or IL-1β, respectively). Per cremaster at least three vessels were analysed and the mean gap size was determined per vessel. Afterwards, the mean gap size per mouse was plotted. Each bar represents results from at least four mice. Significant differences between groups were determined using one way Anova. Significant differences compared to saline injected controls are indicated by * ($p < 0.05$), ** ($p < 0.01$) and *** ($p < 0.001$). Significant differences between different time periods of stimulation are indicated by # ($p < 0.05$) ## ($p < 0.01$) and ### ($p < 0.001$).

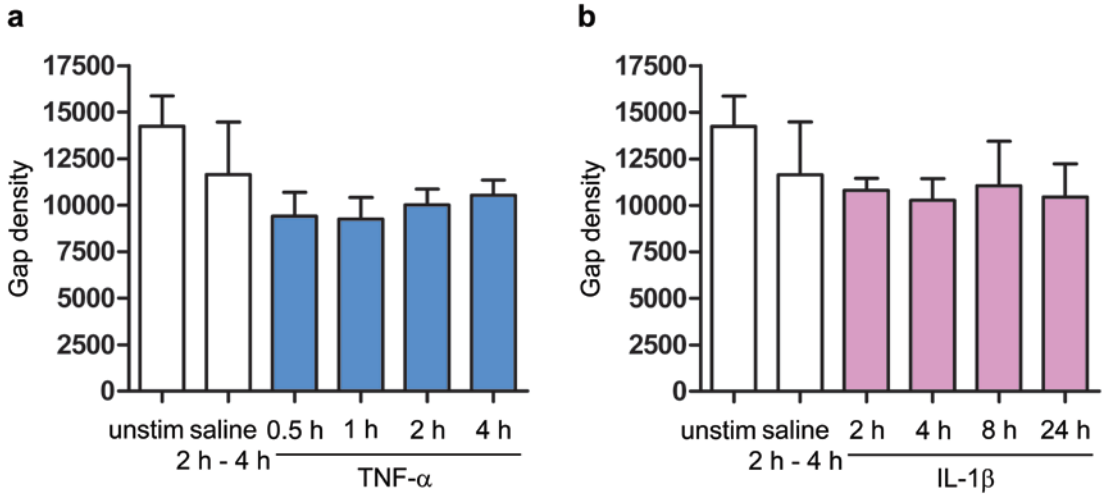

Figure 4.6: Time course of gap density after (a) TNF- α and (b) IL-1β stimulation in the cremaster muscle. Gap density represents the number of gaps per defined vessel area (per mm^2). The confocal images used for analysis were the same as those analysed for Figure 4.5. Significant differences between groups were assessed using one way Anova.

4.2.4 Profile of neutrophil transmigration in TNF-α- and IL-1β-stimulated murine cremaster muscles

All TNF-α- or IL-1β-stimulated cremaster muscles investigated were also stained to visualise neutrophils (MRP-14) to associate the time-dependent enlargement of pericyte gaps in post-capillary venules with the profile of neutrophil transmigration.

Local injection of both TNF-α (300 ng) and IL-1β (50 ng) elicited neutrophil transmigration into the tissue, which also occurred in a time-dependent manner (Figure 4.7, left). TNF-α induced neutrophil transmigration could be detected after 2 h of stimulation and was further increased at the 4 h time point (Figure 4.7 a, left). In this reaction, neutrophil transmigration seemed to be preceded by the enhancement of gaps between adjacent pericytes (Figure 4.7 a, right). As described in section 4.2.3, in TNF-α-stimulated cremasters a change in pericyte shape was noted at 0.5 h, resulting in a 24 % increase in mean gap size compared to saline injected control tissues and after 2 h a significant increase in mean gap size of 72 % could be seen. Within the time-periods investigated, maximum neutrophil transmigration was noted at 4 h post injection of TNF-α, a time-point at which the change in mean pericyte gap size had returned to basal level.

IL-1β induced transmigration peaked at 4 h of stimulation (Figure 4.7 b, left). At this *in vivo* test period the enhancement of gaps between adjacent pericytes was also at its maximum showing a significant 63 % increase in mean gap size compared to saline injected controls (Figure 4.7 b, right). Hence, in this reaction neutrophil transmigration into the tissue was not preceded by pericyte gap enlargement. Time points beyond 4 h appeared to indicate a gradual decrease in mean pericyte gap size and also in the neutrophil transmigration response.

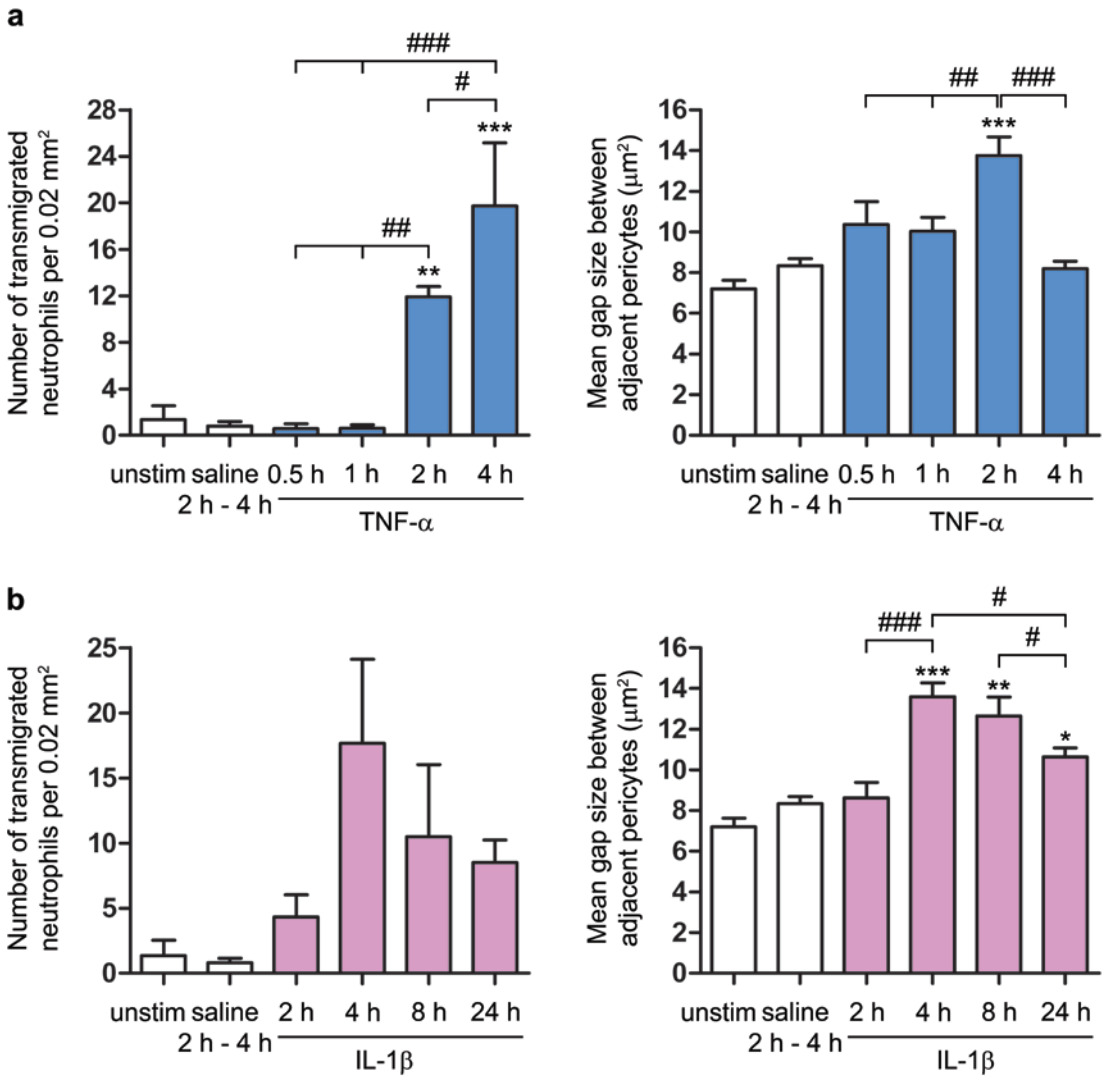

Figure 4.7: Time course of (a) TNF-α- and (b) IL-1β-induced neutrophil transmigration and pericyte shape change in the cremaster muscle. The confocal images used for analysis were the same as those analysed for Figure 4.5. White bars represent unstimulated control samples and blue or pink bars correspond to stimulated cremasters (TNF-α or IL-1β, respectively). Significant differences between groups were determined using one way Anova. Significant differences compared to unstimulated controls are indicated by * ($p < 0.05$), ** ($p < 0.01$) and *** ($p < 0.001$). Significant differences between different time periods of stimulation are indicated by ## ($p < 0.01$) and ### ($p < 0.001$). Left: Number of transmigrated neutrophils per 0.02 mm^2. Transmigrated neutrophils were counted in 3D-reconstructed confocal images and depicted as number of cells per 0.02 mm^2. Per cremaster at least four vessels were analysed. Subsequently, the mean number of transmigrated neutrophils was determined per mouse and plotted. Each bar represents data from at least four mice. Right: Mean gap size graphs, Figure 4.5 re-produced to directly compare changes in mean gap size to the neutrophil transmigration response.

4.2.5 The role of neutrophils in TNF-α- and IL-1β-induced pericyte shape change in the cremaster muscle

As a next step, the involvement of neutrophils in cytokine-induced pericyte shape change was investigated. For this purpose, mice were depleted of their circulating neutrophils using the anti-GR1 antibody RB6-8C5, injected i.p. 24 h prior to local injection of TNF-α and IL-1β and the optimal time points for enhanced pericyte gap sizes were investigated for the two cytokines (i.e. 2 h for TNF-α and 4 h for IL-1β). Neutrophil depletion experiments using IL-1β as a stimulus were performed by Dr. Mathieu-Benoit Voisin.

In neutrophil-depleted mice (but not in control mice, which received an isotype matched control antibody) there was no detectable neutrophil transmigration 2 h after administration of TNF-α. Compared to control mice, neutrophil depleted mice showed a significant increase in mean gap size in the same range at 2 h post administration of TNF-α (control mice: 15.4 $\mu m^2 \pm 1.1$ μm^2, 84 % increase compared to saline injected mice; depleted mice: 13.5 $\mu m2 \pm 0.8$ μm^2, 62 % enlargement) (Figure 4.8). Hence, the results indicate that the increase in mean gap size between adjacent pericytes after TNF-α stimulation (2 h) occurs independently of the presence of neutrophils. Similar results were obtained by Dr. Mathieu-Benoit Voisin, who found that IL-1β induced change in pericyte shape (4 h) occurs independently of neutrophils (data not shown).

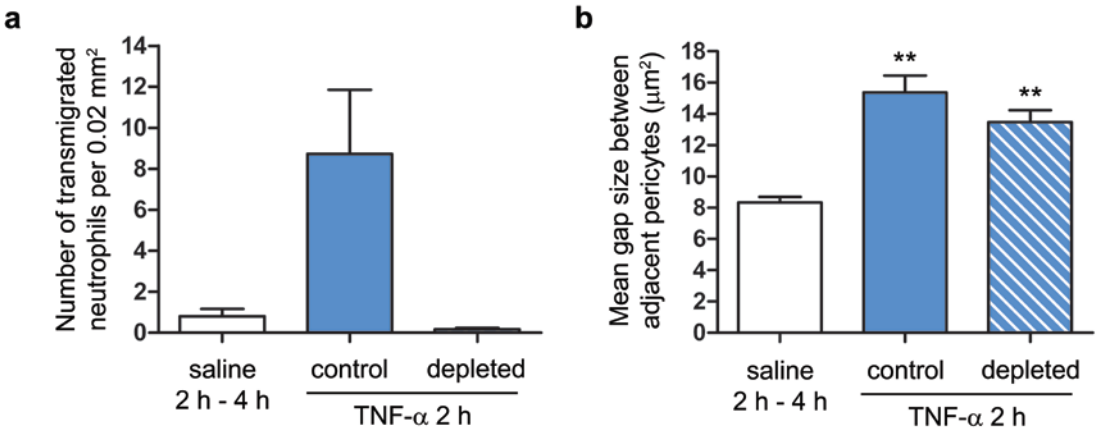

Figure 4.8: TNFα-induced pericyte shape change in the cremaster muscle of neutrophil depleted mice. WT C57BL/6 mice were depleted of their circulating neutrophils via i.p. application of the anti-GR1 antibody RB6-8C5 24 h before i.s. injection of TNF-α (300 ng in 400 µl saline). Control mice were injected i.p. with an isotype matched control antibody (both antibodies were administered at 100 mg/ml). After 2 h of TNF-α stimulation, cremaster muscles were dissected away from the mice, fixed and immunostained for confocal analysis (MRP-14 and α-SMA staining to visualise neutrophils and pericytes, respectively). White bars represent saline-injected controls, blue bars correspond to TNF-α stimulated mice, which received the isotype control antibody, and striped bars depict neutrophil depleted mice, which were stimulated with TNF-α. (a) Number of transmigrated neutrophils per 0.02 mm^2. (b) Mean gap size between adjacent pericytes. Preparation of tissues, image collection and analysis as well as statistical analysis was performed as described for Figure 4.7. At least four vessels were analysed in each cremaster muscle. Afterwards, the mean gap size per mouse was determined and plotted. Each bar represents at least three mice. ** indicate significance levels of $p < 0.01$ compared to saline-treated control mice.

4.2.6 IL-1RI, TNFRI and TNFRII expression on post-capillary venular pericytes and endothelial cells in the murine cremaster muscle

After discovering that the significant increase in mean pericyte gap size upon TNF-α and IL-1β stimulation occurred independently of the presence of neutrophils, I wanted to elucidate whether cremasteric post-capillary pericytes express the receptors for TNF-α and IL-1β *in vivo* and are therefore able to respond directly to these inflammatory cytokines.

Markers for both endothelial cells and pericytes were used in this experiment in order to distinguish receptor expression by the two cellular components of post-capillary venules. Unstimulated male WT C57BL/6 mice were injected i.s. with 2 µg rat anti-mouse PECAM-1 antibody (clone C390, conjugated to Alexa-647) in 400 µl saline to label the endothelium. This protocol for labelling PECAM-1 *in vivo* was employed based on extensive optimisation experiments conducted within our group. After 2 h incubation, mice were sacrificed and the vasculature was washed using 10 ml saline (containing 10 % heparin) to remove all leukocytes from the vascular lumen, which would stain positive for TNFRI and TNFRII. Afterwards, the cremaster muscles were dissected from the mice, fixed in 4 % PFA and whole mounted tissues were subjected to immunofluorescence labelling to visualise the pericyte layer (α-SMA) and IL-1RI, TNFRI or TNFRII.

Expression of IL-1RI, TNFRI and TNFRII could be detected on cremasteric post-capillary venules compared to stainings using isotype matched control IgGs (goat IgG) (Figure 4.9). Cross sections of 3D-reconstructed confocal images indicated that both post-capillary pericytes and endothelial cells expressed all three receptors (Figure 4.10). In cross sections showing the pericyte layer (α-SMA, red channel) and staining for IL-1RI, TNFRI or TNFRII (green channel) receptor immunoreactivity could be seen as a distinct line on the luminal side of the pericytes. This line co-localized with the endothelium (PECAM-1, blue channel). In cross sections depicting endothelial cells and receptor staining, a discrete line of receptor immunoreactivity was observed on the abluminal side of the endothelial layer representing receptors expressed on pericytes.

To completely distinguish IL-1RI, TNFRI and TNFRII expression on pericytes from those on endothelial cells and to quantify the different expression levels, fluorescence intensity analysis using the image analysis software IMARIS was performed as advised by expert users of IMARIS in our group (detailed in 2.6.3). Briefly, to assess the mean fluorescence intensity (MFI) of a particular channel, in this case the green channel (isotype control (goat IgG), IL-1RI, TNFRI or TNFRII staining), on one cell type only, an isosurface has to be created representing exclusively the endothelium or the pericyte sheath. This parameter depicts the limitation of the volume of interest in which IMARIS determines the MFI of other channels. Isosurfaces embodying the endothelial cell or pericyte layer were built by using the channel showing immunofluorescence labeling of PECAM-1 or α-SMA as a source, respectively.

This was achieved easily for the pericyte layer because α-SMA intensity is evenly distributed throughout the pericyte sheath (Figure 4.11 a, top). However, there is an immense difference between PECAM-1 intensity of endothelial junctions and non-junctional areas (endothelial cell bodies). Therefore, to build an isosurface representing the entire endothelial cells, the threshold value has to be decreased severely to also include regions of very low fluorescence intensity (cell bodies). However, when using these settings, regions of high PECAM-1 intensity (endothelial junctions) started reaching into the pericyte isosurface. Consequently, it was technically not possible to build an isosurface representing the complete endothelial layer where regions of high intensity are reaching into the pericyte isosurface. To avoid overlap of the two isosurfaces, I generated three individual PECAM-1 isosurfaces per vessel on endothelial cell body regions avoiding the junctions (Figure 4.11 a, bottom). Using this approach, overlap of PECAM-1 isosurfaces with the pericyte isosurface could be eliminated and PECAM-1 isosurfaces were located on the luminal side of the pericyte isosurface (Figure 4.11 b). Thereby, MFIs could be detected individually for both cell types, however, one has to keep in mind that this technique determines MFIs on endothelial cell bodies only.

The above IMARIS analysis confirmed that both post-capillary pericytes and endothelial cells expressed all three receptors (Figure 4.12). Compared to an isotype control, MFIs of IL-1RI, TNFRI and TNFRII were significantly higher for both the pericyte layer (Figure 4.12 left) and the endothelium (Figure 4.12 right) and

expression levels for each of the receptors (represented as MFIs) were in the same range on the two vascular cell types (Pericytes: TNFRI: 14.6 ± 5.6, TNFRII: 34.9 ± 20.6 and IL-1RI: 10.0 ± 6.8; Endothelial cells: TNFRI: 12.0 ± 4.4, TNFRII: 45.0 ± 20.9 and IL-1RI: 15.5 ± 7.7;). Specificity of the TNFRI and TNFRII antibodies could be verified on cremaster muscles from TNFR double knockout mice (data not shown). By including IL-1 receptor antagonist (IL-1ra) in the staining procedure, staining for IL-1RI could almost be abolished showing the specificity of the anti-IL-1RI antibody (data not shown).

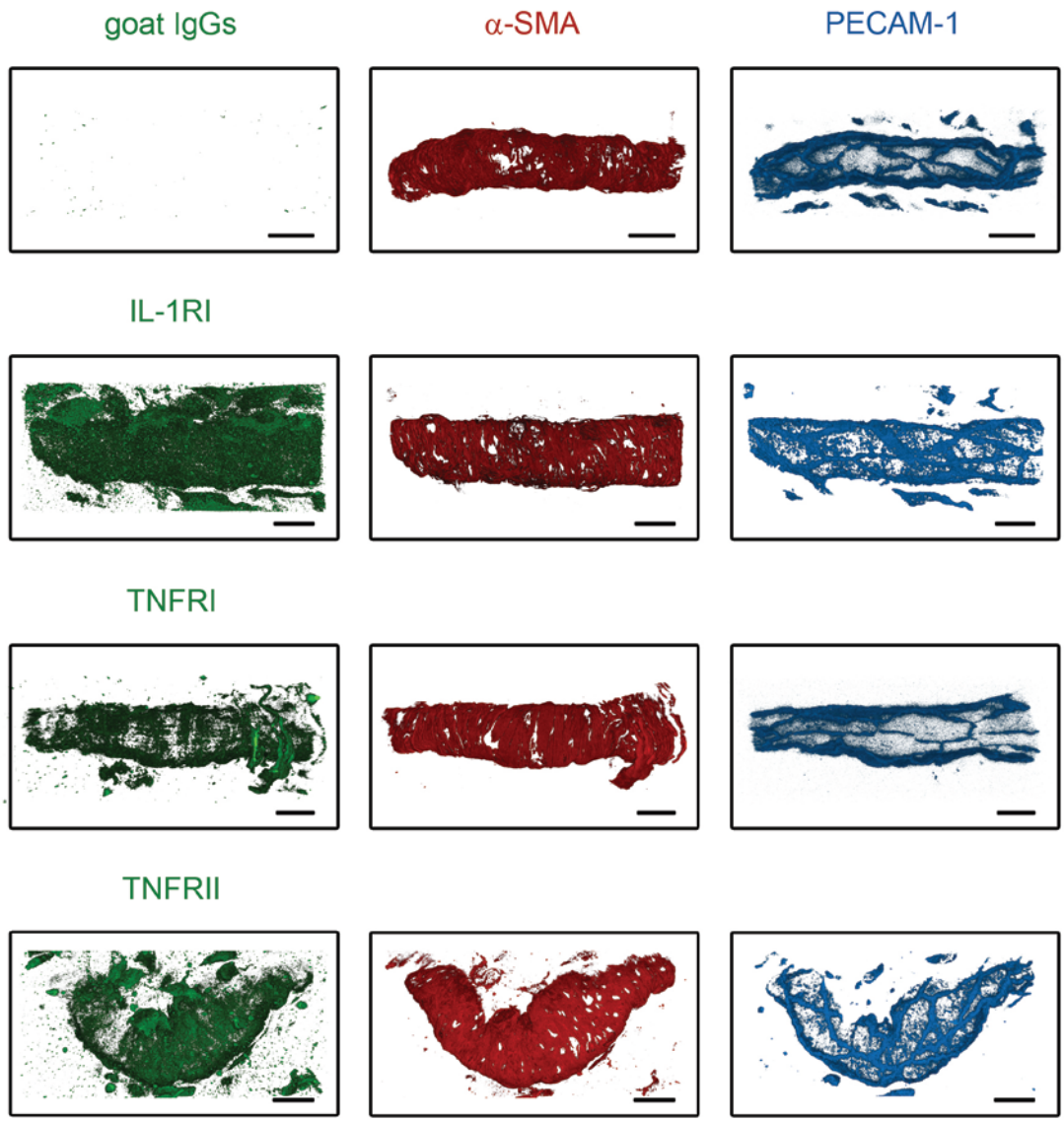

Figure 4.9: IL-1RI, TNFRI and TNFRII expression on post-capillary venules in the cremaster muscle. Unstimulated WT C57BL/6 mice were injected i.s. with 2 µg anti-PECAM-1-Alexa647 antibody in 400 µl saline to label the endothelium (PECAM-1, blue). After 2 h incubation, mice were sacrificed, the vasculature was washed using 10 ml saline (containing 10 % heparin) and cremaster muscles were dissected from the mice. Subsequently, cremasters were fixed in 4 % PFA and whole mount immunofluorescently labelled to visualise the pericyte layer (α-SMA, red) and TNFRI, TNFRII or IL-1RI (green). Representative 3D-reconstructed longitudinal confocal image sections of post-capillary venules are shown. Bars, 20 µm.

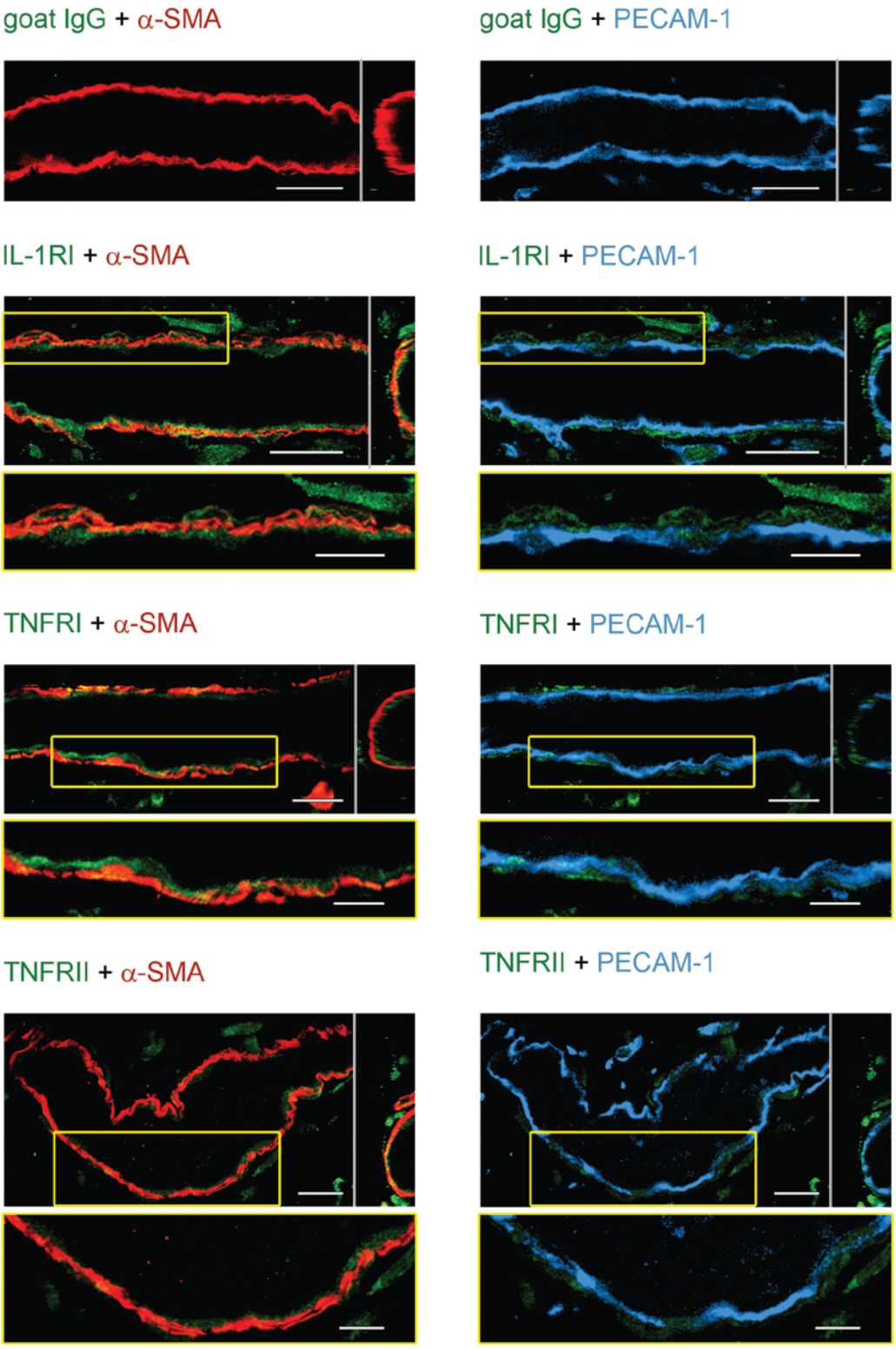

Figure 4.10: Both post-capillary pericytes and endothelial cells express IL-1RI, TNFRI and TNFRII in the cremaster muscle. Preparation of cremaster muscles was performed as describe for Figure 4.9. Confocal images shown in Figure 4.9 are depicted as cross sections. Bars, 20 µm. Yellow boxed region are shown enlarged underneath the appropriate image. Bars, 10 µm.

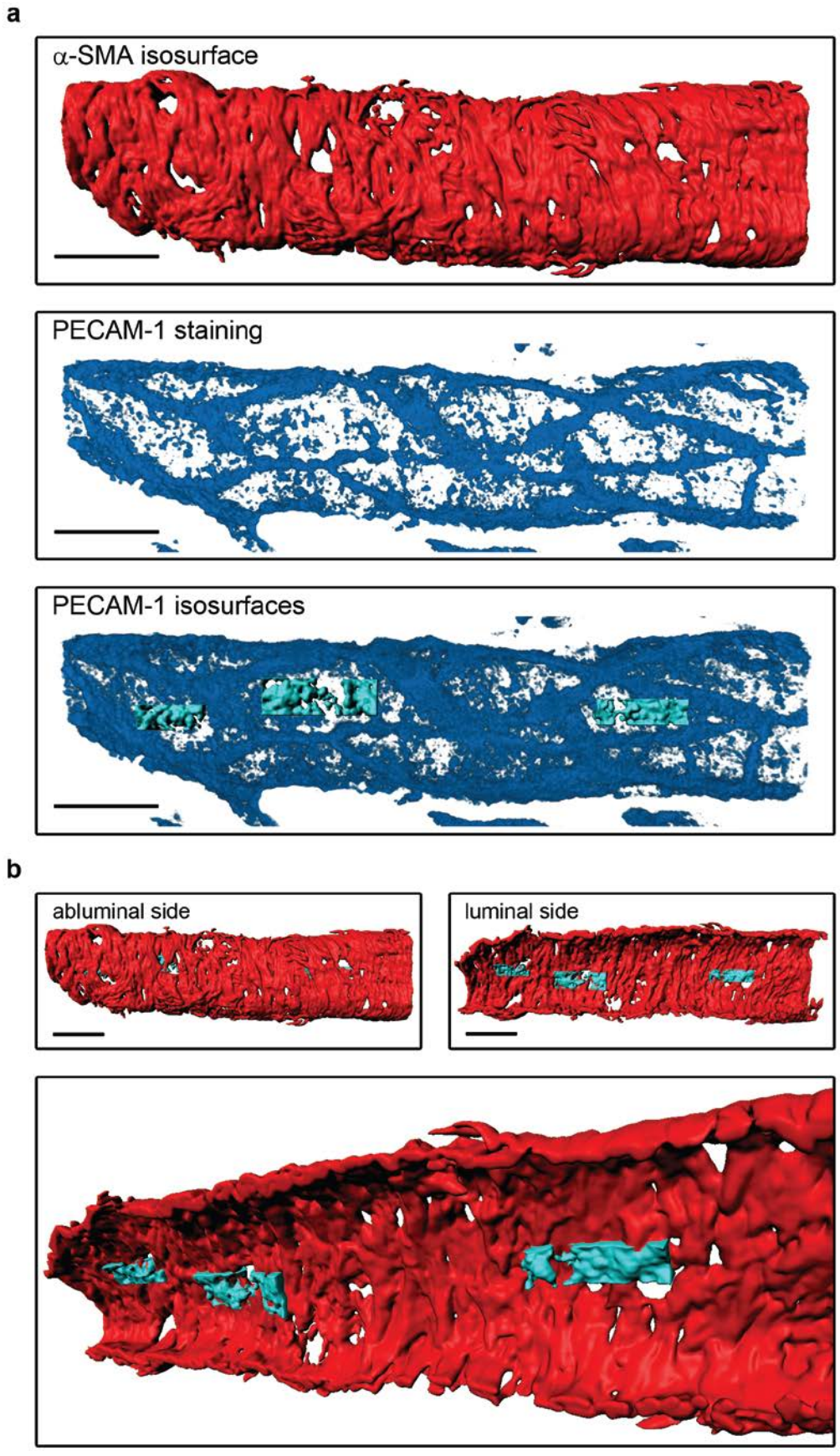
a
α-SMA isosurface
PECAM-1 staining
PECAM-1 isosurfaces
b
abluminal side
luminal side

Figure 4.11: Quantification of mean fluorescence intensity (MFI) of isotype control (goat IgG), IL-RI, TNFRI or TNFRII staining on post-capillary venular pericytes and endothelial cells in the cremaster muscle using IMARIS. (a) Isosurfaces were built representing the pericyte layer (α-SMA, red) or non-junctional regions of endothelial cells (PECAM-1, blue) to be able to determine the MFI of the green channel (goat IgG, IL-1RI, TNFRI or TNFRII) separately on pericytes and endothelial cells. The panel labelled "PECAM-1 staining" shows a representative image of immunofluorescence staining using standard confocal imaging and IMARIS analysis settings for visualisation of PECAM-1. The panel underneath named "PECAM-1 isosurfaces" depicts settings for confocal imaging and IMARIS analysis used to also visualise PECAM-1 expression on non-junctional regions. Three representative PECAM-1 isosurfaces are shown. Bars, 20 μm. (b) Merge of the α-SMA isosurface and the PECAM-1 isosurfaces, abluminal and luminal view showing close association but no overlap of the two isosurfaces. Bars, 20 μm.

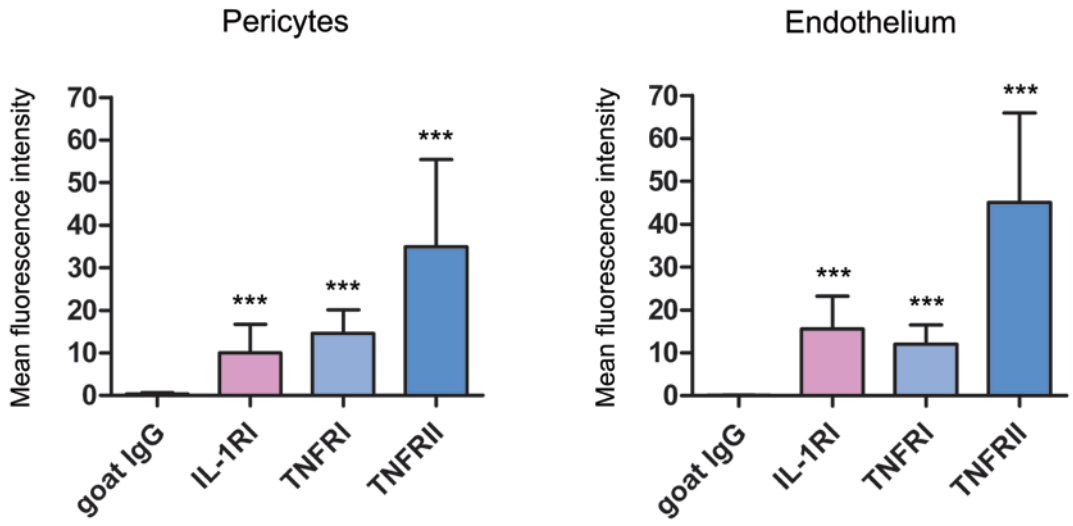

Figure 4.12: Mean fluorescence intensity (MFI) of isotype control (goat IgG), IL-RI, TNFRI or TNFRII staining on post-capillary venular pericytes and endothelial cells in the cremaster muscle. Isosurfaces were built on the pericyte layer and the endothelium as shown in Figure 4.11 and the MFI for goat IgG (white bars), IL-1RI (pink bars), TNFRI (light blue bars) or TNFRII (blue bars) was determined separately for each isosurface. Per vessel three PECAM-1 isosurfaces were analysed to obtain an overall MFI for the endothelium. Per cremaster muscle three vessels were analysed and the resulting MFIs for the pericyte layer and the endothelium were plotted per mouse. Each bar represents data from four mice. Significant differences compared to the isotype control were determined using Student's *t* test and are indicated by *** ($p < 0.001$).

4.3 Discussion

Leukocyte transmigration through venular walls into the surrounding tissue is a crucial event during inflammatory responses. At present very little is known about the mechanisms mediating leukocyte migration through the pericyte sheath and the vascular basement membrane. We previously reported that gaps between adjacent pericytes are co-localised with matrix protein low expression regions in the basement membrane, regions that are preferentially used by leukocytes to penetrate venular walls (Wang et al., 2006; Voisin et al., 2009; Voisin et al., 2010).

To elucidate the role of pericytes in inflammatory conditions, pericyte responses to different inflammatory mediators were investigated in post-capillary venules. Cremaster muscles stimulated via topical application of the chemoattractant LTB_4 or the chemokine CCL2 exhibited no change in pericyte morphology. Intrascrotal injection of TNF-α or IL-1β and I/R injury on the other hand induced pericyte shape change compared to respective controls, which resulted in a significant enhancement of gaps between adjacent cells. Intra dermal injection of TNF-α or IL-1β into the skin of the ear induced pericyte shape change as seen in the cremaster muscle leading to a significant increase in the mean pericyte gap size, showing no evidence for a tissue-specific phenomenon. This part of the study extended previous work from our group and showed for the first time pericyte responsiveness to inflammatory mediators *in vivo* indicating that pericytes might play an important role in leukocyte transmigration during inflammatory conditions.

Other studies indicate that pericytes also play an important role in regulating microvascular permeability. The pro-inflammatory cytokines TNF-α and IL-1β, which induced pericyte responses in the cremaster muscle and the skin of the ear, have been reported to be released in the lung during Acute Respiratory Distress Syndrome (ARDS) leading to an increase in permeability in the microvasculature (Matthay and Zimmerman, 2005). The data shown in this Chapter suggest that the increased permeability might be due to the enhancement of gaps between adjacent pericytes. In agreement to this, pericytes have already been implicated in microvascular permeability and capillary leak (Leveen et al., 1994; Hellstrom et al., 2001). In addition, it has been shown, that histamine and IL-2 stimulation of the rat cremaster muscle leads to an increase in albumin permeability (Sims et al., 1990;

Sims et al., 1994). Interestingly, IL-2 treatment of the rat cremaster muscle was found to alter the distribution of pericytes from a random distribution to localisation around endothelial junctions (Sims et al., 1994).

TNF-α- and IL-1β-induced reactions were selected for more detailed investigations and the responses were characterised regarding the time-course of neutrophil transmigration and pericyte shape change in the cremaster muscle. Local injection of both TNF-α and IL-1β elicited neutrophil transmigration and changes in pericyte shape, which resulted in a significant enhancement of gaps between adjacent pericytes, in a time-dependent manner. Interestingly, with regards to TNF-α, both the on-set and termination of the induced pericyte shape change response was faster than that observed for IL-1β. Additionally, in the TNF-α-induced reaction neutrophil transmigration seemed to be preceded by the pericyte gap enhancement highlighting the existence of different mechanisms of action for these two pro-inflammatory stimuli. IL-1β induced pericyte shape change might involve *de novo* synthesis of secondary mediators such as inflammatory mediators or mediators of intracellular signalling involved in regulating shape change. Differences in the mechanisms of action of TNF-α and IL-1β have also been observed in a previous study demonstrating *in vivo* that intradermal injection of IL-1β induces a slow accumulation of neutrophils in rabbit skin (within 3 to 4 h), which is protein synthesis dependent (Rampart et al., 1989). In the same study neutrophil accumulation induced by TNF-α was rapid (within 30 min) and protein synthesis independent. IL-1β-induced release of secondary inflammatory mediators such as chemokines or chemoattractants could occur either in pericytes themselves or in other cell types such as neutrophils or endothelial cells. IL-1β is known to stimulate intracellular signalling pathways leading to *de novo* protein synthesis of pro-inflammatory cytokines such as IFNα, IFNβ, IL-6 and TNF-α via activation of the transcription factors NFκB and c-JUN (Dinarello, 1996; Muzio et al., 1997; Medzhitov et al., 1998; Kopp et al., 1999). IL-1β and TNF-α has also been shown to stimulate the release of chemokines (e.g. IL-8) and chemoattractants (e.g. LTB_4) in neutrophils and endothelial cells (Strieter et al., 1989; Brain and Williams, 1990; Huber et al., 1991; Barnes et al., 1998). Neutrophils are not likely to be the source of secondary inflammatory mediators in IL-1β-induced pericyte shape change since neutrophil depletion had no effect on the significant increase in mean gap size

observed after IL-1β stimulation. Similar results were obtained for TNF-α induced change in pericyte shape. Hence, in both reactions pericyte gap enhancement did not involve neutrophilic mediators or the presence of neutrophils. However, it remains to be investigated whether IL-1β-induced pericyte shape change is transcriptionally regulated and which mediators and effectors are involved.

In both the TNF-α- and the IL-1β-induced reaction the density of gaps was not altered, suggesting that overall neither a loss nor a generation of new gaps occurred. Existing gaps just increased in size, which might be due to pericyte contractility in response to these inflammatory cytokines. Pericyte contractility upon TNF-α and IL-1β has already been reported for rat lung pericytes *in vitro* (Kerkar et al., 2006). In addition, TNF-α and IL-1β are known to activate small GTPases such as RhoA, Rac 1 and cdc42, which are well known for their ability to regulate the actin cytoskeleton (Puls et al., 1999). Most understood are cdc42 that promotes filopodial extension and may be vital for cell polarity, Rac 1 that promotes an actin-dependent protrusive activity characterized by lamellipodia formation, and RhoA that promotes focal adhesion and microfilament bundle assembly (Jaffe and Hall, 2005). *In vitro* studies using bovine retinal pericytes demonstrated that pericyte contractility is mediated via a RhoA-dependent disassembly of α-SMA stress fibers resulting in a dramatic reduction in cell size (Kolyada et al., 2003). Other Rho GTPases such as the Ras-related small GTPases Rac 1 and cdc42 were shown not to be involved in pericyte shape change (Kolyada et al., 2003; Kutcher et al., 2007; Kutcher and Herman, 2009). Pericyte contraction might facilitate leukocyte transmigration through enhanced permissiveness to migrating cells, contribute to the establishment of chemoattractant gradients or regulate leukocyte transmigration through venular contraction.

To elucidate whether TNF-α or IL-1β could act directly on pericytes, unstimulated cremaster muscles were used for whole mount immunofluorescence labelling and confocal microscopy to visualize and analyse the expression profile of receptors for TNF-α and IL-1β. These receptors have been reported to be present on endothelial cells (Orlinick and Chao, 1998; Eissner et al., 2004; Hehlgans and Pfeffer, 2005; Boraschi and Tagliabue, 2006), but this study demonstrated for the first time IL-1RI, TNFRI and TNFRII expression on the second cellular layer of cremasteric post-capillary venules, the pericyte sheath. Therefore, TNF-α- and IL-1β-induced pericyte

shape change leading to gap enlargement might be a direct effect of these cytokines on pericytes. To further dissect whether TNF-α- and IL-1β-induced reactions could be due to direct stimulation of pericytes or might depend on cross talk with other cell types such as endothelial cells, pericyte responsiveness to these cytokines was investigated *in vitro* using the pericyte-like cell line C3H/10T1/2 (Chapter 5).

Collectively, these findings highlight the possibility that pericytes might play a critical role in facilitating leukocyte transmigration via active shape change during inflammatory conditions. Pericytes might also be involved in T-cell infiltration into the brain during multiple sclerosis. Verbeek et al. have shown that T-Lymphocyte adhesion and migration into the human brain is mediated via the interaction of very late antigen-4 (VLA-4) on T-lymphocytes and VCAM-1, which is expressed on endothelial cells and pericytes (Verbeek et al., 1995).

Pericyte involvement in leukocyte transmigration was further investigated in more detail *in vivo* using 4D real time confocal intravital microscopy (Chapter 6).

Chapter 5: Characterisation of the murine pericyte-like fibroblast cell line C3H/10T1/2 *in vitro*

5.1 Introduction

The *in vivo* findings described in Chapter 4 showed a pronounced change in shape of pericytes in cremasteric post-capillary venules in response to TNF-α and IL-1β stimulation resulting in a significant increase in mean gap size between adjacent cells. Furthermore, this response appeared to occur independently of the presence of neutrophils. To complement these findings and to further dissect whether these reactions could be due to a direct stimulation of pericytes or depend on cross talk with other cell types such as endothelial cells, pericyte responsiveness to these cytokines was investigated *in vitro.*

Isolation of primary pericytes from murine tissues presents technical difficulties due to the lack of specific markers for pericytes. Most methods for isolation and cultivation of pericytes to date are based on the selective culture of cell populations derived from tissues bearing high numbers of pericytes. Hence, mainly rat lung tissues or bovine retinas are used for pericyte isolation, which is followed by a series of phenotypic characterizations (Schor and Schor, 1986; Schor et al., 1995; Khoury and Langleben, 1996). In order to use cells derived from the same species for investigation of pericyte properties *in vitro*, the murine pericyte-like cell line C3H/10T1/2 was used.

The cell line C3H/10T1/2 was established in 1973 from 14- to 17-day-old C3H mouse embryos (Reznikoff et al., 1973). C3H/10T1/2 cells are of mesenchymal origin and display fibroblastic morphology in culture. Being isolated from embryonic mesenchym these cells rather represent mesenchymal stem cells than fibroblasts, smooth muscle cells or pericytes. To date most studies involving C3H/10T1/2 cells have used these cells as fibroblasts (Thorsen et al., 2003; Clemens et al., 2005; Yauk et al., 2008). However, C3H/10T1/2 cells also express vascular smooth muscle cell/pericyte markers and show similar properties to primary murine meningeal perivascular cells (Brachvogel et al., 2007). Hence, C3H/10T1/2 cells are also considered to be smooth muscle cells-/pericyte-like cells and have been used as cultured pericytes in co-culture studies with endothelial cells (Darland and D'Amore, 2001). Clearly results obtained from such studies need to be extrapolated to potential responses exhibited by primary pericytes with caution.

The aim of this Chapter was to characterize the murine pericyte-like cell line C3H/10T1/2 and analyse its properties *in vitro*. To confirm that these cells are an useful tool for analysis of pericyte responses *in vitro*, pericyte-like characteristics such as cell shape and pericyte marker expression were investigated. Subsequently, to complement the *in vivo* findings of TNF-α- and IL-1β-induced pericyte shape change described in the previous Chapter, the responsiveness of C3H/10T1/2 cells to these inflammatory cytokines was investigated *in vitro* in real time using fluorescence time lapse microscopy. Finally, expression of IL-1RI, TNFRI and TNFRII by C3H/10T1/2 cells was explored by flow cytometry.

5.2 Results

5.2.1 Cell morphology and expression of pericyte markers

As a first step, C3H/10T1/2 cells were tested for their pericyte-like characteristics. Cultured C3H/10T1/2 cells showed stellate pericyte-like cell shape with several processes protruding from the body of the cell (Figure 5.1 a and b). Expression of pericyte markers was investigated on these cells by confocal microscopy and flow cytometry. For confocal analysis, C3H/10T1/2 cells were grown on 4-well chamber slides, fixed and immunofluorescently labelled. To examine the expression of pericyte markers by flow cytometry, cells were harvested from culture flasks for subsequent immunofluorescence staining using EDTA only instead of Trypsin/EDTA to avoid shedding of surface molecules.

Confocal analysis showed that C3H/10T1/2 cells strongly expressed the key pericyte marker α-SMA, indicating a pericyte-like phenotype (Figure 5.2 a and b). Co-staining with Wheat Germ Agglutinin, a cell membrane marker, demonstrated α-SMA expression throughout the whole cell body localised along actin fibres (Figure 5.2 a), highlighting the fact that α-SMA staining is an accurate indication of pericyte shape. In addition, the pericyte marker NG2 could be found highly expressed on C3H/10T1/2 cells covering the entire cell surface (Figure 5.2 b).

Flow cytometry analysis confirmed strong expression of α-SMA and NG2 by C3H/10T1/2 cells (Figure 5.2 c). Both pericyte markers showed high relative fluorescence intensity (RFI), which is the x-fold higher mean fluorescence intensity of the sample stained with the specific antibody compared to the respective isotype control sample (mean RFIs from three experiments: α-SMA: 28.1 ± 0.3, NG2: 112.4 ± 21.3).

These data confirm that C3H/10T1/2 cells possess pericyte-like properties and are therefore a useful tool for analysis of pericyte responses *in vitro*.

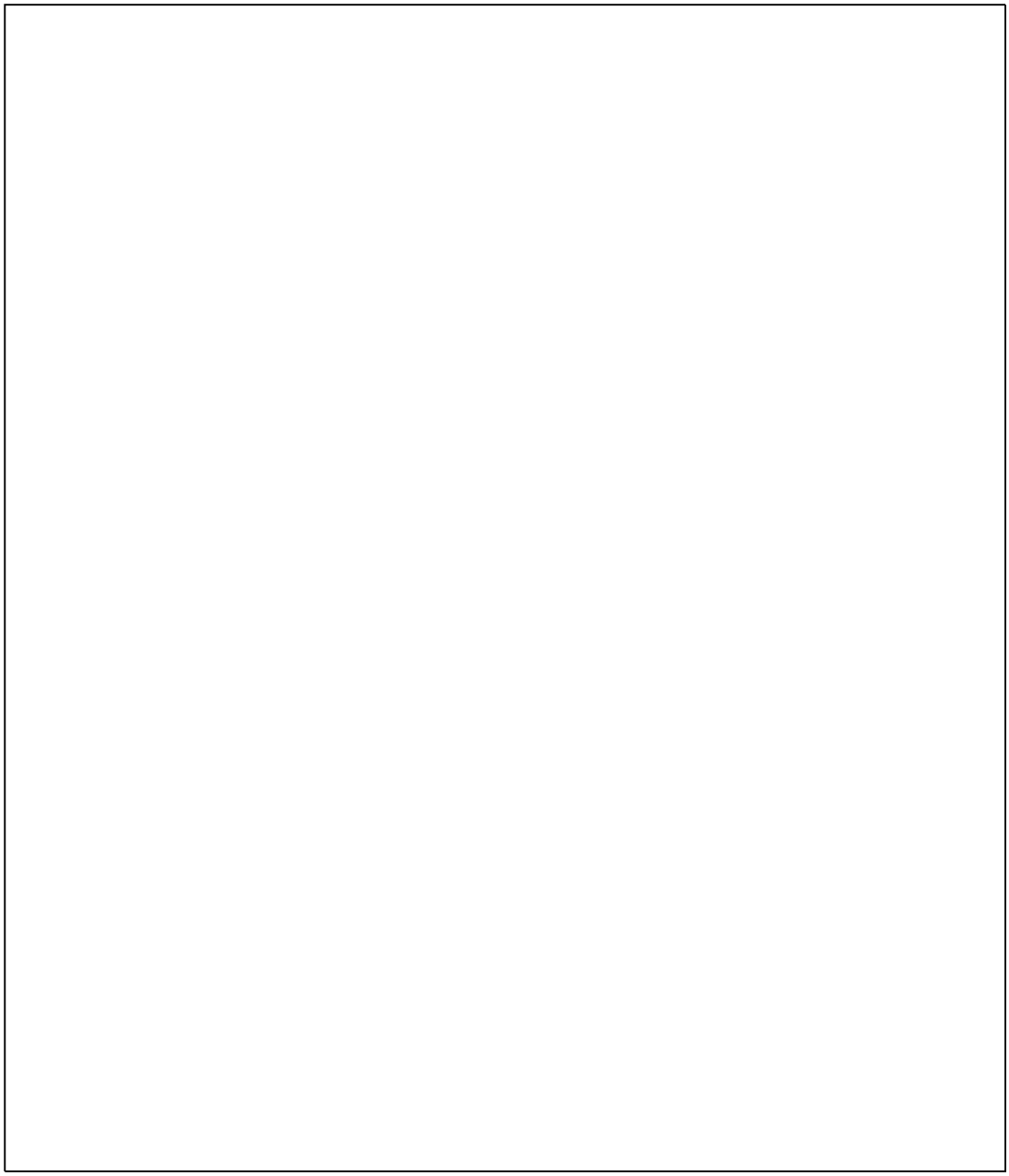

Figure 5.1: Morphology of the murine pericyte-like C3H/10T1/2 cells. Representative phase contrast images of C3H/10T1/2 cells in culture are shown. Several processes were extending from the cell bodies highlighting the stellate cell shape of C3H/10T1/2 cells. (a) 20x phase contrast image. Bar, 50 μm. (b) Enlarged 40x phase contrast images depicting a single cell. Bars, 20 μm.

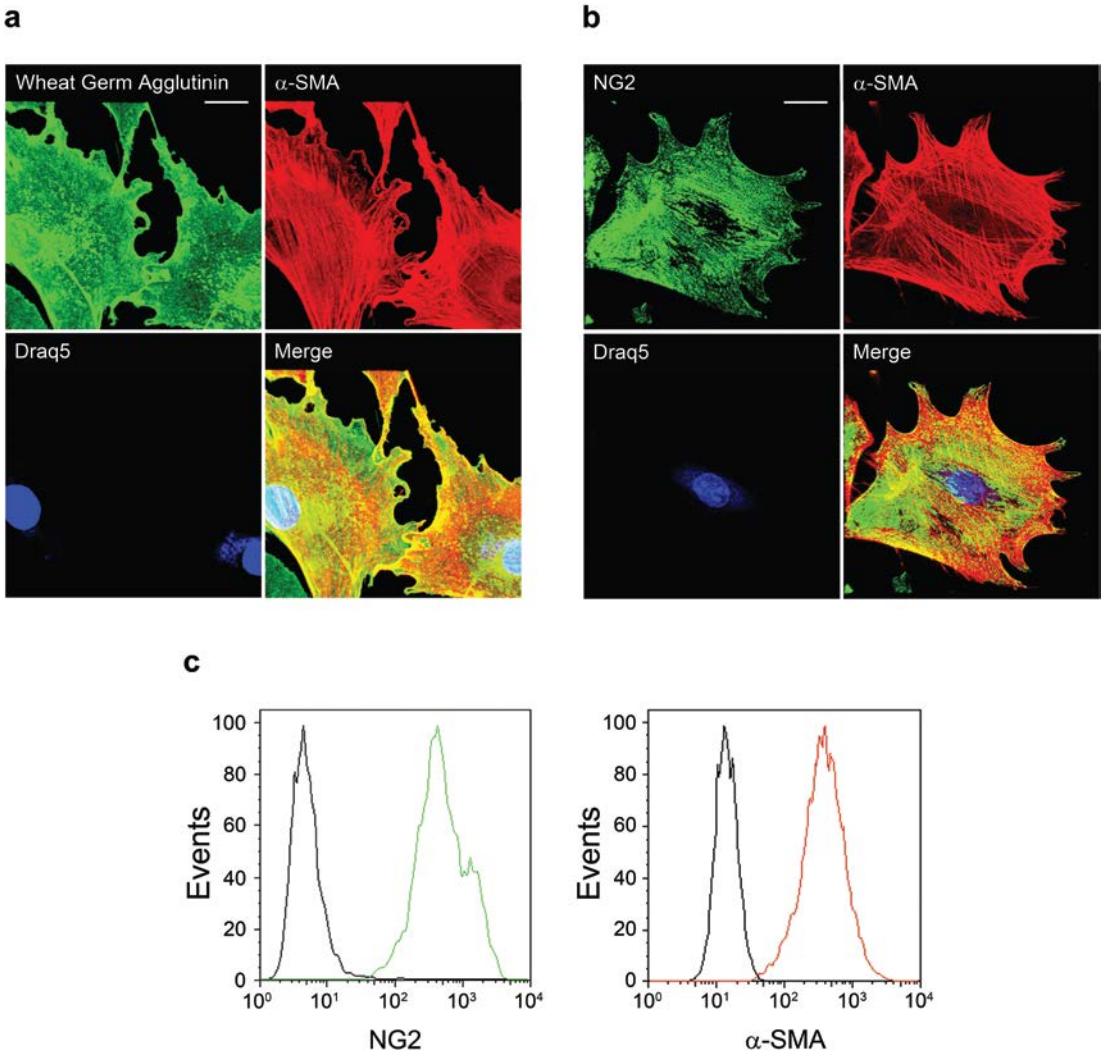

Figure 5.2: Expression of pericyte markers by the pericyte-like C3H/10T1/2 cells. (a and b) Representative confocal images of cells grown on 4-well chamber slides are shown. The cells were fixed and stained with either (a) Wheat Germ Agglutinin (green) or (b) an anti NG2 antibody (green). All cells were also stained to visualise α-SMA (red) and the nucleus using the nuclear dye Draq5 (blue). These images are representative of four experiments. Bars, 20 μm. (c) Expression of NG2 and α-SMA as shown by flow cytometry histograms representative of three experiments. The histograms illustrate the number of events over a spectrum of increasing fluorescence intensities. Histograms resulting from analysis of cells stained with NG2 or α-SMA antibodies are depicted as overlays over histograms of the respective isotype control sample. Black peaks represent labelling using the isotype control antibodies and the green or the red peak shows staining with the specific antibodies against NG2 or α-SMA, respectively.

5.2.2 Effects of TNF-α and IL-1β on cell shape in real time

To extend the findings of TNF-α- and IL-1β-induced pericyte shape change *in vivo* (Chapter 4), responses of C3H/10T1/2 cells to these cytokines were investigated *in vitro* using fluorescence time lapse microscopy.

For real time analysis of C3H/10T1/2 responsiveness to TNF-α and IL-1β, cells were transfected with Lifeact-eGFP and changes in the actin cytoskeleton as well as changes in cell shape were imaged. Cells were seeded into 6-well plates and pictures of three different fields of view per dish were taken every 10 minutes using a motorised fluorescence time lapse microscope. Different doses of TNF-α (10 ng/ml and 100 ng/ml in PBS) and IL-1β (1 ng/ml, 10 ng/ml and 100 ng/ml in PBS) were used for an imaging period of 4 h. After applying the vehicle control (PBS), C3H/10T1/2 cells showed no change in cell shape over time (Figure 5.3, Movie 5.1). However, both TNF-α and IL-1β stimulation led to a striking change in cell shape in a time-dependent manner leading to cell elongation (Figure 5.3, Movie 5.2 and 5.3).

In collaboration with my colleague Dr. Mathieu-Benoit Voisin the image processing software IMARIS was used to quantify cell elongation by manually measuring cell eccentricity, which is the ratio of cell length to cell width (exemplified in Figure 5.4). For all three fields of views cell eccentricity was measured for at least five cells and the mean cell eccentricity was determined for each field of view. The mean cell eccentricity was then plotted per dish (relates to one experiment), normalised to the overall mean at time point 0 h (time point before the addition of cytokines or vehicle control).

Eccentricity measurements confirmed that PBS alone induced no change in cell shape over time (7.8 ± 15.1 % elongation after 4 h) (Figure 5.5). In contrast, TNF-α at all concentrations elicited cell elongation throughout the experiment resulting in a significant change in eccentricity compared to PBS (72.4 ± 22.0 % and 103.4 ± 22.7 % elongation after 4 h of stimulation with 10 ng/ml and 100 ng/ml, respectively). IL-1β at 10 ng/ml and 100 ng/ml also induced a significant change in eccentricity over time (71.5 ± 13.7 % and 100.8 ± 28.9 % elongation after 4 h of stimulation with 10 ng/ml and 100 ng/ml, respectively). Interestingly, as seen in the *in vivo* time course studies of pericyte shape change (Chapter 4), the use of this *in*

vitro model also showed that IL-1β-induced shape change occurs more slowly than the TNF-α-induced response.

Overall these data support the *in vivo* findings of pericyte shape change during inflammatory conditions and confirms the ability of pericytes to change their shape in response to direct stimulation with the inflammatory cytokines TNF-α and IL-1β.

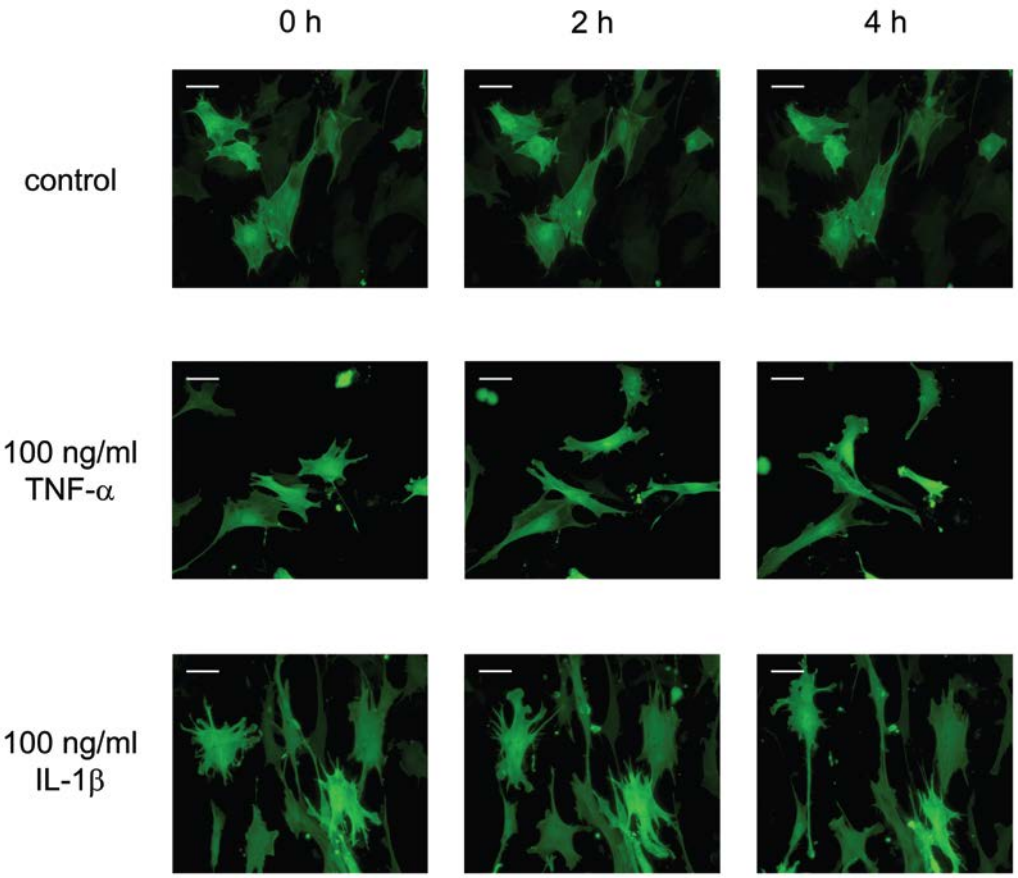

Figure 5.3: Time course of TNF-α- and IL-1β-induced shape change of C3H/10T1/2 cells. Respective fluorescence time lapse microscopy images of Lifeact-eGFP transfected cells are shown for certain time points (0 h (time point before the addition of cytokines or vehicle control (PBS)), 2 h and 4 h after cytokine or PBS application). Bars, 50 μm.

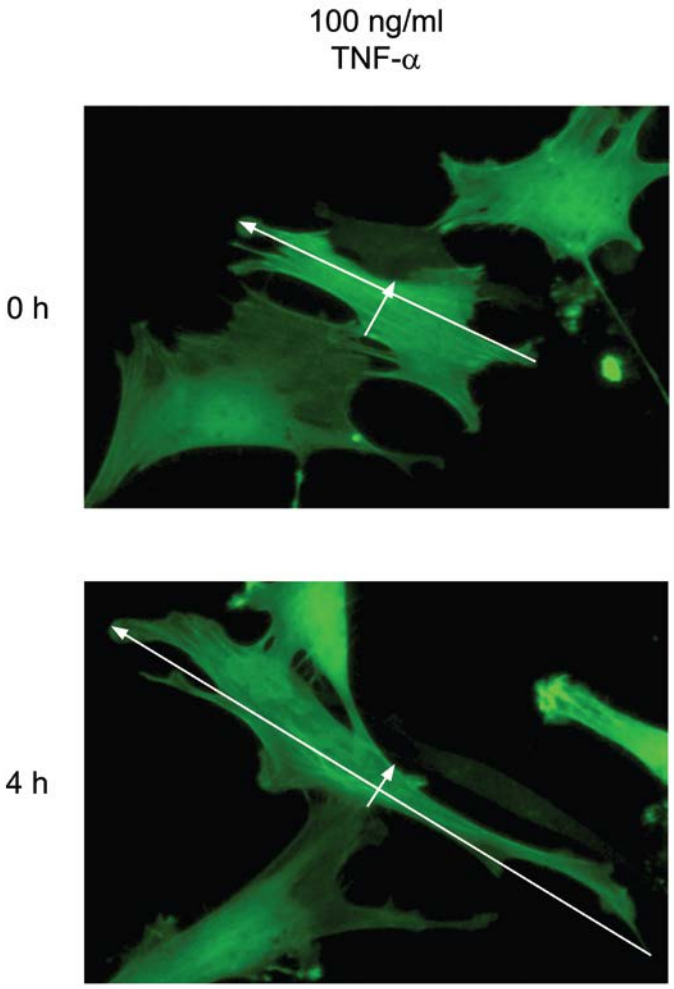

Figure 5.4: Measurement of cell eccentricity using IMARIS to quantify the change in cell shape (elongation). Fluorescence time lapse microscopy images of Lifeact-eGFP transfected cells are shown for start and endpoint of the time course shown in Figure 5.4 using 100 ng/ml TNF-α. White arrows depict measurements to determine cell eccentricity, which is the ratio of cell length to cell width. Cell length is represented by the longest side in directionality of cell elongation. Cell width was measured perpendicularly from the centre point of the cell length measurement.

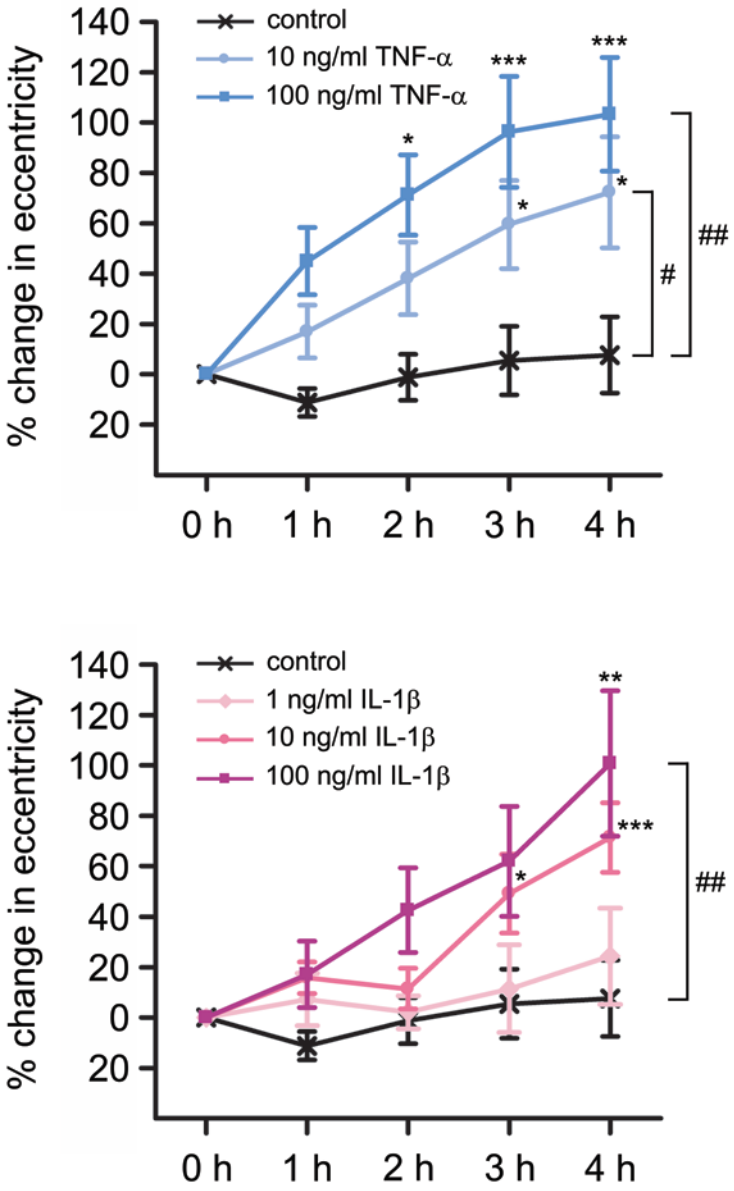

Figure 5.5: Time course of percentage change in C3H/10T1/2 cell eccentricity in response to TNF-α and IL-1β compared to vehicle control (PBS). Pictures of three different fields of view were taken per culture dish every 10 minutes for 4 h. After the first picture, TNF-α (10 or 100 ng/ml), IL-1β (1, 10 or 100 ng/ml) or the vehicle control (PBS) were added to the cells. For all three fields of views cell eccentricity was measured for at least five cells as described in Figure 5.4. Mean cell eccentricity was determined for each field of view and the mean cell eccentricity was then plotted per dish (relates to one experiment) normalised to the overall mean at time point 0 h (time point before addition of the cytokines or the vehicle control (PBS)). Each point represents results from at least seven experiments. Significant differences between groups were determined using one way Anova. Significant differences compared to time point 0 h are indicated by * ($p < 0.05$), ** ($p < 0.01$) and *** ($p < 0.001$). Significant differences at time point 4 h compared to treatment with the vehicle control are indicated by # ($p < 0.05$) and ## ($p < 0.01$).

5.2.3 Expression profile of TNFRI, TNFRII and IL-1RI

To investigate if the observed cytokine-induced shape change of C3H/10T1/2 cells was a result of direct effects of TNF-α and IL-1β on these cells, the expression of the respective receptors for these cytokines was determined. Presence of IL-1RI, TNFRI and TNFRII on C3H/10T1/2 cells was investigated using flow cytometry. Cells were harvested from culture flasks for subsequent immunofluorescence staining.

Flow cytometry analysis demonstrated IL-1RI, TNFRI and TNFRII expression on C3H/10T1/2 cells (Figure 5.6 a). Mean RFIs were low for all three receptors (IL-1RI: 1.9 ± 0.2, TNFRI: 4.2 ± 0.3 and TNFRII: 2.6 ± 0.2), however, statistical significance was noted when compared to the isotype control (armenian hamster IgG_1) (Figure 5.6 b). By including IL-1 receptor antagonist (IL-1ra) in the staining solution, staining for IL-1RI could be abolished showing the specificity of the anti IL-1RI antibody (Figure 5.7). Specificity of the TNFRI and TNFRII antibodies could be verified on blood leukocytes isolated from TNFR double knockout mice (Figure 5.8).

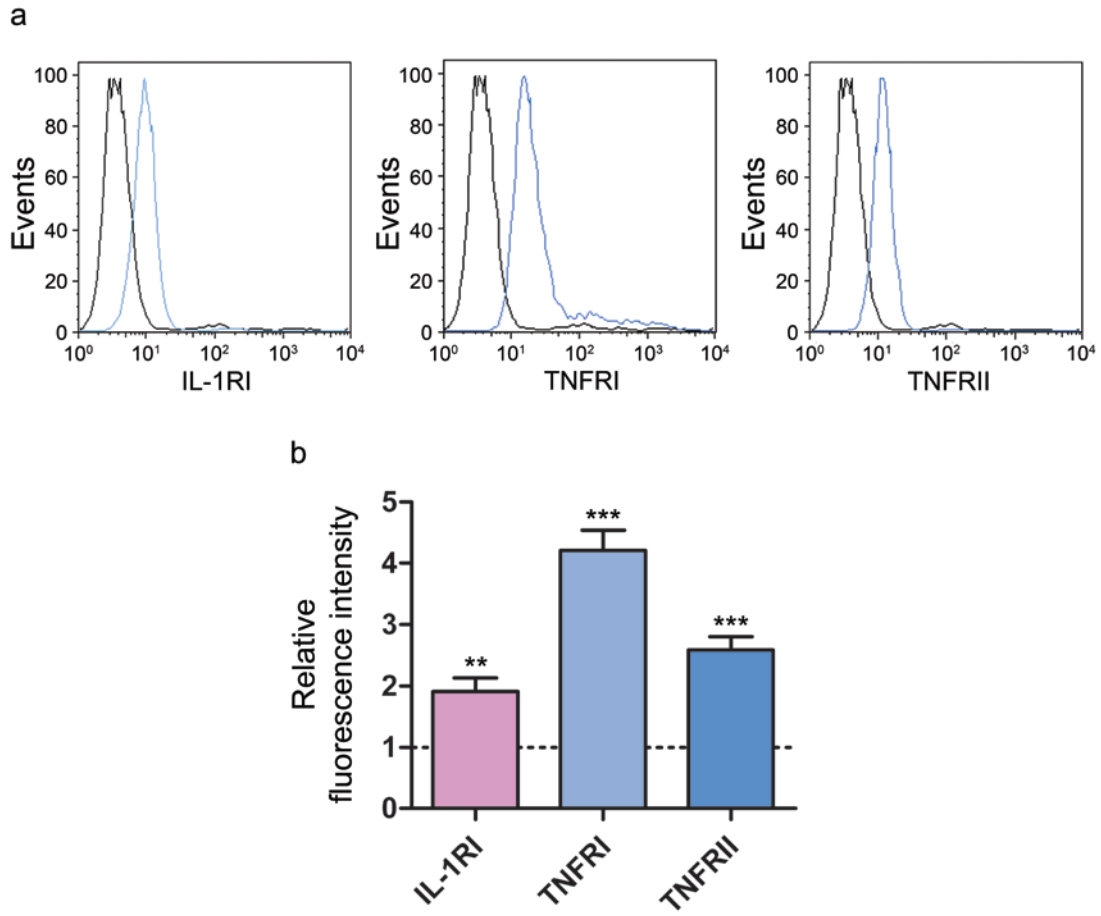

Figure 5.6: C3H/10T1/2 cells expressed IL-1RI, TNFRI and TNFRII as shown by flow cytometry. (a) Representative histograms are depicted illustrating the presence of all three receptors on the cell surface. The histograms illustrate the number of events over a spectrum of increasing fluorescence intensities. Histograms resulting from analysis of cells stained with antibodies for IL-1R, TNFRI and TNFRII are depicted as overlays over the histogram of the isotype control sample (armenian hamster IgG_1). Black peaks represent labelling using the isotype control antibody and blue peaks show staining with the respective specific antibody. (b) The graph shows mean RFIs for IL-1R, TNFRI and TNFRII staining. Each bar represents results from six experiments. The dotted line indicates the isotype control, with an RFI of 1 by definition. Significant differences compared to the isotype control were determined using student's *t* test and are indicated by ** ($p < 0.01$) and *** ($p < 0.001$).

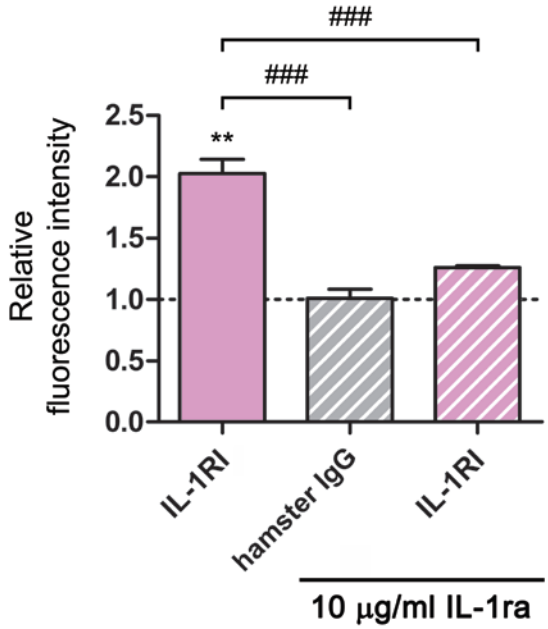

Figure 5.7: Specificity of the armenian hamster anti-mouse IL-1RI antibody. C3H/10T1/2 cells were immunofluorescently labelled for flow cytometry analysis using the armenian hamster anti-mouse IL-1RI antibody or armenian hamster IgG (isotype control, dotted line). Double the amount of antibody solution was prepared, divided in half and either used neat (filled bar) or including IL-1 receptor antagonist (IL-1ra) at 10 µg/ml (striped bars). The graph shows mean RFIs representing results from three experiments. The dotted line indicates the isotype control, with an RFI of 1 by definition. Significant difference of IL-1RI staining compared to staining using armenian hamster IgG (isotype control, dotted line) was determined using student's *t* test and is indicated by ** ($p < 0.01$). Significant differences between groups shown in the graph were determined using one way Anova and are indicated by ### ($p < 0.001$).

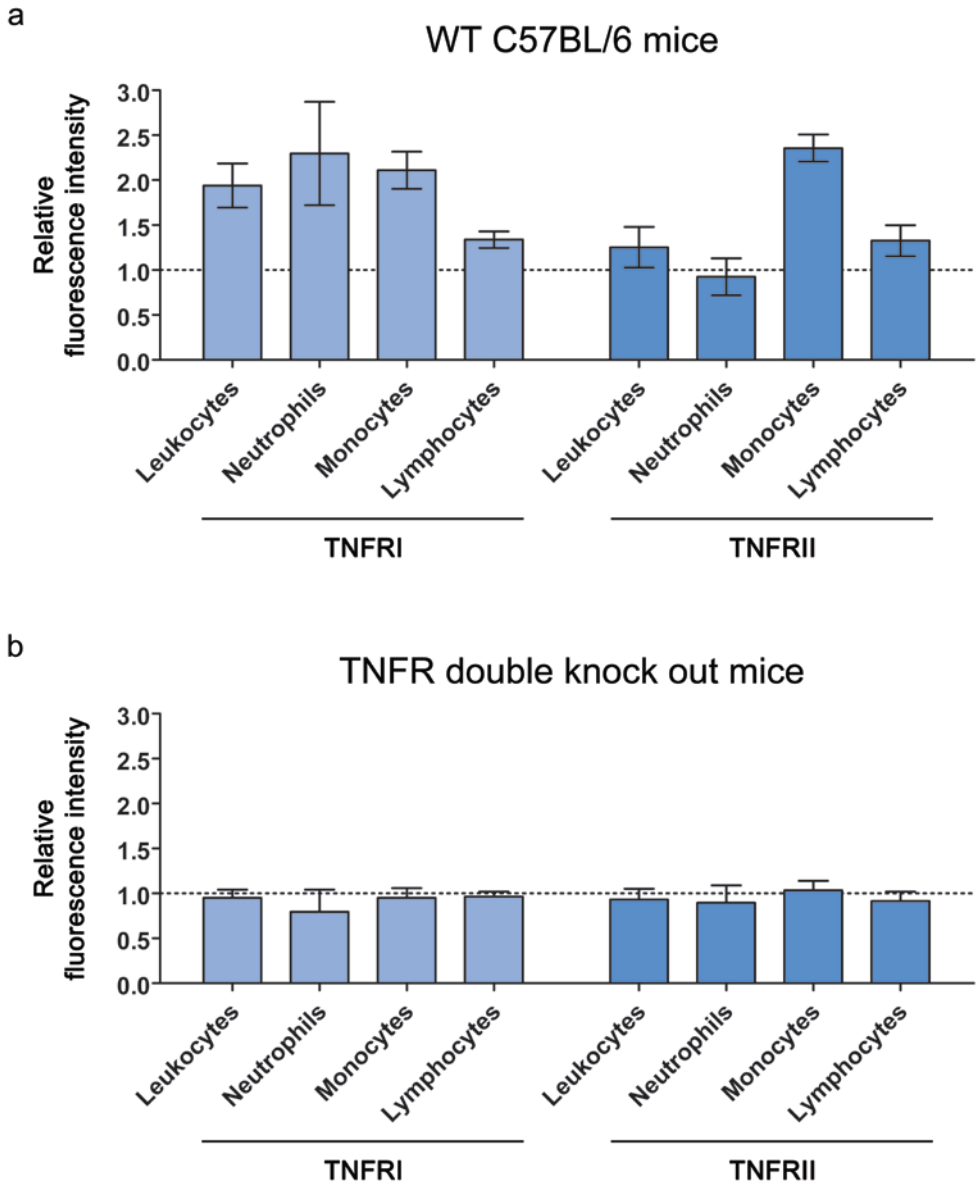

Figure 5.8: Specificity of the armenian hamster anti-mouse TNFRI and anti-mouse TNFRII antibodies. Double the amount of antibody solution was prepared and divided in half and to stain blood leukocytes isolated either from (a) WT C57BL/6 mice or (b) TNFR double knockout mice. The graphs show mean RFIs for TNFRI (light blue bars) and TNFRII (blue bars) staining. Using the flow cytometry analysis software FlowJo expression levels were determined for all live cells (Leukocytes) and additionally for different leukocyte subtypes (Neutrophils, Monocytes and Lymphocytes), which were identified according to cell size and granularity (position in the forward scatter/side scatter profile). Each bar represents results from two experiments. The dotted line indicates staining using armenian hamster IgG (isotype control), with an RFI of 1 by definition. Statistical significance has not been examined since n-numbers were too low.

5.3 Discussion

As described in Chapter 4, *in vivo* studies showed the ability of TNF-α and IL-1β to induce pericyte shape change in a neutrophil-independent manner. In this Chapter, these findings were complemented with *in vitro* analysis of pericyte responsiveness to these cytokines.

Characterisation of C3H/10T1/2 cells demonstrated stellate cell shape with several processes protruding from the body of the cell and expression of key pericyte markers such as the surface marker NG2 and the intracellular marker α-SMA, indicating pericyte-like properties. This confirms what has been shown in a previous study, in which C3H/10T1/2 cells were used as an object of comparison to assess pericyte properties of primary murine meningeal perivascular cells (Brachvogel et al., 2007). Stellate cell shape is expected and has been reported for pericyte-like cells in culture (Canfield et al., 1990). Simultaneous staining with the cell membrane dye Wheat Germ Agglutinin confirmed the value of α-SMA staining as an accurate indication of pericyte shape.

One could argue that the expression of NG2 and α-SMA by C3H/10T1/2 cells seem to indicate that they rather represent vascular smooth muscle cells than pericytes. In Chapter 3, fluorescence immunostaining of whole mounted cremaster muscles *ex vivo* showed that α-SMA is expressed in pericytes surrounding post-capillary and collecting venules as well as in vascular smooth muscles cells of arterioles, arteries and veins. Pericytes on capillaries on the other hand exhibited almost no expression of α-SMA, but were NG2 positive. NG2 was also expressed by vascular smooth muscle cells and nerves. Hence, *in vivo* only vascular smooth muscle cells express both α-SMA and NG2. However, pericytes and vascular smooth muscle cells share numerous characteristics and are of phenotypic complexity (Chapter 3). These phenotypically different subtypes might have lost their specific marker expression during immortalisation of these cells. In addition, 2D culture may induce expression of pericyte markers in these cells in a way not seen in 3D or *in vivo*. Apart from that, C3H/10T1/2 cells are a cell line and hence these cells cannot be considered "authentic" pericytes but have to be considered as pericyte/vascular smooth muscle cell-like cells. Furthermore, *in vitro* experiments can never perfectly mimic complex *in vivo* situation, but they have many important implications and are useful for addressing key questions such as dissecting signalling pathways or, as done in this

study, supplementing *in vivo* findings by looking at a cell type singled out from its environment to investigate whether observed reactions are dependent on cross talks with other cell types. However, to avoid using pericyte-like cells, in future major *in vitro* experiments could be performed using primary murine pericytes freshly isolated from retinas or brain tissues from α-SMA-GFP mice or α-SMA-RFPcherry mice (details about these mice are described in Chapter 2 and 6). Using NG2 staining and fluorescence-activated cell sorting (FACS), different perivascular cell subsets could be selectively collected. Post-capillary pericytes would be represented by α-SMA positive cells, which are at the same time negative for NG2.

In fluorescence time lapse microscopy experiments both TNF-α and IL-1β stimulation led to a respective change in cell shape in a time-dependent manner resulting in a significant cell elongation quantified by measuring cell eccentricity. In addition, TNFRI and TNFRII and IL-1RI were expressed on C3H/10T1/2 cells showing that these pro-inflammatory cytokines can act directly on the cells. This supports the *in vivo* findings of pericyte shape change during inflammatory conditions and provides further evidence to suggest that post-capillary venular pericytes are able to change their shape in direct response to TNF-α and IL-1β. *In vivo*, this active shape change, which led to an increase in mean gap size between adjacent cells, might facilitate neutrophil transmigration via enhanced permissiveness to migrating cells and/or through contributing to the establishment of chemoattractant gradients.

Interestingly, TNF-α-induced cell elongation occurred more rapidly than it did upon IL-1β stimulation. This highlights again the existence of different mechanisms of action for these two pro-inflammatory stimuli and supports the hypothesis that IL-1β induced pericyte shape change might involve *de novo* synthesis of secondary mediators as discussed in Chapter 4.

Stimulation of shape change has previously been demonstrated for pericytes *in vitro*. Primary rat lung pericytes contract in response to the addition of TNF-α and IL-1β (Kerkar et al., 2006). Rat lung pericytes have also been shown to contract after addition of VEGF (Donoghue et al., 2006) or vasoactive agents such as histamine (Kelley et al., 1987), serotonin (Kelley et al., 1987; Speyer et al., 1999) and bradykinin (Speyer et al., 1999) and inflammatory mediators like lipopolysaccharide (LPS) (Khoury and Langleben, 1998; Speyer et al., 2000) and platelet-activating

factor (PAF) (Khoury and Langleben, 1996). Co-cultures of rat lung pericytes and rat pulmonary microvascular endothelial cells exposed to TNF-α, IL-1β and LPS exhibit increased permeability (Edelman et al., 2006; Kerkar et al., 2006). These studies support the possibility that pericyte shape change, which led to an increase in mean gap size between adjacent cells, might not only facilitate neutrophil transmigration but also regulate microvascular permeability. Ultimately, pericyte shape change and its involvement in leukocyte transmigration was investigated *in vivo* in real time using 4D confocal intra vital microscopy (IVM) and the results are detailed in the following Chapter.

Chapter 6: Role of pericyte shape change in leukocyte transmigration *in vivo*

6.1 Introduction

To extend the findings described in Chapters 4 and 5, pericyte shape change and its involvement in leukocyte transmigration was observed and studied *in vivo* in real time. Intravital microscopy (IVM) is a powerful technique for real time *in vivo* investigation of leukocyte/vessel wall interactions in inflammatory reactions and our group recently developed immunofluorescence *in vivo* labelling to be able to visualise different components of the vessel wall for confocal IVM. Pericyte surface markers are not expressed in sufficient abundance on pericytes surrounding cremasteric post-capillary venules in the mouse to enable visualisation by confocal IVM using antibody based approaches (Chapter 3, section 3.2.1). An alternative is to generate mice expressing reporter genes such as Green Fluorescent Protein (GFP)) under the control of cell type specific markers (Maggi and Ciana, 2005). This is achieved either via gene fusion, gene knock in technology or a transgenic approach. Reporter fusion proteins are created through joining the reporter gene to the gene coding for the protein of interest (Maggi and Ciana, 2005). Reporter gene knock-in involves the insertion of the reporter gene into the gene encoding the protein of interest and is therefore a "targeted" gene insertion whereby the endogenous gene is partially deleted (gene knockout) (Koller and Smithies, 1992; Galli-Taliadoros et al., 1995). Transgenic reporter animals are generated by introducing the marker gene into their genome at random sites using the promoter of a gene of interest (Palmiter and Brinster, 1985; Cui et al., 1994). Typically, these technologies of genetic engineering are used to generate genetically modified mice since the technology is more advanced in this species.

To date several different pericyte reporter mice have been generated including promoter-trap transgene XlacZ4 mice (Tidhar et al., 2001), Anxa5-lacZ mice (Brachvogel et al., 2005; Brachvogel et al., 2007), RGS5-GFP mice (Nisancioglu et al., 2008), α-SMA-GFP mice (Yokota et al., 2006) and α-SMA-RFPcherry mice (see 2.1.1). α-SMA-GFP mice and α-SMA-RFPcherry mice are transgenic mice, which express GFP or RFPcherry under the control of the α-SMA promoter, respectively. These two mouse strains could be used for direct *in vivo* imaging of post-capillary venular pericytes using confocal IVM because deployment of fluorescent proteins as pericyte reporter allowed real time imaging since additional staining steps (e.g. using

fluorescent X-gal) were not required. Since α-SMA was used as a marker for pericytes surrounding post-capillary venules throughout this study, this method was advantageous because it permitted direct comparison of data obtained by *ex vivo* immunofluorescence labelling of whole mounted cremaster muscles (Chapters 3 and 4) with real time analysis of post-capillary venular pericytes using direct 4D confocal IVM.

Using these mice, this Chapter aims to investigate pericyte shape change and its involvement in leukocyte transmigration *in vivo* in real time using 4D confocal IVM. Pericyte shape change was imaged using α-SMA-GFP mice and as a start the profile of GFP expression in these mice was assessed in cremasteric blood vessels and compared in cremasteric post-capillary venules with immunofluorescence labelling using the anti-α-SMA antibody that was used throughout this study to visualize pericytes and vascular smooth muscle cells. Expression analysis experiments were also performed using α-SMA-RFPcherry mice expressing the cherry variant of the Red Fluorescent Protein under the control of the α-SMA promoter. The present study is the first to show pericyte shape change resulting in an enlargement of gaps between adjacent cells *in vivo* in real time upon topical application of TNF-α. To examine pericyte involvement in leukocyte transmigration α-SMA-RFPcherryxLys-EGFP mice were used which were generated by crossing α-SMA-RFPcherry mice, with mice that have EGFP knocked into the lysozyme gene (Lys-EGFP mice). Using these mice, we were able to visualise and study for the first time the transmigration of leukocytes (GFP labelled) through gaps between pericytes (RFPcherry labelled) in cremasteric post-capillary venules in real time. Ultimately, using the image analysis software IMARIS we quantified the association of gap size changes with leukocyte transmigration to elucidate whether the transmigrating leukocytes preferentially use enlarged pericyte gaps to migrate into the surrounding tissue.

6.2 Results

6.2.1 Phenotype of α-SMA-GFP and α-SMA-RFPcherry mice

In initial studies, the phenotype of α-SMA-GFP and α-SMA-RFPcherry transgenic mice was assessed by investigating the expression profile of GFP or RFPcherry, as driven by the α-SMA promoter, in cremasteric blood vessels. In order to visualize all types of blood vessels for assessment of their GFP or RFPcherry expression the endothelial marker PECAM-1 was used. Unstimulated male α-SMA-GFP or α-SMA-RFPcherry mice were injected i.s. with 2 µg rat anti-mouse PECAM-1 antibody (clone C390, conjugated to Alexa-647) in 400 µl saline to label the endothelium (as detailed in 4.2.6). After 2 h incubation, cremaster muscles were dissected, fixed and used whole mounted for confocal analysis.

In the cremaster muscle, the expression of GFP or RFPcherry under the control of the α-SMA promoter corresponded to the expression pattern of α-SMA seen by immunofluorescence labelling (as described in 3.2.1). GFP or RFPcherry was strongly expressed in pericytes surrounding post-capillary and collecting venules as well as in smooth muscles cells, which are wrapped tightly around arterioles, arteries and large veins (Figure 6.1 and Figure 6.3, respectively). Pericytes in capillaries on the other hand showed low or no GFP or RFPcherry expression (Figure 6.1 and Figure 6.3, respectively). Interestingly, cell nuclei of smooth muscle cells and all pericyte subtypes were GFP or RFPcherry positive, which is highlighted on capillaries in Figure 6.1 and Figure 6.3, respectively and post-capillary venules shown in Figure 6.2 and Figure 6.4, respectively.

In cremasteric post-capillary venules GFP expression was compared to immunofluorescence labelling using the anti-mouse α-SMA-Cy3 antibody (clone 1A4), which was used throughout this study to visualize pericytes and vascular smooth muscle cells. A similar experiment was performed using α-SMA-RFPcherry mice and the same clone of the anti-mouse α-SMA antibody but conjugated to Alexa-488. Cremaster muscles were isolated from unstimulated α-SMA-GFP or α-SMA-RFPcherry mice, fixed and used whole mounted for immunofluorescence staining and confocal microscopy. The discontinuous nature of the pericyte layer of cremasteric post-capillary venules could also be seen in α-SMA-GFP and

α-SMA-RFPcherry mice and showed comparable localisation with α-SMA expression as visualized by immunofluorescence labelling (Figure 6.2 and Figure 6.4, respectively). Of importance, there is an exact colocalisation of gaps between adjacent pericytes (Figure 6.2 and Figure 6.4, respectively). The only discrepancy between α-SMA-GFP or α-SMA-RFPcherry expression and α-SMA staining could be seen in cell nuclei, which are α-SMA negative but seemed to be GFP or RFPcherry positive (Figure 6.2 and Figure 6.4, respectively). One explanation for this difference might be that the reporter proteins expressed under the control of the α-SMA promoter are dispersed throughout the entire cytosol surrounding and covering the nucleus making it appear to be GFP or RFPcherry positive. α-SMA fibers on the other hand form a network throughout the cytosol, in which very few fibers seemed to be running across the nucleus. Apart from that, this characteristic of GFP and similar reporter proteins to translocate into the nucleus has been observed in numerous studies before.

Based on these findings, α-SMA-GFP and α-SMA-RFPcherry mice provide an excellent tool for direct *in vivo* real time imaging of pericytes surrounding cremasteric post-capillary venules using confocal IVM. In addition, using the same marker permits direct comparison of data obtained by *ex vivo* immunofluorescence labelling of whole mounted cremaster muscles with real time analysis of post-capillary venular pericytes using direct 4D confocal IVM.

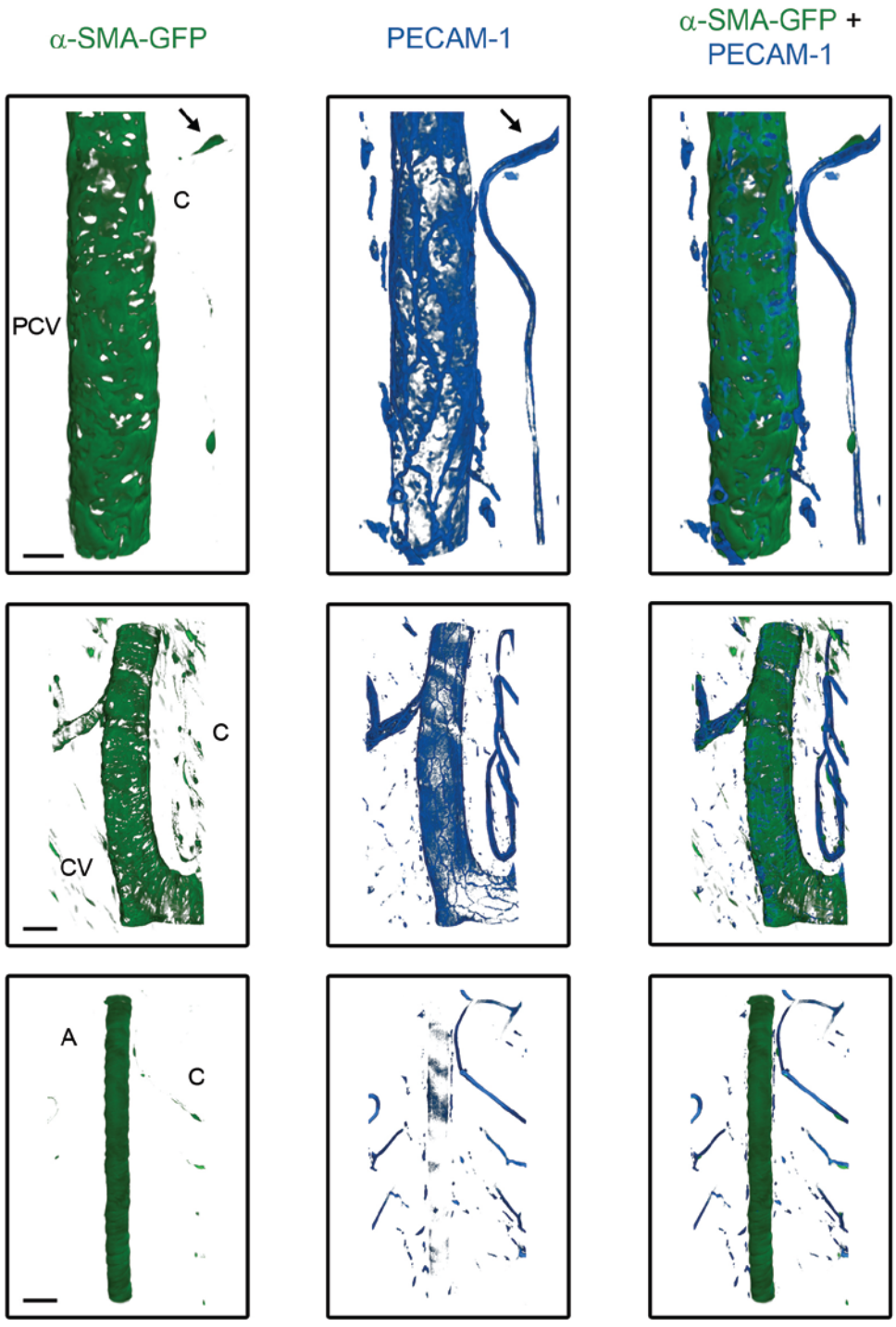

Figure 6.1: Phenotype of α-SMA-GFP mice. GFP expression could be detected in pericytes and vascular smooth muscle cells in the cremaster muscle. Representative 3D-reconstructed longitudinal confocal image sections are shown depicting different vessel types. Unstimulated α-SMA-GFP mice were injected i.s. with 2 µg anti-PECAM-1-Alexa647 antibody in 400 µl saline to label the endothelium (blue). After 2 h incubation, mice were sacrificed, cremaster muscles were dissected, fixed in 4 % PFA and subsequently used whole mounted for confocal microscopy. A, arteriole; C, capillary; CV, collecting venule; PCV, post-capillary venule. The arrow indicates a pericyte nucleus, which seems to contain GFP despite being α-SMA negative. Bars, 20 µm (top row) and 50 µm (middle and bottom row).

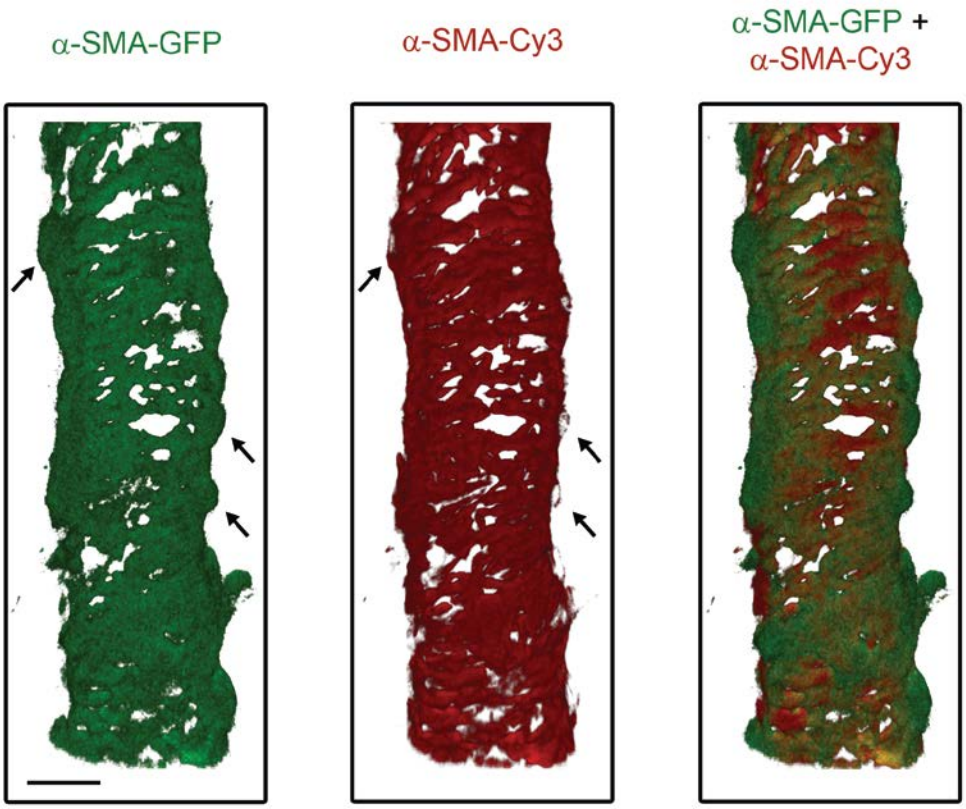

Figure 6.2: The discontinuous nature of the pericyte layer in post-capillary venules could also be seen in α-SMA-GFP mice in line with the α-SMA expression pattern visualized through immunostaining of tissues for α-SMA. A representative 3D-reconstructed longitudinal confocal image section depicting a cremasteric post-capillary venule of an α-SMA-GFP mouse stained to visualise α-SMA is shown. The cremaster muscle was isolated from an unstimulated α-SMA-GFP mouse, fixed in 4 % PFA and used whole mounted for immunofluorescence labelling using the α-SMA-Cy3 antibody (clone 1A4), which was used throughout this study to visualize pericytes and vascular smooth muscle cells. Arrows indicate pericyte nuclei, which seem to contain GFP despite being α-SMA negative. Bar, 20 μm.

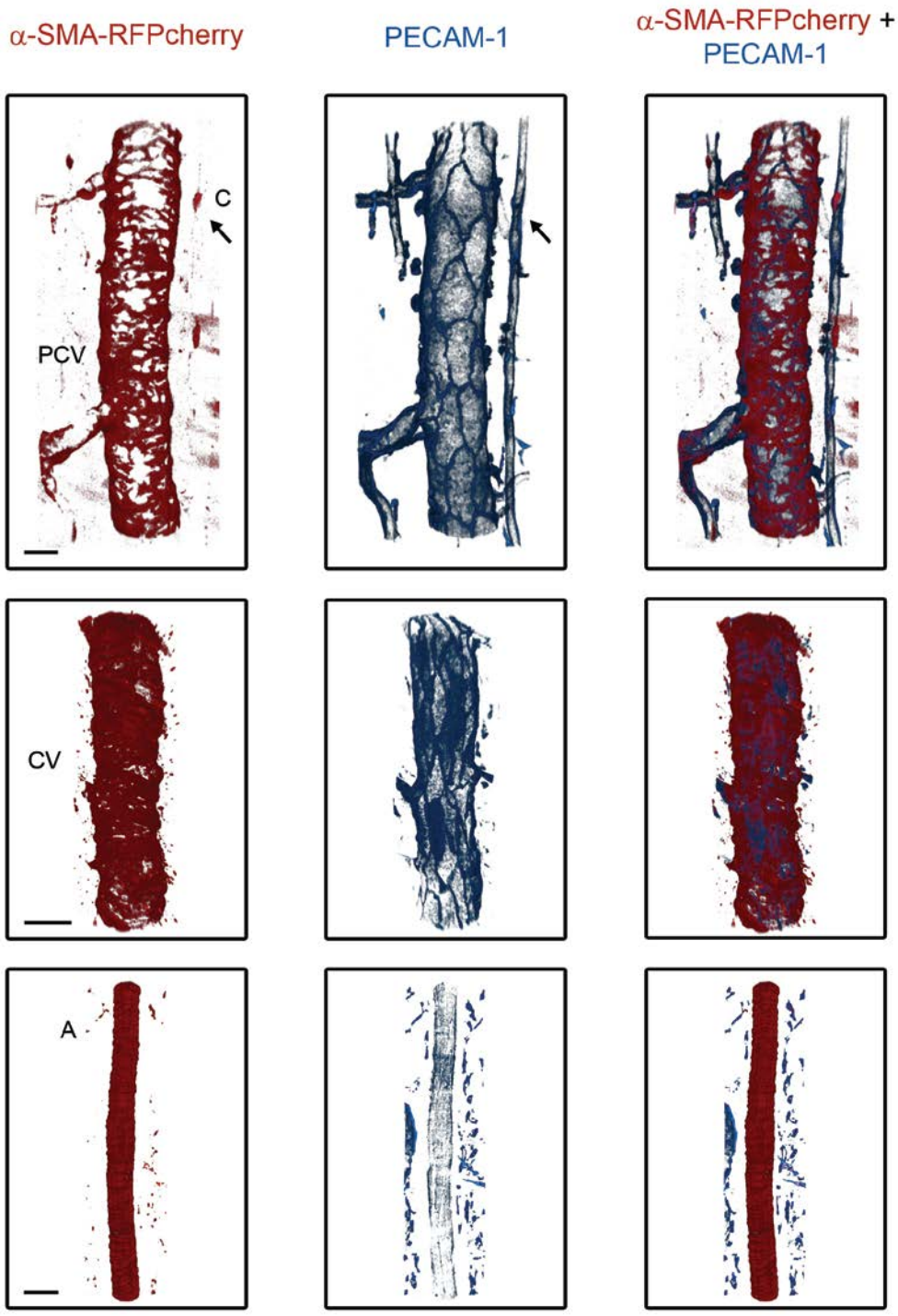

Figure 6.3: Phenotype of α-SMA-RFPcherry mice. RFPcherry expression could be detected in pericytes and vascular smooth muscle cells in the cremaster muscle. Representative 3D-reconstructed longitudinal confocal image sections are shown depicting different vessel types. Unstimulated α-SMA-GFP mice were injected i.s. with 2 µg anti-PECAM-1-Alexa647 antibody in 400 µl saline to label the endothelium (blue). After 2 h incubation, mice were sacrificed, cremaster muscles were dissected, fixed in 4 % PFA and subsequently used whole mounted for confocal microscopy. A, arteriole; C, capillary; CV, collecting venule; PCV, post-capillary venule. The arrow indicates a pericyte nucleus, which seems to contain RFPcherry despite being α-SMA negative. Bars, 20 µm (top row) and 50 µm (middle and bottom row).

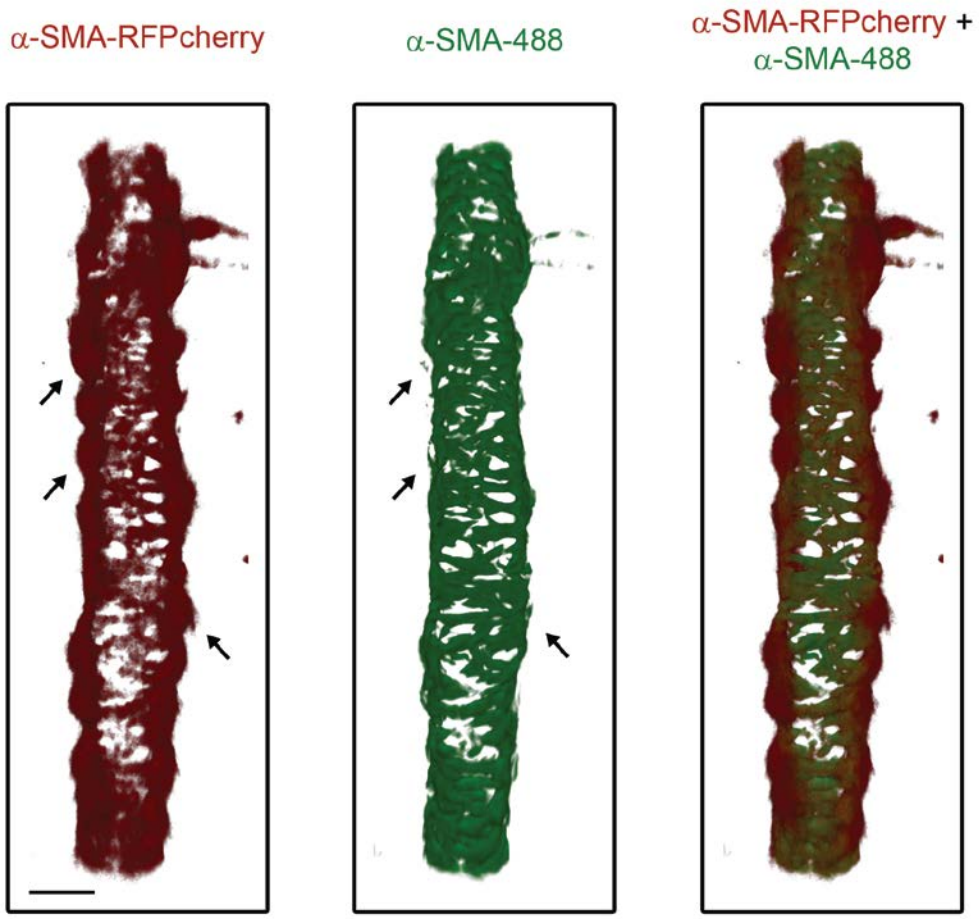

Figure 6.4: The discontinuous nature of the pericyte layer in post-capillary venules could also be seen in α-SMA-RFPcherry mice in line with the α-SMA expression pattern visualized through immunostaining of tissues for α-SMA. A representative 3D-reconstructed longitudinal confocal image section depicting a cremasteric post-capillary venule of an α-SMA-RFPcherry mouse stained to visualise α-SMA is shown. The cremaster muscle was isolated from an unstimulated α-SMA-RFPcherry mouse, fixed in 4 % PFA and used whole mounted for immunofluorescence labelling using an Alexa-488 conjugate of the α-SMA antibody (clone 1A4). Arrows indicate pericyte nuclei, which seem to contain RFPcherry despite being α-SMA negative. Bar, 20 μm.

6.2.2 Confocal Intravital Microscopy to observe TNF-α-induced pericyte shape change in real time in cremasteric post-capillary venules of α-SMA-GFP mice

Based on the findings of TNF-α- and IL-1β-induced pericyte shape change *in vivo*, using *ex vivo* immunofluorescence labelling and confocal microscopy of whole mounted cremaster muscles (Chapter 4), TNF-α-induced pericyte shape change was further investigated in more detail *in vivo* using real time 4D confocal IVM. α-SMA-GFP mice were used for these experiments, because GFP seemed to be brighter then RFPcherry and more stable in terms of laser-induced fluorescence photobleaching.

For real time confocal IVM analysis of pericyte shape change upon TNF-α stimulation, α-SMA-GFP mice were anaesthetised and cremaster muscles were exteriorised and pinned out flat over the optical window of a heated microscope stage. Throughout the experiment, cremaster muscles were constantly superfused with Tyrode's salt solution. Z-stack images of a post-capillary venule were captured every 1 min. After 5 min of imaging, pericyte shape change was induced by adding TNF-α to the Tyrode's solution at 30 ng/ml and images were taken every 1 min for a further 2 h and 30 min. The dose of TNF-α employed for topical application was determined in preliminary studies and the *in vivo* test period was that known to elicit significant pericyte shape change as observed in time-course studies of pericyte shape change induced by local injection of TNF-α (described in Chapter 4). As control, cremasters were superfused with Tyrode's salt solution alone.

When applying Tyrode's salt solution alone, pericytes showed no change in cell shape over time (Figure 6.5 left column, Movie 6.1), whereas topical application of TNF-α led to a change in cell shape in a time-dependent manner resulting in an enlargement of gaps between adjacent cells (Figure 6.5 right column, Movie 6.2). Interestingly, when comparing the confocal IVM observations with the time-course studies of TNF-α-induced pericyte shape change detailed in Chapter 4, similar dynamics were noted despite differences in the method by which TNF-α was administered. In the time-course studies gap enlargement could already be seen after 30 min which continued to peak at the 2 h time point. In the confocal IVM experiments pericyte shape change could also be noted already around 30 min after topical application of

TNF-α and slowly continued to peak at the 2 h time point. These experiments illustrate that TNF-α-induced enlargement of gaps between adjacent pericytes might occur in a continuous manner evolving over a time period of around 2 h. After 2 h of TNF-α stimulation, the enhanced gaps seemed to decrease in size again resulting in gap sizes similar to basal level at the final time point (2 h 30 min).

To asses whether the dose and *in vivo* test period used for topical application of TNF-α induced an inflammatory response in the cremaster muscle, tissues were dissected after confocal IVM, fixed in 4 % PFA and used whole mounted for immunofluorescence labelling to visualise neutrophils (MRP-14, red). Subsequently, cremaster muscles were used whole mounted for confocal microscopy to image the neutrophil transmigration response around the post-capillary venule imaged during confocal IVM. Tyrode's salt solution alone induced no transmigration of neutrophils into the tissue (Figure 6.6 left panel), whereas after topical application of TNF-α transmigrated neutrophils could be detected (Figure 6.6 right panel).

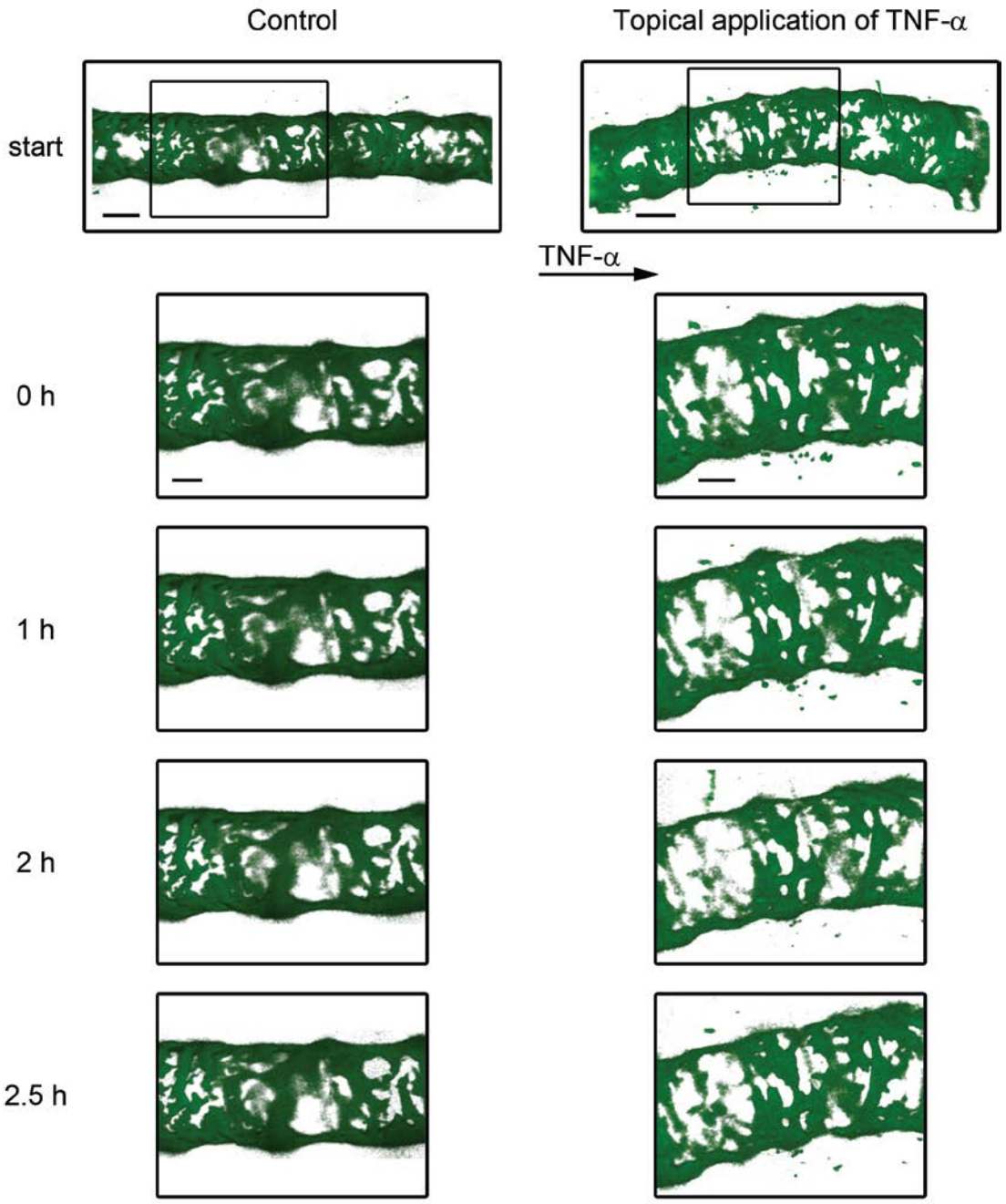

Figure 6.5: Direct 4D confocal IVM to investigate pericyte shape change in response to TNF-α in real time. α-SMA-GFP mice were anaesthetised and cremaster muscles were exteriorised and pinned out flat over the optical window of a heated microscope stage. Cremaster muscles were constantly superfused with Tyrode's solution. The top panel shows two 3D-reconstructed confocal images of cremasteric post-capillary venules at the start of a confocal IVM experiment (left: Tyrode's control experiment, right: Topical application of TNF-α). Bars, 20 μm. After 5 min of imaging, TNF-α was applied by adding it to the Tyrode's solution at 30 ng/ml. Boxed regions are shown enlarged underneath, representing subsections of these venules at indicated time points of the confocal IVM experiment. Bars, 20 μm.

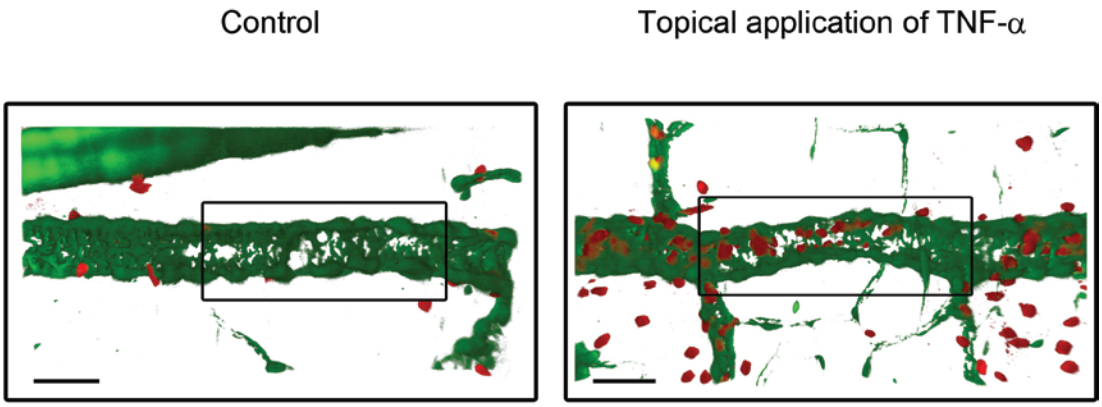

Figure 6.6 Neutrophil transmigration upon topical application of TNF-α during 4D confocal IVM. After confocal IVM (2 h and 30 min of topical application of either Tyrode's solution or TNF-α), cremaster muscles were dissected, fixed in 4 % PFA and used whole mounted for immunofluorescence labelling to visusalise neutrophils (MRP-14, red). The images show 3D-reconstructed longitudinal confocal image sections of the same post-capillary venules shown in Figure 6.3 after MRP-14 staining (left: Tyrode's control experiment, right: Topical application of TNF-α). Bars, 50 µm.

6.2.3 Generation of α-SMA-RFPcherryxLys-EGFP mice

As detailed in section 6.2.1 α-SMA-RFPcherry mice provide an excellent tool for direct *in vivo* real time imaging of pericytes surrounding cremasteric post-capillary venules using confocal IVM. We then obtained mice, which have enhanced Green Fluorescent Protein (eGFP) knocked into the lysozyme gene, exhibiting GFP-labelled neutrophils and monocytes. By crossing these two mouse strains, we generated mice that could be used for 4D confocal IVM to study the transmigration of GFP labelled leukocytes through gaps between RFPcherry labelled pericytes in cremasteric post-capillary venules in real time (Figure 6.7). The α-SMA-RFPcherry mice are transgenic reporter mice and need therefore to be paired with mice that are WT for the transgene to avoid excessive multiplication of the transgene in their genome, which could lead to insertional mutagenesis of endogenous genes (Palmiter and Brinster, 1985). Hence, instead of using C57BL/6 WT mice Lys-EGFP mice were used, which are also on a C57BL/6 background. Litters were for the most part α-SMA-RFPcherry positive and were tested for α-SMA-RFPcherry expression as described in 2.1.2.2. To ensure that all litters from these pairings express GFP, homozygous Lys-EGFP mice were used for breeding (Figure 6.7).

The endothelial cell layer was also visualised in α-SMA-RFPcherryxLys-EFGP mice using immunofluorescence *in vivo* staining for PECAM-1 to observe not only leukocyte transmigration through gaps in the pericyte sheath but also their transmigration through the endothelium and their behaviour whilst migrating in between endothelial and pericyte layer (Figure 6.8). For this purpose, mice were injected i.s. with 2 µg anti-PECAM-1-Alexa647 antibody in 400 µl saline. To elicit leukocyte recruitment 300 ng TNF-α were injected i.s. together with the anti-PECAM-1 antibody. This dose was that known to elicit significant leukocyte transmigration as observed in time-course studies shown in Chapter 4. After 2 h incubation, mice were anaesthetised and cremaster muscles were exteriorised for direct 4D confocal IVM. This time point was chosen since previous findings from our group and time-course studies shown in Chapter 4 indicate that at 2 h after i.s. injection of TNF-α most leukocytes are starting to transmigrate through the endothelium (Figure 6.8).

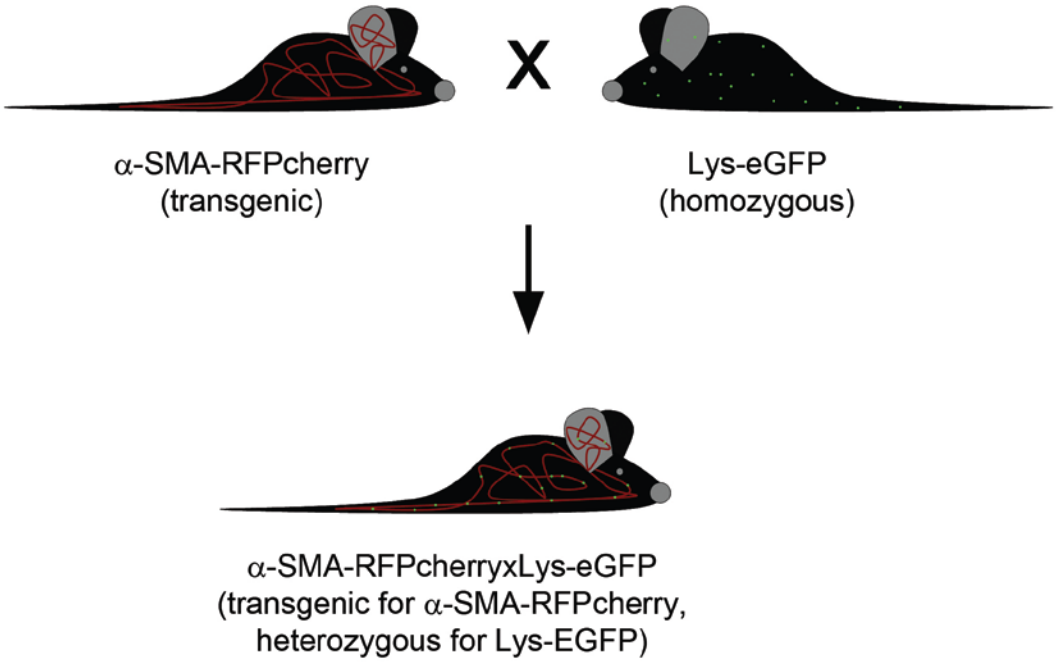

Figure 6.7: Diagram of crossing α-SMA-RFPcherry mice with Lys-EGFP mice to generate α-SMA-RFPcherryxLys-EGFP mice, which exhibit RFPcherry positive pericytes and GFP positive leukocytes. These mice are an excellent tool to observe and study leukocyte-pericyte interactions in real time using confocal IVM.

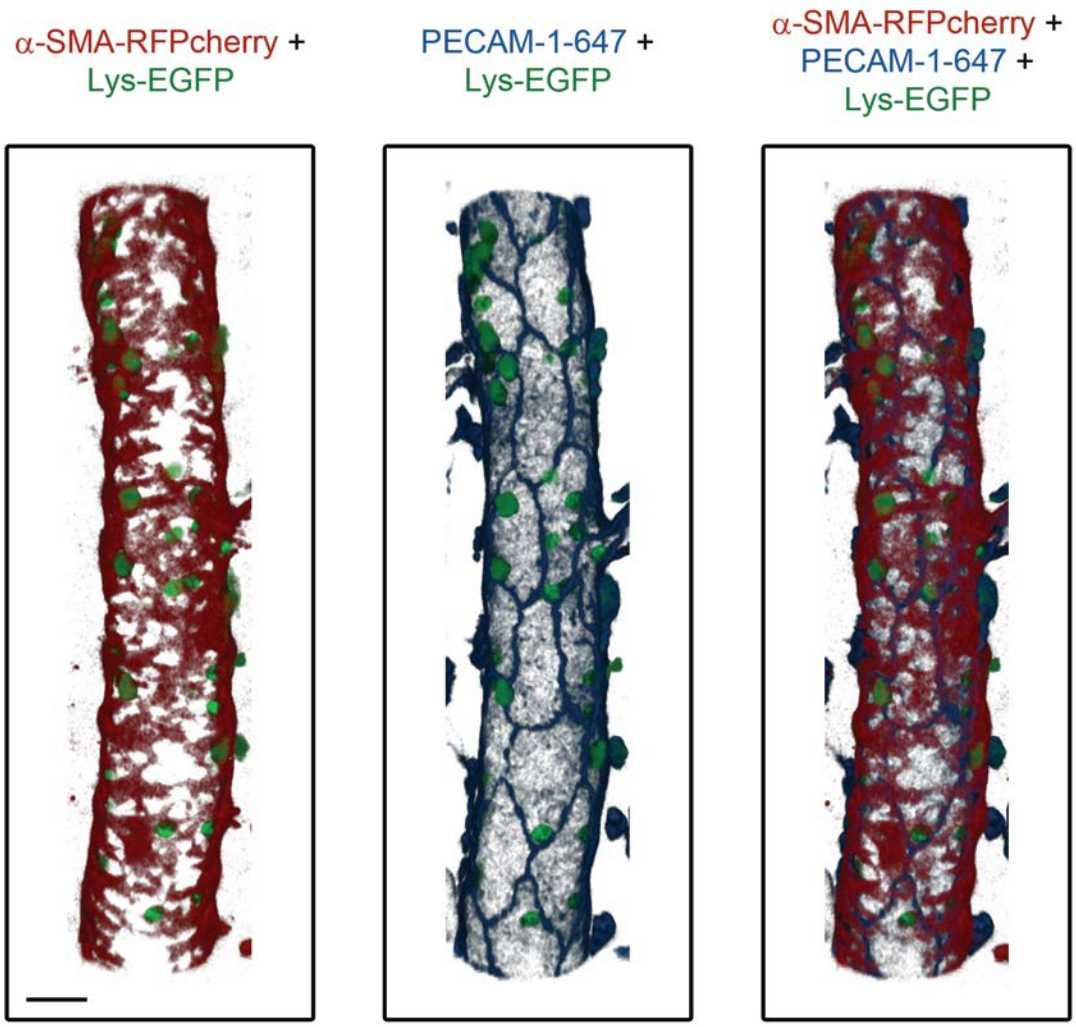

Figure 6.8: The novel α-SMA-RFPcherryxLys-EGFP mouse colony generated during the present project is a powerful tool for direct *in vivo* real time imaging of leukocyte-pericyte interactions in post-capillary venules. α-SMA-RFPcherryxLys-EFGP mice were injected i.s. with 2 µg anti-PECAM-1-Alexa647 antibody and 300 ng TNF-α in 400 µl saline to label the endothelium (blue) and elicit leukocyte recruitment, respectively. After 2 h incubation, mice were anaesthetised and cremaster muscles were exteriorised for direct 4D confocal IVM to observe leukocyte transmigration through the endothelium and the pericyte sheath in real time. The images show a representative 3D-reconstructed longitudinal confocal image section depicting a post-capillary venule of an α-SMA-RFPcherryxLys-EGFP mouse, stained to also visualise the endothelial layer, at the beginning of a confocal IVM experiment. Bar, 20 µm.

6.2.4 Confocal Intravital Microscopy to investigate association of gap size changes with leukocyte transmigration in cremasteric post-capillary venules of α-SMA-RFPcherryxLys-EGFP mice

The previous section showed that PECAM-1 labelled α-SMA-RFPcherryxLys-EGFP mice provide a powerful tool for direct *in vivo* real time imaging of leukocyte transmigration through endothelium and pericyte sheath in cremasteric post-capillary venules.

Using these mice, the involvement of TNF-α-induced pericyte shape change in leukocyte transmigration was investigated by confocal IVM. α-SMA-RFPcherryxLys-EGFP mice were prepared as described in the previous section. 2 h after anti-PECAM-1-Alexa647 and TNF-α injection, mice were anaesthetised and cremaster muscles were exteriorised and pinned out flat over the optical window of a heated microscope stage. Z-stack images of a post-capillary venule were captured every 1 min for 2 h since most leukocytes completed transmigration into the surrounding tissue during this time period (Figure 6.9, Movie 6.3). Throughout the experiment, cremaster muscles were constantly superfused with Tyrode's salt solution.

At the start of the imaging period most leukocytes were observed rolling along the vessel wall. This was followed by firm adhesion to endothelial cells and subsequent transmigration across the endothelium so that 1 h into imaging, the majority of leukocytes were migrating in between the endothelium and the pericyte sheath (Figure 6.9). During the last hour of confocal IVM most leukocytes completed the transmigration process (Figure 6.9). All transmigration events observed occurred via the paracellular route through gaps between adjacent pericytes. To associate changes in the size of gaps between pericytes with leukocyte transmigration, Dr. Mathieu-Benoit Voisin quantified the size of gaps used by leukocytes to breach the pericyte sheath. The mean gap size used for transmigration ($17.1 \pm 4.0\ \mu m^2$) was strikingly higher than the mean gap size of unstimulated cremasteric post-capillary venules but comparable with the mean gap size measured after TNF-α stimulation (results shown in Chapter 4). Upon local TNF-a stimulation for 2 h in the cremaster muscle the frequency of gap sizes within 7 - 16 μm^2 increased from 25 % to 41 % and 50 % of leukocytes used gaps in this range to cross the pericyte layer (frequency profiles are

based on the analysis of the results described in Chapter 4) (Figure 6.10). Another 34 % of leukoctyes used even bigger gaps with sizes ranging from 22 μm^2 to 42 μm^2 (Figure 6.10). Hence, transmigrating leukocytes were preferentially using pericyte gaps that had enlarged upon TNF-α stimulation to migrate into the surrounding tissue. These results suggest that TNF-α-induced pericyte shape change might facilitate leukocyte transmigration during inflammatory conditions.

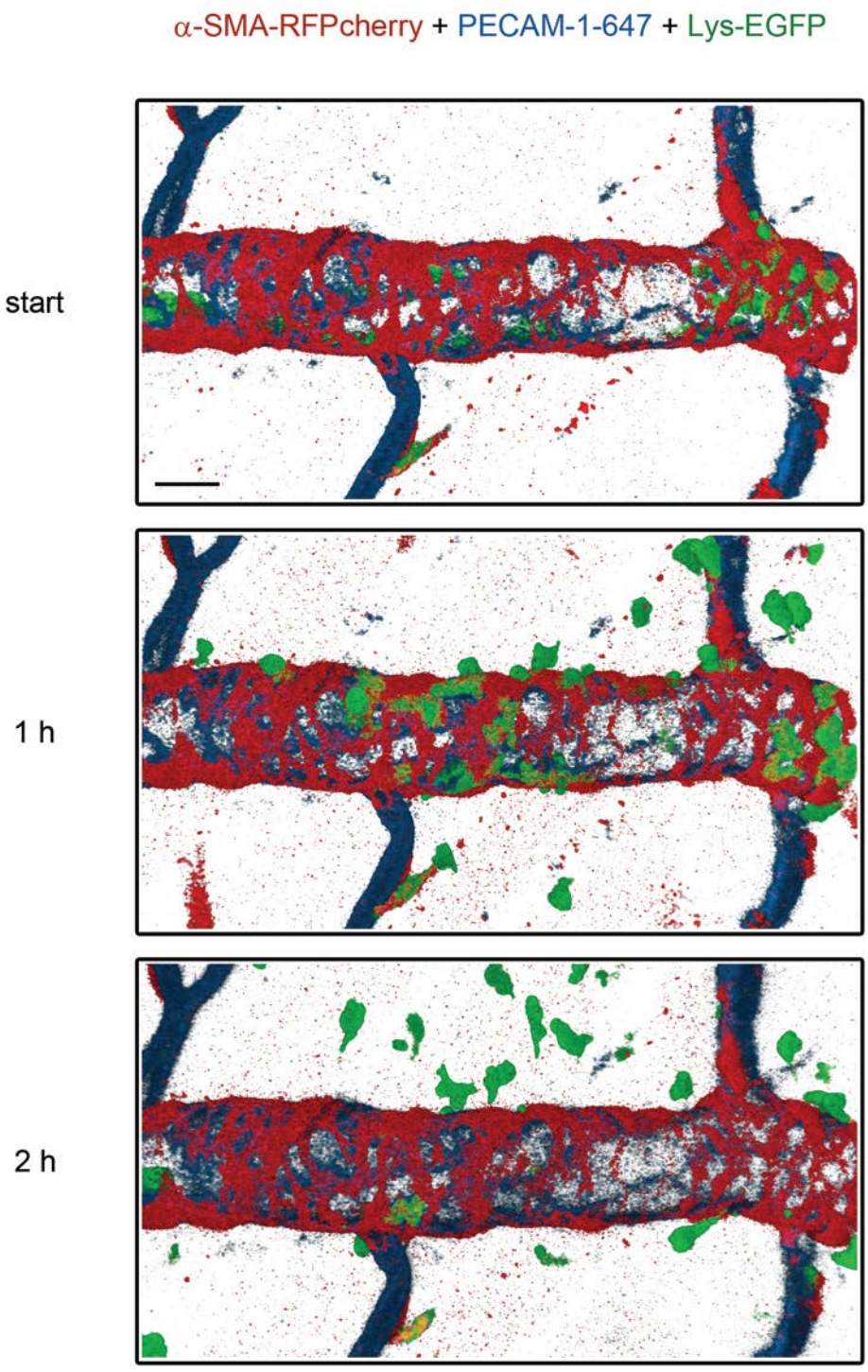

Figure 6.9: Direct 4D confocal IVM to investigate leukocyte transmigration through the endothelium and the pericyte sheath. α-SMA-RFPcherryxLys-EGFP mice were prepared as described in Figure 6.8. 2 h after anti-PECAM-1-Alexa647 and TNF-α injection, mice were anaesthetised and cremaster muscles were exteriorised and pinned out flat over the optical window of a heated microscope stage. Throughout the experiment, cremaster muscles were constantly superfused with Tyrode's solution. The images show 3D-reconstructed longitudinal confocal image sections of the same post-capillary venule at indicated time points of a confocal IVM experiment. Bar, 20 μm.

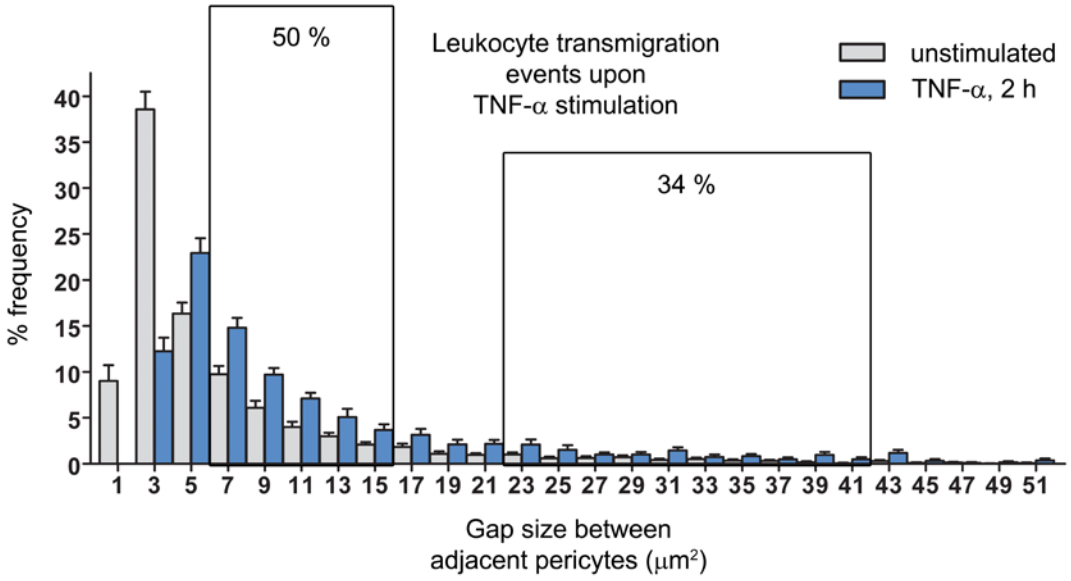

Figure 6.10: Range of sizes of gaps between adjacent pericytes preferentially used by leukocytes to cross the pericyte sheath. The graph shows the frequency of different sizes of gaps between adjacent pericytes in cremasteric post-capillary venules in percent (quantified as described in 2.6.3). Frequency profiles were generated by analysis of the results shown in Chapter 4 (Figure 4.5). Results are from n = 4 – 5 cremaster muscles and at least three venules were analysed in each. Gap sizes in the depicted range (1 – 51 μm^2) represent 98 % and 96 % of all detected gaps in unstimulated (light grey bars) and TNF-α-stimulated (blue bars) cremasteric venules, respectively. Boxed regions highlight ranges of gap sizes preferentially used by leukocytes to transmigrate through the pericyte layer as observed in confocal IVM experiments using α-SMA-RFPcherryxLys-EGFP mice (shown in Figure 6.9). The numbers inside the boxes represent the frequency of leukocyte transmigration events in the respective range of gap sizes in percent. 3D reconstructed images from these experiments were analysed to determine the sizes of gaps used by transmigrating leukocytes per experiments (quantified as described in 2.6.3). These data were obtained using four mice (equivalent to four confocal IVM experiments).

6.3 Discussion

To extend the findings described in Chapters 4 and 5, pericyte shape change and its involvement in leukocyte transmigration was observed and studied *in vivo* in real time using 4D confocal IVM. Since to date no pericyte surface marker for pericytes surrounding cremasteric post-capillary venules in the mouse is known that could be used for immunofluorescence *in vivo* labelling, the transgenic pericyte marker mouse strains α-SMA-GFP and α-SMA-RFPcherry were used. Phenotypic assessment of α-SMA-GFP and α-SMA-RFPcherry mice revealed that in cremasteric blood vessels GFP or RFPcherry expression corresponded directly with the expression pattern of α-SMA seen by immunofluorescence labelling to visualise α-SMA. Collectively, the finding indicate that these mice provide an excellent tool for direct *in vivo* real time imaging of cremasteric post-capillary venular pericytes.

Pericyte shape change was imaged using α-SMA-GFP mice, showing for the first time *in vivo* that pericytes in post-capillary venules change their shape in response to stimulation with the inflammatory cytokine TNF-α resulting in an enlargement of gaps between adjacent cells. This confirms the results obtained in time-course studies of TNF-α-induced pericyte shape change detailed in Chapter 4 as similar reaction profiles were noted. The confocal IVM experiments further elucidated the TNF-α-induced reaction showing that the enlargement of gaps between pericytes occurs in a continuous manner. The TNF-α stimulation protocol also induced neutrophil transmigration as shown by MRP-14 staining of tissues.

To examine pericyte involvement in leukocyte transmigration *in vivo* α-SMA-RFPcherry mice were crossed with Lys-EGFP mice to generate α-SMA-RFPcherryxLys-EGFP mice. This novel mouse colony enabled for the first time visualisation and study of leukocyte transmigration (GFP labelled) through the pericyte sheath (RFPcherry labelled) surrounding cremasteric post-capillary venules in real time. All transmigration events observed occurred via the paracellular route through gaps between adjacent pericytes. Quantifications of the size of gaps used by transmigrating leukocytes revealed that leukocytes seem to preferentially use enlarged pericyte gaps to migrate into the surrounding tissue. The majority of neutrophils transmigrated just after the 2 h time point, when the gap size was at its maximum, highlighting the possibility that pericyte shape change might play a critical role in facilitating leukocyte transmigration during inflammatory conditions. Pericyte shape

change resulting in significant enlargement of gaps between adjacent cells might therefore support leukocyte transmigration. This may occur via a number of means such as enhancing the permissiveness of the pericyte sheath to migrating cells and contributing to the establishment of chemoattractant gradients. Chemoattractants and chemokines could also be presented on the surface of pericytes, facilitating the interaction of leukocytes with pericytes. In this context, *in vitro* studies have shown that pericytes express glucosaminoglycans (GAGs) on their cell surface (Stramm et al., 1987) which are known to bind chemoattractants and chemokines (Johnson et al., 2005). Pericyte might also play a part in the enlargement of regions of low matrix protein deposition in the vascular basement membrane (termed low expression regions, LE regions or LERs) since pericytes express receptors for main basement membrane components including the integrins $\alpha_1\beta_1$, $\alpha_2\beta_1$ (collagen receptors), $\alpha_3\beta_1$, $\alpha_6\beta_1$, $\alpha_7\beta_1$, $\alpha_6\beta_4$ (laminin receptors), $\alpha_4\beta_1$ and $\alpha_5\beta_1$ (fibronectin receptors) (Silva et al., 2008). Previous studies from our group show that LERs are directly in line with gaps in the pericyte layer and also increase significantly in size in response to inflammatory mediators such as TNF-α, IL-1β, CCL2 and LTB_4 (Wang et al., 2006; Voisin et al., 2009; Voisin et al., 2010). These studies also highlight the fact that transmigrating leukocytes preferentially use permissive sites consisting of gaps combined with aligned LERs to migrate through venular walls. In addition, different leukocyte subtypes might use different mechanisms to breach the pericyte sheath and might therefore depend differently on pericyte responses. For example our group has previously reported that although both neutrophils and monocytes preferentially use LERs for penetrating the vascular basement membrane, these leukocyte subtypes use different and independent mechanisms (Voisin et al., 2009). Finally, pericyte shape change, which might be due to a contractile response, could also act to regulate leukocyte transmigration through venular contraction terminating the response.

Overall, confocal IVM using α-SMA-RFPcherryxLys-EGFP mice presents a powerful tool for direct *in vivo* real time imaging of leukocyte-pericyte interactions and could be used for further investigations into the mechanisms that regulate and mediate leukocyte transmigration through the pericyte layer. Compared to time-course studies using *ex vivo* immunofluorescence labelling and confocal microscopy, pericyte responses to different inflammatory stimuli can be investigated in a more detailed manner since it is now possible to investigate changes in pericyte shape by observing

the same vessel over time and taking 3D confocal images every minute. As a result, this technique also reduces the time needed and the number of mice used to complete a full time-course study. Finally, this advanced 4D imaging technique together with IMARIS now enables imaging and analysis of leukocyte-pericyte interactions, which cannot be investigated by *ex vivo* confocal analysis. Interestingly, confocal IVM experiments combined with IMARIS quantifications currently conducted by Dr. Mathieu-Benoit Voisin show that after transmigration through the endothelium leukocytes crawl along pericyte processes when in between the endothelial and the pericyte layer. This process seems to involve the presence of ICAM-1. Additional, immunofluorescence *in vivo* labelling to visualise PECAM-1 allows observing and examining leukocyte transmigration through both cellular components of the venular wall. However, this method is limited to shorter time-course experiments since mice can only be kept alive for a certain time period (up to 4 h – 6 h).

Chapter 7: General Discussion

7.1 Project overview

The recruitment of leukocytes from the circulation to sites of inflammation is a crucial event during inflammatory responses. In the last decade the understanding of the mechanisms involved in leukocyte transmigration through the endothelium has improved substantially (Ley et al., 2007; Woodfin et al., 2010) and recently some progress has been made in understanding how leukocytes breach the underlying vascular basement membrane and migrate within the extravascular tissue (Wang et al., 2006; Voisin et al., 2009; Nourshargh et al., 2010; Voisin et al., 2010). However, to date the role of pericytes in leukocyte migration has not been investigated. Therefore, this study aimed to elucidate the potential role of pericytes in regulating leukocyte transmigration and to identify the corresponding mechanisms by which leukocytes penetrate the pericyte sheath. The findings of this work contribute to our understanding of the events that mediate leukocyte transmigration during inflammatory conditions.

7.1.1 Identification and characterisation of pericytes in different types of blood vessels and in different vascular beds in the mouse

Due to the lack of specific markers for pericytes, initial studies investigated the expression profile of various commonly used pericyte markers in the cremaster muscle using immunofluorescence staining and confocal microscopy. These experiments showed that α-SMA and NG2 are highly expressed by cremasteric pericytes. However, the expression of these markers differed among pericytes depending on the vessel type. Only α-SMA was found to be expressed by pericytes surrounding post-capillary venules. Hence, α-SMA was used for the rest of this study as a marker to visualise post-capillary venular pericytes in the murine cremaster muscle as well as in various other murine tissues.

In common with pericyte marker expression, differences were also evident in pericyte shape when comparing different vessel types in the cremaster muscle. Capillary pericytes showed an elongated cell body consisting of two major processes from which numerous small processes originated. Pericytes in post-capillary venules were irregular in shape and orientation and exhibited multiple major processes

forming a discontinuous layer with gaps between adjacent cells. This confirmed previous observations that had been made using electron microscopy (Shimada et al., 1992) or immunofluorescence staining and confocal microscopy (Morikawa et al., 2002; Wang et al., 2006). Pericytes on collecting venules exhibited many major processes, however, mainly arranged circumferentially. Interestingly, the transition between the different pericyte phenotypes - marker expression as well as morphology - occurred gradually.

Pericyte morphology was also compared among post-capillary venules of different vascular beds, such as the cremaster muscle, the mesentery, the skin of the ear, the peritoneal wall and the diaphragm using immunofluorescence staining and confocal microscopy of whole mounted tissues. This study demonstrated, that in all vascular beds investigated the pericyte layer surrounding post-capillary venules is discontinuous with significant gaps between adjacent cells (Voisin et al., 2010). However, a significant diversity in pericyte shape and coverage was noted among these tissues, resulting in different mean size and density of gaps between pericytes. This highlights the existence of a wide range of vascular pericyte coverage, which has been reported previously to differ among organs (Diaz-Flores et al., 1991; Shepro and Morel, 1993; Egginton et al., 1996). This diversity could lead to differences in pericyte function and vascular permeability as well as contribute to tissue-specific mechanisms of leukocyte transmigration, which has been discussed in relation to the functional needs of different organs (Butcher and Picker, 1996; Petri et al., 2008).

All the tissues investigated were also immunostained to visualise the vascular basement membrane component type IV collagen. In these vascular beds the collagen IV layer surrounding post-capillary venules was expressed in a heterogeneous manner and exhibited LERs which were directly aligned with gaps between adjacent pericytes. The same was true for laminin-511 and we obtained similar results for laminin-411 and nidogen in cremasteric post-capillary venules (Voisin et al., 2010). These findings suggest that pericytes are an important source for these basement membrane components and that their venular coverage determines the properties of the venular basement membrane (Figure 7.1). Several *in vitro* studies have shown that pericytes can generate key basement membrane constituents such as collagen IV, laminin and fibronectin (Cohen et al., 1980;

Mandarino et al., 1993; Stratman et al., 2009). Immunostaining for perlecan also revealed a heterogeneous expression. However, perlecan LERs were mainly located at venular regions covered by pericytes indicating that pericytes are not involved in the generation of this basement membrane component. Overall, both endothelial cells and pericytes have been linked to the generation of the venular basement membrane, however, differences may exist between the relative contributions of these two cell types to the different basement membrane components.

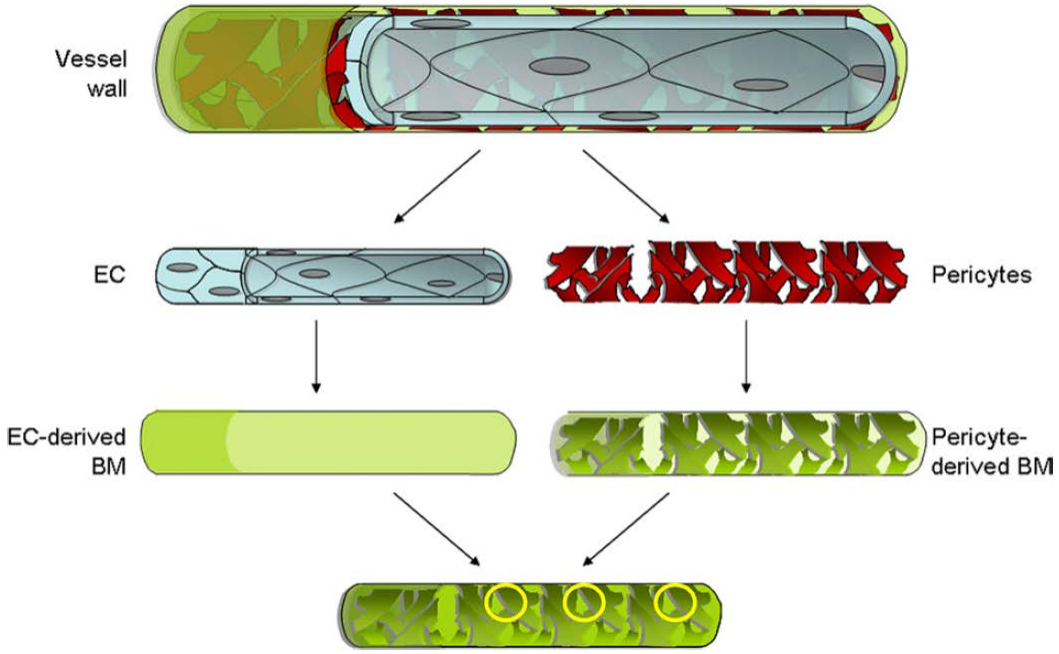

Figure 7.1: Both endothelial cells and pericytes contribute to the generation of the venular basement membrane leading to a heterogeneous expression profile of most basement membrane components. The schematic diagram illustrates the formation of venular basement membrane components, which are synthesized by both cellular components of venules (endothelial cells and pericytes). Endothelial cells form a confluent layer, which results in the generation of a continuous layer of basement membrane (left). In contrast to that, the pericyte sheath is discontinuous leading to a heterogeneous expression profile of basement membrane components (right). Therefore, the morphology and expression profile of the two cell types govern the properties of the basement membrane, especially the formation of LERs (yellow circles). Taken from Voisin et al., 2010.

7.1.2 TNF-α and IL-1β stimulation induced shape change in post-capillary venular pericytes *in vivo* and in murine pericyte-like C3H/10T1/2 cells *in vitro*

Previous findings from our group have shown that transmigrating neutrophils preferentially use the permissive sites formed by pericyte gaps and aligned LERs illustrating a functional implication of pericytes in leukocyte trafficking, especially

concerning pericyte morphology and pericyte coverage (Wang et al., 2006; Voisin et al., 2009; Voisin et al., 2010).

To elucidate the role of pericytes in inflammatory conditions, pericyte responses to different inflammatory mediators were investigated in cremasteric post-capillary venules. Topical application of the chemoattractant LTB_4 or the chemokine CCL2 onto the exteriorised cremaster muscle induced no change in pericyte morphology at the time points analysed. In contrast, I/R injury or intrascrotal injection of the inflammatory cytokines TNF-α or IL-1β elicited pericyte shape change resulting in a significant enhancement of gaps between adjacent cells (Figure 7.2). Intra dermal injection of TNF-α or IL-1β into the skin of the ear also induced a significant increase in the mean pericyte gap size, showing no evidence for a tissue-specific phenomenon. This part of the study showed for the first time pericyte responsiveness to inflammatory mediators *in vivo* indicating that pericyte shape change might play a role in leukocyte transmigration during inflammatory scenarios.

TNF-α- and IL-1β-induced reactions were selected for more detailed investigations and the responses were characterised regarding the time-course of neutrophil transmigration and pericyte shape change in the cremaster muscle. Local injection of both TNF-α and IL-1β elicited neutrophil transmigration and a significant enhancement of gaps between adjacent pericytes in a time-dependent manner. Interestingly, with regards to TNF-α, both the on-set and termination of the induced pericyte shape change response was faster than that observed for IL-1β highlighting the existence of different mechanisms of action for these two pro-inflammatory stimuli. IL-1β induced pericyte shape change might involve *de novo* synthesis of secondary mediators such as inflammatory mediators or mediators of intracellular signalling involved in regulating shape change. In both the TNF-α- and the IL-1β-induced reaction the density of gaps was not altered, suggesting that overall neither a loss nor a generation of new gaps occurred. Existing gaps just increased in size, which might be due to pericyte contractility in response to these inflammatory cytokines, since pericyte contractility upon TNF-α and IL-1β treatment has already been reported for rat lung pericytes *in vitro* (Kerkar et al., 2006) (Figure 7.3). In addition, TNF-α and IL-1β are known to activate small GTPases such as RhoA, Rac 1 and cdc42, which are well known for their ability to regulate the actin cytoskeleton (Puls et al., 1999). To investigate the involvement of neutrophils in pericyte shape

change TNF-α- and IL-1β-induced reactions were studied in neutrophil depleted mice. Neutrophil depleted mice showed the same significant increase in mean gap size after TNF-α and IL-1β stimulation indicating that in both reactions pericyte gap enhancement did not involve neutrophilic mediators or the presence of neutrophils.

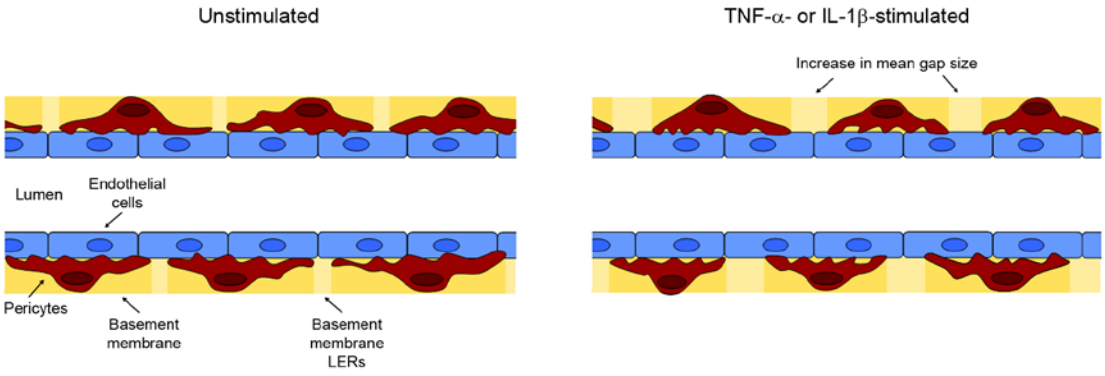

Figure 7.2: Schematic illustration of TNF-α- and IL-1β-induced pericyte shape change resulting in an increase in the mean size of gaps between adjacent pericytes. Left: Components of post-capillary venular walls in unstimulated tissues: Endothelial cells (blue), pericytes (red, with gaps between adjacent cells) and the vascular basement membrane (yellow, including LERs). Right: Local injection of TNF-α or IL-1β induced changes in pericyte morphology leading to a significant increase in the average pericyte gap size. In addition, our group has also shown that LERs, which are directly in line with gaps in the pericyte layer, significantly increase in size (Wang et al., 2006; Voisin et al., 2009; Voisin et al., 2010).

The *in vivo* findings of TNF-α- and IL-1β-induced pericyte shape change were complemented with *in vitro* analysis of pericyte responsiveness to these inflammatory cytokines using the murine pericyte-like cell line C3H/10T1/2. By performing *in vitro* experiments, pericytes could be investigated singled out from their environment to elucidate whether the responses observed *in vivo* were dependent on cross talks with other cell types (e.g. endothelial cells). Fluorescence time lapse microscopy experiments showed that both TNF-α and IL-1β stimulation led to a respective change in cell shape in a time-dependent manner resulting in a significant cell elongation quantified by measuring cell eccentricity. This supports the *in vivo* findings of pericyte shape change during inflammatory conditions and provides further evidence to suggest that post-capillary venular pericytes are able to change their shape in direct response to TNF-α and IL-1β (Figure 7.3). Interestingly, TNF-α-induced cell elongation occurred more rapidly than it did upon IL-1β stimulation highlighting again the existence of different mechanisms of action for

these two pro-inflammatory stimuli and supports the hypothesis that IL-1β induced pericyte shape change might involve *de novo* synthesis of secondary mediators.

To elucidate whether TNF-α or IL-1β can act directly on pericytes the expression profiles of the respective receptors (TNFRI/II and IL-1RI) were investigated *in vitro* and *in vivo*. These receptors have been reported to be present on endothelial cells (Orlinick and Chao, 1998; Eissner et al., 2004; Hehlgans and Pfeffer, 2005; Boraschi and Tagliabue, 2006), but this study demonstrated for the first time IL-1RI, and TNFRI/II expression on the second cellular layer of cremasteric post-capillary venules, the pericyte sheath, *in vivo* and on C3H/10T1/2 cells *in vitro*. Therefore, TNF-α- and IL-1β-induced pericyte shape change leading to gap enhancement might well be a direct effect of these cytokines on pericytes (Figure 7.3).

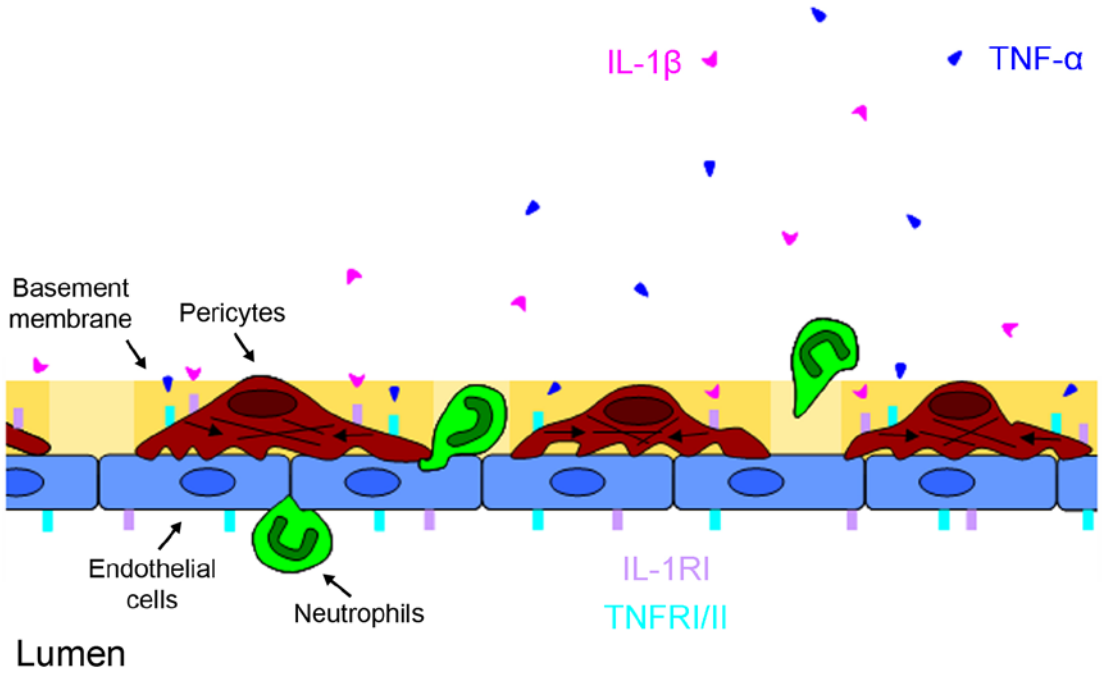

Figure 7.3: Schematic illustration of pericytes facilitating leukocyte transmigration via gap opening upon direct TNF-α and IL-1β stimulation. Components of post-capillary venular walls are illustrated under TNF-α or IL-1β stimulation: Endothelial cells (blue), pericytes (red, with enhanced gaps between adjacent cells) and the vascular basement membrane (yellow, including increased LERs). Both endothelial cells and pericytes expressed IL-1RI (light pink) and TNFRI and II (light blue). Therefore locally administered TNF-α (blue) or IL-1β (pink) can act directly on pericytes inducing the increase in mean gap size in the pericyte layer. Gap enhancement might be due to a contractile response of pericyte to TNF-α and IL-1β stimulation. Pericyte contraction and the formation of stress fibers are depicted inside the cells as black arrows and black lines, respectively. Enhanced gaps were used by transmigrating neutrophils (green) as gates to cross the pericyte sheath.

7.1.3 Role of pericyte shape change in leukocyte transmigration *in vivo*

The above findings highlight the possibility that pericytes might play a regulatory role in facilitating leukocyte transmigration via active shape change during inflammatory conditions. Therefore, pericyte shape change and its involvement in leukocyte transmigration were further investigated in more detail *in vivo* using 4D real time confocal intravital microscopy. Since to date no pericyte surface marker for pericytes surrounding cremasteric post-capillary venules in the mouse is known that could be used for immunofluorescence *in vivo* labelling, the transgenic pericyte marker mouse strains α-SMA-GFP and α-SMA-RFPcherry were used. GFP and RFPcherry expression in cremasteric blood vessels corresponded directly with the expression pattern of α-SMA seen by immunofluorescence labelling.

Using α-SMA-GFP mice, this study showed for the first time *in vivo* in real time that pericytes in post-capillary venules change their shape in response to stimulation with the inflammatory cytokine TNF-α resulting in an enlargement of gaps between adjacent cells. This confirms the time-course studies of TNF-α-induced pericyte shape change as similar reaction profiles were noted. Furthermore, this experiment showed that the enlargement of gaps between pericytes occurs in a continuous manner.

To examine pericyte involvement in leukocyte transmigration *in vivo*, α-SMA-RFPcherry mice were crossed with Lys-EGFP mice to generate α-SMA-RFPcherryxLys-EGFP mice. This novel mouse colony enabled for the first time visualisation and study of leukocyte transmigration (GFP labelled) through the pericyte sheath (RFPcherry labelled) around cremasteric post-capillary venules in real time. All transmigration events observed occurred via the paracellular route through gaps between adjacent pericytes. Quantifications of the size of gaps used by transmigrating leukocytes revealed that leukocytes seem to preferentially use enlarged pericyte gaps to migrate into the surrounding tissue (Figure 7.3). Hence, pericyte shape change resulting in significant enlargement of gaps between adjacent cells seems to support leukocyte transmigration, but the underlying mechanisms remain to be investigated. Pericyte shape change, which might be due to a contractile response, might enhance the permissiveness of the pericyte sheath to migrating cells and could contribute to the establishment of chemoattractant gradients (Figure 7.4).

In addition, chemokines and chemoattractants could also be presented on the surface of pericytes, facilitating the interaction of leukocytes with pericytes (Figure 7.4). Pericyte contraction could also act to regulate leukocyte transmigration through venular contraction terminating the response. Finally, pericytes might also play a part in the enlargement of basement membrane LERs since pericytes express receptors for main basement membrane components including the integrins $\alpha_1\beta_1$, $\alpha_2\beta_1$ (collagen receptors), $\alpha_3\beta_1$, $\alpha_6\beta_1$, $\alpha_7\beta_1$, $\alpha_6\beta_4$ (laminin receptors), $\alpha_4\beta_1$ and $\alpha_5\beta_1$ (fibronectin receptors) (Silva et al., 2008). Experimental approaches to investigate these potential mechanisms in future and additional future directions are detailed in the following sections.

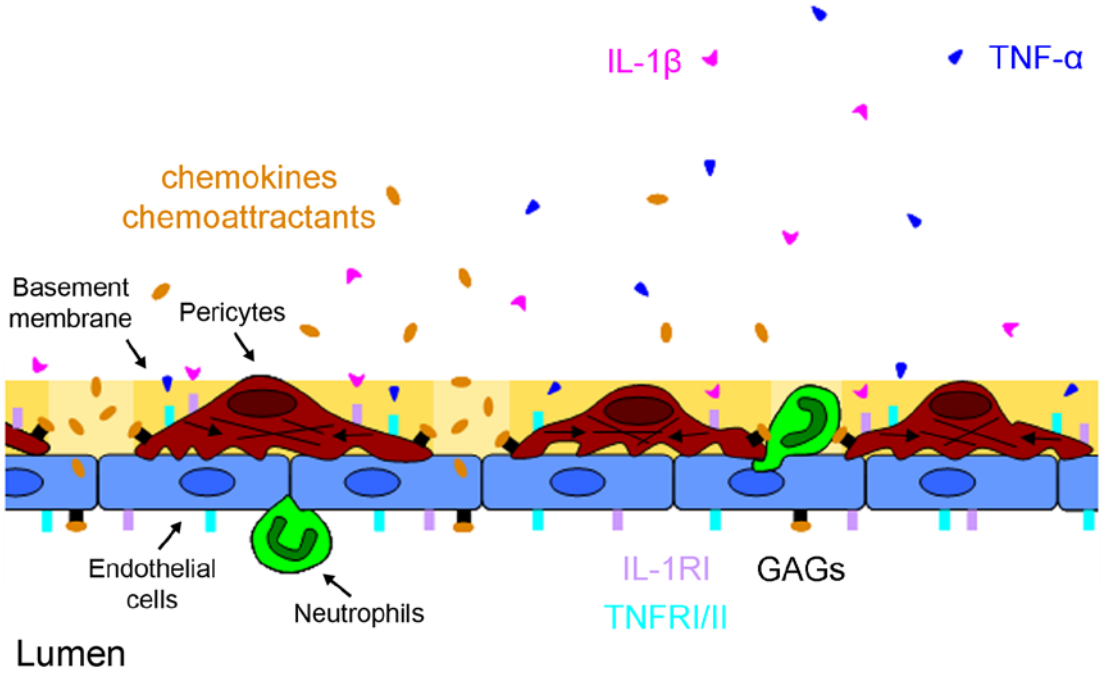

Figure 7.4: Hypothetical scenario of additional means by which enlarged pericyte gaps could aide leukocyte transmigration. Apart from increased permissiveness to transmigrating neutrophils as shown in Figure 7.3 enhanced pericyte gaps could also be more accessible to chemokines and chemoattractants (orange) and hence contribute to the establishment of chemoattractant gradients (depicted as an accumulation of chemokines and chemoattractants in gaps between adjacent pericytes). In addition, chemokines and chemoattractants could also be presented on the surface of pericytes bound to glycosaminoglycans (GAGs, black), facilitating the interaction of leukocytes with pericytes.

7.2 Future directions

7.2.1 Analysis into the mechanisms by which pericytes mediate leukocyte transmigration through enhanced gaps between adjacent cells

This study demonstrated that in the murine cremaster muscle TNF-α or IL-1β induce enlargement of gaps between adjacent pericytes and that this response supports neutrophil transmigration through the pericyte sheath. Future experiments should investigate the underlying mechanisms of pericyte shape change and elucidate how pericytes mediate neutrophil guidance towards as well as through enlarged gaps.

The reaction profiles of pericyte shape change observed for TNF-α and IL-1β differed in terms of reaction speed *in vitro* and *in vivo* highlighting the existence of different mechanisms of action for these two pro-inflammatory stimuli. On-set and termination of pericyte shape change was slower when induced by IL-1β stimulation indicating that IL-1β induced pericyte shape change might involve *de novo* synthesis of secondary mediators. Secondary mediators could be inflammatory mediators (e.g. chemokines) or mediators of intracellular signalling pathways important for cell shape change. Dependence of pericyte shape change on *de novo* protein synthesis could be determined by using inhibitors of transcription or protein biosynthesis such as actinomycin D or cycloheximide, respectively. Depending on the outcome, secondary mediators could be identified in the cremaster muscle using immunofluorescence labelling and confocal microscopy. In addition, initial *in vitro* experiments should be performed using the murine pericyte-like cell line C3H/10T1/2 or even primary murine pericytes (potential isolation procedure is detailed in section 7.2.2). Secreted proteins could be detected in cell culture supernatants and changes in the expression of intracellular proteins could be investigated upon cell lysis by using enzyme-linked immunosorbent assay (ELISA) or Western Blot. In addition, gene expression arrays could be used to screen numerous genes for changes in expression.

As indicated in Figure 7.3, TNF-α- and IL-1β-induced pericyte shape change leading to gap enhancement might be due to pericyte contraction. Pericyte contractility upon TNF-α and IL-1β treatment has already been reported for rat lung pericytes *in vitro*

(Kerkar et al., 2006). Furthermore, TNF-α and IL-1β are known to activate small GTPases such as RhoA, Rac 1 and cdc42, which are known to regulate the actin cytoskeleton (Puls et al., 1999). *In vitro* studies using bovine retinal pericytes demonstrated that RhoA but not Rac 1 and cdc42 mediates pericyte contractility (Kolyada et al., 2003; Kutcher et al., 2007; Kutcher and Herman, 2009). To elucidate whether TNF-α- and IL-1β-induced pericyte shape change is RhoA dependent, *in vivo* shape change experiments including RhoA inhibitors could be performed. However, these inhibitors could cause enormous side effects *in vivo,* since inhibition of RhoA would occur in every cell type. These side effects could then have an influence on pericyte responses. Therefore, *in vitro* time lapse experiments of TNF-α- and IL-1β-induced pericyte shape change including RhoA inhibitors might be more suitable, especially if primary murine pericytes can be used. Recently, mice have been generated that express the actin probe Lifeact-GFP (Riedl et al., 2010). These mice could provide a powerful tool to investigate the formation of actin stress fibers upon TNF-α or IL-1β stimulation *in vivo* in real time using confocal IVM, provided that it is possible to distinguish pericytes from endothelial cells, since all cells express Lifeact-GFP in these mice.

Especially important future experiments are investigations into the mechanisms by which neutrophils are attracted to enlarged pericyte gaps. Interestingly, confocal IVM experiments combined with IMARIS quantifications, conducted by Dr. Mathieu-Benoit Voisin, showed that after transendothelial migration neutrophils crawl along pericyte processes to reach preferred gaps to exit the pericyte layer toward the extravascular space. This process involved the presence of ICAM-1 since including an ICAM-1 blocking antibody abolished abluminal crawling of neutrophils. Immunofluorescence labelling of cremaster muscles showed that apart from endothelial cells pericyte on post-capillary venules also express ICAM-1, which is increased post TNF-α stimulation. These results suggest a close interaction of neutrophils with pericytes, which could be ICAM-1 mediated. In addition, the cell adhesion molecule VCAM-1 has been implicated in T cell adhesion to TNF-α-stimulated pericytes *in vitro* and has been shown to be expressed by brain pericytes during multiple sclerosis (Verbeek et al., 1995), suggesting that this molecule could also contribute to neutrophil-pericyte interactions upon TNF-α stimulation *in vivo*. Therefore, the presence of cell adhesion molecules such as VCAM-1 and integrins

and their implication in neutrophil transmigration should be investigated via immunofluorescence staining and confocal IVM, respectively.

Enlargement of gaps between adjacent pericytes could support neutrophil transmigration via the establishment of chemoattractant gradients since pericyte gaps could be more permissive to chemokines and chemoattractants. Therefore, immunofluorescence staining could be performed to elucidate the localisation of chemoattractant molecules to determine whether they accumulate in pericyte gaps. Chemokines and chemoattractants could also be presented on the surface of pericytes, facilitating the interaction of neutrophils with pericytes. In this context, *in vitro* studies have shown that pericytes express glucosaminoglycans (GAGs) on their cell surface (Stramm et al., 1987) which are known to bind chemoattractants and chemokines (Johnson et al., 2005). Hence, immunofluorescence staining to visualise chemokines and GAGs could be performed *in vivo*.

Furthermore, pericytes could facilitate neutrophil transmigration via the generation and release of pro-inflammatory mediators or proteases during inflammatory reactions. Therefore, their ability to generate pro-inflammatory mediators or proteases should be investigated. This could be done *in vitro* upon TNF-α and IL-1β stimulation by either using flow cytometry analysis of permeabilised cells or ELISA/Western Blot analysis of cell culture supernatants and cell lysates.

The present study together with other studies from our group showed LERs of most basement membrane components are directly aligned with gaps between adjacent pericytes and that they form permissive regions which are preferentially used by transmigrating neutrophils (Wang et al., 2006; Voisin et al., 2009; Voisin et al., 2010). These findings also suggest that pericytes are an important source for most basement membrane components. Several *in vitro* studies have shown that pericytes can generate key basement membrane constituents such as collagen IV, laminin and fibronectin (Cohen et al., 1980; Mandarino et al., 1993; Stratman et al., 2009). However, to date neither *in vitro* nor *in vivo* studies have been performed that directly compare the ability of endothelial cells and pericytes to generate different components of the vascular basement membrane in terms of relative contributions. Hence, *in vitro* experiments could be performed to investigate the expression of basement membrane components either *in vitro* by Real time PCR (RT-PCR) or flow cytometry of permeabilised cells or *in vivo* via immunofluorescence staining and

confocal microscopy. In addition, the presence of basement membrane components in cell culture supernatants could be examined under basal as well as inflammatory conditions using ELISA or Western Blot.

7.2.2 Isolation of primary murine pericytes

In the present study, the pericyte-like C3H/10T1/2 cells were used for *in vitro* studies into pericyte properties, but C3H/10T1/2 cells are a cell line and cannot be considered to be "authentic" pericytes. To avoid using pericyte-like cells in future, the isolation of primary murine pericytes should be established. However, isolation of primary pericytes from murine tissues presents technical difficulties due to the lack of specific markers for pericytes. Most methods for isolation and cultivation of pericytes to date are based on the selective culture of cell populations derived from tissues that exhibit high numbers of pericytes. Therefore, tissues from larger animals are used as a source (mainly rat lung and bovine retina). To date only two studies exist describing the isolation of primary pericytes from murine tissue (Tidhar et al., 2001; Brachvogel et al., 2007), but these studies isolate all perivascular cells including smooth muscle cells. Primary murine pericytes could be isolated from α-SMA-GFP mice or α-SMA-RFPcherry mice using NG2 staining and fluorescence-activated cell sorting (FACS). Using this approach, different perivascular cell subsets could be selectively collected to investigate their properties *in vitro*, isolated from other cell types. In addition, co-culture experiments with murine endothelial cells could be established. These could be used to investigate whether endothelial cells support and hence possibly even enhance pericyte shape change upon TNF-α and IL-1β stimulation, since they also express the respective receptors and have been reported to exhibit close interaction with pericytes. For instance, communication and exchange of small molecules has been shown *in vitro* to occur between microvascular endothelial cells and pericytes via gap junction (Larson et al., 1987). Furthermore, pericyte-endothelial cell co-cultures could be compared to pericytes alone in terms of permissiveness to neutrophils under both basal and inflammatory conditions.

7.2.3 Investigation into pericyte responsiveness in other vascular beds in the mouse

Investigations into pericyte responses could be extended to post-capillary venules in other vascular beds. Local injection of TNF-α and IL-1β induced pericyte shape change in both the cremaster muscle and the skin of the ear, which indicates that this might not be a tissue-specific phenomenon. However, this should be investigated in additional vascular beds. Using immunofluorescence staining and confocal microscopy, the effect of TNF-α or IL-1β stimulation on pericyte shape could also be investigated in tissues such as the mesentery. Furthermore, pericytes and their responses could also be characterized on post-capillary venules in tissues that are not thin and transparent enough to be used whole mounted for confocal microscopy such as brain, heart and kidney. Tissue sections that are thick enough to allow for imaging of whole vessels (100 - 200 µm thick) could be cut from these tissues using a vibratome. Subsequently, these sections could be used for fluorescence immunostaining and confocal analysis.

Especially interesting are investigations into pericyte responses in the mesentery, since gaps between adjacent pericytes are already quite large under basal conditions (more than twice as large as in the cremaster). In this tissue, pericyte responses to inflammatory stimuli could even be investigated *in vivo* in real time using confocal intravital microscopy (IVM) and α-SMA-GFP or α-SMA-RFPcherry mice. In addition, pericyte gaps and potential gap enhancement could be associated with neutrophil transmigration in α-SMA-RFPcherryxLys-EGFP mice as done for the cremaster muscle.

7.2.4 Pericyte responses to other pro-inflammatory stimuli and during chronic inflammatory conditions

The effects of other inflammatory stimuli on pericyte shape change and gap enhancement should also be investigated in more detail regarding their reaction profile *in vitro* and *in vivo*. Apart from the effects of TNF-α and IL-1β, this study has looked at pericyte responses to stimulation with the chemokine CCL2 and the chemoattractant LTB_4, both of which did not induce changes in pericyte shape. However, just a single time point was investigated. Therefore time-course studies or, depending on the reaction speed, even confocal IVM should be performed. Other

stimuli that do not induce neutrophil infiltration such as histamine or serotonin could also be investigated, since TNF-α-and IL-1β-induced pericyte shape change occurred in a neutrophil independent manner. Furthermore, pericyte responses could be studied in experimental mouse models of chronic inflammatory conditions such as inflammatory bowel disease or autoimmune diseases (e.g. multiple sclerosis, mouse model: Experimental autoimmune encephalomyelitis (EAE)), since all investigated reactions to date have been acute inflammatory responses.

In addition, since this study could demonstrate that pericytes express receptors for TNF-α and IL-1β, the expression of receptors for other inflammatory stimuli that caused pericyte responses could be examined and the expression profile of all receptors could be investigated under basal and inflammatory conditions.

7.2.5 Do different leukocyte subtypes use different mechanisms to migration through the pericyte sheath?

Concerning transmigration through LERs in the venular basement membrane different leukocyte subtype use different mechanisms to breach this barrier (Voisin et al., 2009). Hence, monocyte might also behave differently in penetrating the pericyte layer when compared to neutrophils. Therefore, monocyte-pericyte interactions and monocyte transmigration through the pericyte sheath should be studied in future. For this purpose, neutrophil depleted mice together with immunofluorescence staining to visualise monocytes and pericytes could be used for confocal microscopy.

References

Alexopoulou, A.N., Couchman, J.R., and Whiteford, J.R. (2008). **The CMV early enhancer/chicken beta actin (CAG) promoter can be used to drive transgene expression during the differentiation of murine embryonic stem cells into vascular progenitors**. BMC Cell Biol *9*, 2.

Alliot, F., Rutin, J., Leenen, P.J., and Pessac, B. (1999). **Pericytes and periendothelial cells of brain parenchyma vessels co-express aminopeptidase N, aminopeptidase A, and nestin**. J Neurosci Res *58*, 367-378.

Allport, J.R., Muller, W.A., and Luscinskas, F.W. (2000). **Monocytes induce reversible focal changes in vascular endothelial cadherin complex during transendothelial migration under flow**. J Cell Biol *148*, 203-216.

Alon, R., Hammer, D.A., and Springer, T.A. (1995). **Lifetime of the P-selectin-carbohydrate bond and its response to tensile force in hydrodynamic flow**. Nature *374*, 539-542.

Armulik, A., Abramsson, A., and Betsholtz, C. (2005). **Endothelial/pericyte interactions**. Circ Res *97*, 512-523.

Arnaout, M.A., Mahalingam, B., and Xiong, J.P. (2005). **Integrin structure, allostery, and bidirectional signaling**. Annu Rev Cell Dev Biol *21*, 381-410.

Asa, D., Raycroft, L., Ma, L., Aeed, P.A., Kaytes, P.S., Elhammer, A.P., and Geng, J.G. (1995). **The P-selectin glycoprotein ligand functions as a common human leukocyte ligand for P- and E-selectins**. J Biol Chem *270*, 11662-11670.

Bagley, R.G., Honma, N., Weber, W., Boutin, P., Rouleau, C., Shankara, S., Kataoka, S., Ishida, I., Roberts, B.L., and Teicher, B.A. (2008). **Endosialin/TEM 1/CD248 is a pericyte marker of embryonic and tumor neovascularization**. Microvasc Res *76*, 180-188.

Baluk, P., Hashizume, H., and McDonald, D.M. (2005). **Cellular abnormalities of blood vessels as targets in cancer**. Curr Opin Genet Dev *15*, 102-111.

Bardin, N., Anfosso, F., Masse, J.M., Cramer, E., Sabatier, F., Le Bivic, A., Sampol, J., and Dignat-George, F. (2001). **Identification of CD146 as a component of the endothelial junction involved in the control of cell-cell cohesion**. Blood *98*, 3677-3684.

Bargatze, R.F., Kurk, S., Butcher, E.C., and Jutila, M.A. (1994). **Neutrophils roll on adherent neutrophils bound to cytokine-induced endothelial cells via L-selectin on the rolling cells**. J Exp Med *180*, 1785-1792.

Barnes, P.J., Chung, K.F., and Page, C.P. (1998). **Inflammatory mediators of asthma: an update**. Pharmacol Rev *50*, 515-596.

Barreiro, O., de la Fuente, H., Mittelbrunn, M., and Sanchez-Madrid, F. (2007). **Functional insights on the polarized redistribution of leukocyte integrins and their ligands during leukocyte migration and immune interactions**. Immunol Rev *218*, 147-164.

Barreiro, O., Yanez-Mo, M., Serrador, J.M., Montoya, M.C., Vicente-Manzanares, M., Tejedor, R., Furthmayr, H., and Sanchez-Madrid, F. (2002). **Dynamic interaction of VCAM-1 and ICAM-1 with moesin and ezrin in a novel endothelial docking structure for adherent leukocytes**. J Cell Biol *157*, 1233-1245.

Barreiro, O., Zamai, M., Yanez-Mo, M., Tejera, E., Lopez-Romero, P., Monk, P.N., Gratton, E., Caiolfa, V.R., and Sanchez-Madrid, F. (2008). **Endothelial adhesion receptors are recruited to adherent leukocytes by inclusion in preformed tetraspanin nanoplatforms**. J Cell Biol *183*, 527-542.

Berlin, C., Bargatze, R.F., Campbell, J.J., von Andrian, U.H., Szabo, M.C., Hasslen, S.R., Nelson, R.D., Berg, E.L., Erlandsen, S.L., and Butcher, E.C. (1995). **alpha 4 integrins mediate lymphocyte attachment and rolling under physiologic flow**. Cell *80*, 413-422.

Bevilacqua, M.P., Pober, J.S., Mendrick, D.L., Cotran, R.S., and Gimbrone, M.A., Jr. (1987). **Identification of an inducible endothelial-leukocyte adhesion molecule**. Proc Natl Acad Sci U S A *84*, 9238-9242.

Bevilacqua, M.P., Stengelin, S., Gimbrone, M.A., Jr., and Seed, B. (1989). **Endothelial leukocyte adhesion molecule 1: an inducible receptor for neutrophils related to complement regulatory proteins and lectins**. Science *243*, 1160-1165.

Bixel, M.G., Petri, B., Khandoga, A.G., Khandoga, A., Wolburg-Buchholz, K., Wolburg, H., Marz, S., Krombach, F., and Vestweber, D. (2007). **A CD99-related antigen on endothelial cells mediates neutrophil but not lymphocyte extravasation in vivo**. Blood *109*, 5327-5336.

Boraschi, D., and Tagliabue, A. (2006). **The interleukin-1 receptor family**. Vitam Horm *74*, 229-254.

Borges, E., Eytner, R., Moll, T., Steegmaier, M., Campbell, M.A., Ley, K., Mossmann, H., and Vestweber, D. (1997a). **The P-selectin glycoprotein ligand-1 is important for recruitment of neutrophils into inflamed mouse peritoneum**. Blood *90*, 1934-1942.

Borges, E., Tietz, W., Steegmaier, M., Moll, T., Hallmann, R., Hamann, A., and Vestweber, D. (1997b). **P-selectin glycoprotein ligand-1 (PSGL-1) on T helper 1 but not on T helper 2 cells binds to P-selectin and supports migration into inflamed skin**. J Exp Med *185*, 573-578.

Brachvogel, B., Moch, H., Pausch, F., Schlotzer-Schrehardt, U., Hofmann, C., Hallmann, R., von der Mark, K., Winkler, T., and Poschl, E. (2005). **Perivascular cells expressing annexin A5 define a novel mesenchymal stem cell-like population with the capacity to differentiate into multiple mesenchymal lineages**. Development *132*, 2657-2668.

Brachvogel, B., Pausch, F., Farlie, P., Gaipl, U., Etich, J., Zhou, Z., Cameron, T., von der Mark, K., Bateman, J.F., and Poschl, E. (2007). **Isolated Anxa5+/Sca-1+ perivascular cells from mouse meningeal vasculature retain their perivascular phenotype in vitro and in vivo**. Exp Cell Res *313*, 2730-2743.

Brain, S.D., and Williams, T.J. (1990). **Leukotrienes and inflammation**. Pharmacol Ther *46*, 57-66.

Brighton, C.T., Lorich, D.G., Kupcha, R., Reilly, T.M., Jones, A.R., and Woodbury, R.A., 2nd (1992). **The pericyte as a possible osteoblast progenitor cell**. Clin Orthop Relat Res, 287-299.

Butcher, E.C. (1991). **Leukocyte-endothelial cell recognition: three (or more) steps to specificity and diversity**. Cell *67*, 1033-1036.

Butcher, E.C., and Picker, L.J. (1996). **Lymphocyte homing and homeostasis**. Science *272*, 60-66.

Campbell, J.J., Hedrick, J., Zlotnik, A., Siani, M.A., Thompson, D.A., and Butcher, E.C. (1998). **Chemokines and the arrest of lymphocytes rolling under flow conditions**. Science *279*, 381-384.

Canfield, A.E., Allen, T.D., Grant, M.E., Schor, S.L., and Schor, A.M. (1990). **Modulation of extracellular matrix biosynthesis by bovine retinal pericytes in vitro: effects of the substratum and cell density**. J Cell Sci *96 (Pt 1)*, 159-169.

Canfield, A.E., Sutton, A.B., Hoyland, J.A., and Schor, A.M. (1996). **Association of thrombospondin-1 with osteogenic differentiation of retinal pericytes in vitro**. J Cell Sci *109 (Pt 2)*, 343-353.

Carman, C.V. (2009). **Mechanisms for transcellular diapedesis: probing and pathfinding by 'invadosome-like protrusions'**. J Cell Sci *122*, 3025-3035.

Carman, C.V., Sage, P.T., Sciuto, T.E., de la Fuente, M.A., Geha, R.S., Ochs, H.D., Dvorak, H.F., Dvorak, A.M., and Springer, T.A. (2007). **Transcellular diapedesis is initiated by invasive podosomes**. Immunity *26*, 784-797.

Carman, C.V., and Springer, T.A. (2004). **A transmigratory cup in leukocyte diapedesis both through individual vascular endothelial cells and between them**. J Cell Biol *167*, 377-388.

Cepinskas, G., Sandig, M., and Kvietys, P.R. (1999). **PAF-induced elastase-dependent neutrophil transendothelial migration is associated with the mobilization of elastase to the neutrophil surface and localization to the migrating front**. J Cell Sci *112 (Pt 12)*, 1937-1945.

Cera, M.R., Fabbri, M., Molendini, C., Corada, M., Orsenigo, F., Rehberg, M., Reichel, C.A., Krombach, F., Pardi, R., and Dejana, E. (2009). **JAM-A promotes neutrophil chemotaxis by controlling integrin internalization and recycling**. J Cell Sci *122*, 268-277.

Chan-Ling, T., Page, M.P., Gardiner, T., Baxter, L., Rosinova, E., and Hughes, S. (2004). **Desmin ensheathment ratio as an indicator of vessel stability: evidence in normal development and in retinopathy of prematurity**. Am J Pathol *165*, 1301-1313.

Chan, J.R., Hyduk, S.J., and Cybulsky, M.I. (2001). **Chemoattractants induce a rapid and transient upregulation of monocyte alpha4 integrin affinity for vascular cell adhesion molecule 1 which mediates arrest: an early step in the process of emigration**. J Exp Med *193*, 1149-1158.

Chesnutt, B.C., Smith, D.F., Raffler, N.A., Smith, M.L., White, E.J., and Ley, K. (2006). **Induction of LFA-1-dependent neutrophil rolling on ICAM-1 by engagement of E-selectin**. Microcirculation *13*, 99-109.

Cho, H., Kozasa, T., Bondjers, C., Betsholtz, C., and Kehrl, J.H. (2003). **Pericyte-specific expression of Rgs5: implications for PDGF and EDG receptor signaling during vascular maturation**. Faseb J *17*, 440-442.

Cinamon, G., Shinder, V., Shamri, R., and Alon, R. (2004). **Chemoattractant signals and beta 2 integrin occupancy at apical endothelial contacts combine with shear stress signals to promote transendothelial neutrophil migration**. J Immunol *173*, 7282-7291.

Clemens, F., Verma, R., Ramnath, J., and Landolph, J.R. (2005). **Amplification of the Ect2 proto-oncogene and over-expression of Ect2 mRNA and protein in nickel compound and methylcholanthrene-transformed 10T1/2 mouse fibroblast cell lines**. Toxicol Appl Pharmacol *206*, 138-149.

Cohen, M.P., Frank, R.N., and Khalifa, A.A. (1980). **Collagen production by cultured retinal capillary pericytes**. Invest Ophthalmol Vis Sci *19*, 90-94.

Collett, G.D., and Canfield, A.E. (2005). **Angiogenesis and pericytes in the initiation of ectopic calcification**. Circ Res *96*, 930-938.

Constantin, G., Majeed, M., Giagulli, C., Piccio, L., Kim, J.Y., Butcher, E.C., and Laudanna, C. (2000). **Chemokines trigger immediate beta2 integrin affinity and mobility changes: differential regulation and roles in lymphocyte arrest under flow**. Immunity *13*, 759-769.

Corada, M., Chimenti, S., Cera, M.R., Vinci, M., Salio, M., Fiordaliso, F., De Angelis, N., Villa, A., Bossi, M., Staszewsky, L.I., *et al.* (2005). **Junctional adhesion molecule-A-deficient polymorphonuclear cells show reduced diapedesis in peritonitis and heart ischemia-reperfusion injury**. Proc Natl Acad Sci U S A *102*, 10634-10639.

Courtoy, P.J., and Boyles, J. (1983). **Fibronectin in the microvasculature: localization in the pericyte-endothelial interstitium**. J Ultrastruct Res *83*, 258-273.

Cuevas, P., Gutierrez-Diaz, J.A., Reimers, D., Dujovny, M., Diaz, F.G., and Ausman, J.I. (1984). **Pericyte endothelial gap junctions in human cerebral capillaries**. Anat Embryol (Berl) *170*, 155-159.

Cui, C., Wani, M.A., Wight, D., Kopchick, J., and Stambrook, P.J. (1994). **Reporter genes in transgenic mice**. Transgenic Res *3*, 182-194.

D'Amore, P.A., and Smith, S.R. (1993). **Growth factor effects on cells of the vascular wall: a survey**. Growth Factors *8*, 61-75.

Dangerfield, J., Larbi, K.Y., Huang, M.T., Dewar, A., and Nourshargh, S. (2002). **PECAM-1 (CD31) homophilic interaction up-regulates alpha6beta1 on transmigrated neutrophils in vivo and plays a functional role in the ability of alpha6 integrins to mediate leukocyte migration through the perivascular basement membrane**. J Exp Med *196*, 1201-1211.

Darland, D.C., and D'Amore, P.A. (2001). **TGF beta is required for the formation of capillary-like structures in three-dimensional cocultures of 10T1/2 and endothelial cells**. Angiogenesis *4*, 11-20.

Dejana, E. (2004). **Endothelial cell-cell junctions: happy together**. Nat Rev Mol Cell Biol *5*, 261-270.

Despoix, N., Walzer, T., Jouve, N., Blot-Chabaud, M., Bardin, N., Paul, P., Lyonnet, L., Vivier, E., Dignat-George, F., and Vely, F. (2008). **Mouse CD146/MCAM is a marker of natural killer cell maturation**. Eur J Immunol *38*, 2855-2864.

Diaz-Flores, L., Gutierrez, R., Lopez-Alonso, A., Gonzalez, R., and Varela, H. (1992). **Pericytes as a supplementary source of osteoblasts in periosteal osteogenesis**. Clin Orthop Relat Res, 280-286.

Diaz-Flores, L., Gutierrez, R., Varela, H., Rancel, N., and Valladares, F. (1991). **Microvascular pericytes: a review of their morphological and functional characteristics**. Histol Histopathol *6*, 269-286.

Dimitroff, C.J., Lee, J.Y., Rafii, S., Fuhlbrigge, R.C., and Sackstein, R. (2001). **CD44 is a major E-selectin ligand on human hematopoietic progenitor cells**. J Cell Biol *153*, 1277-1286.

Dinarello, C.A. (1996). **Biologic basis for interleukin-1 in disease**. Blood *87*, 2095-2147.

Doherty, M.J., Ashton, B.A., Walsh, S., Beresford, J.N., Grant, M.E., and Canfield, A.E. (1998). **Vascular pericytes express osteogenic potential in vitro and in vivo**. J Bone Miner Res *13*, 828-838.

Donoghue, L., Tyburski, J.G., Steffes, C.P., and Wilson, R.F. (2006). **Vascular endothelial growth factor modulates contractile response in microvascular lung pericytes**. Am J Surg *191*, 349-352.

Dunne, J.L., Ballantyne, C.M., Beaudet, A.L., and Ley, K. (2002). **Control of leukocyte rolling velocity in TNF-alpha-induced inflammation by LFA-1 and Mac-1**. Blood *99*, 336-341.

Edelman, D.A., Jiang, Y., Tyburski, J., Wilson, R.F., and Steffes, C. (2006). **Pericytes and their role in microvasculature homeostasis**. J Surg Res *135*, 305-311.

Egginton, S., Hudlicka, O., Brown, M.D., Graciotti, L., and Granata, A.L. (1996). **In vivo pericyte-endothelial cell interaction during angiogenesis in adult cardiac and skeletal muscle**. Microvasc Res *51*, 213-228.

Eissner, G., Kolch, W., and Scheurich, P. (2004). **Ligands working as receptors: reverse signaling by members of the TNF superfamily enhance the plasticity of the immune system**. Cytokine Growth Factor Rev *15*, 353-366.

Elshal, M.F., Khan, S.S., Takahashi, Y., Solomon, M.A., and McCoy, J.P., Jr. (2005). **CD146 (Mel-CAM), an adhesion marker of endothelial cells, is a novel marker of lymphocyte subset activation in normal peripheral blood**. Blood *106*, 2923-2924.

Eriksson, E.E., Xie, X., Werr, J., Thoren, P., and Lindbom, L. (2001). **Importance of primary capture and L-selectin-dependent secondary capture in leukocyte accumulation in inflammation and atherosclerosis in vivo**. J Exp Med *194*, 205-218.

Etchevers, H.C., Vincent, C., Le Douarin, N.M., and Couly, G.F. (2001). **The cephalic neural crest provides pericytes and smooth muscle cells to all blood vessels of the face and forebrain**. Development *128*, 1059-1068.

Farrington-Rock, C., Crofts, N.J., Doherty, M.J., Ashton, B.A., Griffin-Jones, C., and Canfield, A.E. (2004). **Chondrogenic and adipogenic potential of microvascular pericytes**. Circulation *110*, 2226-2232.

Faust, N., Varas, F., Kelly, L.M., Heck, S., and Graf, T. (2000). **Insertion of enhanced green fluorescent protein into the lysozyme gene creates mice with green fluorescent granulocytes and macrophages**. Blood *96*, 719-726.

Feng, D., Nagy, J.A., Pyne, K., Dvorak, H.F., and Dvorak, A.M. (1998). **Neutrophils emigrate from venules by a transendothelial cell pathway in response to FMLP**. J Exp Med *187*, 903-915.

Finger, E.B., Puri, K.D., Alon, R., Lawrence, M.B., von Andrian, U.H., and Springer, T.A. (1996). **Adhesion through L-selectin requires a threshold hydrodynamic shear**. Nature *379*, 266-269.

Finlay, B.B., and Hancock, R.E. (2004). **Can innate immunity be enhanced to treat microbial infections?** Nat Rev Microbiol *2*, 497-504.

Forbes, M.S., Rennels, M.L., and Nelson, E. (1977). **Ultrastructure of pericytes in mouse heart**. Am J Anat *149*, 47-70.

Fujimoto, K. (1995). **Pericyte-endothelial gap junctions in developing rat cerebral capillaries: a fine structural study**. Anat Rec *242*, 562-565.

Fujimoto, T., and Singer, S.J. (1987). **Immunocytochemical studies of desmin and vimentin in pericapillary cells of chicken**. J Histochem Cytochem *35*, 1105-1115.

Gallatin, W.M., Weissman, I.L., and Butcher, E.C. (1983). **A cell-surface molecule involved in organ-specific homing of lymphocytes**. Nature *304*, 30-34.

Galli-Taliadoros, L.A., Sedgwick, J.D., Wood, S.A., and Korner, H. (1995). **Gene knock-out technology: a methodological overview for the interested novice**. J Immunol Methods *181*, 1-15.

Geng, J.G., Bevilacqua, M.P., Moore, K.L., McIntyre, T.M., Prescott, S.M., Kim, J.M., Bliss, G.A., Zimmerman, G.A., and McEver, R.P. (1990). **Rapid neutrophil adhesion to activated endothelium mediated by GMP-140**. Nature *343*, 757-760.

Gerhardt, H., and Betsholtz, C. (2003). **Endothelial-pericyte interactions in angiogenesis**. Cell Tissue Res *314*, 15-23.

Gerhardt, H., Wolburg, H., and Redies, C. (2000). **N-cadherin mediates pericytic-endothelial interaction during brain angiogenesis in the chicken**. Dev Dyn *218*, 472-479.

Giagulli, C., Ottoboni, L., Caveggion, E., Rossi, B., Lowell, C., Constantin, G., Laudanna, C., and Berton, G. (2006). **The Src family kinases Hck and Fgr are dispensable for inside-out, chemoattractant-induced signaling regulating beta 2 integrin affinity and valency in neutrophils, but are required for beta 2 integrin-mediated outside-in signaling involved in sustained adhesion**. J Immunol *177*, 604-611.

Gilbertson-Beadling, S.K., and Fisher, C. (1993). **A potential role for N-cadherin in mediating endothelial cell-smooth muscle cell interactions in the rat vasculature**. Lab Invest *69*, 203-209.

Goetz, D.J., Greif, D.M., Ding, H., Camphausen, R.T., Howes, S., Comess, K.M., Snapp, K.R., Kansas, G.S., and Luscinskas, F.W. (1997). **Isolated P-selectin glycoprotein ligand-1 dynamic adhesion to P- and E-selectin**. J Cell Biol *137*, 509-519.

Grabovsky, V., Feigelson, S., Chen, C., Bleijs, D.A., Peled, A., Cinamon, G., Baleux, F., Arenzana-Seisdedos, F., Lapidot, T., van Kooyk, Y., *et al.* (2000). **Subsecond induction of alpha4 integrin clustering by immobilized chemokines stimulates leukocyte tethering and rolling on endothelial vascular cell adhesion molecule 1 under flow conditions**. J Exp Med *192*, 495-506.

Greenberg, J.I., Shields, D.J., Barillas, S.G., Acevedo, L.M., Murphy, E., Huang, J., Scheppke, L., Stockmann, C., Johnson, R.S., Angle, N., and Cheresh, D.A. (2008). **A role for VEGF as a negative regulator of pericyte function and vessel maturation**. Nature *456*, 809-813.

Halden, Y., Rek, A., Atzenhofer, W., Szilak, L., Wabnig, A., and Kungl, A.J. (2004). **Interleukin-8 binds to syndecan-2 on human endothelial cells**. Biochem J *377*, 533-538.

Hallmann, R., Horn, N., Selg, M., Wendler, O., Pausch, F., and Sorokin, L.M. (2005). **Expression and function of laminins in the embryonic and mature vasculature**. Physiol Rev *85*, 979-1000.

Hammer, D.A., and Apte, S.M. (1992). **Simulation of cell rolling and adhesion on surfaces in shear flow: general results and analysis of selectin-mediated neutrophil adhesion**. Biophys J *63*, 35-57.

Hehlgans, T., and Pfeffer, K. (2005). **The intriguing biology of the tumour necrosis factor/tumour necrosis factor receptor superfamily: players, rules and the games**. Immunology *115*, 1-20.

Hellstrom, M., Gerhardt, H., Kalen, M., Li, X., Eriksson, U., Wolburg, H., and Betsholtz, C. (2001). **Lack of pericytes leads to endothelial hyperplasia and abnormal vascular morphogenesis**. J Cell Biol *153*, 543-553.

Herman, I.M., and D'Amore, P.A. (1985). **Microvascular pericytes contain muscle and nonmuscle actins**. J Cell Biol *101*, 43-52.

Hirschi, K.K., and D'Amore, P.A. (1996). **Pericytes in the microvasculature**. Cardiovasc Res *32*, 687-698.

Hixenbaugh, E.A., Goeckeler, Z.M., Papaiya, N.N., Wysolmerski, R.B., Silverstein, S.C., and Huang, A.J. (1997). **Stimulated neutrophils induce myosin light chain phosphorylation and isometric tension in endothelial cells**. Am J Physiol *273*, H981-988.

Hobbs, J.A., May, R., Tanousis, K., McNeill, E., Mathies, M., Gebhardt, C., Henderson, R., Robinson, M.J., and Hogg, N. (2003). **Myeloid cell function in MRP-14 (S100A9) null mice**. Mol Cell Biol *23*, 2564-2576.

Hsu-Lin, S., Berman, C.L., Furie, B.C., August, D., and Furie, B. (1984). **A platelet membrane protein expressed during platelet activation and secretion. Studies using a monoclonal antibody specific for thrombin-activated platelets**. J Biol Chem *259*, 9121-9126.

Huang, A.J., Furie, M.B., Nicholson, S.C., Fischbarg, J., Liebovitch, L.S., and Silverstein, S.C. (1988). **Effects of human neutrophil chemotaxis across human endothelial cell monolayers on the permeability of these monolayers to ions and macromolecules**. J Cell Physiol *135*, 355-366.

Huang, A.J., Manning, J.E., Bandak, T.M., Ratau, M.C., Hanser, K.R., and Silverstein, S.C. (1993). **Endothelial cell cytosolic free calcium regulates neutrophil migration across monolayers of endothelial cells**. J Cell Biol *120*, 1371-1380.

Huang, M.T., Larbi, K.Y., Scheiermann, C., Woodfin, A., Gerwin, N., Haskard, D.O., and Nourshargh, S. (2006). **ICAM-2 mediates neutrophil transmigration in vivo: evidence for stimulus specificity and a role in PECAM-1-independent transmigration**. Blood *107*, 4721-4727.

Huber, A.R., Kunkel, S.L., Todd, R.F., 3rd, and Weiss, S.J. (1991). **Regulation of transendothelial neutrophil migration by endogenous interleukin-8**. Science *254*, 99-102.

Hughes, S., and Chan-Ling, T. (2004). **Characterization of smooth muscle cell and pericyte differentiation in the rat retina in vivo**. Invest Ophthalmol Vis Sci *45*, 2795-2806.

Hungerford, J.E., and Little, C.D. (1999). **Developmental biology of the vascular smooth muscle cell: building a multilayered vessel wall**. J Vasc Res *36*, 2-27.

Huo, Y., Hafezi-Moghadam, A., and Ley, K. (2000). **Role of vascular cell adhesion molecule-1 and fibronectin connecting segment-1 in monocyte rolling and adhesion on early atherosclerotic lesions**. Circ Res *87*, 153-159.

Issekutz, A.C., Rowter, D., and Springer, T.A. (1999). **Role of ICAM-1 and ICAM-2 and alternate CD11/CD18 ligands in neutrophil transendothelial migration**. J Leukoc Biol *65*, 117-126.

Jaffe, A.B., and Hall, A. (2005). **Rho GTPases: biochemistry and biology**. Annu Rev Cell Dev Biol *21*, 247-269.

Johnson, Z., Proudfoot, A.E., and Handel, T.M. (2005). **Interaction of chemokines and glycosaminoglycans: a new twist in the regulation of chemokine function with opportunities for therapeutic intervention**. Cytokine Growth Factor Rev *16*, 625-636.

Johnston, G.I., Cook, R.G., and McEver, R.P. (1989). **Cloning of GMP-140, a granule membrane protein of platelets and endothelium: sequence similarity to proteins involved in cell adhesion and inflammation**. Cell *56*, 1033-1044.

Joyce, N.C., DeCamilli, P., and Boyles, J. (1984). **Pericytes, like vascular smooth muscle cells, are immunocytochemically positive for cyclic GMP-dependent protein kinase**. Microvasc Res *28*, 206-219.

Joyce, N.C., Haire, M.F., and Palade, G.E. (1985a). **Contractile proteins in pericytes. I. Immunoperoxidase localization of tropomyosin**. J Cell Biol *100*, 1379-1386.

Joyce, N.C., Haire, M.F., and Palade, G.E. (1985b). **Contractile proteins in pericytes. II. Immunocytochemical evidence for the presence of two isomyosins in graded concentrations**. J Cell Biol *100*, 1387-1395.

Jung, U., Norman, K.E., Scharffetter-Kochanek, K., Beaudet, A.L., and Ley, K. (1998). **Transit time of leukocytes rolling through venules controls cytokine-induced inflammatory cell recruitment in vivo**. J Clin Invest *102*, 1526-1533.

Jutila, M.A., and Kurk, S. (1996). **Analysis of bovine gamma delta T cell interactions with E-, P-, and L-selectin. Characterization of lymphocyte on lymphocyte rolling and the effects of O-glycoprotease**. J Immunol *156*, 289-296.

Kalluri, R. (2003). **Basement membranes: structure, assembly and role in tumour angiogenesis**. Nat Rev Cancer *3*, 422-433.

Kansas, G.S. (1996). **Selectins and their ligands: current concepts and controversies**. Blood *88*, 3259-3287.

Katayama, Y., Hidalgo, A., Chang, J., Peired, A., and Frenette, P.S. (2005). **CD44 is a physiological E-selectin ligand on neutrophils**. J Exp Med *201*, 1183-1189.

Kelley, C., D'Amore, P., Hechtman, H.B., and Shepro, D. (1987). **Microvascular pericyte contractility in vitro: comparison with other cells of the vascular wall**. J Cell Biol *104*, 483-490.

Kerkar, S., Williams, M., Blocksom, J.M., Wilson, R.F., Tyburski, J.G., and Steffes, C.P. (2006). **TNF-alpha and IL-1beta increase pericyte/endothelial cell co-culture permeability**. J Surg Res *132*, 40-45.

Khoury, J., and Langleben, D. (1996). **Platelet-activating factor stimulates lung pericyte growth in vitro**. Am J Physiol *270*, L298-304.

Khoury, J., and Langleben, D. (1998). **Effects of endotoxin on lung pericytes in vitro**. Microvasc Res *56*, 71-84.

Kim, M., Carman, C.V., and Springer, T.A. (2003). **Bidirectional transmembrane signaling by cytoplasmic domain separation in integrins**. Science *301*, 1720-1725.

Kinashi, T. (2005). **Intracellular signalling controlling integrin activation in lymphocytes**. Nat Rev Immunol *5*, 546-559.

Koller, B.H., and Smithies, O. (1992). **Altering genes in animals by gene targeting**. Annu Rev Immunol *10*, 705-730.

Kolyada, A.Y., Riley, K.N., and Herman, I.M. (2003). **Rho GTPase signaling modulates cell shape and contractile phenotype in an isoactin-specific manner**. Am J Physiol Cell Physiol *285*, C1116-1121.

Kopp, E., Medzhitov, R., Carothers, J., Xiao, C., Douglas, I., Janeway, C.A., and Ghosh, S. (1999). **ECSIT is an evolutionarily conserved intermediate in the Toll/IL-1 signal transduction pathway**. Genes Dev *13*, 2059-2071.

Kunkel, E.J., and Ley, K. (1996). **Distinct phenotype of E-selectin-deficient mice. E-selectin is required for slow leukocyte rolling in vivo**. Circ Res *79*, 1196-1204.

Kutcher, M.E., and Herman, I.M. (2009). **The pericyte: cellular regulator of microvascular blood flow**. Microvasc Res *77*, 235-246.

Kutcher, M.E., Kolyada, A.Y., Surks, H.K., and Herman, I.M. (2007). **Pericyte Rho GTPase mediates both pericyte contractile phenotype and capillary endothelial growth state**. Am J Pathol *171*, 693-701.

Larson, D.M., Carson, M.P., and Haudenschild, C.C. (1987). **Junctional transfer of small molecules in cultured bovine brain microvascular endothelial cells and pericytes**. Microvasc Res *34*, 184-199.

Laudanna, C., Kim, J.Y., Constantin, G., and Butcher, E. (2002). **Rapid leukocyte integrin activation by chemokines**. Immunol Rev *186*, 37-46.

Lawrence, M.B., Kansas, G.S., Kunkel, E.J., and Ley, K. (1997). **Threshold levels of fluid shear promote leukocyte adhesion through selectins (CD62L,P,E)**. J Cell Biol *136*, 717-727.

Lawrence, M.B., and Springer, T.A. (1991). **Leukocytes roll on a selectin at physiologic flow rates: distinction from and prerequisite for adhesion through integrins**. Cell *65*, 859-873.

Leveen, P., Pekny, M., Gebre-Medhin, S., Swolin, B., Larsson, E., and Betsholtz, C. (1994). **Mice deficient for PDGF B show renal, cardiovascular, and hematological abnormalities**. Genes Dev *8*, 1875-1887.

Levinovitz, A., Muhlhoff, J., Isenmann, S., and Vestweber, D. (1993). **Identification of a glycoprotein ligand for E-selectin on mouse myeloid cells**. J Cell Biol *121*, 449-459.

Ley, K., Laudanna, C., Cybulsky, M.I., and Nourshargh, S. (2007). **Getting to the site of inflammation: the leukocyte adhesion cascade updated**. Nat Rev Immunol *7*, 678-689.

Ley, K., and Zhang, H. (2008). **Dances with leukocytes: how tetraspanin-enriched microdomains assemble to form endothelial adhesive platforms**. J Cell Biol *183*, 375-376.

Li, Q., Yu, Y., Bischoff, J., Mulliken, J.B., and Olsen, B.R. (2003). **Differential expression of CD146 in tissues and endothelial cells derived from infantile haemangioma and normal human skin**. J Pathol *201*, 296-302.

Lindahl, P., Johansson, B.R., Leveen, P., and Betsholtz, C. (1997). **Pericyte loss and microaneurysm formation in PDGF-B-deficient mice**. Science *277*, 242-245.

Linder, S., and Aepfelbacher, M. (2003). **Podosomes: adhesion hot-spots of invasive cells**. Trends Cell Biol *13*, 376-385.

Little, T.L., Xia, J., and Duling, B.R. (1995). **Dye tracers define differential endothelial and smooth muscle coupling patterns within the arteriolar wall**. Circ Res *76*, 498-504.

Lo, S.K., Lee, S., Ramos, R.A., Lobb, R., Rosa, M., Chi-Rosso, G., and Wright, S.D. (1991). **Endothelial-leukocyte adhesion molecule 1 stimulates the adhesive activity of leukocyte integrin CR3 (CD11b/CD18, Mac-1, alpha m beta 2) on human neutrophils**. J Exp Med *173*, 1493-1500.

Maggi, A., and Ciana, P. (2005). **Reporter mice and drug discovery and development**. Nat Rev Drug Discov *4*, 249-255.

Mandarino, L.J., Sundarraj, N., Finlayson, J., and Hassell, H.R. (1993). **Regulation of fibronectin and laminin synthesis by retinal capillary endothelial cells and pericytes in vitro**. Exp Eye Res *57*, 609-621.

Marmon, S., Hinchey, J., Oh, P., Cammer, M., de Almeida, C.J., Gunther, L., Raine, C.S., and Lisanti, M.P. (2009). **Caveolin-1 expression determines the route of neutrophil extravasation through skin microvasculature**. Am J Pathol *174*, 684-692.

Marshall, B.T., Long, M., Piper, J.W., Yago, T., McEver, R.P., and Zhu, C. (2003). **Direct observation of catch bonds involving cell-adhesion molecules**. Nature *423*, 190-193.

Matthay, M.A., and Zimmerman, G.A. (2005). **Acute lung injury and the acute respiratory distress syndrome: four decades of inquiry into pathogenesis and rational management**. Am J Respir Cell Mol Biol *33*, 319-327.

McEver, R.P., and Martin, M.N. (1984). **A monoclonal antibody to a membrane glycoprotein binds only to activated platelets**. J Biol Chem *259*, 9799-9804.

Medzhitov, R., Preston-Hurlburt, P., Kopp, E., Stadlen, A., Chen, C., Ghosh, S., and Janeway, C.A., Jr. (1998). **MyD88 is an adaptor protein in the hToll/IL-1 receptor family signaling pathways**. Mol Cell *2*, 253-258.

Middleton, J., Neil, S., Wintle, J., Clark-Lewis, I., Moore, H., Lam, C., Auer, M., Hub, E., and Rot, A. (1997). **Transcytosis and surface presentation of IL-8 by venular endothelial cells**. Cell *91*, 385-395.

Millan, J., Hewlett, L., Glyn, M., Toomre, D., Clark, P., and Ridley, A.J. (2006). **Lymphocyte transcellular migration occurs through recruitment of endothelial ICAM-1 to caveola- and F-actin-rich domains**. Nat Cell Biol *8*, 113-123.

Moore, K.L., Patel, K.D., Bruehl, R.E., Li, F., Johnson, D.A., Lichenstein, H.S., Cummings, R.D., Bainton, D.F., and McEver, R.P. (1995). **P-selectin glycoprotein ligand-1 mediates rolling of human neutrophils on P-selectin**. J Cell Biol *128*, 661-671.

Mor, A., Dustin, M.L., and Philips, M.R. (2007). **Small GTPases and LFA-1 reciprocally modulate adhesion and signaling**. Immunol Rev *218*, 114-125.

Morikawa, S., Baluk, P., Kaidoh, T., Haskell, A., Jain, R.K., and McDonald, D.M. (2002). **Abnormalities in pericytes on blood vessels and endothelial sprouts in tumors**. Am J Pathol *160*, 985-1000.

Muller, W.A. (2003). **Leukocyte-endothelial-cell interactions in leukocyte transmigration and the inflammatory response**. Trends Immunol *24*, 327-334.

Murfee, W.L., Skalak, T.C., and Peirce, S.M. (2005). **Differential arterial/venous expression of NG2 proteoglycan in perivascular cells along microvessels: identifying a venule-specific phenotype**. Microcirculation *12*, 151-160.

Muzio, M., Ni, J., Feng, P., and Dixit, V.M. (1997). **IRAK (Pelle) family member IRAK-2 and MyD88 as proximal mediators of IL-1 signaling**. Science *278*, 1612-1615.

Nayak, R.C., Berman, A.B., George, K.L., Eisenbarth, G.S., and King, G.L. (1988). **A monoclonal antibody (3G5)-defined ganglioside antigen is expressed on the cell surface of microvascular pericytes**. J Exp Med *167*, 1003-1015.

Nehls, V., and Drenckhahn, D. (1991). **Heterogeneity of microvascular pericytes for smooth muscle type alpha-actin**. J Cell Biol *113*, 147-154.

Newcomb, P.M., and Herman, I.M. (1993). **Pericyte growth and contractile phenotype: modulation by endothelial-synthesized matrix and comparison with aortic smooth muscle**. J Cell Physiol *155*, 385-393.

Nisancioglu, M.H., Mahoney, W.M., Jr., Kimmel, D.D., Schwartz, S.M., Betsholtz, C., and Genove, G. (2008). **Generation and characterization of rgs5 mutant mice**. Mol Cell Biol *28*, 2324-2331.

Norman, K.E., Moore, K.L., McEver, R.P., and Ley, K. (1995). **Leukocyte rolling in vivo is mediated by P-selectin glycoprotein ligand-1**. Blood *86*, 4417-4421.

Nourshargh, S., Hordijk, P.L., and Sixt, M. (2010). **Breaching multiple barriers: leukocyte motility through venular walls and the interstitium**. Nat Rev Mol Cell Biol *11*, 366-378.

Nourshargh, S., Krombach, F., and Dejana, E. (2006). **The role of JAM-A and PECAM-1 in modulating leukocyte infiltration in inflamed and ischemic tissues**. J Leukoc Biol *80*, 714-718.

Orlidge, A., and D'Amore, P.A. (1986). **Cell specific effects of glycosaminoglycans on the attachment and proliferation of vascular wall components**. Microvasc Res *31*, 41-53.

Orlidge, A., and D'Amore, P.A. (1987). **Inhibition of capillary endothelial cell growth by pericytes and smooth muscle cells**. J Cell Biol *105*, 1455-1462.

Orlinick, J.R., and Chao, M.V. (1998). **TNF-related ligands and their receptors**. Cell Signal *10*, 543-551.

Ozerdem, U., Grako, K.A., Dahlin-Huppe, K., Monosov, E., and Stallcup, W.B. (2001). **NG2 proteoglycan is expressed exclusively by mural cells during vascular morphogenesis**. Dev Dyn *222*, 218-227.

Ozerdem, U., Monosov, E., and Stallcup, W.B. (2002). **NG2 proteoglycan expression by pericytes in pathological microvasculature**. Microvasc Res *63*, 129-134.

Palmiter, R.D., and Brinster, R.L. (1985). **Transgenic mice**. Cell *41*, 343-345.

Pan, J., and McEver, R.P. (1995). **Regulation of the human P-selectin promoter by Bcl-3 and specific homodimeric members of the NF-kappa B/Rel family**. J Biol Chem *270*, 23077-23083.

Peppiatt, C.M., Howarth, C., Mobbs, P., and Attwell, D. (2006). **Bidirectional control of CNS capillary diameter by pericytes**. Nature *443*, 700-704.

Petri, B., Phillipson, M., and Kubes, P. (2008). **The physiology of leukocyte recruitment: an in vivo perspective**. J Immunol *180*, 6439-6446.

Phillipson, M., Heit, B., Colarusso, P., Liu, L., Ballantyne, C.M., and Kubes, P. (2006). **Intraluminal crawling of neutrophils to emigration sites: a molecularly distinct process from adhesion in the recruitment cascade**. J Exp Med *203*, 2569-2575.

Phillipson, M., Heit, B., Parsons, S.A., Petri, B., Mullaly, S.C., Colarusso, P., Gower, R.M., Neely, G., Simon, S.I., and Kubes, P. (2009). **Vav1 is essential for mechanotactic crawling and migration of neutrophils out of the inflamed microvasculature**. J Immunol *182*, 6870-6878.

Pober, J.S., Lapierre, L.A., Stolpen, A.H., Brock, T.A., Springer, T.A., Fiers, W., Bevilacqua, M.P., Mendrick, D.L., and Gimbrone, M.A., Jr. (1987). **Activation of cultured human endothelial cells by recombinant lymphotoxin: comparison with tumor necrosis factor and interleukin 1 species**. J Immunol *138*, 3319-3324.

Puls, A., Eliopoulos, A.G., Nobes, C.D., Bridges, T., Young, L.S., and Hall, A. (1999). **Activation of the small GTPase Cdc42 by the inflammatory cytokines TNF(alpha) and IL-1, and by the Epstein-Barr virus transforming protein LMP1**. J Cell Sci *112 (Pt 17)*, 2983-2992.

Rajantie, I., Ilmonen, M., Alminaite, A., Ozerdem, U., Alitalo, K., and Salven, P. (2004). **Adult bone marrow-derived cells recruited during angiogenesis comprise precursors for periendothelial vascular mural cells**. Blood *104*, 2084-2086.

Rampart, M., Fiers, W., de Smet, W., and Herman, A.G. (1989). **Different pro-inflammatory profiles of interleukin 1 (IL 1) and tumor necrosis factor (TNF) in an in vivo model of inflammation**. Agents Actions *26*, 186-188.

Reznikoff, C.A., Brankow, D.W., and Heidelberger, C. (1973). **Establishment and characterization of a cloned line of C3H mouse embryo cells sensitive to postconfluence inhibition of division**. Cancer Res *33*, 3231-3238.

Riedl, J., Crevenna, A.H., Kessenbrock, K., Yu, J.H., Neukirchen, D., Bista, M., Bradke, F., Jenne, D., Holak, T.A., Werb, Z., *et al.* (2008). **Lifeact: a versatile marker to visualize F-actin**. Nat Methods *5*, 605-607.

Riedl, J., Flynn, K.C., Raducanu, A., Gartner, F., Beck, G., Bosl, M., Bradke, F., Massberg, S., Aszodi, A., Sixt, M., and Wedlich-Soldner, R. (2010). **Lifeact mice for studying F-actin dynamics**. Nat Methods *7*, 168-169.

Rose, D.M., Alon, R., and Ginsberg, M.H. (2007). **Integrin modulation and signaling in leukocyte adhesion and migration**. Immunol Rev *218*, 126-134.

Rot, A. (2005). **Contribution of Duffy antigen to chemokine function**. Cytokine Growth Factor Rev *16*, 687-694.

Rowe, R.G., and Weiss, S.J. (2008). **Breaching the basement membrane: who, when and how?** Trends Cell Biol *18*, 560-574.

Rupp, C., Dolznig, H., Puri, C., Sommergruber, W., Kerjaschki, D., Rettig, W.J., and Garin-Chesa, P. (2006). **Mouse endosialin, a C-type lectin-like cell surface receptor: expression during embryonic development and induction in experimental cancer neoangiogenesis**. Cancer Immun *6*, 10.

Ryschich, E., Kerkadze, V., Lizdenis, P., Paskauskas, S., Knaebel, H.P., Gross, W., Gebhard, M.M., Buchler, M.W., and Schmidt, J. (2006). **Active leukocyte crawling in microvessels assessed by digital time-lapse intravital microscopy**. J Surg Res *135*, 291-296.

Salas, A., Shimaoka, M., Kogan, A.N., Harwood, C., von Andrian, U.H., and Springer, T.A. (2004). **Rolling adhesion through an extended conformation of integrin alphaLbeta2 and relation to alpha I and beta I-like domain interaction**. Immunity *20*, 393-406.

Sato, Y., and Rifkin, D.B. (1989). **Inhibition of endothelial cell movement by pericytes and smooth muscle cells: activation of a latent transforming growth factor-beta 1-like molecule by plasmin during co-culture**. J Cell Biol *109*, 309-315.

Schenkel, A.R., Mamdouh, Z., and Muller, W.A. (2004). **Locomotion of monocytes on endothelium is a critical step during extravasation**. Nat Immunol *5*, 393-400.

Schlingemann, R.O., Oosterwijk, E., Wesseling, P., Rietveld, F.J., and Ruiter, D.J. (1996). **Aminopeptidase a is a constituent of activated pericytes in angiogenesis**. J Pathol *179*, 436-442.

Schor, A.M., Canfield, A.E., Sutton, A.B., Arciniegas, E., and Allen, T.D. (1995). **Pericyte differentiation**. Clin Orthop Relat Res, 81-91.

Schor, A.M., and Schor, S.L. (1986). **The isolation and culture of endothelial cells and pericytes from the bovine retinal microvasculature: a comparative study with large vessel vascular cells**. Microvasc Res *32*, 21-38.

Schrage, A., Loddenkemper, C., Erben, U., Lauer, U., Hausdorf, G., Jungblut, P.R., Johnson, J., Knolle, P.A., Zeitz, M., Hamann, A., and Klugewitz, K. (2008). **Murine CD146 is widely expressed on endothelial cells and is recognized by the monoclonal antibody ME-9F1**. Histochem Cell Biol *129*, 441-451.

Shamri, R., Grabovsky, V., Gauguet, J.M., Feigelson, S., Manevich, E., Kolanus, W., Robinson, M.K., Staunton, D.E., von Andrian, U.H., and Alon, R. (2005). **Lymphocyte arrest requires instantaneous induction of an extended LFA-1 conformation mediated by endothelium-bound chemokines**. Nat Immunol *6*, 497-506.

Shattil, S.J. (2005). **Integrins and Src: dynamic duo of adhesion signaling**. Trends Cell Biol *15*, 399-403.

Shaw, S.K., Bamba, P.S., Perkins, B.N., and Luscinskas, F.W. (2001). **Real-time imaging of vascular endothelial-cadherin during leukocyte transmigration across endothelium**. J Immunol *167*, 2323-2330.

Shepro, D., and Morel, N.M. (1993). **Pericyte physiology**. Faseb J *7*, 1031-1038.

Shimada, T., Kitamura, H., and Nakamura, M. (1992). **Three-dimensional architecture of pericytes with special reference to their topographical relationship to microvascular beds**. Arch Histol Cytol *55 Suppl*, 77-85.

Silva, R., D'Amico, G., Hodivala-Dilke, K.M., and Reynolds, L.E. (2008). **Integrins: the keys to unlocking angiogenesis**. Arterioscler Thromb Vasc Biol *28*, 1703-1713.

Sima, A.A., Chakrabarti, S., Garcia-Salinas, R., and Basu, P.K. (1985). **The BB-rat--an authentic model of human diabetic retinopathy**. Curr Eye Res *4*, 1087-1092.

Simon, S.I., Hu, Y., Vestweber, D., and Smith, C.W. (2000). **Neutrophil tethering on E-selectin activates beta 2 integrin binding to ICAM-1 through a mitogen-activated protein kinase signal transduction pathway**. J Immunol *164*, 4348-4358.

Simonavicius, N., Robertson, D., Bax, D.A., Jones, C., Huijbers, I.J., and Isacke, C.M. (2008). **Endosialin (CD248) is a marker of tumor-associated pericytes in high-grade glioma**. Mod Pathol *21*, 308-315.

Sims, D.E. (2000). **Diversity within pericytes**. Clin Exp Pharmacol Physiol *27*, 842-846.

Sims, D.E., Miller, F.N., Donald, A., and Perricone, M.A. (1990). **Ultrastructure of pericytes in early stages of histamine-induced inflammation**. J Morphol *206*, 333-342.

Sims, D.E., Miller, F.N., Horne, M.M., and Edwards, M.J. (1994). **Interleukin-2 alters the positions of capillary and venule pericytes in rat cremaster muscle**. J Submicrosc Cytol Pathol *26*, 507-513.

Singbartl, K., Thatte, J., Smith, M.L., Wethmar, K., Day, K., and Ley, K. (2001). **A CD2-green fluorescence protein-transgenic mouse reveals very late antigen-4-dependent CD8+ lymphocyte rolling in inflamed venules**. J Immunol *166*, 7520-7526.

Sixt, M., Engelhardt, B., Pausch, F., Hallmann, R., Wendler, O., and Sorokin, L.M. (2001). **Endothelial cell laminin isoforms, laminins 8 and 10, play decisive roles in T cell recruitment across the blood-brain barrier in experimental autoimmune encephalomyelitis**. J Cell Biol *153*, 933-946.

Skalli, O., Pelte, M.F., Peclet, M.C., Gabbiani, G., Gugliotta, P., Bussolati, G., Ravazzola, M., and Orci, L. (1989). **Alpha-smooth muscle actin, a differentiation marker of smooth muscle cells, is present in microfilamentous bundles of pericytes**. J Histochem Cytochem *37*, 315-321.

Speyer, C.L., Steffes, C.P., and Ram, J.L. (1999). **Effects of vasoactive mediators on the rat lung pericyte: quantitative analysis of contraction on collagen lattice matrices**. Microvasc Res *57*, 134-143.

Speyer, C.L., Steffes, C.P., Tyburski, J.G., and Ram, J.L. (2000). **Lipopolysaccharide induces relaxation in lung pericytes by an iNOS-independent mechanism**. Am J Physiol Lung Cell Mol Physiol *278*, L880-887.

Spillmann, D., Witt, D., and Lindahl, U. (1998). **Defining the interleukin-8-binding domain of heparan sulfate**. J Biol Chem *273*, 15487-15493.

Springer, T.A. (1994). **Traffic signals for lymphocyte recirculation and leukocyte emigration: the multistep paradigm**. Cell *76*, 301-314.

Springer, T.A. (1995). **Traffic signals on endothelium for lymphocyte recirculation and leukocyte emigration**. Annu Rev Physiol *57*, 827-872.

Staunton, D.E., Dustin, M.L., and Springer, T.A. (1989). **Functional cloning of ICAM-2, a cell adhesion ligand for LFA-1 homologous to ICAM-1**. Nature *339*, 61-64.

Stramm, L.E., Li, W., Aguirre, G.D., and Rockey, J.H. (1987). **Glycosaminoglycan synthesis and secretion by bovine retinal capillary pericytes in culture**. Exp Eye Res *44*, 17-28.

Stratman, A.N., Malotte, K.M., Mahan, R.D., Davis, M.J., and Davis, G.E. (2009). **Pericyte recruitment during vasculogenic tube assembly stimulates endothelial basement membrane matrix formation**. Blood *114*, 5091-5101.

Strieter, R.M., Kunkel, S.L., Showell, H.J., Remick, D.G., Phan, S.H., Ward, P.A., and Marks, R.M. (1989). **Endothelial cell gene expression of a neutrophil chemotactic factor by TNF-alpha, LPS, and IL-1 beta**. Science *243*, 1467-1469.

Su, W.H., Chen, H.I., Huang, J.P., and Jen, C.J. (2000). **Endothelial [Ca(2+)](i) signaling during transmigration of polymorphonuclear leukocytes**. Blood *96*, 3816-3822.

Sumagin, R., and Sarelius, I.H. (2006). **TNF-alpha activation of arterioles and venules alters distribution and levels of ICAM-1 and affects leukocyte-endothelial cell interactions**. Am J Physiol Heart Circ Physiol *291*, H2116-2125.

Sundberg, C., Ivarsson, M., Gerdin, B., and Rubin, K. (1996). **Pericytes as collagen-producing cells in excessive dermal scarring**. Lab Invest *74*, 452-466.

Thompson, R.D., Noble, K.E., Larbi, K.Y., Dewar, A., Duncan, G.S., Mak, T.W., and Nourshargh, S. (2001). **Platelet-endothelial cell adhesion molecule-1 (PECAM-1)-deficient mice demonstrate a transient and cytokine-specific role for PECAM-1 in leukocyte migration through the perivascular basement membrane**. Blood *97*, 1854-1860.

Thorsen, V.A., Vorland, M., Bjorndal, B., Bruland, O., Holmsen, H., and Lillehaug, J.R. (2003). **Participation of phospholipase D and alpha/beta-protein kinase C in growth factor-induced signalling in C3H10T1/2 fibroblasts**. Biochim Biophys Acta *1632*, 62-71.

Tidhar, A., Reichenstein, M., Cohen, D., Faerman, A., Copeland, N.G., Gilbert, D.J., Jenkins, N.A., and Shani, M. (2001). **A novel transgenic marker for migrating limb muscle precursors and for vascular smooth muscle cells**. Dev Dyn *220*, 60-73.

Varki A, C.R., Esko JD, Freeze HH, Stanley P, Bertozzi CR, Hart GW and Etzler ME, ed. (2009). Essentials of Glycobiology, 2nd edn (Cold Spring Harbor (NY, USA): Cold Spring Harbor Laboratory Press).

Verbeek, M.M., Otte-Holler, I., Ruiter, D.J., and de Waal, R.M. (1999). **Human brain pericytes as a model system to study the pathogenesis of cerebrovascular amyloidosis in Alzheimer's disease**. Cell Mol Biol (Noisy-le-grand) *45*, 37-46.

Verbeek, M.M., Westphal, J.R., Ruiter, D.J., and de Waal, R.M. (1995). **T lymphocyte adhesion to human brain pericytes is mediated via very late antigen-4/vascular cell adhesion molecule-1 interactions**. J Immunol *154*, 5876-5884.

Vestweber, D., and Blanks, J.E. (1999). **Mechanisms that regulate the function of the selectins and their ligands**. Physiol Rev *79*, 181-213.

Voisin, M.B., Probstl, D., and Nourshargh, S. (2010). **Venular basement membranes ubiquitously express matrix protein low-expression regions: characterization in multiple tissues and remodeling during inflammation**. Am J Pathol *176*, 482-495.

Voisin, M.B., Woodfin, A., and Nourshargh, S. (2009). **Monocytes and neutrophils exhibit both distinct and common mechanisms in penetrating the vascular basement membrane in vivo**. Arterioscler Thromb Vasc Biol *29*, 1193-1199.

Wallow, I.H., Bindley, C.D., Reboussin, D.M., Gange, S.J., and Fisher, M.R. (1993). **Systemic hypertension produces pericyte changes in retinal capillaries**. Invest Ophthalmol Vis Sci *34*, 420-430.

Wang, S., Dangerfield, J.P., Young, R.E., and Nourshargh, S. (2005). **PECAM-1, alpha6 integrins and neutrophil elastase cooperate in mediating neutrophil transmigration**. J Cell Sci *118*, 2067-2076.

Wang, S., Voisin, M.B., Larbi, K.Y., Dangerfield, J., Scheiermann, C., Tran, M., Maxwell, P.H., Sorokin, L., and Nourshargh, S. (2006). **Venular basement membranes contain specific matrix protein low expression regions that act as exit points for emigrating neutrophils**. J Exp Med *203*, 1519-1532.

Weber, C., Fraemohs, L., and Dejana, E. (2007). **The role of junctional adhesion molecules in vascular inflammation**. Nat Rev Immunol *7*, 467-477.

Woltmann, G., McNulty, C.A., Dewson, G., Symon, F.A., and Wardlaw, A.J. (2000). **Interleukin-13 induces PSGL-1/P-selectin-dependent adhesion of eosinophils, but not neutrophils, to human umbilical vein endothelial cells under flow**. Blood *95*, 3146-3152.

Woodfin, A., Reichel, C.A., Khandoga, A., Corada, M., Voisin, M.B., Scheiermann, C., Haskard, D.O., Dejana, E., Krombach, F., and Nourshargh, S. (2007). **JAM-A mediates neutrophil transmigration in a stimulus-specific manner in vivo: evidence for sequential roles for JAM-A and PECAM-1 in neutrophil transmigration**. Blood *110*, 1848-1856.

Woodfin, A., Voisin, M.B., Imhof, B.A., Dejana, E., Engelhardt, B., and Nourshargh, S. (2009). **Endothelial cell activation leads to neutrophil transmigration as supported by the sequential roles of ICAM-2, JAM-A, and PECAM-1**. Blood *113*, 6246-6257.

Woodfin, A., Voisin, M.B., and Nourshargh, S. (2010). **Recent developments and complexities in neutrophil transmigration**. Curr Opin Hematol *17*, 9-17.

Xie, J., Li, R., Kotovuori, P., Vermot-Desroches, C., Wijdenes, J., Arnaout, M.A., Nortamo, P., and Gahmberg, C.G. (1995). **Intercellular adhesion molecule-2 (CD102) binds to the leukocyte integrin CD11b/CD18 through the A domain**. J Immunol *155*, 3619-3628.

Yamagishi, S., Fujimori, H., Yonekura, H., Tanaka, N., and Yamamoto, H. (1999). **Advanced glycation endproducts accelerate calcification in microvascular pericytes**. Biochem Biophys Res Commun *258*, 353-357.

Yao, L., Pan, J., Setiadi, H., Patel, K.D., and McEver, R.P. (1996). **Interleukin 4 or oncostatin M induces a prolonged increase in P-selectin mRNA and protein in human endothelial cells**. J Exp Med *184*, 81-92.

Yao, L., Setiadi, H., Xia, L., Laszik, Z., Taylor, F.B., and McEver, R.P. (1999). **Divergent inducible expression of P-selectin and E-selectin in mice and primates**. Blood *94*, 3820-3828.

Yauk, C.L., Polyzos, A., Rowan-Carroll, A., Kortubash, I., Williams, A., and Kovalchuk, O. (2008). **Tandem repeat mutation, global DNA methylation, and regulation of DNA methyltransferases in cultured mouse embryonic fibroblast cells chronically exposed to chemicals with different modes of action**. Environ Mol Mutagen *49*, 26-35.

Yokota, T., Kawakami, Y., Nagai, Y., Ma, J.X., Tsai, J.Y., Kincade, P.W., and Sato, S. (2006). **Bone marrow lacks a transplantable progenitor for smooth muscle type alpha-actin-expressing cells**. Stem Cells *24*, 13-22.

Zarbock, A., Abram, C.L., Hundt, M., Altman, A., Lowell, C.A., and Ley, K. (2008). **PSGL-1 engagement by E-selectin signals through Src kinase Fgr and ITAM adapters DAP12 and FcR gamma to induce slow leukocyte rolling**. J Exp Med *205*, 2339-2347.

Zarbock, A., and Ley, K. (2008). **Mechanisms and consequences of neutrophil interaction with the endothelium**. Am J Pathol *172*, 1-7.